
Multi-photon entanglement and applications in quantum information

Christian I. T. Schmid



München 2008

Multi-photon entanglement and applications in quantum information

Christian I. T. Schmid

Dissertation
an der Fakultät für Physik
der Ludwig–Maximilians–Universität
München

vorgelegt von
Christian I. T. Schmid
aus Landshut

München, den 30.05.2008

Erstgutachter / First referee: Prof. Dr. Harald Weinfurter
Zweitgutachter / Second referee: Prof. Dr. Axel Schenzle
Tag der mündlichen Prüfung / Day of oral exam: 23.07.2008

Contents

Zusammenfassung / Abstract	xiii
Introduction and outline	1
1 Basic concepts in quantum information	5
1.1 Classical vs. quantum states	5
1.1.1 Description of physical states	5
1.1.2 Superposition principle, entanglement and violation of local realism	7
1.2 (Quantum)-information	12
1.2.1 Information encoded in physical systems – (qu)bits	13
1.2.2 Entanglement of qubits	15
1.2.3 Processing of information	27
1.3 Photons as qubits	31
1.3.1 Encoding of information in polarization and its manipulation	32
1.3.2 Generation of photons	33
1.3.3 Building blocks of typical setups	37
2 Tools for optical quantum information processing	43
2.1 Controlled phase gate	43
2.1.1 The setup	44
2.1.2 A model for gate characterization	46
2.1.3 Experimental results	47
2.2 One setup for the observation of a whole family of states	50
2.2.1 The theoretical concept and the class of states	50
2.2.2 Interesting states in terms of correlations	54
2.2.3 Experiment	56
2.2.4 Discussion of the results	64
2.3 Conclusion	66
3 Applications of a controlled phase gate	67
3.1 Teleportation and entanglement swapping	67
3.1.1 The protocols	68
3.1.2 The implementation	70
3.1.3 Experimental results for teleportation	71
3.1.4 Experimental results for entanglement swapping	75
3.1.5 Discussion	78
3.2 Concurrence	79

3.2.1	Theory	80
3.2.2	Experimental implementation	81
3.2.3	Results	82
3.2.4	Influence of imperfect gate operation	83
3.2.5	Discussion	84
3.3	Cluster state	85
3.3.1	The linear four-photon Cluster state	85
3.3.2	Experimental results	87
3.3.3	Measurement based quantum computation	88
3.3.4	Discussion	90
3.4	Conclusion	91
4	Discriminating entangled states	93
4.1	The problem of state discrimination	93
4.2	Characteristic Bell inequalities – principle idea	94
4.3	Examples with experimental results	95
4.3.1	The four qubit cluster state	95
4.3.2	The four-qubit singlet state	97
4.3.3	The symmetric dicke state with two excitations	98
4.4	Non-Bell operators	101
4.5	Conclusion	105
5	Application of four-photon states in quantum games	107
5.1	Basics of (quantum) game theory	107
5.2	The quantum Minority game	108
5.3	Theory	109
5.4	Experimental implementation and results	113
5.5	Conclusion	117
	Conclusion and outlook	118
A	Experimentally measured expectation values and their errors	123
A.1	Evaluation of expectation values of operators	123
A.2	Errors of expectation values	125
A.3	Examples	126
B	Supplementary information and measured data	129
B.1	For Chap. 2	129
B.1.1	A product of two Bell pairs: $ \Psi'(0)\rangle$	129
B.1.2	Still unknown: $ \Psi'(\sqrt{\frac{1}{6}(3-\sqrt{3})})\rangle$	130
B.1.3	The symmetric four-qubit Dicke state: $ \Psi'(\frac{1}{\sqrt{3}})\rangle$	131
B.1.4	Still unknown: $ \Psi'(\frac{1}{\sqrt{2}})\rangle$	132
B.1.5	Psi-four: $ \Psi_4\rangle$	133
B.1.6	Still unknown: $ \Psi'(\sqrt{\frac{1}{6}(3+\sqrt{3})})\rangle$	135
B.1.7	GHZ: $ \Psi'(1)\rangle$	136
B.2	For Chap. 3	137

B.3 For Chap. 4	137
Acronyms and abbreviations	139
Bibliography	141
Danksagung / Acknowledgements	155
Curriculum Vitae	156
Publication list	158

List of Figures

1.1	State space in classical and quantum mechanics	6
1.2	Bloch sphere	14
1.3	Reflection symmetries for qubits	20
1.4	Equivalence classes of three-qubit states	22
1.5	Witness	24
1.6	Circuit symbols	30
1.7	SPDC	35
1.8	Polarization analysis	39
2.1	Controlled phase gate	44
2.2	Quantum process tomography	48
2.3	Dip measurement	49
2.4	One setup for many states	52
2.5	Probability	53
2.6	Correlations	56
2.7	GHZ and Bell terms	57
2.8	Dip measurement	58
2.9	State vectors	61
2.10	Correlation measurement $ \Psi_4^-\rangle$	62
2.11	Fidelities	64
2.12	Resulting fidelities	64
3.1	Circuit diagram for quantum teleportation	68
3.2	Teleportation, entanglement swapping	71
3.3	Teleported states	72
3.4	Teleportation process tomography matrix	75
3.5	Swapped states	76
3.6	Fidelity of swapped states	77
3.7	Concurrence	82
3.8	Concurrence simulation	84
3.9	Cluster states	86
3.10	Correlation measurement $ C_4\rangle$	87
3.11	Measurement based quantum computation	89
4.1	Correlation measurement $ C_4\rangle$	97
4.2	Correlation measurement \mathbb{B}_{Ψ_4}	99
4.3	Dicke state setup	102

4.4	Correlation measurement $\mathbb{B}_{D_4^{(2)}}$	103
5.1	Payoff in the quantum Minority game	112
5.2	Experimentally measured payoffs	114
A.1	Scaling of errors	127

List of Tables

2.1	Correlations of $ \Psi'(\alpha)\rangle$	54
3.1	Fidelities of teleported output states	74
3.2	Fidelities and negativities of swapped states	77
3.3	Violation of local realism	78
4.1	Maximal expectation values of \mathbb{B}_{C_4}	96
4.2	Maximal expectation values of \mathbb{B}_{Ψ_4}	98
4.3	Maximal expectation values of $\mathbb{B}_{D_4^{(2)}}$	101
4.4	Maximal expectation values for characteristic non-Bell operators	104
5.1	Payoff in the quantum Minority game	113
5.2	Measured payoff values	115
5.3	Measured payoffs in other bases	117
A.1	Scaling of errors	128
B.1	Theoretical values for the non-zero correlations of the state $ \Psi'(0)\rangle$	129
B.2	Measured values for the non-zero correlations of the state $ \Psi'(0)\rangle$	130
B.3	Theoretical values for the non-zero correlations of the state $ \Psi'(\sqrt{\frac{1}{6}(3-\sqrt{3})})\rangle$	130
B.4	Measured values for the non-zero correlations of the state $ \Psi'(\sqrt{\frac{1}{6}(3-\sqrt{3})})\rangle$	131
B.5	Theoretical values for the non-zero correlations of the state $ \Psi'(\frac{1}{\sqrt{3}})\rangle$	131
B.6	Measured values for the non-zero correlations of the state $ \Psi'(\frac{1}{\sqrt{3}})\rangle$	132
B.7	Theoretical values for the non-zero correlations of the state $ \Psi'(\frac{1}{\sqrt{2}})\rangle$	132
B.8	Measured values for the non-zero correlations of the state $ \Psi'(\frac{1}{\sqrt{2}})\rangle$	133
B.9	Theoretical values for the non-zero correlations of the state $ \Psi_4^-\rangle$	133
B.10	Theoretical values for the non-zero correlations of the state $ \Psi_4^+\rangle$	134
B.11	Measured values for the non-zero correlations of the state $ \Psi_4^-\rangle$	134
B.12	Measured values for the non-zero correlations of the state $ \Psi_4^+\rangle$	135
B.13	Theoretical values for the non-zero correlations of the state $ \Psi'(\sqrt{\frac{1}{6}(3+\sqrt{3})})\rangle$	135
B.14	Measured values for the non-zero correlations of the state $ \Psi'(\sqrt{\frac{1}{6}(3+\sqrt{3})})\rangle$	136
B.15	Theoretical values for the non-zero correlations of the state $ \Psi'(1)\rangle$	136
B.16	Measured values for the non-zero correlations of the state $ \Psi'(1)\rangle$	137
B.17	Measured values for the non-zero correlations of the state $ C_4\rangle$	137

B.18 Measured values for the non-zero correlations of the state $|D_4^{(2)}\rangle$ 138

Zusammenfassung

Fast 55 Jahre vergingen bis die Entdeckung des Phänomens der Verschränkung durch Einstein, Podolski, Rosen und Schrödinger Ende des zwanzigsten Jahrhunderts Einzug in die Labore hielt. Mittlerweile wurde eine Vielfalt von verschränkten Zuständen untersucht; die größte davon in Systemen photonischer Qubits. Alle modernen Experimente zu viel-Photonen Verschränkung lassen sich in drei wesentliche Bestandteile untergliedern: Eine Photonenquelle, ein Netzwerk aus linearen optischen Komponenten welches die Photonen verarbeitet, und eine bedingte Detektion der Photonen am Ausgang des Netzwerks.

Die vorliegende Arbeit führt zwei neue Netzwerke ein und präsentiert deren Anwendungen in verschiedenen Problemstellungen der Quanteninformation. Als Photonenquelle dient hierbei der Prozeß der spontanen parametrischen Fluoreszenz in unterschiedlichen Konfigurationen.

Das erste Netzwerk ist ein neuartiges Kontroll-Phasengatter das sich gegenüber früheren Realisierungen vor allem durch seine hohe Stabilität auszeichnet. Wie anhand mehrerer Beispiele gezeigt wird, eignet es sich besonders für den Einsatz in mehr-Photonen Experimenten. Mit Hilfe des Gatters werden alle vier Bell Zustände in einem Teleportations- und „entanglement swapping“ Experiment unterschieden. Ein ähnlicher experimenteller Aufbau erlaubt ferner die direkte Messung der Verschränkung zweier Kopien eines Zustands in Form der „Concurrence“. Ausgehend von zwei Bell Zuständen wird das Gatter darüberhinaus zur Beobachtung eines Vier-Photonen „Cluster Zustands“ verwendet. Die Analyse der Ergebnisse konzentriert sich dabei auf die Hauptanwendung von Cluster Zuständen, das meßbasierte Quantenrechnen.

Das zweite Netzwerk bildet, zusammen mit der Emission zweiter Ordnung der parametrischen Fluoreszenz als Input, eine einstellbare Quelle verschiedenster Zustände. Während die Beobachtung eines Zustands bisher einen individuell maßgeschneiderten Versuchsaufbau benötigte, können mit dem neuen Netzwerk viele verschiedene Zustände innerhalb desselben Aufbaus beobachtet werden. Dies erfordert lediglich die Veränderung eines einzelnen, leicht zugänglichen experimentellen Parameters. Die so erzeugten Zustände besitzen eine Reihe nützlicher Eigenschaften und spielen eine zentrale Rolle in vielen Anwendungen. Hier werden sie zur Lösung eines vier-Parteien Quanten „Minority“ Spiels verwendet. Es wird gezeigt, dass die Quanten Version des Spiels durch den Einsatz von vier-Qubit Verschränkung sein klassisches Pendant an Möglichkeiten deutlich übertrifft.

Mit Hilfe experimenteller Daten beider Netzwerke wird eine neue Methode der Unterscheidung vier-Qubit verschränkter Zustände vorgestellt. Obwohl theoretische Klassifizierungen verschränkter Zustände existieren, gab es bisher keine einfache experimentelle Methode einen beobachteten Zustand der einen oder anderen Klasse zuzuordnen. Das hier vorgestellte Konzept ermöglicht eine experimentelle Klassifizierung basierend auf Operatoren die aus zustandsabhängigen Korrelationsmessungen bestimmt werden.

Abstract

Since the awareness of entanglement was raised by Einstein, Podolski, Rosen and Schrödinger in the beginning of the last century, it took almost 55 years until entanglement entered the laboratories as a new resource. Meanwhile, entangled states of various quantum systems have been investigated. So far, their biggest variety was observed in photonic qubit systems. Thereby, the setups of today's experiments on multi-photon entanglement can all be structured in the following way: They consist of a photon source, a linear optics network by which the photons are processed and the conditional detection of the photons at the output of the network.

In this thesis, two new linear optics networks are introduced and their application for several quantum information tasks is presented. The workhorse of multi-photon quantum information, spontaneous parametric down conversion, is used in different configurations to provide the input states for the networks.

The first network is a new design of a controlled phase gate which is particularly interesting for applications in multi-photon experiments as it constitutes an improvement of former realizations with respect to stability and reliability. This is explicitly demonstrated by employing the gate in four-photon experiments. In this context, a teleportation and entanglement swapping protocol is performed in which all four Bell states are distinguished by means of the phase gate. A similar type of measurement applied to the subsystem parts of two copies of a quantum state, allows further the direct estimation of the state's entanglement in terms of its concurrence. Finally, starting from two Bell states, the controlled phase gate is applied for the observation of a four photon cluster state. The analysis of the results focuses on measurement based quantum computation, the main usage of cluster states.

The second network, fed with the second order emission of non-collinear type II spontaneous parametric down conversion, constitutes a tunable source of a whole family of states. Up to now the observation of one particular state required one individually tailored setup. With the network introduced here many different states can be obtained within the same arrangement by tuning a single, easily accessible experimental parameter. These states exhibit many useful properties and play a central role in several applications of quantum information. Here, they are used for the solution of a four-player quantum Minority game. It is shown that, by employing four-qubit entanglement, the quantum version of the game clearly outperforms its classical counterpart.

Experimental data obtained with both networks are utilized to demonstrate a new method for the experimental discrimination of different multi-partite entangled states. Although theoretical classifications of four-qubit entangled states exist, so far there was no experimental tool to easily assign an observed state to the one or the other class. The new tool presented here is based on operators which are formed by the correlations between local measurement settings that are typical for the respective quantum state.

Introduction and outline

*Das, wobei unsere Berechnungen
versagen, nennen wir Zufall.*

Albert Einstein

In the early twentieth century, the development of quantum mechanics coerced physicists into radically changing the concepts they used to describe the world. The new theory, though being incredibly successful, discomfited even its own founders and caused debates lasting until today. Albert Einstein, who was one of the first to apply and generalize Planck's quantum hypothesis, never liked the consequences following from quantum theory. In particular, he thought that randomness is rather something for which the calculus fails, than an inherent principle of nature. He explicitly expressed his concerns about the random character of quantum effects in a seminal work together with Boris Podolsky and Nathan Rosen in the year 1935 [1]. In their argument, Einstein, Podolski, Rosen (**EPR**) pointed first at something which was, still in the same year, named "*entanglement*" by Erwin Schrödinger [2]. Schrödinger described entanglement as a situation which can regularly occur if two or more bodies enter a situation in which they influence each other and separate again. Each of the bodies might be maximally known prior to the interaction. However, there is no necessity that the knowledge, though remaining maximal, splits into a logical sum of knowledges about the individual bodies after they have separated again. As a consequence, the entangled particles, even if they are spatially spread, behave as a whole and have to be treated as such.

For a long time, entanglement was considered as nothing but a weird effect, useless besides being topic for philosophical discussions. It was not until the end of the twentieth century that entanglement turned out to be not only the "great difference" between classical and quantum physics, but the essential ingredient of a new field of research – *quantum information* [3]. This branch of physics is a quantum theory of information that applies quantum effects, and in particular entanglement, to enhance conventional information processing. On a more fundamental level it is even a completion of classical information theory. As such it includes two complementary kinds of information, classical and quantum information. While the commonly known "bit" is a measure of classical information, the newly introduced "qubit" corresponds to the quantum mechanical counterpart [4].

The physical implementation of single qubits as two level quantum systems, as well as the quantitative study of their entanglement and their interaction with classical information are essential prerequisites to harness the power of quantum mechanics for applications in quantum information science. The cornerstone for this was already put in the 1970's when many techniques for controlling single quanta of various kinds started to be developed. Methods have been invented to hold single ions in traps, move single atoms, transfer single electrons

within the operation of electronic devices and process single photons by means of linear optical elements.

Each of the different qubit realizations has its own advantages within the different branches of quantum information science which can be roughly divided into *quantum computation* and *quantum communication*. The former deals with the processing of quantum information, for which it was shown that it solves certain computational tasks more efficiently than classical computers. The latter studies quantum protocols for information transfer for which it opens up new possibilities, such as, e.g., the unconditionally secure key exchange in cryptographic applications [5]. Both fields are linked and attended by the study of the entanglement of qubits. The investigation of entanglement in the context of information theory leads thereby in turn to a deeper understanding of quantum theory itself.

For quantum communication, photons are the most suited system as they are the fastest carrier of information and couple only very weakly to the environment, thus profiting from extremely low decoherence. In contrast, for quantum computation, localized systems exhibiting a controllable interaction, like atoms or ions seem to be the preferable implementations. Surprisingly, as long as only the processing, but not the storage of information is concerned, photons offer also interesting possibilities for quantum computation. As was shown, universal linear optics quantum computation is indeed possible in principle [6]. Linear optical elements, such as phase shifters and beam splitters, though not able to let photons interact, can make them interfere. In combination with proper single-photon sources and photon-number resolving detectors this can be used for a realization of logical operations (for a review see [7]). In order to make the operations near deterministic, which is essential to combine them in scalable circuits, this approach requires a commensurate overhead of resources in form of, e.g., ancillary (entangled) qubit states. At the moment this is technically still too demanding. However, the additional resources are dispensable, and a probabilistic functioning tolerable, as long as only a limited number of quantum logic operations is sufficient for the solution of a given task. Following these suggestions, photon interference in linear optical networks could be successfully used for the (non-deterministic) implementation of various quantum computation primitives (for a review see [8, 9]). Moreover it allowed also the observation and characterization of a multitude of different entangled states.

Referring to this progress, in this thesis, two new linear optics networks are introduced. The workhorse of multi-photon quantum information, spontaneous parametric down conversion (SPDC), is used in different configurations to provide the input states for the networks. Accordingly, the aim of the work at hand is twofold: On the one hand, it should be shown that the presented networks face up to the current technical challenges of quantum computation as well as quantum communication. This is demonstrated by their application for several quantum information tasks. On the other hand, by implementing these tasks, the networks can serve for an experimental characterization and a better understanding of different kinds of multi-photon entanglement.

The first network is a controlled phase (CPHASE) gate which belongs to the set of universal quantum logic gates necessary for quantum computation. It is one of the fundamental two-qubit gates that allow to entangle and disentangle qubits. In this respect it applies in basic protocols, such as quantum teleportation and entanglement swapping [10, 11]. The CPHASE operation represents furthermore the central interaction in the generation principle of cluster states. These are particular entangled states which themselves provide again a resource for an alternative way of quantum computation [12, 13]. The design of the CPHASE gate presented here distinguishes itself from previous realizations [14–17] due to its interferometric stability

and reliability. This property makes it particularly interesting for applications in multi-photon experiments.

Usually in experiments aiming at the study of multi-photon entanglement, the observation of *one* particular state required *one* individually tailored setup. The second network which is presented breaks with this inflexibility. Once fed with the second order emission of non-collinear type II SPDC, it constitutes a tunable source of a whole family of states. The states of the family can be conveniently chosen by the variation of a single, easily accessible experimental parameter. They differ strongly in their entanglement properties and can be used in several applications. The ability to obtain different states within the same setup allows to experimentally study the performance of a given quantum information task depending on the kind of entanglement that is used. For example, quantum game theory studies competitive situations within quantum communication settings. In strategic situations the optimal results for the involved parties might depend on the type of entangled state that is used as resource. The investigation of such scenarios requires a source which provides more than just one type of state.

The observation of different types of entangled states demands also tools for their characterization, or a scheme to classify them. Indeed, it turns out that the establishment of classifications is an endeavor which becomes increasingly difficult with a rising number of qubits. For two qubits the situation is still simple as there is only one type of entanglement. Schemes to theoretically classify entangled states of three and four qubits exist [18–21]. They assume that two states belong to the same class if they can be converted into each other by means of local operations and classical communication. In the case of three qubits, this leads to a set of only a few classes which is still manageable, also experimentally. For four qubits, however, infinitely many classes exist, and so far there was no experimental tool to easily assign an observed state to the one or the other. There are methods to experimentally acquire full information about an observed state, but they are laborious and often not practicable [22]. Within this work, a new approach is introduced which focuses on a very restricted but relevant part of information about a state. It relies on characteristic operators which allow to discriminate an observed state from states of other entanglement classes. These operators are constructed from the correlations of local measurement settings that are typical for the respective quantum state. For the entangled states observed with the two networks they provide an efficient tool for their characterization.

The thesis is structured as follows: The first chapter addresses readers who are not familiar with the field. It recapitulates fundamentals of quantum mechanics and introduces definitions and notions which are frequently used in quantum information and required for the comprehension of the subsequent chapters. In the second chapter the layout and the functioning of the two new linear optics networks is presented and their applicability for different tasks is tested in chapters three and five. Chapter four introduces the characteristic operators for state discrimination. Finally, they are applied for the analysis of data obtained with both networks.

Chapter 1

Basic concepts in quantum information

This chapter gives an introduction to basic concepts in quantum information. It should facilitate the comprehension of the subsequent chapters for a reader who is not familiar with the field. Starting from the principle differences between classical and quantum mechanics it establishes fundamental terms like the *superposition principle* as well as *entanglement* and *violation of local realism* for bi- and multi-partite quantum systems. As will be shown, these typical quantum effects, though seemingly strange from an everyday life perspective, have intriguing and very practical applications in information tasks. Since single photons are the quantum system of choice throughout all the experiments presented in this thesis, this chapter finally provides insight in their generation and detection. The inherent benefits and disadvantages of the components of a typical setup are discussed briefly with respect to the experiments presented in the following chapters.

1.1 Classical vs. quantum states

The description of a physical state in quantum mechanics is almost as axiomatic as in classical Newtonian mechanics. However, there is a principal difference in the mathematical framework which has far-ranging consequences. Quantum mechanical phenomena like *entanglement* and *violation of local realism* emerge naturally as a consequence of the *superposition principle*, which is inherent to a description of physical states as elements of an abstract vector space, the Hilbert space.

1.1.1 Description of physical states

The physical state, with regard to a given underlying physical theory, is the minimal set of physical quantities that provides maximal information about the considered physical system.

In Newtonian mechanics the state of a physical system is fully described by its generalized coordinate \vec{q} and generalized momentum \vec{p} . The space of all possible states of the system is called *phase space*, and each state is uniquely represented by a point (\vec{q}, \vec{p}) in this space. Based on Newton's laws of motion the knowledge of \vec{q} and \vec{p} does not only provide complete information about the state at an initial time t_0 , but allows further to make predictions about the state of the system at any later time t . The dynamics of a particle with mass m subject

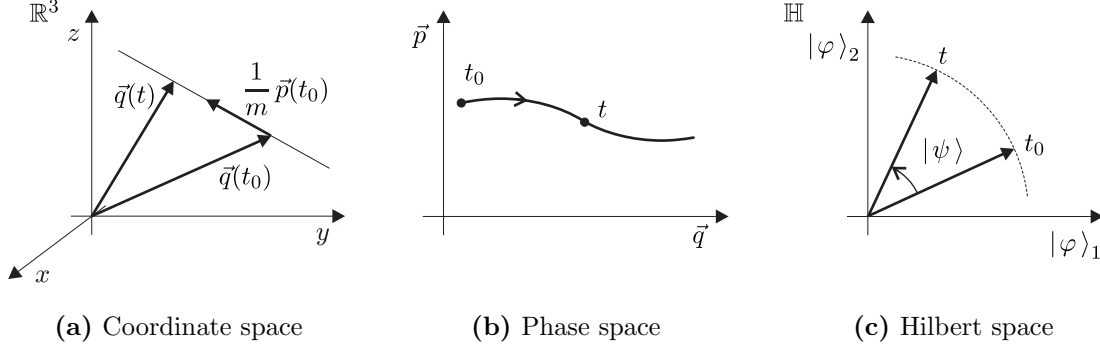


Figure 1.1: (a) In classical mechanics the state and the dynamics of a system is completely determined by the knowledge of the generalized position \vec{q} and the generalized momentum \vec{p} at a given initial time t_0 . (b) The state of a classical system is represented as a point (\vec{q}, \vec{p}) in phase space. The time evolution corresponds to a trajectory, i.e., a sequence of points. (c) In quantum mechanics the state of a physical system is represented by a vector $|\psi\rangle$ of a Hilbert space spanned by a set of basis vectors $\{|\varphi\rangle_1, |\varphi\rangle_2, \dots\}$. The dynamics equals a rotation of the state vector.

to a force \vec{F} is accordingly described by

$$\vec{F} = 0 : \quad \vec{q}(t) = \vec{q}(t_0) + \frac{1}{m} \vec{p}(t_0) t$$

and

$$\left. \begin{aligned} \dot{\vec{q}}(t) &\equiv \frac{d}{dt} \vec{q}(t) = \frac{1}{m} \vec{p}(t) \\ \dot{\vec{p}}(t) &\equiv \frac{d}{dt} \vec{p}(t) = \vec{F}(\vec{q}, \dot{\vec{q}}, t) \end{aligned} \right\} \quad m \ddot{\vec{q}}(t) \equiv m \frac{d^2}{dt^2} \vec{q}(t) = \vec{F}(\vec{q}, \dot{\vec{q}}, t)$$

(see Fig. 1.1(a)). Thus, the time evolution is represented by a trajectory, i.e., a sequence of points in phase space (see Fig. 1.1(b)).

By contrast, in quantum mechanics, the complete information about a physical state is provided by a vector $|\psi\rangle$ of an, in general, infinite-dimensional and complex vector space \mathbb{H} . This space is called *Hilbert space* and might be seen as a mathematical extension of the well-known vector algebra of Euclidean space to infinite dimensions. The dynamics of a system, characterized by the Hamiltonian \mathbb{H} , is described by the Schrödinger equation and can be interpreted as a rigid rotation of the state vector in this space (see Fig. 1.1(c)):

$$\frac{d}{dt} |\psi(t)\rangle = -\frac{i}{\hbar} \mathbb{H}_t |\psi(t)\rangle, \quad (1.1)$$

with the general solution $|\psi(t)\rangle = \mathbf{U}(t, t_0) |\psi(t_0)\rangle$ and $\mathbf{U}(t, t_0) \mathbf{U}^\dagger(t, t_0) = \mathbb{1} = \mathbf{U}^\dagger(t, t_0) \mathbf{U}(t, t_0)$.

In classical statistical physics it is sometimes not possible to describe the state of a system as a single point in phase space. In such an instance, due to macroscopic information about the system, the state can only be represented by a probability distribution $\rho(\vec{q}_j, \vec{p}_j)$ that specifies the probability to find the system in a particular state (\vec{q}_j, \vec{p}_j) . The analogue description of a system in quantum mechanics, in case of a lack of complete knowledge about the state, is given by the so-called density operator ρ . It is a Hermitian, positive-semidefinite operator of trace one. For a finite dimensional Hilbert space \mathbb{H} of dimension N , defined by a complete

set of orthonormal basis vectors $\{|\varphi_j\rangle\}$, it can be written as

$$\rho = \sum_{i=1}^N a_i |\varphi_i\rangle\langle\varphi_i|, \quad (1.2)$$

with $a_i \geq 0$, $\sum_{i=1}^N a_i = 1$ and $\langle\varphi_j|$ the dual vector to $|\varphi_j\rangle$. It provides the probabilities a_j to find the system in the state $|\varphi_j\rangle$ and its time evolution is in analogy to Eqn. (1.1) given by

$$\frac{\partial}{\partial t} \rho(t) = -\frac{i}{\hbar} [\mathbf{H}_t, \rho], \quad (1.3)$$

with the commutator $[\mathbf{H}_t, \rho] = \mathbf{H}_t \rho - \rho \mathbf{H}_t$.

Properties of a system's state that can be determined by a sequence of physical operations are called observables. In quantum mechanics, observables are represented by Hermitian operators whose spectrum denotes the set of possible measurement results. The expectation value of an observable \mathbf{A} for a system in the state $|\psi\rangle$ or ρ is given by

$$\langle\mathbf{A}\rangle_\psi \equiv \langle\psi|\mathbf{A}|\psi\rangle \quad \text{or} \quad \langle\mathbf{A}\rangle_\rho \equiv \text{tr}(\mathbf{A}\rho), \quad (1.4)$$

respectively. It can be seen as the average outcome of a measurement repeated (infinitely) many times or as the average outcome of a measurement performed on (infinitely) many copies of the system.

1.1.2 Superposition principle, entanglement and violation of local realism

In the preceding section it was established that the quantum mechanical description of the world deals with physical states being vectors of a vector space. One characteristic feature of a vector space is a defined binary operation that maps two elements of the space onto another element of the same space. This, usually referred to as vector addition, means that the result of two vectors being added will be again a vector. Although it seems not worth being mentioned from a mathematical point of view and was tacitly assumed in Sec. 1.1.1, it has intriguing implications concerning the interpretation of vectors as physical states. In fact it turns out to be the essential difference between classical and quantum mechanics and leads to a number of peculiar phenomena as shall be seen in the following.

Superposition principle

\mathcal{S} be an N -dimensional quantum system and \mathbf{A} be an observable of the system with spectrum $\text{sp}_{\mathbf{A}} = \{a_1, \dots, a_N\}$ and corresponding non-degenerate eigenvectors $\{|\alpha_1\rangle, \dots, |\alpha_N\rangle\} \in \mathbb{H}_{\mathcal{S}}$. As \mathbf{A} is an observable of the system, each $|\alpha_j\rangle$ is a valid state of \mathcal{S} . However, due to the vector addition any linear superposition

$$|\psi\rangle = \sum_{i=1}^N b_i |\alpha_i\rangle \quad \text{with } b_i \in \mathbb{C} \quad \text{and} \quad \sum_{i=1}^N |b_i|^2 = 1 \quad (1.5)$$

is also an element of the Hilbert space $\mathbb{H}_{\mathcal{S}}$ and hence a valid state of \mathcal{S} . That this concept, called *superposition principle*, is astonishing and surely unknown to classical mechanics is best seen by applying it to a macroscopic example, as first done by Erwin Schrödinger [2]:

\mathcal{S} be a cat and \mathbb{A} its state of health with, for reason of simplicity only two, eigenstates $|dead\rangle$ and $|alive\rangle$. In agreement with the above considerations

$$|\psi\rangle = \frac{1}{\sqrt{2}}(|dead\rangle + |alive\rangle)$$

has to be a valid state of the cat as well. The fact that naturally a real cat was never observed in such a state, pending between dead and alive or being neither nor, is a problem of lacking coherence in macroscopic systems. Superposition states like the one above occur only in a coherent system, i.e., a system whose Hamiltonian is a (time dependent) function of observables of only that system. A process, like in the above scenario, e.g., the cat crossing a street, is coherent if the observables at the end of the process are functions only of the observables of the same system at the beginning. These conditions are clearly not fulfilled for the example of the cat. To keep at the language of the example, the cat's state of health, after having passed the street, might strongly depend on a car coming along the street or not during the crossing. So, a more realistic description of the cat would be the "classical" state

$$\rho_{cat} = \frac{1}{2}(|dead\rangle\langle dead| + |alive\rangle\langle alive|)$$

expressing that the cat is indeed in a well defined state of health, either *dead* or *alive*, it is just not known, due to lack of information about the system. This example seems weird but it nicely illustrates the principle difference between the state given by a coherent superposition or a statistical mixture. In a macroscopic system all the constituting quanta face a continuous interaction, means disturbance, by their environment leading to a loss of coherence. Therefore, in every-day life typical quantum phenomena are usually not observed.

However, on a microscopic scale coherent systems as well as coherent processes can be realized and superposition states are existent.

Entanglement

The phenomenon *entanglement*, a term coined also by Erwin Schrödinger [2], appears as natural consequence of the superposition principle when going from a single indecomposable system to systems composed of two and more subsystems.

$\mathcal{S}_1, \dots, \mathcal{S}_n$ be n quantum systems and $\mathbb{H}_{\mathcal{S}_1}, \dots, \mathbb{H}_{\mathcal{S}_n}$ the corresponding Hilbert space of each. In a classical description the state space of the total system would be the Cartesian product of the n subsystem spaces and consequently the state of the total system would be a product state of the n subsystems. Contrary, in quantum physics, the state space of the total system \mathbb{H} is given as the tensor product of the subsystem spaces, $\mathbb{H} = \mathbb{H}_{\mathcal{S}_1} \otimes \mathbb{H}_{\mathcal{S}_2} \otimes \dots \otimes \mathbb{H}_{\mathcal{S}_n}$. The superposition principle implies that the state of the total system can be written in the form

$$|\psi\rangle = \sum_{i_1, \dots, i_n} b_{i_1, \dots, i_n} |\varphi_{i_1}\rangle \otimes |\varphi_{i_2}\rangle \otimes \dots \otimes |\varphi_{i_n}\rangle \quad (1.6)$$

with $|\varphi_{i_j}\rangle \in \mathbb{H}_{\mathcal{S}_j}$. In general $|\psi\rangle$ is not a product of states $|\psi_j\rangle \in \mathbb{H}_{\mathcal{S}_j}$ of the subsystems, $|\psi\rangle \neq |\psi_1\rangle \otimes |\psi_2\rangle \otimes \dots \otimes |\psi_n\rangle \equiv |\psi_1 \psi_2 \dots \psi_n\rangle$. A first phenomenological definition of entanglement can hence be stated as follows:

Definition 1.1.1 (Entanglement.) *A pure state of a composed quantum system is called entangled if it cannot be written as a product of states of the individual subsystems.*

In case of mixed states the situation is more difficult and entanglement is not equivalent to being non-product. Rather, a mixed state ρ of n subsystems is called entangled if it cannot be written as a convex combination of product states [23]:

$$\rho \neq \sum_i a_i \rho_{i_1} \otimes \rho_{i_2} \otimes \cdots \otimes \rho_{i_n}. \quad (1.7)$$

Short review of Def. 1.1.1 suggests the necessity of its refinement also in another direction. While being clear what "non-product" means for systems composed of two subsystems (bipartite systems), it might lead to ambiguities for systems of more than two components. However, a more careful discussion about the meaning of "being entangled or not" shall be held off for now on Sec. 1.2.2.

In any case, entangled states give rise to the third phenomenon discussed in this section, *violation of local realism*.

Reality or locality? – EPR's paradoxon and Bell's inequality

In the year 1935 Albert Einstein, Boris Podolski and Nathan Rosen (EPR) published an article on the question whether the quantum mechanical description of physical reality could be considered complete [1]. Its content triggered not only physical and philosophical discussions lasting to date, but is also of importance for the work presented in this thesis and shall be shortly recapitulated in the following.

In order to do this, two definitions made by EPR are required:

Definition 1.1.2 (Completeness) *A physical theory is complete, iff every element of the physical reality has a counterpart in the physical theory.*

Definition 1.1.3 (Reality) *If, without in any way disturbing the system, the value of a physical quantity can be predicted with certainty (i.e., with probability equal to unity), then there exists an element of physical reality corresponding to this physical quantity.*

Based on these definitions EPR derive a proposition of the form A or B ($A \vee B$) and show that the negation of A implies the negation of B ($\neg A \rightarrow \neg B$) from what they finally conjecture that A has to be true. For deduction of the former they consider a single particle state, whereas a two-particle entangled state is used for the demonstration of the latter.

\mathbf{P} and \mathbf{Q} be the operators corresponding to the momentum and position observable of a single particle with one degree of freedom, respectively. $|\psi\rangle$ be the state of the particle and an eigenstate of \mathbf{P} . Consequently, in the coordinate basis it holds that

$$\langle q|\mathbf{P}|q\rangle = -i\hbar \frac{\partial}{\partial q}, \quad \langle q|\mathbf{Q}|q\rangle = q, \quad (1.8)$$

and one can choose, e.g.,

$$\psi(q) \equiv \langle q|\psi\rangle = \exp\left(\frac{i}{\hbar} p_0 q\right), \quad (1.9)$$

with p_0 as constant and q the variable position of the particle. Obviously $\mathbf{P}|\psi\rangle = p_0|\psi\rangle$, $\langle \mathbf{P} \rangle_\psi = p_0$ and the momentum of the particle can be predicted to have certainly the value p_0 . According to Def. 1.1.3 it must be thus an object of physical reality. In contrast, the position of the particle \mathbf{Q} is completely indefinite and its value cannot be *predicted* but just *determined* by a measurement. The latter would clearly mean a disturbance of the system

changing its state. In fact, measuring \mathbf{Q} (or any other observable), leaves the system in an eigenstate of \mathbf{Q} (or the corresponding operator). As $[\mathbf{Q}, \mathbf{P}] = i\hbar \neq 0$ these operators do not have common eigenvectors and therefore the values for both observables cannot be predicted with certainty simultaneously.

From the above considerations and Def. 1.1.2 EPR formulate the proposition

Proposition 1.1.4 (1) *The quantum mechanical description of physical reality, representing states as vectors and observables as operators, is not complete, or,*
(2) *two physical observables represented by two non-commuting operators cannot have simultaneous reality.*

How does the situation described above change for a state of *two* particles that is entangled?

$|\Psi\rangle$ be an entangled state of two particles. It can be chosen exemplarily as

$$\langle q_1 q_2 | \Psi \rangle \equiv \Psi(q_1, q_2) = \int_{-\infty}^{\infty} \exp\left(\frac{i}{\hbar}(q_1 p - q_2 p + q_0 p)\right) dp \quad (1.10)$$

with q_0 being some constant. In analogy to Eqn. (1.8) it holds for the momentum and position observables of the first and second particle

$$\langle q_1 | \mathbf{P}_1 | q_1 \rangle = -i\hbar \frac{\partial}{\partial q_1}, \quad \langle q_2 | \mathbf{P}_2 | q_2 \rangle = -i\hbar \frac{\partial}{\partial q_2}, \quad \langle q_1 | \mathbf{Q}_1 | q_1 \rangle = q_1, \quad \langle q_2 | \mathbf{Q}_2 | q_2 \rangle = q_2. \quad (1.11)$$

Once the two particles are in the state $|\Psi\rangle$ they are space-like separated from each other and do not interact in any way. This ensures that whatever measurement is carried out on one particle cannot influence results obtained for measurements performed on the other one.

As a consequence of the entanglement contained in $|\Psi\rangle$ it is possible to predict the value for the momentum of the second particle by measuring the momentum of the first particle. This can be easily seen by slightly rewriting Eqn. (1.10),

$$\Psi(q_1, q_2) = \int_{-\infty}^{\infty} \underbrace{\exp\left(\frac{i}{\hbar} q_1 p\right)}_{1^{\text{st}} \text{ particle}} \underbrace{\exp\left(-\frac{i}{\hbar} (q_2 - q_0) p\right)}_{2^{\text{nd}} \text{ particle}} dp. \quad (1.12)$$

Obviously both parts of $\Psi(q_1, q_2)$ describing particle one and two are each eigenfunctions of \mathbf{P}_1 and \mathbf{P}_2 , respectively and, whenever particle one is measured to have momentum p , particle two must have momentum $-p$. Similarly, a measurement of position on particle one, enables the prediction of position for particle two. In order to understand this, Eqn. (1.10) has to be (fourier) basis transformed,

$$\Psi(q_1, q_2) = 2\pi\hbar \int_{-\infty}^{\infty} \underbrace{\delta(q_1 - q)}_{1^{\text{st}} \text{ particle}} \underbrace{\delta(q - q_2 + q_0)}_{2^{\text{nd}} \text{ particle}} dq, \quad (1.13)$$

where $\delta(\cdot)$ is the Dirac delta function. In the new basis representation both parts of $\Psi(q_1, q_2)$ are eigenfunctions of \mathbf{Q}_1 and \mathbf{Q}_2 , respectively and, finding particle one at position q implies particle two will be found at $q + q_0$. This is of course not surprising as $|\Psi\rangle$ is, by construction, eigenvector of the operators $\mathbf{P}_1 \otimes \mathbf{P}_2$ as well as of $\mathbf{Q}_1 \otimes \mathbf{Q}_2$, but it shows another characteristic

feature of entangled states: The measurement outcomes for measurements on an entangled state are correlated in more than just one basis.

In conclusion, both the momentum and the position of particle two can be predicted with certainty by a measurement of the corresponding quantity on particle one. As the particles are space-like separated, the measurement on subsystem one cannot influence subsystem two. Consequently, according to Def. 1.1.3 the position *and* momentum of particle two are objects of physical reality. As this proves Prop. 1.1.4 (2) to be wrong, EPR reason Prop. 1.1.4 (1) to be true. This reasoning is of course strongly dependent on the definition of reality and the authors were well aware of the fact that *"one would not arrive at our conclusion if one insisted that two or more physical quantities can be regarded as simultaneous elements of reality only when they can be simultaneously measured or predicted."* However, according to EPR no reasonable conception of reality could permit that the existence of properties like **P** or **Q** of one subsystem depend on measurements carried out on another system in the absence of any interaction. Abiding such a concept would require either non-local *"spooky actions at a distance"*, like Einstein said, or the abandonment of an objective reality. Indeed the latter, like Schrödinger's cat, seems even more weird when again translated to the macroscopic world. Abraham Pais, Einstein's biographer, reports: *"I recall that during one walk Einstein suddenly stopped, turned to me and asked whether I really believed that the moon exists only when I look at it."* [24] Hence, it was the credo of EPR that quantum mechanics, though logically consistent, is an incomplete manifestation of a more fundamental theory capable of explaining these phenomena in a local and objectively realistic manner [25]. As the quantum mechanical state vector does not a priori determine the result for an individual measurement, it was thought that such a predetermination could be established in a new theory by a more complete specification of the state in terms of additional parameters. These parameters were just conjectured and should hence not be accessible by measurement wherefore they are often referred to as "hidden" variables.

In the year 1964 John Bell showed that such a theory, if it may exist at all, cannot meet all of the concerns raised by EPR [26]. In particular, it cannot simultaneously be realistic, Lorentz invariant and consistent with the statistical predictions made by quantum mechanics.

Five years later John Clauser, Michael Horne, Abner Shimony and Richard Holt (CHSH) published a generalization of Bell's considerations in a form which is suitable to be experimentally tested and which shall be sketched shortly in the following [27].

A source emit pairs of particles in an entangled state. After the emission, the particles be subjected to measurements at space-like separated locations. Two dichotomic observables **A**, **A'** and **B**, **B'** with spectrum $\{\pm 1\}$ be measured each on particle one and two respectively. The allegedly complete description of the initial quantum state be given in terms of the hidden variables λ with probability distribution $\varrho(\lambda)$, fixing the measurement results for any possible measurement setting. The results A_i, A'_i for measurements on particle one and B_i, B'_i for measurements on particle two might depend on λ . However, the condition of locality, ensured by the space-like separation of the measurement apparatus, requires that both A_i and A'_i do *not* depend on B_i or B'_i , nor B_i and B'_i on A_i or A'_i . Consequently, the correlation E of the

measurement results, i.e., the weighted mean of their product is given by

$$\begin{aligned} E(\mathbf{A}, \mathbf{B}) &= \int \mathbf{A}(\lambda)\mathbf{B}(\lambda)\varrho(\lambda)d\lambda \\ E(\mathbf{A}, \mathbf{B}') &= \int \mathbf{A}(\lambda)\mathbf{B}'(\lambda)\varrho(\lambda)d\lambda \\ E(\mathbf{A}', \mathbf{B}) &= \int \mathbf{A}'(\lambda)\mathbf{B}(\lambda)\varrho(\lambda)d\lambda \\ E(\mathbf{A}', \mathbf{B}') &= \int \mathbf{A}'(\lambda)\mathbf{B}'(\lambda)\varrho(\lambda)d\lambda. \end{aligned} \quad (1.14)$$

As the possible measurement outcomes are ± 1 it holds for a single measurement run j that

$$\mathbf{A}_j\mathbf{B}_j + \mathbf{A}_j\mathbf{B}'_j + \mathbf{A}'_j\mathbf{B}_j - \mathbf{A}'_j\mathbf{B}'_j = \underbrace{\mathbf{A}_j}_{\pm 1} \underbrace{(\mathbf{B}_j + \mathbf{B}'_j)}_{\substack{+2 \\ 0 \\ -2}} + \underbrace{\mathbf{A}'_j}_{\pm 1} \underbrace{(\mathbf{B}_j - \mathbf{B}'_j)}_{\substack{0 \\ \pm 2 \\ 0}} = \pm 2 \quad (1.15)$$

and accordingly

$$-2 \leq E(\mathbf{A}, \mathbf{B}) + E(\mathbf{A}, \mathbf{B}') + E(\mathbf{A}', \mathbf{B}) - E(\mathbf{A}', \mathbf{B}') \leq +2. \quad (1.16)$$

In contrast, for particular entangled states $|\psi\rangle$ of two subsystems and appropriate choices of $\mathbf{A}, \mathbf{A}', \mathbf{B}, \mathbf{B}'$ quantum mechanics predicts

$$-2\sqrt{2} \leq \langle \mathbf{A} \otimes \mathbf{B} \rangle_\psi + \langle \mathbf{A} \otimes \mathbf{B}' \rangle_\psi + \langle \mathbf{A}' \otimes \mathbf{B} \rangle_\psi - \langle \mathbf{A}' \otimes \mathbf{B}' \rangle_\psi \leq +2\sqrt{2}. \quad (1.17)$$

The comparison of Eqn. (1.16) and Eqn. (1.17) shows that the quantum mechanical statistical prediction for measurement results cannot be reproduced in its entirety by a theory which is local (in the sense of Eqn. (1.14)) and realistic (in the sense of assigning predetermined values to each measurement) at the same time. The experimentally demonstrated violation of Eqn. (1.16) [28–30] proves that a local realistic theory is not only unable to account for the predictions made by quantum mechanics, but, that it is even not capable of describing nature. It is a fact to be accepted that the world is not local *and* realistic after the belief of EPR¹. It might be either or neither of both, a question which is still not answered to date. However, very recently it was demonstrated that a whole class of non-local realistic theories (based on a set of rather sensible restrictions) conflicts with the observations made in experiments [33]. A fact which makes the authors *"believe that our results lend strong support to the view that any future extension of quantum theory that is in agreement with experiments must abandon certain features of realistic descriptions."*

1.2 (Quantum)-information

The preceding section has established that the mathematical framework of quantum mechanics leads to a number of phenomena which might seem counterintuitive from an every day life perspective. It is surely legitimate to philosophize about the implications on the world view of such a physical description of nature. However, once taking quantum mechanics, though probably being weird, as granted (and in 100 years there was no single experiment performed

¹The ultimate, incontrovertible proof of this "fact" requires still the closure of basically two loopholes (see, e.g., [31]) in a single experiment, each of which apart has been already darned [30, 32]. However, it is the personal belief of the author that any kind of experiment to be performed in this respect will only corroborate what might be today still a conjecture.

proving it to be possibly wrong), the question about the usefulness and applicability of its non-classical effects for practical tasks arises.

Indeed, it turns out that the quantum mechanical description of physical systems opens up several new vistas when applied to information theory.

As this thesis deals with some of these applications, in the following the required basic notions of quantum information are introduced.

1.2.1 Information encoded in physical systems – (qu)bits

The term information itself has slightly different connotations in different branches of science. In every field dealing with its communication or processing, information is however understood as a structure or pattern imprinted on a physical system, i.e., as something that can be distinguished. Hence, as every distinction requires *at least* two discriminative options the simplest possible system which is capable of containing information is one with a degree of freedom that can take one out of at least two distinct values. In classical physics such a system would be one that possesses (at least) two states described by a single (at least) two-valued physical quantity. The observable corresponding to this physical quantity is called "bit" and provides the answer to a single "yes/no"-question. It is easy to imagine that the answer to every possible question can be obtained by a sequence of properly chosen "yes/no"-questions. Thus, a bit can be also seen as the unit in which information is measured. Various practical realizations of a one-bit system are conceivable as, e.g., a coin lying "head-up" or "tail-up", or, more sophisticated, an electrical circuit carrying current or not. As the notion of information is obviously tightly bound to the description of physical systems it must consequently change with the transition from classical to quantum physics.

In analogy to the classical bit, Benjamin Schumacher coined in the year 1995 the term "qubit" or "quantum bit" [4].

Definition 1.2.1 (qubit) *A qubit is a two-state quantum system, i.e., it is the minimal quantum physical system whose non-trivial observables have spectrum two.*

The state space of the qubit is a two dimensional Hilbert space \mathbb{H}_2 with a set of orthonormal basis vectors $\{|0\rangle, |1\rangle\}$. These basis vectors which are usually referred to as "computational basis" are the pendants to the two distinct states of a classical one-bit system associated with the logical values "0" and "1" or "yes" and "no". However, in contrast to the classical bit, a quantum bit is not a two-valued quantity, but a quantum system described by a state vector (see Def. 1.2.1). This implies that due to the superposition principle (cp. Sec. 1.1.2) the most general state of a qubit is given by any superposition of the two basis vectors, i.e., as

$$|\varpi\rangle_{\theta,\varphi} = \exp(i\gamma) \left(\cos\left(\frac{\theta}{2}\right) |0\rangle + \exp(i\varphi) \sin\left(\frac{\theta}{2}\right) |1\rangle \right) \quad (1.18)$$

with $\theta \in [0, \pi[$ and $\varphi, \gamma \in [0, 2\pi[$. As the global phase γ is not a physical observable it is irrelevant and can be omitted. Thus qubit states can be seen as elements of the complex projective line² which is isomorphic to a three dimensional sphere. This leads to a nice visualization of qubits as points (θ, φ) on the surface of a sphere of radius one, the Bloch sphere (see Fig. 1.2), with coordinate vector $\vec{r} = (\cos(\varphi) \sin(\theta), \sin(\varphi) \sin(\theta), \cos(\theta))$. In contrast to classical bits the information needed to *describe* a qubit is in general infinite as it requires two

² $\{(a, b) \in \mathbb{C}^2 \mid a, b \in \mathbb{C}, a \vee b \neq 0, (a, b) = (ca, cb) \forall c \in \mathbb{C} \setminus \{0\}\}$

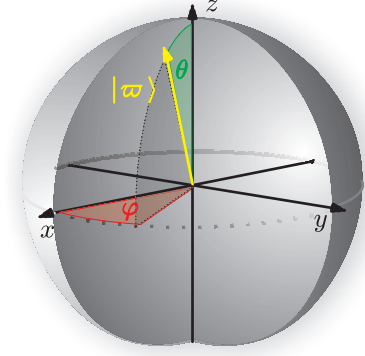


Figure 1.2: Visualization of qubit states. A pure qubit state $|\varpi\rangle_{\theta,\varphi} = \cos(\frac{\theta}{2})|0\rangle + \exp(i\varphi)\sin(\frac{\theta}{2})|1\rangle$ can be represented as a point (θ, φ) on the surface of a three dimensional sphere, the Bloch sphere. The point is characterized by the coordinate vector $\vec{r} = (\cos(\varphi)\sin(\theta), \sin(\varphi)\sin(\theta), \cos(\theta))$ with $\theta \in [0, \pi]$ and $\varphi \in [0, 2\pi]$. The pole points $(\frac{\pi}{2}, 0), (\frac{\pi}{2}, \pi)$ correspond to the eigenstates of σ_x , $(\frac{\pi}{2}, \frac{\pi}{2}), (\frac{\pi}{2}, \frac{3\pi}{2})$ to the one of σ_y and $(0, 0), (0, \pi)$ to the one of σ_z .

real numbers (θ, φ) . The information which can be *read out* of or *transmitted* by one qubit corresponds, however, to only one classical bit [34], as all of its observables are by Def. 1.2.1 dichotomic.

For the representation of operators acting on \mathbb{H}_2 it is convenient to choose the Pauli spin operators $\{\sigma_x, \sigma_y, \sigma_z\}$ together with the identity $\mathbb{1}$ as they form a orthogonal basis in the corresponding operator space. Throughout this work the following definition is used

$$\begin{aligned} \sigma_x|+\rangle &= +1|+\rangle \equiv +\frac{1}{\sqrt{2}}(|0\rangle + |1\rangle), & \sigma_x|-\rangle &= -1|-\rangle \equiv -\frac{1}{\sqrt{2}}(|0\rangle - |1\rangle) \\ \sigma_y|R\rangle &= +1|R\rangle \equiv +\frac{1}{\sqrt{2}}(|0\rangle + i|1\rangle), & \sigma_y|L\rangle &= -1|L\rangle \equiv -\frac{1}{\sqrt{2}}(|0\rangle - i|1\rangle) \\ \sigma_z|0\rangle &= +1|0\rangle, & \sigma_z|1\rangle &= -1|1\rangle, \end{aligned} \quad (1.19)$$

$$\mathbb{1}|\varpi\rangle = +1|\varpi\rangle, \quad \forall |\varpi\rangle \in \mathbb{H}_2 \quad (1.20)$$

and

$$\sigma_x^2 = \sigma_y^2 = \sigma_z^2 = \mathbb{1}, \quad \det(\sigma_i) = -1, \quad \text{tr}(\sigma_i) = 0, \quad \sigma_i\sigma_j = \delta_{ij}\mathbb{1} + i\varepsilon_{ijk}\sigma_k, \quad (1.21)$$

with

$$\delta_{ij} = \begin{cases} 1, & \text{for } i = j \\ 0, & \text{for } i \neq j \end{cases}, \quad \varepsilon_{ijk} = \begin{cases} +1, & \text{for even permutations of } \{ijk\} \\ -1, & \text{for odd permutations of } \{ijk\} \\ 0, & \text{otherwise.} \end{cases}, \quad i, j, k \in \{x, y, z\}. \quad (1.22)$$

As can be seen from Eqn. (1.19) the eigenvectors of the Pauli operators form the pole points of the Bloch sphere (Fig. 1.2). In order to use matrix algebra it is common practice to represent the computational basis vectors as

$$|0\rangle = \begin{pmatrix} 1 \\ 0 \end{pmatrix}, \quad |1\rangle = \begin{pmatrix} 0 \\ 1 \end{pmatrix} \quad (1.23)$$

such that the operators read

$$\mathbb{1} = \begin{pmatrix} 1 & 0 \\ 0 & 1 \end{pmatrix}, \quad \sigma_x = \begin{pmatrix} 0 & 1 \\ 1 & 0 \end{pmatrix}, \quad \sigma_y = \begin{pmatrix} 0 & -i \\ i & 0 \end{pmatrix}, \quad \sigma_z = \begin{pmatrix} 1 & 0 \\ 0 & -1 \end{pmatrix}. \quad (1.24)$$

An arbitrary, general observable $\sigma_{\theta,\varphi}$ of a qubit can be written in terms of the Pauli operators as

$$\sigma_{\theta,\varphi} = \vec{r} \cdot \vec{\sigma} = \cos(\varphi) \sin(\theta) \sigma_x + \sin(\varphi) \sin(\theta) \sigma_y + \cos(\theta) \sigma_z \quad \text{with } \vec{\sigma} = \begin{pmatrix} \sigma_x \\ \sigma_y \\ \sigma_z \end{pmatrix}. \quad (1.25)$$

From Eqn. (1.21) can be derived that the eigenvalues of the Pauli operators, and consequently for all $\sigma_{\theta,\varphi}$ are ± 1 in agreement with Def. 1.2.1. The projector $\mathbb{P}_{\theta,\varphi}^{\pm}$ on the eigenvector of $\sigma_{\theta,\varphi}$ with positive or negative eigenvalue, respectively, is expressed as

$$\mathbb{P}_{\theta,\varphi}^{\pm} = \frac{\mathbb{1} \pm \sigma_{\theta,\varphi}}{2}. \quad (1.26)$$

In Sec. 1.1.1 it was stated that the dynamics of quantum states equals their rigid rotation in state space. For qubits the time evolution is therefore usually given by unitary operations which are elements of the special unitary group $SU(2)$. As the Pauli operators are (up to a constant factor) the generators of $SU(2)$, they can be also used to write an arbitrary general unitary single qubit operation $\mathbf{U} \in U(2) = U(1) \times SU(2)$ as [35]

$$\mathbf{U}(\alpha, \gamma, \theta, \varphi) = \underbrace{\exp(i\alpha)}_{\text{phase}} \underbrace{\exp\left(-i\frac{\gamma}{2}\vec{r} \cdot \vec{\sigma}\right)}_{\text{rotation}} = \exp(i\alpha) \left(\cos\left(\frac{\gamma}{2}\right) \mathbb{1} - i \sin\left(\frac{\gamma}{2}\right) \sigma_{\theta,\varphi} \right). \quad (1.27)$$

In terms of the Bloch sphere representation this form suggests the interpretation of a qubit evolution as a rotation by the angle γ about the axis \vec{r} followed by the application of a phase α . In the language of information theory transformations of the form Eqn. (1.27) represent gates, acting on qubits and processing information. One important example is the so called Hadamard gate $\text{HAD} = \mathbf{U}\left(\frac{\pi}{2}, \pi, 0, \frac{\pi}{2}\right) = \frac{1}{\sqrt{2}}(\sigma_x + \sigma_z)$ which transforms between the eigenstates of σ_x and σ_z ;

$$\text{HAD} = \begin{cases} |0\rangle \rightarrow \frac{1}{\sqrt{2}}(|0\rangle + |1\rangle) \\ |1\rangle \rightarrow \frac{1}{\sqrt{2}}(|0\rangle - |1\rangle) \end{cases}, \quad \frac{1}{\sqrt{2}} \begin{pmatrix} 1 & 1 \\ 1 & -1 \end{pmatrix}. \quad (1.28)$$

This gate is often used in quantum information algorithms to generate equally weighted superpositions of the computational basis states. A prominent example thereof is the Deutsch algorithm [36] (and its extension [37]) which constitutes the first proof that the superposition principle enables a speedup in quantum computation compared to any classical information processing.

1.2.2 Entanglement of qubits

As seen in the previous section, the main difference between classical and quantum bits is the fact that qubits are in general not in one of the two computational basis states but in an arbitrary superposition thereof. This implies that qubits, also in contrast to classical bits, can be entangled. In Sec. 1.1.2 it was adumbrated that the definition of "entangled" as being "non-product" might require detailed refinement in terms of the number of subsystems under consideration. This shall now be supplemented in the following in particular with respect to qubits as individual subsystems.

Two-qubit entanglement

The state space of two qubits is the four-dimensional Hilbert space $\mathbb{H}_2 \otimes \mathbb{H}_2$. A natural extension of the one-qubit case might be to choose a set of four basis vectors as $\{|00\rangle, |01\rangle, |10\rangle, |11\rangle\}$ in analogy to the logical states of two classical bits "00", "01", "10", "11". However, the general state of two qubits does not need to be a product state of the two subsystems (see Sec. 1.1.2), and just as well four orthonormal entangled states can form a set of basis vectors. One simple, but important example are the four Bell states, named after John Bell and featuring in his inequality [38]:

$$\begin{aligned} |\phi^\pm\rangle &= \frac{1}{\sqrt{2}} (|00\rangle \pm |11\rangle) \\ |\psi^\pm\rangle &= \frac{1}{\sqrt{2}} (|01\rangle \pm |10\rangle). \end{aligned} \quad (1.29)$$

From an information theoretic point of view, the entanglement of qubits has interesting implications on the encoding of information in quantum physical systems. In accordance with the one-qubit case of the previous section the information, necessary to characterize the state of the two qubits is infinite, but the information which can be transmitted and read by two qubits is limited and restricted to two classical bits. In classical systems the two bits of information are carried each by the individual subsystem. This can be described by two propositions, like for example, "(1) the logical state of the first subsystem is 0" and "(2) the logical state of the second subsystem is also 0", corresponding to the state "00" for the total system. In contrast, in the quantum case there are two, fundamentally different possibilities to distribute the two bits of readable information. The first is analogous to the classical one and corresponds to product states. Thereby each of the two bits of readable information is also carried by one of the two qubits. For instance, the state $|00\rangle$ corresponds to the propositions "(1) the logical state of the first qubit is 0 in the computational basis" and "(2) the logical state of the second qubit is also 0 in the computational basis". The second encoding possibility corresponds to entangled states and is not possible for classical bits. In entangled states of the form Eqn. (1.29) the two bits of readable information are uniformly spread out on both qubits. This means the system as a whole carries all the information while no information is contained in the individual subsystem. Thus, the information is not encoded in the state of the individual subsystem but in the relations or correlations which the subsystems possess with respect to each other. This could be formulated for example in two propositions of the form "(1) the logical state of both qubits is the same for a measurement $\sigma_z \otimes \sigma_z$ " and "(2) the logical state of both qubits is the same for a measurement $\sigma_x \otimes \sigma_x$ ", what corresponds to the state³ $|\phi^+\rangle$ [39].

These statements can be easily quantified by introducing various concepts. The first was the von Neumann entropy as a measure of information contained in quantum systems. It can be regarded as the extension of classical entropy concepts to the field of quantum mechanics.

Definition 1.2.2 (von Neumann entropy) *The von Neumann entropy S_{vN} for a quantum*

³A third proposition like "(3) the logical state of both qubits is opposite for a measurement $\sigma_y \otimes \sigma_y$ " is redundant as there is only one unique common eigenvector of $\sigma_x \otimes \sigma_x$ and $\sigma_z \otimes \sigma_z$ with positive eigenvalue for both operators. Thus (3) follows from (1) and (2).

state described by the density operator ρ is given as

$$S_{\text{vN}}(\rho) \equiv -\text{tr}(\rho \log_N \rho) = -\sum_i \lambda_i \log_N \lambda_i,$$

where N is the dimension of the Hilbert space and λ_i are the eigenvalues of ρ .

For practical issues it is sometimes convenient to consider alternatively the so-called linear entropy as its calculation does not require diagonalization of the density operator.

Definition 1.2.3 (Linear entropy and purity) *The linear entropy S_{lin} for a quantum state described by the density operator ρ is given as*

$$S_{\text{lin}}(\rho) \equiv \frac{N}{N-1} (1 - P(\rho)),$$

where N is the dimension of the Hilbert space and $P(\rho) \equiv \text{tr}(\rho^2)$ the purity of ρ .

As can be easily verified, for any Bell state $|\text{bs}\rangle \in \{|\phi^\pm\rangle, |\psi^\pm\rangle\}$ the entropy of the total system $\rho_{\text{bs}} = |\text{bs}\rangle\langle\text{bs}|$ is minimal and hence the information maximal,

$$S_{\text{vN}}(\rho_{\text{bs}}) = S_{\text{lin}}(\rho_{\text{bs}}) = 0.$$

In turn, the entropy of each of the two subsystems, given after tracing the other subsystem $\rho_1 = \text{tr}_2(\rho_{\text{bs}})$ and $\rho_2 = \text{tr}_1(\rho_{\text{bs}})$, is maximal, what corresponds to no information content

$$S_{\text{vN}}(\rho_1) = S_{\text{vN}}(\rho_2) = S_{\text{lin}}(\rho_1) = S_{\text{lin}}(\rho_2) = 1.$$

The two propositions about the above example of the product state $|00\rangle$ could be equally well stated as "(1) the logical state of the first qubit in the computational basis is 0" and "(2) the logical state of both qubits is the same for a measurement $\sigma_z \otimes \sigma_z$ ". This means that the amount of information used to describe the correlations of two-qubit *product* states equals one, whereas it is in contrast greater than one for *entangled* states⁴. Indeed the latter can be shown to be a necessary and sufficient condition for two-qubit states to violate a Bell inequality of the form of Eqn. (1.16) [40], and it is even suggested to be a possible definition of two-qubit entanglement [41]. Yet, the commonly accepted definition is Def. 1.1.1 which is unambiguous in the case of two qubits.

In view of practical applications it might be desirable to have a criterion, or even a measure, at hand to decide whether or how strongly a particular state under consideration is entangled. A criterion which will also be used in this thesis, was provided by Asher Peres in the year 1996 [42]. It is called positive partial transpose (PPT) and requires the following definition.

Definition 1.2.4 (Partial transpose) *The quantum state of a bipartite system be given in terms of the density matrix ρ . The matrix elements of ρ in a particular basis be $\langle m\mu|\rho|n\nu\rangle$, with $|m\rangle, |n\rangle$ and $|\mu\rangle, |\nu\rangle$ as basis vectors of the first and second subsystem respectively:*

The new matrix ρ^{T_2} with matrix elements

$$\langle m\mu|\rho^{T_2}|n\nu\rangle \equiv \langle m\nu|\rho|n\mu\rangle$$

is called the partial transpose of ρ (with respect to the second subsystem). (Analogous definition holds for ρ^{T_1}).

⁴A similar statement appeared already in the discussion about the violation of local realism in Sec. 1.1.2 in the form that the outcomes for measurements on entangled states are correlated in more than one basis.

Peres' criterion states that

Proposition 1.2.5 (Positive partial transpose) ρ separable $\Rightarrow \rho^{T_2} = \sum_i p_i \rho_{i_1} \otimes \rho_{i_2}^T$ and $\rho^{T_2} \geq 0$.

This means that whenever the partial transpose of a density matrix is found to have negative eigenvalues, the state is entangled. The reverse is in general not true, besides for the special case of two qubits (or one qubit and one qutrit⁵) [43]. The transformation defined by Def. 1.2.4 can be seen as a time reversal on one subsystem [44]. Thus, Prop. 1.2.5 has a physical interpretation in the sense that separable states do not correlate local time flows. If the time reversal on just one subsystem leads to a non-physical state of the total system, the time flows must have been correlated and the state entangled.

In order to go beyond a pure detection of the entanglement contained in a state in terms of its quantification, some criteria have to be introduced. Several conditions for entanglement measures exist [45, 46] but the following three ones are indispensable and define so-called entanglement monotones [47]:

Definition 1.2.6 (Entanglement monotone) $\rho \in \mathbb{H}$ be a density operator of two or more subsystems. The map $M : \mathbb{H} \rightarrow \mathbb{R}^+$ is called entanglement monotone if it satisfies the conditions:

1. $M(\rho) \geq 0 \forall \rho \in \mathbb{H}$ and $M(\rho) = 0$ if ρ is separable.
2. $M(\Lambda_{\text{LOCC}}\rho) \leq M(\rho)$
3. $\sum_i a_i M(\rho_i) \geq M(\sum_i a_i \rho_i)$, with $\rho_i \in \mathbb{H}$, $a_i \in \mathbb{R}$ and $\sum_i |a_i| = 1$.

The first condition is a quite obvious one. If an entanglement measure would not be zero for separable states, which do by definition not contain any entanglement, it would be no sensible quantification of entanglement. It might be just surprising that it is not demanded that the measure is zero if and *only* if the state is separable. This is, however, for good reason as there are states which contain a form of entanglement that is not useful for quantum information applications⁶ [48, 49]. These states, though being entangled, can have $M = 0$. (Again this suggests that there are different types of entanglement, but this is only relevant for more than two qubits and will be matter of the subsequent section.)

The second condition states that entanglement cannot be increased with local operations and classical communication (LOCC). This means, whatever is done to each subsystem locally (*local operations*) cannot, even conditioned on the prior or subsequent exchange of classical information (*classical communication*), enhance the amount of entanglement in a system [50, 51]. This seems reasonable with regard to the discussions in Sec. 1.1.2 and particularly in view of applications in quantum communication tasks where a couple of remote parties share parts of an entangled state and interact with each other solely by a classical transmission channel (see Sec. 3.1).

The third condition implies that discarding information should not lead to an increase of entanglement.

⁵Analogously to Def. 1.2.1, a qutrit is a three-state quantum system, i.e., it is the minimal quantum physical system whose non-trivial observables have spectrum three.

⁶These states are called "bound"-entangled and are also the ones which do not have a negative partial transpose. They will not be discussed any further as they have no relevance for the work presented in this thesis.

For pure states the von Neumann entropy of the reduced system, i.e., after tracing one subsystem, is already an entanglement measure [52]. For mixed states it is, however, not suitable, as it is not clear whether the lack of information in the subsystem results from entanglement or from lack of purity in the total system. Still, it can be generalized in a way that it applies also to mixed states. The resulting measure is called *entanglement of formation* [51]. An arbitrary state $\rho = \sum_i a_i |\varphi_i\rangle\langle\varphi_i|$ can be decomposed as a convex sum of projectors on pure states $|\varphi_i\rangle$. The entanglement of formation \mathcal{E}_{of} is then given as the averaged von Neumann entropy of the pure states' reduced density matrices, minimized over all possible decompositions of ρ ,

$$\mathcal{E}_{\text{of}}(\rho) \equiv \inf_{\{\text{dec}\}} \sum_i a_i S_{\text{vN}}(\text{tr}_1(|\varphi_i\rangle\langle\varphi_i|)). \quad (1.30)$$

In the defining form of Eqn. (1.30) the measure is not very practicable as the involved optimization is not easy to handle analytically. Fortunately the evaluation of \mathcal{E}_{of} can be reduced to the determination of a quantity which is for itself an entanglement measure and is called *concurrence* [53, 54]. It will be of particular interest in Sec. 3.2.

Definition 1.2.7 (Concurrence) *The map $\mathcal{C} : \mathbb{H} \rightarrow [0, 1]$ of a two-qubit state $\rho \in \mathbb{H}$ is called concurrence, with*

$$\mathcal{C}(\rho) \equiv \max\left(0, \sqrt{\lambda_1} - \sqrt{\lambda_2} - \sqrt{\lambda_3} - \sqrt{\lambda_4}\right)$$

where $\lambda_1, \dots, \lambda_4$ are the eigenvalues of the non-Hermitian operator $\rho(\sigma_y \otimes \sigma_y)\rho^*(\sigma_y \otimes \sigma_y)$ in decreasing order and ρ^* the complex conjugate of ρ .

The entanglement of formation is then given as

$$\mathcal{E}_{\text{of}}(\mathcal{C}) = \mathfrak{h}\left(\frac{1 + \sqrt{1 - \mathcal{C}^2}}{2}\right), \quad (1.31)$$

with $\mathfrak{h}(x) = -x \log_2 x - (1 - x) \log_2(1 - x)$. The operation involved in Def. 1.2.7 of applying σ_y on the complex conjugate maps every qubit on its antipode on the Bloch sphere. Thus, it shall be termed *universal not* (UNOT). For a physical realization of qubits in terms of spin one-half particles this corresponds again to a time reversal. Consequently, the concurrence can be seen as the overlap of a state with its (universal) bit-flipped counterpart. It is worth to note that the universal not when applied on both qubits, though changing the state of each individual subsystem does *not* change the correlations which the subsystems possess with respect to each other (see Fig. 1.3(b)) [55]. As the information contained in a maximally entangled state is encoded solely in these correlations, but not in the state of the individual subsystems (see page 16 et seqq.), it does not change under such a transformation leading to a maximal value for the concurrence. In contrast, for a separable state the information is exclusively encoded in the states of the individual subsystems. Thus the application of UNOT results in the orthogonal state and zero value of concurrence.

In the formulation of the PPT criterion the UNOT (up to a local unitary⁷) is applied to just one of the subsystems. For the case of two qubits, this leads to an inversion of the state of one qubit *and* in addition to an inversion of the correlations between the subsystems (see Fig. 1.3(a)). Hence, it is plausible that the change in the correlations might affect an

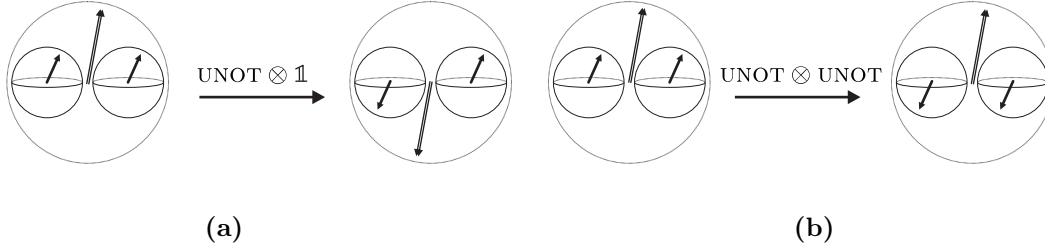


Figure 1.3: Reflection symmetries of two qubits involved in the determination of entanglement. Small arrows represent Bloch vectors of qubits, double arrows correlations between qubits. (a) Transformation $\text{UNOT} \otimes \mathbb{1}$ involved in the PPT criterion. Inversion of the state of one subsystem changes the correlations between the subsystems. The transformation can be interpreted as local time reversal on one of the subsystems. As separable states do not correlate local time flows they are unaffected by this operation. (b) Transformation $\text{UNOT} \otimes \text{UNOT}$ involved in the determination of the concurrence. Inversion of the states of both subsystems leaves the correlations between them unchanged. As for entangled states the information is encoded solely in the correlations but not in the individual subsystems, the total state stays the same. For separable states it is the direct opposite.

entangled state while being irrelevant for product states. This is also in accordance with the statement that the local time flows are not correlated for separable states.

Another entanglement measure which can be equally well applied to pure and mixed states is deduced from Prop. 1.2.5 and called logarithmic negativity [56].

Definition 1.2.8 (Logarithmic negativity) *The map $\mathcal{N} : \mathbb{H} \rightarrow [0, 1]$ of a state $\rho \in \mathbb{H}$ of a bipartite system is called logarithmic negativity, with*

$$\mathcal{N}(\rho) \equiv \log_2(2 \mathfrak{n}(\rho) + 1) \quad \text{and} \quad \mathfrak{n}(\rho) \equiv \sum_i \frac{|\lambda_i^T| - \lambda_i^T}{2},$$

where λ_i^T are the eigenvalues of the partial transpose of ρ .

As already denoted by the name, it expresses the degree to which the partial transpose of a state fails to be positive. It will be used for the characterization of experimental states in Sec. 3.1.4. Although \mathcal{N} is not convex, it was recently proven to be non-increasing under PPT preserving operations, of which LOCC operations are a subset. Therefore it is a good entanglement measure [57].

Summarized in a nutshell, for two qubits, the term being entangled is well defined and several tools for the detection and quantification of entanglement are available. As shall be seen in the following an understanding of this kind of multi-qubit entanglement is the less tangible the more qubits are involved.

Three-qubit entanglement

When defining "entangled" as being non-product it might be, to a particular extent, unclear what this means for systems composed out of three qubits A, B, C . For such systems different partitions with respect to factorizing are conceivable: $ABC, A - BC, AB - C, AC - B,$

⁷For density operators the transposition equals the complex conjugation.

$A - B - C$, where the dash denotes which subsystem is considered as separable from the others. The first or the last partition are surely entangled or separable, respectively. The remaining ones are, however, in a way both. Therefore, when dealing with multi-partite systems it is reasonable to distinguish between full separability [58] and partial separability [23]:

Definition 1.2.9 (Full separability) ρ be a density operator describing n systems $\mathcal{S}_1, \dots, \mathcal{S}_n$ with Hilbert space $\mathbb{H} = \mathbb{H}_{\mathcal{S}_1} \otimes \dots \otimes \mathbb{H}_{\mathcal{S}_n}$. ρ is called fully separable iff

$$\rho = \sum_{i=1}^k a_i \rho_{i_1} \otimes \dots \otimes \rho_{i_n},$$

with $\rho_{i_l} \in \mathbb{H}_{\mathcal{S}_l}$ and $k \leq \dim(\mathbb{H})^2$. (The number of states in the convex combination is thereby limited by Caratheodory's bound k [45, 49, 59].)

Definition 1.2.10 (Partial separability) ρ be a density operator describing n systems $\mathcal{S}_1, \dots, \mathcal{S}_n$ with Hilbert space $\mathbb{H} = \mathbb{H}_{\mathcal{S}_1} \otimes \dots \otimes \mathbb{H}_{\mathcal{S}_n}$. ρ is called separable with respect to a given partition $\{I_1, \dots, I_m\}$, where I_i are disjoint subsets of the set of indices $I = \{1, \dots, n\}$, $\bigcup_{l=1}^m I_l = I$, iff

$$\rho = \sum_i a_i \rho_{i_1} \otimes \dots \otimes \rho_{i_m},$$

where ρ_{i_l} be defined on $\bigotimes_j \mathbb{H}_{\mathcal{S}_j}$ and j runs over all elements of I_l . (It is also said, ρ is m -separable with respect to partition $\{I_1, \dots, I_m\}$).

A state of n systems which is neither fully nor partially separable is called genuine n -partite entangled. Consequently, for three qubits a coarse, minimal distinction of states would be according to three-partite entangled, bi-separable and separable. This does, however, not sufficiently cope with the given situation.

A partial ordering of states as more or less entangled, deduced from Def. 1.2.6 by stating that, (i) two states are equally entangled if they are related by local unitary (LU) operations [47, 60] and (ii) the entanglement of a state cannot increase under LOCC, has several distinct maxima. Thus, obviously different kinds of three-partite entanglement exist. In fact, to label all the equivalence classes introduced by this partial order needs even a continuous parameter, i.e., infinitely many kinds of entanglement are distinguished [61]. Fortunately the situation can be simplified by alternatively stipulating that two states are equivalent if they are related by stochastic local operations and classical communication (SLOCC) [18]. In such an ordering, the conversion between states is still achieved through LOCC, but not with certainty, rather with a non-vanishing probability of success. As a result two distinguished kinds of tri-partite entanglement remain, the Greenberger, Horne, Zeilinger (GHZ)- and W-class, which are named after their two representatives states [62]:

$$|\text{GHZ}\rangle = \frac{1}{\sqrt{2}} (|000\rangle + |111\rangle) \quad (1.32)$$

$$|\text{W}\rangle = \frac{1}{\sqrt{3}} (|001\rangle + |010\rangle + |100\rangle). \quad (1.33)$$

Each pure state of three qubits, as long as it is not (partially/fully) separable, can be transformed either in the one or the other form, depending to which class it belongs. The

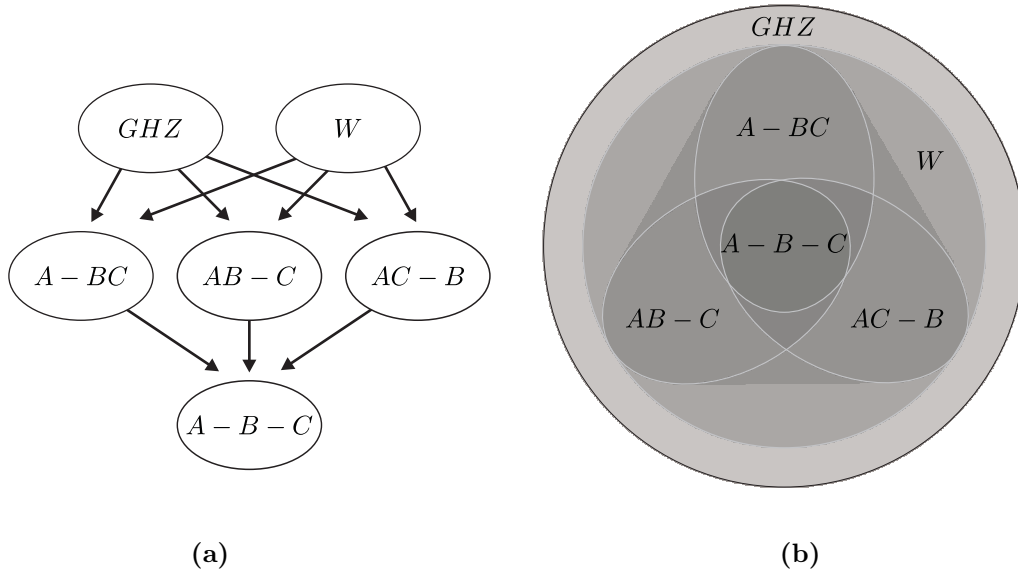


Figure 1.4: Different equivalence classes of three-qubit states with respect to **SLOCC**. (a) Equivalence under **SLOCC** induces a partial order on the space of three qubit pure states. In contrast to the two-qubit case just a distinction between fully separable or entangled is not adequate. Even a classification according to separable ($A - B - C$), bi-separable ($A - BC$, $AB - C$, $AC - B$) and entangled (ABC) is not sufficient as there are two distinct types of three qubit entanglement (GHZ , W). (b) Schematic representation of the sets of mixed three-qubit states. The sets are nested according to their degree of entanglement, starting from the set of separable states ($A - B - C$) and ending at the two different sets of tri-partite entangled states W and GHZ . Mixed states of a particular set are given in terms of a convex combination of pure states of the respective set, including all embedded subsets.

partial order induced by **SLOCC** is displayed as a whole in Fig. 1.4(a). In contrast, for two qubits the classification according to **SLOCC** coincides with the distinction between separable and entangled and the only form of two-qubit entanglement is the one represented by one of the four Bell states (Eqn. (1.29)) [50]. Although w- and **GHZ**-states cannot be transformed into each other by means of **SLOCC**, the set of pure w-states has measure zero among the set of all pure three-qubit states, and each w-state can be infinitely well approximated by a **GHZ**-state. This is, however, different for mixed states in a generalization of the **SLOCC** classification [63]. In such a generalization the set of separable states $\{A - B - C\}$ contains all states that can be decomposed as a convex combination of pure separable states. All states that can be expressed as a convex combination of separable or any kind of bi-separable states form the set of bi-separable mixed states $\{A - BC, AB - C, AC - B\}$. Convex combinations of states from $\{A - B - C\}$, $\{A - BC, AB - C, AC - B\}$, and pure w-states constitute the set of mixed w-states W , and GHZ is the set of all physical three-qubit states (see Fig. 1.4(b)). All sets are convex and compact and the set $W \setminus \{A - BC, AB - C, AC - B\}$ is not of measure zero anymore.

Given a three-qubit state it might be desirable to decide to which of the **SLOCC** classes it belongs. For pure states $\rho_{ABC} = |\chi\rangle\langle\chi|$ this can be achieved by the determination of a quantity which is deduced from the concurrence and called *tangle* [64]. The tangle τ analyzes

in which way the entanglement is distributed among the subsystems A , B and C ,

$$\tau(\rho_{ABC}) \equiv \mathcal{C}_{A-BC}^2(\rho_{ABC}) - \mathcal{C}^2(\text{tr}_C(\rho_{ABC})) - \mathcal{C}^2(\text{tr}_B(\rho_{ABC})). \quad (1.34)$$

Thereby $\mathcal{C}_{A-BC}(\rho_{ABC}) = 2\sqrt{\det(\text{tr}_{BC}(\rho_{ABC}))}$ specifies the entanglement (measured by the concurrence) between subsystem A and the joint subsystem BC which is treated as a single object. The remaining terms in Eqn. (1.34) denote the entanglement between the pairs of qubits, $A - B$ and $A - C$. Thus, the value of the tangle, which does not depend on the chosen partition, measures the degree to which entanglement is contained solely in individual pairs of qubits. Vanishing tangle at non-zero concurrence between all pairs of qubits indicates W-class states, whereas states with non-zero tangle belong to the GHZ-class. This illustrates nicely that these two classes exhibit indeed two different kinds of three-partite entanglement and what the difference exactly is. In a W-state, Eqn. (1.33), the three-qubit entanglement is established by entanglement between all pairs ($\tau = 0$), whereas in a GHZ-state, Eqn. (1.32), the entanglement is totally "smeared" among all constituents ($\tau = 1$). An important consequence of this fact in practice is that a GHZ-state becomes completely disentangled if one qubit is lost. In contrast W-states retain still bi-partite entanglement after tracing over one of the qubits.

A generalization of the tangle to mixed states is not straight forward and will not be pursued any further in this thesis (one attempt in this direction might be found in [65, 66]). Instead, another very useful tool for the characterization of qubit entanglement shall shortly be recapitulated in the following, as it will be of importance for the evaluation of experimental data: *entanglement witnesses* [43, 67].

The concept of entanglement witnesses is based on the previously mentioned topological structure of the set of mixed states and its partition in subsets with respect to the SLOCC equivalence of its elements. It is known from the Hahn-Banach theorem that, laxly stated, for a set which is convex and compact, and a point which is not an element of the set, there exists a hyperplane separating the point from the set. Such a hyperplane in the state space of three qubits can be defined, in complete analogy to three-dimensional Euclidian space, as the set of all points ρ for which $\text{tr}(\mathbf{W}\rho) = 0$, where \mathbf{W} is a Hermitian operator⁸. Accordingly, points to the left or the right of the hyperplane have positive or negative expectation value for \mathbf{W} , respectively. If the hyperplane defined by the operator \mathbf{W} lies between an entangled state ρ_{ent} and the set of separable states, the operator \mathbf{W} witnesses the entanglement of ρ_{ent} :

Definition 1.2.11 (Entanglement witness) *A Hermitian operator \mathbf{W} is called entanglement witness for the state ρ_{ent} iff*

$$\text{tr}(\mathbf{W}\rho_{\text{ent}}) < 0 \quad \text{and} \quad \text{tr}(\mathbf{W}\rho) \geq 0 \quad \text{for all separable } \rho.$$

Proposition 1.2.12 *A state ρ is entangled iff there exists an entanglement witness for ρ .*

In case that the expectation value of a witness operator, measured in an experiment, is negative, the state under investigation is entangled. Unfortunately the reverse is not true, that means that a witness provides only a sufficient but not necessary condition to test for entanglement. If a state is not detected to be entangled it might be that it *is* indeed not

⁸In this analogy \mathbf{W} corresponds to the normal vector of a plane in Euclidean space and $\text{tr}(\cdot)$ resembles the usual scalar product in \mathbb{R}^3 .

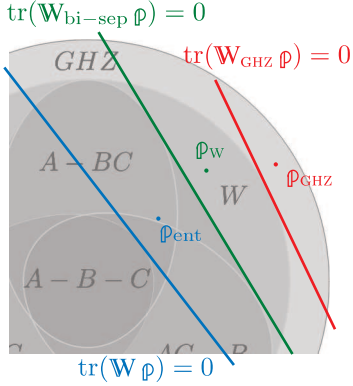


Figure 1.5: Entanglement witnesses. An entanglement witness \mathbf{W} defines a hyperplane, $\text{tr}(\mathbf{W}\rho) = 0$, in the convex set of mixed qubit states. All states lying right or left of the plane have positive or negative expectation value for the operator \mathbf{W} , respectively. Thus, depending on the location of the hyperplane, a negative expectation value of the operator indicates that a state is entangled ($\text{tr}(\mathbf{W}\rho_{\text{ent}}) < 0$), tri-partite entangled ($\text{tr}(\mathbf{W}_{\text{bi-sep}}\rho_{\text{W}}) < 0$) or GHZ-type entangled ($\text{tr}(\mathbf{W}_{\text{GHZ}}\rho_{\text{GHZ}}) < 0$).

entangled, or that the witness was not properly chosen. Choosing a witness optimally is in practice a non-trivial task as it requires a kind of a priori knowledge about the state for which the operator should be constructed. Intuitively it is obvious to require the hyperplane, defined by the witness operator, to be tangential to the set from which a particular state should be separated in order to detect as many states as possible [68, 69].

The structure of state space suggests furthermore that witnesses cannot only be used to distinguish separable from entangled, but also tri-partite entangled from bi-separable and GHZ- from W-class states. To this end the conditions in Def. 1.2.11 have to be accordingly modified:

$$\text{tr}(\mathbf{W}_{\text{bi-sep}}\rho_{\text{W}}) < 0 \quad \text{and} \quad \text{tr}(\mathbf{W}_{\text{bi-sep}}\rho) \geq 0 \quad \forall \rho \in \{A-BC, AB-C, AC-B\} \quad (1.35)$$

would detect a state ρ_{W} as being not bi-separable and

$$\text{tr}(\mathbf{W}_{\text{GHZ}}\rho_{\text{GHZ}}) < 0 \quad \text{and} \quad \text{tr}(\mathbf{W}_{\text{GHZ}}\rho) \geq 0 \quad \forall \rho \in W \quad (1.36)$$

witnesses GHZ-type entanglement for a state $\rho_{\text{GHZ}} \in \text{GHZ}$, see Fig. 1.5. One particular explicit form of these two witnesses would be [63]:

$$\mathbf{W}_{\text{bi-sep}} = \frac{1}{2} \mathbb{1}^{\otimes 3} - |\text{GHZ}\rangle\langle\text{GHZ}| \quad \text{or} \quad \mathbf{W}_{\text{bi-sep}} = \frac{2}{3} \mathbb{1}^{\otimes 3} - |\text{W}\rangle\langle\text{W}| \quad (1.37)$$

and

$$\mathbf{W}_{\text{GHZ}} = \frac{3}{4} \mathbb{1}^{\otimes 3} - |\text{GHZ}\rangle\langle\text{GHZ}|. \quad (1.38)$$

In general, a possible way to construct a witness operator that detects entanglement in the vicinity of a pure state $|\psi\rangle$ of d qubits is always

$$\mathbf{W} = \alpha \mathbb{1}^{\otimes d} - |\psi\rangle\langle\psi|, \quad \text{with} \quad \alpha = \max_{|\phi\rangle \in D} |\langle\phi|\psi\rangle|^2, \quad (1.39)$$

where $|\phi\rangle$ are states of the set D against which should be separated (see e.g. [70]).

There is an interesting connection between entanglement witnesses and the PPT-criterion (Prop. 1.2.5) which is worth to be noted. Prop. 1.2.5 is a special case that can be deduced from a more general theorem which was proven in [43] and reads:

Proposition 1.2.13 ρ be a density operator acting on $\mathbb{H}_a \otimes \mathbb{H}_b$. Then ρ is bi-separable iff for any positive (but not completely positive) map⁹ $\Lambda_{\mathbb{H}_b}$

$$(\mathbb{1}_{\mathbb{H}_a} \otimes \Lambda_{\mathbb{H}_b}) \rho \geq 0.$$

Obviously transposition T is a positive map, thus the partial transposition (Def. 1.2.4) is of the form $(\mathbb{1} \otimes \Lambda)$ and Prop. 1.2.5 follows from Prop. 1.2.13. As any positive map for two qubits (or one qubit and one qutrit) can be written as a sum of a completely positive map and a completely positive map times transposition [71, 72], Prop. 1.2.5 provides a sufficient and necessary condition in these cases (cp. page 18).

The correspondence between Prop. 1.2.13 and witnesses is established by the so-called Choi-Jamiołkowski isomorphism [73, 74],

$$\mathbf{W} = (\mathbb{1}_{\mathbb{H}} \otimes \Lambda_{\mathbb{H}}) \mathbf{P}, \quad (1.40)$$

where $\mathbf{P} = |\psi\rangle\langle\psi|$ denotes a pure projector onto $|\psi\rangle = \frac{1}{\sqrt{d}} \sum_{i=0}^{d-1} |i\rangle \otimes |i\rangle$ with $d = \dim(\mathbb{H})$ and $|i\rangle$ basis vectors in \mathbb{H} . Thus, a witness operator can be expressed in terms of positive maps and Prop. 1.2.12 as a whole is equivalent to Prop. 1.2.13. However, a particular witness is *not* equivalent to an associated positive map. The latter proves a stronger condition as it expresses an operator inequality whereas the former relates to a scalar expression. This is already relevant for the simple case of two qubits where the transposition map detects all entangled states (in the sense of PPT), while the corresponding witness¹⁰ does not detect any symmetric pure state to be entangled [23]. In view of the intuitive geometric picture this can be understood in the sense that infinitely many tangents would be necessary to characterize the convex set completely, as long as it is not a polytope. Still, for practical purposes the witnesses are more suitable, as it is in general hard to test that the condition in Prop. 1.2.13 holds for *any* positive map.

Another interesting connection, which was pointed out first by Barbara Terhal [67] and which will be of particular importance in Chap. 4, is the one between witnesses and Bell inequalities. Though the latter make no assumptions on the structure of some Hilbert space of an investigated system, but solely on the obtainable statistics of measurement results and their correlations, they are a kind of non-optimal witness; at least from a quantum information point of view. The operator measured in the CHSH inequality is of the form (cp. Eqn. (1.17))

$$\mathbf{B}_{\text{CHSH}} = \mathbf{A} \otimes \mathbf{B} + \mathbf{A} \otimes \mathbf{B}' + \mathbf{A}' \otimes \mathbf{B} - \mathbf{A}' \otimes \mathbf{B}', \quad (1.41)$$

from which a corresponding witness operator can be easily constructed,

$$\mathbf{W}_{\text{CHSH}} = 2(\mathbb{1} \otimes \mathbb{1}) - \mathbf{B}_{\text{CHSH}}. \quad (1.42)$$

It is obvious that, for every state ρ_{CHSH} violating the CHSH inequality, the operator \mathbf{W}_{CHSH} is indeed a witness, as $\text{tr}(\mathbf{W}_{\text{CHSH}} \rho_{\text{CHSH}}) < 0$ and $\text{tr}(\mathbf{W}_{\text{CHSH}} \rho) > 0$ for all separable states ρ . However, as already mentioned, the witness is not optimal as it is tangential to the set of

⁹A positive map is a linear map that takes positive operators to positive operators. A positive map is completely positive if any extension to a larger Hilbert space \mathbb{H} of arbitrary dimension, $(\mathbb{1}_{\mathbb{H}} \otimes \Lambda)$ is a positive map. Clearly, for completely positive maps the condition would be true for all ρ and thus not reasonable to test for separability.

¹⁰This witness is given in terms of the swap operator $\mathbf{V} = \sum_{i,j} |i\rangle\langle j| \otimes |j\rangle\langle i|$ which exchanges the subsystems (cp. e.g. [58]).

all states obeying a local realistic description, but not to the set of separable states which is a subset thereof. Indeed, there are states which are entangled but do not violate a Bell inequality [58].

The concept of entanglement witnesses appears generally in various contexts and its investigation and further development is an ongoing and very active field of research (see e.g. [75–78]). The latter fact is for good reason, as, from an experimental point of view, entanglement witnesses are one of the most important tools for the characterization, not only of three-, but also of multi-qubit entangled states.

Multi-qubit entanglement

The preceding paragraphs showed that in contrast to two qubits, for three qubits it is important to ask not only whether or how strongly but also in which way a state is entangled. The latter question, giving rise to very few possible answers for three qubits, turns out to face an unlimited amount of answers in the case of four qubits.

This means that for four qubits infinitely many, instead of only six (see Fig. 1.4), SLOCC classes can be distinguished. In the year 2002 Frank Verstraete *et al.* [19] were able to group these classes into nine SLOCC families of pure states, corresponding to nine different ways of entangling four qubits. Eight of them concern the distribution of two- and three-qubit entanglement among four subsystems (analogous to the w-class in the three qubit case) and one family is distinguished in a particular respect which shall be shortly discussed in the following. This family, which will be matter of experimental studies in Sec. 2.2 and Chap. 5, is of the form

$$G_{abcd} = \frac{a+d}{2} (|0000\rangle + |1111\rangle) + \frac{a-d}{2} (|0011\rangle + |1100\rangle) \\ + \frac{b+c}{2} (|0101\rangle + |1010\rangle) + \frac{b-c}{2} (|0110\rangle + |1001\rangle), \quad (1.43)$$

where a , b , c and d are complex parameters with non-negative real part. Each choice of these parameters represents an SLOCC class on its own, but the states of each class share a common property: All local density operators obtained by tracing all but one qubit have maximal entropy, means zero information content. In the case of two qubits this property is characteristic for (maximally) entangled states (cp. page 17) and for three qubits it is the GHZ state who exhibits this feature and is usually considered to have the "highest" three-qubit entanglement (see page 21 et seq.). Indeed, in [19] it is shown that states from G_{abcd} maximize several entanglement monotones and are therefore considered to have maximal four-qubit entanglement¹¹. This might also be the reason why most of the four-qubit states, studied so far and featuring in several applications of quantum information, belong to this class.

Very recently an alternative and complementary classification of SLOCC-families for four qubits was provided in a publication by Lamata *et al.* [20, 21]. In their inductive approach the classification of, in general, N -qubit states is based upon the classification of $(N - 1)$ -qubit states which is assumed to be known afore. Deviating from [19] the authors come to the conclusion that four qubits can be entangled in eight different ways, but claim their method to be more along the "philosophy" of the seminal work ([18]) done for the classification of three qubit states.

¹¹Naturally these statements do not apply to the very special choices of a , b , c , d for which G_{abcd} equals $|bs\rangle \otimes |bs\rangle$.

Without forming any opinion about the two alternative classification schemes, – an advantage of the latter is surely its possible generalization to arbitrary qubit numbers –, the former will be referred to within this work for purely practical reasons that shall become clear in Sec. 2.2.

Common to all the above mentioned attempts of establishing a systematic order of multi-qubit entanglement is the classification of states according to their invariance with respect to local operations. This corresponds to dividing the states' Hilbert space into orbits generated by the respective transformation group and finding a representation for the states that separates local and non-local parameters with respect to the action of the local operations. The difficulty in the transition to higher qubit numbers can be thereby nicely revealed:

An arbitrary state of a fixed number of qubits is described by a set of complex (or real) parameters equal the dimension of the Hilbert space. Some of these parameters, – the invariants under the local transformations –, specify the equivalence class to which the state belongs. The remaining ones describe where the state is situated within the class; they correspond to the dimension of the orbit and do change under the local operations [61]. As the dimension of the orbits grows polynomially in the number of qubits, while the dimension of the state space, as is known, increases exponentially, almost all parameters have non-local significance for large qubit numbers. The qualitative scaling dependence is irrespective of the type of local operation, (though the quantitative is not). In the example of N qubits the state is described by $2(2^N - 1)$ real parameters and an SLOCC operation which is an element of the special linear group $SL(2, \mathbb{C})$ is specified by six real parameters¹². Thus, the set of equivalence classes under SLOCC depends at least on $2(2^N - 1) - 6N$ parameters [18]. This clarifies why a finite number of SLOCC classes is still possible in the case of three qubits, whereas infinitely many classes, labeled by a set of continuous parameters are obtained for $N = 4$. Furthermore, analogous considerations demonstrate that LU operations, which are elements of $U(2)$ (or $SU(2)$) and defined by four (or three) parameters, are not sufficient even for the characterization of only three qubits by a finite set of equivalence classes.

1.2.3 Processing of information

So far the formal notions of separable and entangled states of qubits were established. The following paragraphs are devoted to the generation of states and the processing of the information carried by them.

Whenever a computer performs a computation, it modifies a given input information according to definite rules, what will finally yield a desired output information. From a physical point of view, this computation is associated with the time evolution of the initial (input) state of a system, to a final state which is to be read out. When extending these concepts from the classical to the quantum domain, it seems sensible to associate the time evolution with a unitary process transforming the quantum state of the computer. In analogy to classical computers where the transformations are mediated by logical gates within the design of a circuit, unitary operations acting on qubits can be thought of as *quantum gates*. It can be shown that an arbitrary unitary operation on any finite number of qubits can be decomposed as a product of one- and two-qubit transformations. In turn, any of the latter can be expressed by compositions of single-qubit gates and one distinguished two-qubit gate,

¹²In [18] it was proved that two states are equivalent under SLOCC if an invertible local operator \mathbf{A} relating them exists. So, $\det(\mathbf{A}) \neq 0$, and it can be fixed to be $\det(\mathbf{A}) = 1$, as the state transformed by $c\mathbf{A}$ would only differ by the constant complex factor c ; so $\mathbf{A} \in SL(2, \mathbb{C})$.

the so-called controlled not (**CNOT**) [79–81]. This means, the $\text{CNOT} = \frac{1}{2}(\mathbb{1} \otimes \mathbb{1} + \mathbb{1} \otimes \sigma_x + \sigma_z \otimes \mathbb{1} - \sigma_z \otimes \sigma_x)$ together with the set of single-qubit operations is *universal* with respect to computation. Therefore its action and the one of other related two- and one-qubit gates shall be shortly discussed.

The **CNOT** gate has two input qubits, one labeled as the *control*, the other as the *target* qubit. Conditioned on the logical state of the control qubit, the state of the target qubit will be either flipped or not. The action of the gate on the computational basis states is given as

$$\text{CNOT} = \begin{cases} |00\rangle \rightarrow |00\rangle \\ |01\rangle \rightarrow |01\rangle \\ |10\rangle \rightarrow |11\rangle \\ |11\rangle \rightarrow |10\rangle \end{cases}, \quad \begin{pmatrix} 1 & 0 & 0 & 0 \\ 0 & 1 & 0 & 0 \\ 0 & 0 & 0 & 1 \\ 0 & 0 & 1 & 0 \end{pmatrix}, \quad (1.44)$$

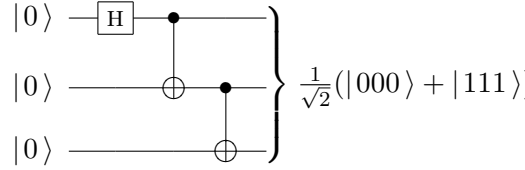
where the first qubit holds the role of the control, the second of the target qubit. Three of the gate’s symbols commonly used in quantum circuits are displayed in Fig. 1.6(e). Due to the flip operation on the second qubit, the **CNOT** is also sometimes referred to as ”controlled X-gate”, as σ_x exchanges the two computational basis states (see Fig. 1.6(a), 1.6(e) right, and Eqn. (1.19)). From another point of view, the **CNOT** is the pendant of the classical exclusive or (**XOR**) gate, since the logical state of the control qubit is added modulo two to the state of the target qubit. This fact is in particular symbolically expressed in Fig. 1.6(e) center. The most important application of the **CNOT** gate is to (dis)entangle qubits. Whenever the state of the control qubit is a superposition of the computational basis states the output of the gate will be an entangled state (and vice versa). For instance, if the superposition is generated by the **HAD** gate (see Fig. 1.6(c) and Eqn. (1.28)), the following circuit transforms between the Bell- and the product basis of two qubits (cp. Eqn. (1.29)):

$$\left. \begin{array}{l} |0\rangle \text{---} \boxed{\text{H}} \text{---} \bullet \text{---} \\ |0\rangle \text{---} \oplus \text{---} \end{array} \right\} \frac{1}{\sqrt{2}}(|00\rangle + |11\rangle) \quad (1.45)$$

$$\begin{aligned} \text{CNOT} \cdot (\text{HAD} \otimes \mathbb{1})|00\rangle &= \text{CNOT} \frac{1}{\sqrt{2}}(|0\rangle + |1\rangle)|0\rangle = \text{CNOT} \frac{1}{\sqrt{2}}(|00\rangle + |10\rangle) \\ &= \frac{1}{\sqrt{2}}(|00\rangle + |11\rangle) = |\phi^+\rangle, \end{aligned}$$

and analogous for $|01\rangle \rightleftharpoons |\psi^+\rangle$, $|10\rangle \rightleftharpoons |\phi^-\rangle$ and $|11\rangle \rightleftharpoons |\psi^-\rangle$. This is, of course, not restricted to the case of two qubits. Very recently it was shown that any three qubit state, particularly any entangled state, can be prepared from a product state by using at most three **CNOT** gates [82]. Thereby the Hilbert space of pure three-qubit states is divided in orbits, each spanned by a different number of applications of (non-local) **CNOT** gates (in contrast to the previous section where the orbits were generated by local operations, cp. page 27). In this way four classes of states are derived. The canonical form of the **GHZ** state (Eqn. (1.32))

is in the one whose elements can be obtained by two **CNOT** applications. A possible circuit is

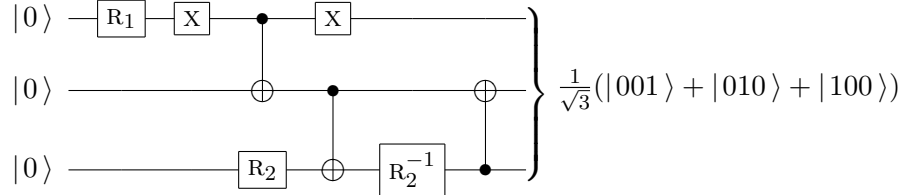


$$\left. \begin{array}{l} |0\rangle \text{---} \boxed{\text{H}} \text{---} \bullet \text{---} \\ |0\rangle \text{---} \oplus \text{---} \bullet \text{---} \\ |0\rangle \text{---} \oplus \text{---} \end{array} \right\} \frac{1}{\sqrt{2}}(|000\rangle + |111\rangle) \quad (1.46)$$

$$\begin{aligned} & (\mathbb{1} \otimes \text{CNOT}) \cdot (\text{CNOT} \otimes \mathbb{1}) \cdot (\text{HAD} \otimes \mathbb{1} \otimes \mathbb{1}) |000\rangle = \dots \\ & \dots = \frac{1}{\sqrt{2}}(|000\rangle + |111\rangle) = |\text{GHZ}\rangle. \end{aligned}$$

In turn, starting already from the **GHZ** state any other class can be reached within two **CNOT** operations. Remarkably, any pure three-qubit state can thus be transformed into any other by at most four **CNOT** gates.

The generation of the three-qubit **w** state, with a product state as origin, is a little bit more complicated, as it requires special single qubit rotations (see Fig. 1.6(d)) and three **CNOT** gates [83],



$$\left. \begin{array}{l} |0\rangle \text{---} \boxed{R_1} \text{---} \boxed{\text{X}} \text{---} \bullet \text{---} \boxed{\text{X}} \text{---} \\ |0\rangle \text{---} \oplus \text{---} \bullet \text{---} \\ |0\rangle \text{---} \boxed{R_2} \text{---} \oplus \text{---} \boxed{R_2^{-1}} \text{---} \bullet \text{---} \end{array} \right\} \frac{1}{\sqrt{3}}(|001\rangle + |010\rangle + |100\rangle)$$

$$\begin{aligned} & (\mathbb{1} \otimes \overline{\text{CNOT}}) \cdot (\mathbb{1} \otimes \mathbb{1} \otimes R_2^{-1}) \cdot (\sigma_x \otimes \text{CNOT}) \cdot (\text{CNOT} \otimes R_2) \cdot (\sigma_x \otimes \mathbb{1} \otimes \mathbb{1}) \cdot (R_1 \otimes \mathbb{1} \otimes \mathbb{1}) |000\rangle = \dots \\ & \dots = \frac{1}{\sqrt{3}}(|001\rangle + |010\rangle + |100\rangle) = |\text{w}\rangle, \end{aligned} \quad (1.47)$$

where $R_1 = \frac{1}{\sqrt{3}} \begin{pmatrix} \sqrt{2} & -1 \\ 1 & \sqrt{2} \end{pmatrix}$, $R_2 = \begin{pmatrix} \cos(\frac{\pi}{8}) & -\sin(\frac{\pi}{8}) \\ \sin(\frac{\pi}{8}) & \cos(\frac{\pi}{8}) \end{pmatrix}$ and $\overline{\text{CNOT}} \equiv \text{SWAP} \cdot \text{CNOT} \cdot \text{SWAP}$ is a swapped **CNOT** gate in which the roles of control and target qubit are exchanged (see Fig. 1.6(g)). The thereby introduced operation $\text{SWAP} = \frac{1}{2}(\mathbb{1} \otimes \mathbb{1} + \sigma_x \otimes \sigma_x + \sigma_y \otimes \sigma_y + \sigma_z \otimes \sigma_z)$ is another two qubit gate, which is often useful on its own as it exchanges two qubits

$$\text{SWAP} = \begin{cases} |00\rangle \rightarrow |00\rangle \\ |01\rangle \rightarrow |10\rangle \\ |10\rangle \rightarrow |01\rangle \\ |11\rangle \rightarrow |11\rangle \end{cases}, \quad \begin{pmatrix} 1 & 0 & 0 & 0 \\ 0 & 0 & 1 & 0 \\ 0 & 1 & 0 & 0 \\ 0 & 0 & 0 & 1 \end{pmatrix}. \quad (1.48)$$

In a slightly different notation it appeared in the context of entanglement witnesses for two qubits on page 25 and footnote 10. Yet, the **SWAP** operation can be basically expressed as a sequence of three **CNOT** gates (see Fig. 1.6(f)).

Last but not least, a further two-qubit gate which is closely related to the **CNOT**, and whose applications constitute in fact a significant part of the work in this thesis (see Sec. 2.1 and Chap. 3), is the **CPHASE** gate. As the name already suggests it involves as well a control and a target qubit: Depending on the logical state of the control qubit the $\text{CPHASE} = \frac{1}{2}(\mathbb{1} \otimes \mathbb{1} + \mathbb{1} \otimes \sigma_z + \sigma_z \otimes \mathbb{1} - \sigma_z \otimes \sigma_z)$ applies a relative phase shift of π in the computational basis

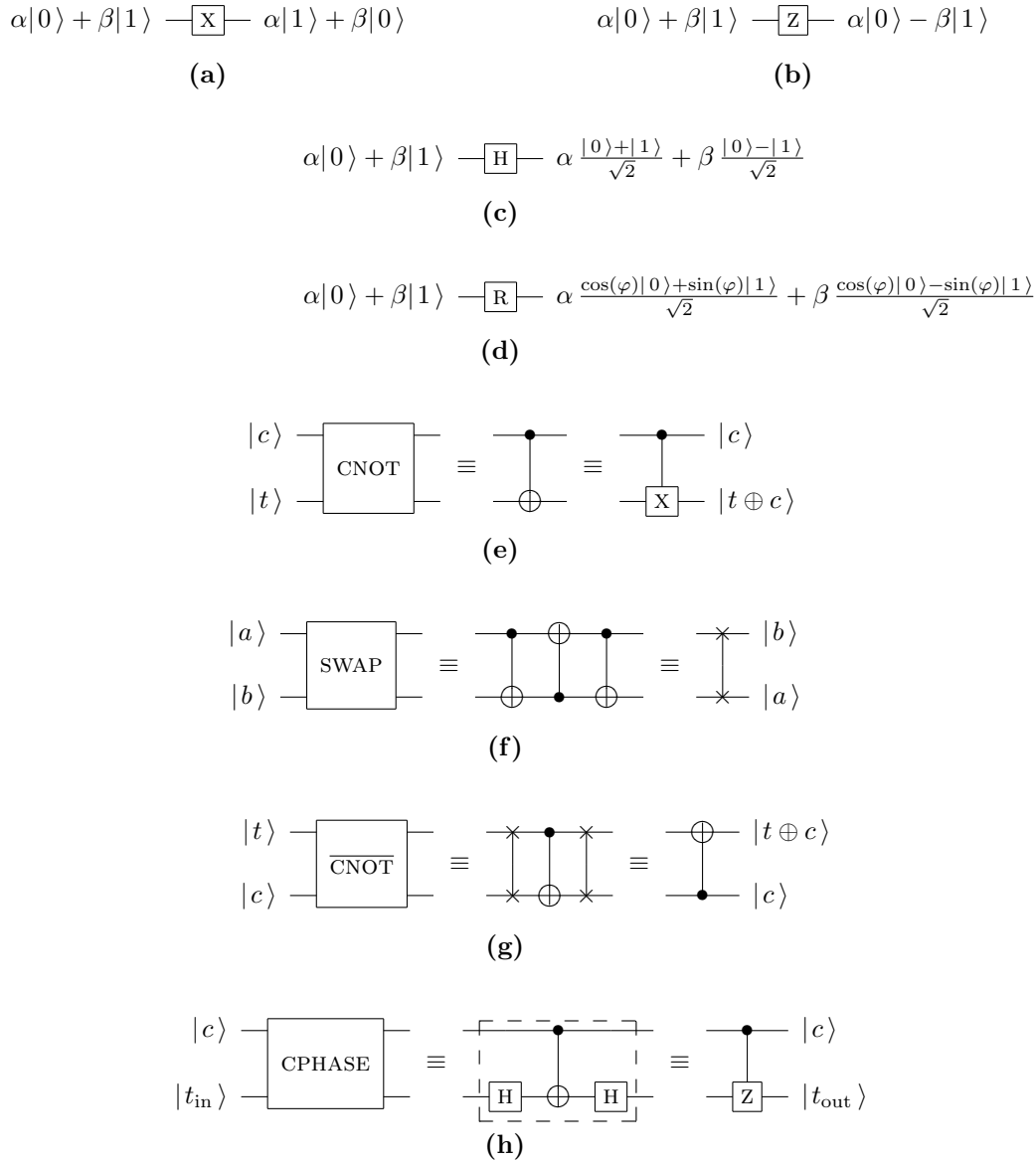


Figure 1.6: Quantum circuit symbols of important single- and two-qubit gates. **(a)** The σ_x operation applies a bit flip in the computational basis on the input, whereas **(b)** the σ_z gate introduces a relative phase of π between the computational basis states. **(c)** The Hadamard gate, as a superposition of both operations generates an equally weighted superposition of the computational basis states. It can be also seen as a basis transformation between the σ_x - and σ_z -basis. **(d)** The one-qubit rotation gate rotates the state of the input in the xz -plane of the Bloch sphere by an angle φ . **(e)** The **CNOT** gate flips the state of the target qubit conditioned on the logical value of the control qubit. Therefore it can be also regarded as a controlled z -gate (right). From another point of view it represents the pendant to the classical **XOR**, as the bit value of the control qubit is added modulo two to the one of the target qubit (center). **(f)** The **SWAP** operation exchanges two qubits. It can be expressed in terms of three **CNOT** gates (center). **(g)** In a swapped **CNOT** gate the roles of control and target qubit are exchanged. **(h)** The **CPHASE** gate applies a relative phase shift of π in the computational basis components of the state of the target qubit, conditioned on the state of the control qubit. Therefore it is also sometimes named controlled z -gate (right). The **CPHASE** equals the **CNOT** besides a basis rotation of the target qubit by 45° , mediated e.g. by a **HAD** gate (center).

states of the target qubit. Therefore it also often referred to as "controlled z-gate" as σ_z adds a π phase shift to the state $|1\rangle$ while leaving $|0\rangle$ unchanged (see Fig. 1.6(h) right). The basis representation reads

$$\text{CPHASE} = \begin{cases} |00\rangle \rightarrow |00\rangle \\ |01\rangle \rightarrow |01\rangle \\ |10\rangle \rightarrow |10\rangle \\ |11\rangle \rightarrow -|11\rangle \end{cases}, \quad \begin{pmatrix} 1 & 0 & 0 & 0 \\ 0 & 1 & 0 & 0 \\ 0 & 0 & 1 & 0 \\ 0 & 0 & 0 & -1 \end{pmatrix}. \quad (1.49)$$

Interestingly, the **CPHASE** equals a **CNOT** in which the basis of the target qubit is rotated by 45° , i.e., these two gates differ only by a **HAD**-gate applied to the target qubit (see Fig. 1.6(h) center)

$$\text{CPHASE} = (\mathbb{1} \otimes \text{HAD}) \cdot \text{CNOT} \cdot (\mathbb{1} \otimes \text{HAD}). \quad (1.50)$$

This fact suggests that the **CPHASE** gate can be used as well to transform between a product and an entangled state basis. However, these bases will differ from the canonical ones by the additional rotation (see Sec. 3.1).

1.3 Photons as qubits

So far, a theoretical framework has been introduced, which is basically needed for the discussion of the experimental results presented in the subsequent chapters. What is, however, still missing is a short overview on the actual practical possibilities for implementations of entangled qubit states in physical systems. This should be made up for in the subsequent paragraphs before the presentation of the underlying new results of this work starts with the next chapter.

The definition of a qubit (Def. 1.2.1) suggests that any quantum physical system which possesses two distinct states can be used for a practical implementation. Still, several other requirements might seem to be sensible with respect to applications in quantum information [84]. Naturally, the qubit should be well characterized in the sense that its defining internal parameters as well as its external coupling to environmental influences and other qubits are accurately known. The physical system supporting the qubit should be scalable, i.e., it should have the capacity for more qubits, as a single qubit is hardly useful for any sensible application. Further, it should be possible to initialize the qubit in a well defined state and apply to it the previously mentioned set of universal quantum gates. In this connection it is of course important that the time scale on which the gates act on the qubits is sufficiently small compared to the time in which the state decoheres; or, to put it the other way round, the decoherence time of the qubit should be small compared to the gate operation time. Finally, obtaining results of any computation requires the ability to measure specific qubits. In particular with respect to communication it is reasonable to have additionally a well controllable interface at hand between stationary qubits, adapted for the localized *processing* of information and mobile qubits, suited for the remote *transportation* of information.

Obviously there is not *the* ideal qubit, and the used physical system has to be chosen according to the actual task to be accomplished. Several different realizations already exist as for example trapped ions, quantum dots, atoms in optical lattices etc., all of them each in a different stage of development (for a survey see [85]). However, especially for quantum

communication photons are doubtlessly the preferred choice for many obvious reasons. Basically all of the above criteria are met by them, still some certainly better than others as shall become clear in the course of these last paragraphs of the chapter.

1.3.1 Encoding of information in polarization and its manipulation

Due to the algebra presented on page 14 et seqq. the intuitive association with a qubit is a spin one-half particle. Spin one particles like photons do not seem to be the proper system at first glance, due to their three level scheme. Yet, photons have the peculiarity to possess only doubly degenerate eigenvalues for the momentum, and so, to never occur in a spin zero state. This is closely related to the fact that they do not have a rest mass; consequently there is no rest frame in which they could exhibit the full symmetry with respect to the rotation group in three dimensions. The angular momentum along the direction of motion of a photon propagating in well defined spatial mode, has therefore two values, ± 1 . With this restriction, the photon's spin relates to the polarization of its vector wave function (see, e.g., [86]). Thus, the photon's polarization represents a two-state quantum system which is indeed well described by the spin one-half algebra and suitable for representing a qubit. Such photonic qubits are used for all the experiments discussed in this work and the following convention is chosen:

The computational basis states $|0\rangle$ and $|1\rangle$ are encoded in the states $|H\rangle_i$ and $|V\rangle_i$, denoting the state of a single photon in the spatial mode i with linear horizontal and linear vertical polarization, respectively. Most of the time the spatial mode will be evident from the context and hence the subscript be omitted,

$$|0\rangle \leftrightarrow |H\rangle, \quad |1\rangle \leftrightarrow |V\rangle. \quad (1.51)$$

In agreement with this encoding the eigenstates of σ_x are given as linear diagonal polarization states ($|\pm\rangle$) and the eigenstates of σ_y as right ($|R\rangle$) and left ($|L\rangle$) circular polarization states.

The polarization of photons can be easily manipulated by so-called linear retarders made of uniaxial birefringent crystals (see, e.g., [87]). Of particular importance are half-wave plates (HWP) and quarter-wave plates (QWP) which introduce a relative phase shift of π and $\frac{\pi}{2}$, respectively, between the ordinary and extraordinary polarization modes of the crystal. For an angle of θ between the principal axis and the vector of horizontal polarization the explicit form of their transformation on the basis vectors is given by [88] (cp. Eqn. (1.27))

$$\text{HWP}(\theta) = \mathbf{U}\left(\frac{\pi}{2}, \pi, 2\theta, 0\right) = \begin{pmatrix} \cos(2\theta) & \sin(2\theta) \\ \sin(2\theta) & -\cos(2\theta) \end{pmatrix}, \quad (1.52a)$$

$$\text{QWP}(\theta) = \mathbf{U}\left(-\frac{\pi}{4}, -\frac{\pi}{2}, 2\theta, 0\right) = \begin{pmatrix} \cos^2(\theta) - i \sin^2(\theta) & (1+i) \cos(\theta) \sin(\theta) \\ (1+i) \cos(\theta) \sin(\theta) & -i \cos^2(\theta) + \sin^2(\theta) \end{pmatrix} \quad (1.52b)$$

The combination of two QWPs and one HWP allows for the implementation of any single-qubit unitary operation and especially it holds that $\text{HWP}(0) = \sigma_z$, $\text{HWP}(\frac{\pi}{4}) = \sigma_x$, $\text{HWP}(\frac{\pi}{8}) = \text{HAD}$. For practical reasons it is sometimes convenient to have a linear retarder with an adjustable retardation that serves as a variable phase shifter. For this purpose several experiments in this work use a pair of Yttrium Vanadate (YVO₄) crystals. These birefringent crystals are cut, like wave plates, such that the principal axis lies in a plane parallel to the surface and they are aligned in a way that horizontal and vertical polarization correspond to the normal

modes. The axes of two crystals within a pair are oriented perpendicular with respect to each other to compensate for dispersion effects. If a crystal is rotated around its axis, the optical thickness, and so the retardation can be changed (for details, see [89] page 41 et seqq.).

In general, from an experimental point of view, the implementation of single-qubit gates for photonic qubits is not a challenge. As photons have zero charge they scarcely interact with their environment and, moreover, they do not have any linear self-interaction¹³, as for example electrons. Therefore photons exhibit exceptional long decoherence times compared to any time experimentally required for the gate operations. This fact, though being a virtue concerning *single*-qubit operations, turns out to be a serious vice with regard to *two*-qubit gates. It is easy to imagine that any *controlled* gate operation, like the **CNOT**, must be based on some kind of interaction between the involved qubits. In order to solve this problem, non-linear effects in solid states could be used in principle, but in practice they are unfortunately often not available at the required strength. It is possible to realize any discrete unitary operation that relates a finite number of input and output modes with linear optics only [90]. However, linear optical elements cannot make photons interact, but only interfere. Consequently, the realized unitary operation is separable in the sense that it can be decomposed in operations acting on each qubit individually. This means the "interaction" provided by linear optics is not sufficient to implement a two-qubit gate as, e.g., the **CNOT** in a deterministic manner for the polarization qubits used in this thesis [91]. This, at first, fatal result with respect to linear optics quantum computation (**LOQC**) was mitigated in a seminal work by Emanuel Knill, Raymond Laflamme and Gerard Milburn (**KLM**) [6]. They introduce the required non-linearity in the form of ancillary modes, auxiliary entangled states, photon counting and conditional detection. The latter means that particular events are selected or actions performed, conditioned on the detection of photons in distinguishable modes. Using this approach all linear optics quantum logic (**LOQL**) can be made near deterministic, i.e., its probability of failure can be made arbitrarily small, with increasing resources. Although it seems that this solution would just shift the problem of performing a computation to the one of creating the auxiliary resource states, it can be shown that even if these states can be generated only probabilistically this does *not* affect the overall computation. (A tutorial introduction to quantum computation with linear optics realizations can be found for instance in [92].) The experiments presented in this thesis use as well the technique of conditional detection and interferometric linear optics setups. Still, the optical networks are probabilistic, as building them strictly in the spirit of **KLM** would require an unrealistic and not manageable amount of resources with current state of the art technology. The input states are generated by the process of **SPDC** what is subject of the following section.

1.3.2 Generation of photons

As stated above, though photons do not have a linear self-interaction in general, non-linear effects can occur in a solid state. If an electromagnetic field interacts with a dielectric medium, it generates electric dipole moments whose macroscopic sum results in the polarization density \vec{P} . In an anisotropic crystal, i.e., in a crystal in which the relation between \vec{P} and the incident electromagnetic field \vec{E} depends on the direction of the latter, the components P_i of the

¹³Self-interaction means an interaction between two particles of the same kind.

polarization are given in the form [87],

$$P_i = \epsilon_0 \sum_j \chi_{ij}^{(1)} E_j + 2 \sum_{jk} \chi_{ijk}^{(2)} E_j E_k + 4 \sum_{jkl} \chi_{ijkl}^{(3)} E_j E_k E_l + \dots, \quad (1.53)$$

where $i, j, k, l = 1, 2, 3$ and ϵ_0 is the permittivity of the vacuum; $\chi_{ij}^{(1)}$ is the susceptibility tensor of the medium and $\chi_{ijk}^{(2)}, \chi_{ijkl}^{(3)}$ its pendants for non-linear effects of second and third order, respectively. The contribution of the second order term in Eqn. (1.53) is typically ten orders of magnitude lower than the one of the linear term. Therefore it can be usually neglected for weak fields. In contrast, for a strong pump field with frequency ω_p it leads to the generation of two new fields of frequency ω_s and ω_i . In terms of photons, i.e., in the language of second quantization, this corresponds to the spontaneous conversion of a pump photon with energy $\hbar\omega_p$ and momentum $\hbar\vec{k}_p$ into two photons with energies $\hbar\omega_s, \hbar\omega_i$ and momenta $\hbar\vec{k}_s, \hbar\vec{k}_i$. These are usually referred to as *signal* and *idler* photon. This process resembles the phenomenon of three-wave mixing or parametric amplification known from classical electrodynamics. There, two fields of evanescent intensity are amplified by the presence of a strong pump field in a non-linear medium. However, the *spontaneous* conversion, the conversion without the prior presence of a weak field, is purely quantum. Its mathematical treatment can be found in standard literature like, e.g., [93].

In the conversion process energy and momentum have to be conserved [94],

$$\omega_p = \omega_s + \omega_i \quad (1.54a)$$

$$\vec{k}_p = \vec{k}_s + \vec{k}_i. \quad (1.54b)$$

For a uniaxial non-linear crystal two types of **SPDC** are distinguished according to the polarization of the down converted photons:

Type I: Signal and idler are ordinarily polarized with respect to the principal axis of the crystal.

Type II: Signal and idler are orthogonally polarized, one ordinarily, the other extraordinarily.

In both cases, the pump photons are extraordinarily polarized, which means the polarization vector lies in the plane spanned by the principal axis of the crystal and the wave vector of the pump photon; ordinarily means the polarization vector is normal to this plane. Throughout this thesis only the second type of **SPDC** will be relevant.

Due to Eqns. 1.54a and 1.54b the pairwise generated photons are strongly correlated with respect to their energy, momentum and also polarization. The latter can be exploited to directly obtain polarization-entangled states from the **SPDC** as shall be seen later on [95]. In all experiments presented in the work at hand, the down conversion photons are intended to be processed in linear optics networks which might comprise interference. Consequently, the photonic qubits should ideally not differ in any other degree of freedom than their spatial mode and polarization. Therefore, a proper experimental arrangement ensures that only photons with degenerate solutions for Eqn. (1.54a) are fed into the network, i.e., only photons which have a spectral distribution around the same central wavelength.

Eqn. (1.54b) implies that the **SPDC** emission is conic and symmetric around the pump beam [96]. The orthogonality in the polarization leads, however, to emission cones which are

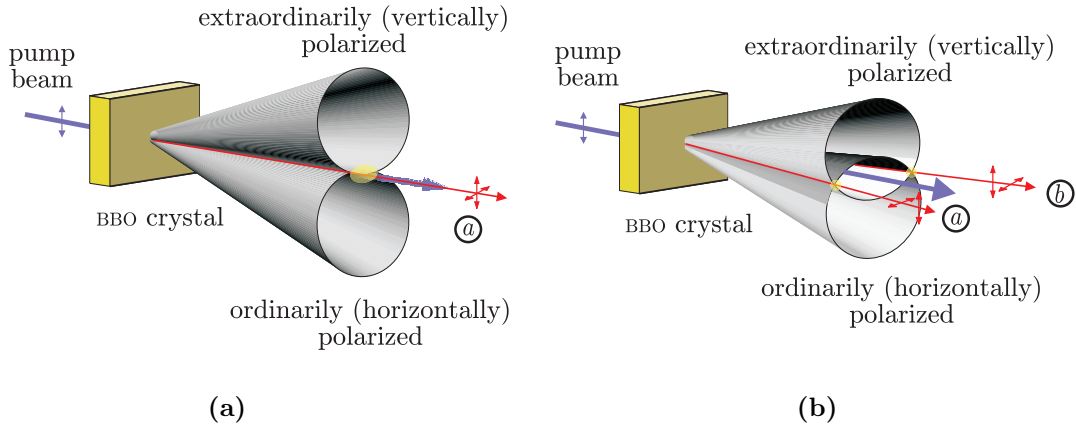


Figure 1.7: Type II degenerate spontaneous parametric down conversion. A uniaxial nonlinear crystal **BBO** is pumped by **UV** pulses. With a small but non-vanishing probability the pump photons undergo a conversion process into two photons of half the wavelength. Due to energy and momentum conservation these photons are orthogonally polarized and emitted onto two cones. **(a)** In the collinear case the cones touch each other along a line. Photons coupled along this intersection line (spatial mode *a*) cannot be assigned to one of the two cones. Thus no information is available about their polarization, a fact that is essential to obtain entanglement. **(b)** In the non-collinear case the cones cross and intersect along two lines defining two spatial modes *a* and *b*. Photons emitted into these two modes cannot be assigned to one of the cones. After proper compensation of walk-off effects caused by birefringence of the **BBO** the photons are found to be in a polarization-entangled Bell state.

not concentric (see Fig. 1.7). The opening angle of each cone as well as the angle between the cone axes depends on the angle enclosed by the pump wave vector and the principal axis of the crystal. According to the relative orientation of the cones with respect to each other two cases of type II **SPDC** are distinguished which shall be discussed in more detail in the following paragraphs: The non-collinear case, in which the cones intersect (Fig. 1.7(b)) and the collinear case in which the cones just touch each other (Fig. 1.7(a)) [97, 98].

Collinear spontaneous parametric down conversion

For a specific angle between the wave vector of the pump beam and the principal axis of the crystal, the down conversion emission cones are tangent to one another along a line which is defined by the pump beam direction (see Fig. 1.7(a)). The state of the photons which are emitted in the spatial mode *a* defined by this line is best described in terms of the bosonic creation and annihilation operators, \mathbf{a}^\dagger , \mathbf{a} , acting on the vacuum $|0\rangle$,

$$Z \exp\left(-i\sqrt{2}\alpha \mathbf{a}_H^\dagger \mathbf{a}_V^\dagger\right) |0\rangle. \quad (1.55)$$

Thereby, Z is a normalization constant, α depends on parameters of the crystal and is approximately proportional to the pump beam intensity. Furthermore it holds that

$$[\mathbf{a}_i^\dagger, \mathbf{a}_j^\dagger] = 0 = [\mathbf{a}_i, \mathbf{a}_j], \quad [\mathbf{a}_i, \mathbf{a}_j^\dagger] = \delta_{ij}, \quad \text{with } i, j \in \{H, V\}, \quad (1.56)$$

and $\mathbf{a}_i^\dagger |ni\rangle = \sqrt{n+1} |(n+1)i\rangle_a$ creates, $\mathbf{a}_i |ni\rangle = \sqrt{n} |(n-1)i\rangle_a$ annihilates a horizontally or vertically polarized photon in the spatial mode a . Expanding Eqn. (1.55) results in

$$Z \left(1 - \underbrace{i\sqrt{2}\alpha \mathbf{a}_H^\dagger \mathbf{a}_V^\dagger}_{2 \text{ photons}} - \underbrace{\alpha^2 (\mathbf{a}_H^\dagger \mathbf{a}_V^\dagger)^2}_{4 \text{ photons}} + \underbrace{i\frac{\sqrt{2}}{3}\alpha^3 (\mathbf{a}_H^\dagger \mathbf{a}_V^\dagger)^3}_{6 \text{ photons}} + \dots \right) |0\rangle, \quad (1.57)$$

and demonstrates nicely what happens in the down conversion process: In zero order the pump beam passes the crystal without any conversion taking place. In first order a pair of photons is created in the state $|H, V\rangle_a$ what happens with probability $2Z^2\alpha^2$. In second and third order 4 and 6 photons, in the states $|2H, 2V\rangle_a$ and $|3H, 3V\rangle_a$ are created with probabilities $4Z^2\alpha^4$ and $8Z^2\alpha^6$, respectively, and so forth. Usually, for a continuous wave (CW) pump the latter probabilities are so small that the higher order events can be neglected. However, for very high pump field intensities, as they occur, e.g., in short laser pulses the second and third order contributions can be relevant and used for the experimental generation of multi-photon states; see for instance [99].

Non-collinear spontaneous parametric down conversion

When, starting from the collinear configuration, the angle between the pump wave vector and the principal axis of the crystal is increased, the down conversion emission cones tilt towards the pump beam direction and intersect each other along two lines (see Fig. 1.7(b)). These intersection lines define two spatial modes a and b . If the photons which are emitted along these crossing modes do not differ in any other degree of freedom than their spatial mode and polarization, a polarization entangled state can be directly obtained from the SPDC process [95]. The reason is, that for each of these photons the spatial mode does not reveal any information about the cone to which the photon belongs and hence does not offer any polarization information [100],

$$\begin{aligned} & Z \exp \left(-i\alpha (\mathbf{a}_H^\dagger \mathbf{b}_V^\dagger + \mathbf{a}_V^\dagger \mathbf{b}_H^\dagger) |0\rangle \right) \\ &= Z \left(1 - \underbrace{i\alpha (\mathbf{a}_H^\dagger \mathbf{b}_V^\dagger + \mathbf{a}_V^\dagger \mathbf{b}_H^\dagger)}_{2 \text{ photons}} - \underbrace{\frac{\alpha^2}{2} (\mathbf{a}_H^\dagger \mathbf{b}_V^\dagger + \mathbf{a}_V^\dagger \mathbf{b}_H^\dagger)^2}_{4 \text{ photons}} + \dots \right) |0\rangle. \end{aligned} \quad (1.58)$$

In first order this results in the Bell state

$$|\psi^+\rangle = \frac{1}{\sqrt{2}} (|H_a V_b\rangle + |V_a H_b\rangle) \quad (1.59)$$

emitted with probability $2Z^2\alpha^2$ in the two modes a and b . The second order term leads with probability $3Z^2\alpha^4$ to an emission of four photons in the following superposition of photon number states

$$\frac{1}{\sqrt{3}} (|2H_a, 2V_b\rangle + |2V_a, 2H_b\rangle + |H_a, V_a, H_b, V_b\rangle). \quad (1.60)$$

It is worth to be noted that, due to bosonic bunching, the terms where two photons of identical polarization are emitted in the same spatial mode have higher amplitude, what means that this state is not just a product of two pairs of the form of Eqn. (1.59). The above

description is, however, only valid if the uncertainty about the temporal origin of each of the photons is smaller than their coherence time. In order to ensure this condition, the spectral bandwidth of the selected photons has to be smaller than that of the pumping field [101]. Alternatively, the state of Eqn. (1.60) is observed when the photons are detected within a time window which is smaller than the inverse of the bandwidth of the radiation [11]. These conditions are not trivial and can be hard to achieve in practice, particularly for the usage of a **CW** pump laser, because of its typically narrow spectral bandwidth [102]. For high enough intensities also in the **CW** case the second order emission can become relevant, but leads usually to the incoherent emission of two independent pairs (see e.g. [103]). Such *double* pair emissions might cause problems in form of unwanted noise for quantum information applications working with *single* photon pairs like, e.g., quantum cryptography [5].

For short pump pulses, like the ones used in the experiments presented in this work, the state of Eqn. (1.60) can be obtained by filtering the down conversion emission to a reasonable bandwidth (see next section). "Reasonable" in this context refers to the fact that every kind of filtering comprises in practice a trade-off between quality of the obtained state and observed count rate¹⁴ [104].

1.3.3 Building blocks of typical setups

The previous considerations suggest that every setup of a linear optics quantum information experiment can be divided into three building blocks: A photon source providing the qubits, a linear optics network processing the information, and finally, a detection system registering the qubits at the output of the network. These typical parts, as they were used in the experiments presented later, shall be shortly discussed in the following.

Photon source

As already stated before, all experiments described in this thesis use as photon source solely **SPDC** of type II in the collinear and non-collinear configuration. The process is pumped by femtosecond **UV** pulses at a central wavelength of 390 nm and an average mean power between 600 and 800 mW leading to a down conversion emission in the near infrared (**IR**) at around 780 nm. The short pulses for the pump combine high peak intensities with short creation time windows of the down converted photons; features, which are both highly desired in multi-photon experiments to achieve a non-vanishing, coherent emission in the second order. The **UV** pump is obtained from the second harmonic generation (**SHG**) of femtosecond **IR** pulses in a 3 mm long Lithium Borate (**LBO**) crystal. These **IR** pulses have a pulse length of approximately 130 fs, an average mean power of 2.1 W at a wavelength of 780 nm and are generated by a commercial mode-locked Titanium doped Sapphire (**Ti:Sa**) laser (Tsunami[®], Spectra-Physics[®]) at a repetition rate of 82 MHz. The **Ti:Sa** is pumped by a **CW** solid-state (diode pumped, frequency doubled Neodymium doped Yttrium Vanadate (**Nd:YVO₄**)) laser (Millennia[®], Spectra-Physics[®]) with an output power of 10 W at 532 nm.

After the **LBO** crystal the **UV** emission is shaped by two cylindrical lenses to obtain a circular beam profile in the focus. A couple of reflections at dichroic mirrors which are highly reflective for **UV** and highly transmissive for **IR** serve to filter residual **IR** light in the **UV** beam

¹⁴Naturally, also for long pump pulses, or maybe even nearly **CW** pump beams, a state of the form of Eqn. (1.60) could be theoretically observed by accordingly strong filtering. However, practically no photon emission would be left in such a case.

prior to the SPDC. The focus of the UV beam, whose diameter is chosen to be 200 μm for the non-collinear and 100 μm for the collinear case, is located at the down conversion crystal, which is a 2 mm long BBO crystal cut for collinear SHG. For the collinear configuration, also dichroic mirrors are used to separate the IR down conversion emission from the residual UV pump light. In both configurations walk-off effects caused by the birefringence of the down conversion crystal are compensated by a combination of a HWP, switching horizontal and vertical polarization, and a 1 mm BBO crystal. The spatial mode(s) specified by the intersection line(s) of the down conversion emission cones is (are) fixed and exactly defined by coupling the photons into single mode fibres [105]. Coarse spectral filtering is achieved by spatially selecting the degenerate SPDC emission, while narrow band interference filters with a bandwidth of typically 2 or 3 nm define precisely the final spectral range of the photonic qubits.

The broad spectral band width of the short pump pulses, though being essential to obtain coherence in the second order emission, is also disadvantageous in some respects. Usually, due to Eqn. (1.54) for a narrow band or CW pump there is a strict relation between the emission angle of the down converted photons (with respect to the pump direction) and their wavelength [106]. This leads to a dependence of the spectral from the angular width coupled by the single mode fibres, which can be used for spectral filtering, and to optimize the photon collection efficiency [105]. As a consequence of the broad band width of pump pulses, comprising not a single but a whole range of pump wave vectors, Eqn. (1.54) is relaxed and the relation between the emission direction and the wavelength washed out. Therefore the angular range defined by the coupling optics together with the single mode fiber alone is not sufficient for a spectral selection of the down conversion photons, and the use of additional interference filters is indispensable. The latter, though being not a problem per se, leads together with the lack of angular-spectral correlation in the emission to a noticeable decrease of the photon pair collection efficiency¹⁵.

Another effect caused by the usage of very short pump pulses, is that signal and idler emission have different spectral width [107, 108]. This leads on the one hand to a polarization dependency of the pair collection efficiency by the same reasons as described above, and on the other hand to a partial distinguishability of the photons within a pair which involves problems, particularly when these photons are processed in optical networks that include interference [109, 110].

Linear optics networks

The design of the linear optics network used in a particular experiment depends very strongly on the state to be observed or the task to be accomplished. Two network examples and their applications are discussed in Chap. 2 and the further course of this thesis. Therefore their treatment shall be kept very short in this place.

In general, their advantage is that linear optical elements, such as beam splitters and phase shifters are easy to handle experimentally. The major drawback is, as was already mentioned in Sec. 1.3.1, that they function probabilistically.

For instance, starting from Eqn. (1.60), two beam splitters, one placed in each mode a and b (and two phase shifters), are sufficient to obtain genuine four-photon entangled states

¹⁵The filters are typically centered around the degenerate wavelength. Thus it is easy to imagine that for an emission which originates from the conversion of a pump photon with a wavelength slightly off the central one, one photon of the pair is collected by the optics while the other is cut by the filter.

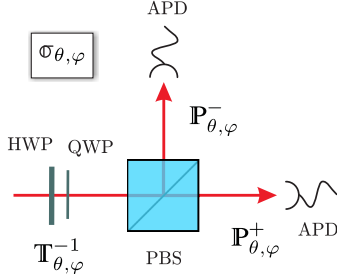


Figure 1.8: Polarization analysis (PA). Every observable $\sigma_{\theta, \varphi}$ can be measured by the use of a PBS preceded by HWP and QWP. The PBS transmits horizontally polarized photons while reflecting vertically polarized photons. The wave plates have to be set such that they implement the operation $\mathbb{T}_{\theta, \varphi}^{-1}$ transforming between the eigenstates of $\sigma_{\theta, \varphi}$ and σ_z . Detecting a photon in the transmitted or reflected output mode of the PBS corresponds then to $\mathbb{P}_{\theta, \varphi}^{\pm}$, i.e., to projecting the state of the photon onto the positive or negative eigenvector of $\sigma_{\theta, \varphi}$, respectively.

directly from SPDC [100, 111, 112] which are useful for many quantum information applications [113–115] (see also Sec. 2.2). However, the states can be observed only under the condition that after the beam splitter one photon is found in each of the output modes prior to the detection. This happens only with a certain probability.

Detection system

The detection system in all experiments presented in this work consists of passively quenched Silicon APDs¹⁶ operated in Geiger mode with typical detection efficiencies in the near IR of 38% to 48%. The detectors are preceded in each mode by a polarization analysis (PA) consisting of a HWP and a QWP followed by a PBS. The latter transmits horizontal polarization while reflecting vertical polarization. By properly setting the angle of the wave plates, any two points, lain diametric, on the Bloch sphere, can be analyzed. For example, putting the HWP at an angle of $\frac{\pi}{8}$ rotates the polarization of a photon being initially in one of the eigenstates of σ_x , $|+\rangle$ or $|-\rangle$ to $|H\rangle$ or $|V\rangle$, respectively. For this particular setting, finding a photon *after* the HWP and the PBS in the transmitted (reflected) mode, means that the photon has been in the state $|+\rangle$ ($|-\rangle$) *before* the PA. Analogously, setting the QWP to an angle of $\frac{\pi}{4}$ corresponds to the analysis of $|R\rangle$ and $|L\rangle$, the eigenstates of σ_y (cp. Eqn. (1.19) and Eqn. (1.52)). Any general operator $\sigma_{\theta, \varphi}$ (cp. Eqn. (1.25)) can be measured this way by accordingly adjusting the angular setting of the HWP and QWP. More precisely, the HWP and QWP have to implement the transformation $\mathbb{T}_{\theta, \varphi}^{-1}$ that transforms the eigenvectors of $\sigma_{\theta, \varphi}$ into the ones of σ_z ,

$$\sigma_z = \mathbb{T}_{\theta, \varphi}^{-1} \cdot \sigma_{\theta, \varphi} \cdot \mathbb{T}_{\theta, \varphi}, \quad \text{with} \quad (1.61)$$

$$\mathbb{T}_{\theta, \varphi} = \begin{pmatrix} \cos\left(\frac{\theta}{2}\right) & \sin\left(\frac{\theta}{2}\right) \\ \exp(i\varphi) \sin\left(\frac{\theta}{2}\right) & -\exp(i\varphi) \cos\left(\frac{\theta}{2}\right) \end{pmatrix} \quad (1.62a)$$

$$\text{and } \mathbb{T}_{\theta, \varphi}^{-1} = \mathbb{T}_{\theta, \varphi}^{\dagger} = \begin{pmatrix} \cos\left(\frac{\theta}{2}\right) & \exp(-i\varphi) \sin\left(\frac{\theta}{2}\right) \\ \sin\left(\frac{\theta}{2}\right) & -\exp(-i\varphi) \cos\left(\frac{\theta}{2}\right) \end{pmatrix}. \quad (1.62b)$$

Detecting the photon in the transmitted mode of the PBS corresponds then to the projection $\mathbb{P}_{\theta, \varphi}^{+}$ (cp. Eqn. (1.26)), while a detection in the reflected mode projects according to $\mathbb{P}_{\theta, \varphi}^{-}$. For a photon in the polarization state ρ , the expectation value

$$\text{tr}(\rho \sigma_{\theta, \varphi}) = \text{tr}\left(\rho (\mathbb{P}_{\theta, \varphi}^{+} - \mathbb{P}_{\theta, \varphi}^{-})\right) = \text{tr}(\rho \mathbb{P}_{\theta, \varphi}^{+}) - \text{tr}(\rho \mathbb{P}_{\theta, \varphi}^{-}) = \wp^{+} - \wp^{-} \quad (1.63)$$

¹⁶The diodes were purchased from PerkinElmer.[®]

is consequently given by the difference of the probabilities \wp^+ and \wp^- to find the photon in the transmitted and reflected output mode of the PBS, respectively. These probabilities can experimentally be approximated by the corresponding relative frequencies obtained from statistically sampling detector "clicks" during a fixed measurement time (for further details and error considerations see App. A). However, in order to determine the relative frequencies correctly, the detection efficiencies of the two detectors behind the PBS have to be measured independently as they happen to be different. Accordingly, prior to any further data evaluation the raw count rates are corrected by the gauged relative efficiencies of the detectors for the approximation of \wp^+ and \wp^- .

For the measurement of multi-qubit observables a PA is placed in each output mode of the linear optics network. The conditional detection requires the registration of coincidence events, i.e., the "simultaneous" detection of two, three or more photons within a given time window. To this end the electronic signal of each APD is fed into an ultra-fast coincidence logic which is capable to register any possible coincidence event for up to eight input signals [116]. The time window, within which the signals are considered to be coincident, is adjusted to be less than 12 ns to ensure that photons generated in subsequent pump pulses cannot lead to a coincidence event.

Advantages and challenges

Before proceeding with the next chapter the most important advantages and experimental challenges of setups conceived in the way explained before shall be summarized.

The main hurdle which causes diverse problems during all the experiments of the type described before concerns the probabilistic nature of each of the three building blocks. First, of all the photon generation is probabilistic and not very efficient; typical values for the creation probabilities $2\alpha^2$ (see page 36 et seq.) are 0.008 and 0.034 for the non-collinear and collinear SPDC process, respectively. The usage of higher pump intensities provides only a limited remedy in this respect as the "signal-to-noise" ratio is getting worse. This has to be understood in the following way: For every experiment aiming at the generation of n photons, all higher orders of SPDC with an emission of more than n photons can lead to faulty n -photon noise events due to non-perfect efficiencies in the detection system¹⁷. Second, the linear optics networks, as long as they are not built along the lines of KLM which would require an enormous overhead of resources, work only with a certain probability. This makes cascading of several logical circuits on larger scales impossible. Third and last, the detection system is not perfect. This is a limiting factor for going to higher qubit numbers as the probability for a coincidence detection decreases exponentially with the number of photons.

All these facts lead to an increasing measurement time in order to approximate any measured expectation value (Eqn. (1.63)) with a sensible error. Yet, as the alignment of every setup does not remain unchanged for an arbitrary amount of time the development of stable linear optics setups and efficient measurement procedures is highly desirable; an ambition that will be faced also at some places in the following chapters.

An important advantage of photonic qubits is that they show exceptional long coherence times and can be easily and fast transported over larger distances by glass fibres or directly through free space. Further, they can be conveniently manipulated by linear optical elements. The required technical effort is relatively small compared to other experiments based on, for

¹⁷That means $n + x$ photons are emitted out of which only n are detected. These detected n photons need not necessarily have to have the same polarization state as the photons of a "real" n -photon emission.

example, atomic or semi-conductor systems which involve the usage of ultra-high vacuum or cryogenic apparatus. The ongoing and fast developing technical progress on the source- and detection-side will help to, at least partly, overcome the above problems. Even if near-deterministic linear optics setups are not experimentally feasible with current state-of-the-art technology, their probabilistic functioning is still very useful in many applications in which only a limited number of logic operations is required. This is going to be demonstrated in the following.

Chapter 2

Linear optics setups as tools for quantum information

Besides an overview of the basic notions and concepts of quantum information, the previous chapter showed that linear optics networks are important ingredients in photonic quantum information processing.

This chapter introduces two new networks which will be used for several applications in the course of this thesis.

The first is an all linear optics **CPHASE** gate [117, 118] (see also [119, 120]) whose novel design is a simplification of former approaches with respect to experimental stability. As the gate itself and the methods used for its characterization are described very detailed in [121], this chapter just recapitulates the main results for reasons of completeness. This comprises in particular the explanation of the gate's functionality and the characterization of its performance by quantum state tomography. From the latter, a matrix is derived which describes the experimentally realized process and which will be used for simulations in Chap. 3.

The second network which is presented in this chapter is a particular setup which allows the observation of a whole family of states (see Sec. 1.2.2) [122]. This family is discussed, and the experimental results for the observation of some particular interesting members are presented.

2.1 A simple linear optics controlled phase gate

In the preceding chapter it was stated that the **CNOT** gate, together with single qubit operations, is universal for quantum computation in the sense that it provides a basis for the decomposition of any unitary transformation acting on a finite number of qubits. As the **CPHASE** gate differs from the **CNOT** solely by an additional single qubit rotation this universality holds equally well for the phase gate (see Sec. 1.2.3). Thus the **CPHASE** gate is an essential tool in many quantum information applications and its experimental implementation is of high importance. For the reasons discussed in Sec. 1.2.3 the realization of large linear optics quantum networks along the lines of **KLM** is not feasible with current state of the art technology. However, as long as, for a given task, the action of a limited number of logic operations is sufficient, and thus a probabilistic functioning tolerable, simple solutions for the realization of two qubit logic gates exist.

Recently, different schemes were introduced [14–17] which use a combination of first- and

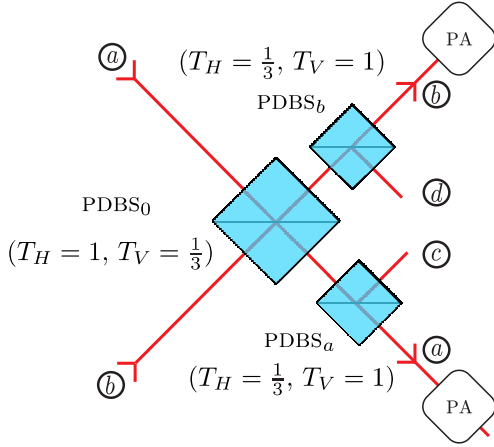


Figure 2.1: Controlled phase gate (CPHASE). The phase is introduced by the second order interference of two input modes a and b on a polarization dependent beam splitter (PDBS₀) which has transmission for horizontal polarization $T_H^0 = 1$ and for vertical polarization $T_V^0 = \frac{1}{3}$. To obtain equal output amplitudes for any input state, polarization dependent beam splitters with reversed splitting ratio PDBS _{a,b} are placed in each mode after PDBS₀. The gate operation is applied in case of a coincidence detection between the PA in modes a and b .

second-order interference to obtain the CPHASE action with $\frac{1}{9}$ probability. Yet, since first-order interference requires stability of the setup on the order of less than the photons' wavelength, for multi-photon experiments more simple and stable implementations are desirable, as discussed at the end of the previous chapter.

In the following, an alternative setup is presented, which uses only a single two-photon interference at a polarization dependent beam splitter. The stability requirements are thereby relaxed to the coherence length of the detected photons ($\approx 150 \mu\text{m}$) and can easily be fulfilled without any active stabilization of the involved optical path lengths. This enables the usage of this gate in several quantum information applications as will be shown later on.

2.1.1 The setup

The theoretical description of the action of the gate was introduced in Sec. 1.2.3. In order to implement the controlled phase shift with linear optics, second order interference on a polarization dependent beam splitter (PDBS) is employed. The layout of the experimental setup is shown in Fig. 2.1. Two input modes a and b are overlapped at PDBS₀ which has perfect transmission for horizontal polarization, $T_H^0 = 1$, while reflecting vertical polarization with probability¹ $R_V^0 = \frac{2}{3}$. The CPHASE action is performed under the condition that one photon is found in each output of the PDBS₀ leading to a coincidence detection between one detector of the PA in mode a and one in mode b . Prior to the PA, beam splitters with the reversed splitting ratio, PDBS _{a} and PDBS _{b} , are put in each mode to ensure equal amplitudes for every possible combination of input states by attenuating horizontal polarization, $T_H^{a,b} = \frac{1}{3}$. As every operation is characterized by its action on the basis states, it is sufficient to consider the effect of the CPHASE gate on the computational basis. This shall be done in detail in the following to better understand how the interference leads to the desired transformation. To this end, the beam splitters are best described by their action on the bosonic creation and

¹All types of beam splitters are considered to be rather loss-free, i.e., the transmission of the PDBS for vertical polarization $T_V = 1 - R_V = \frac{1}{3}$.

annihilation operators,

$$\text{PDBS}_0 : \begin{cases} \mathbf{a}_H^\dagger \rightarrow \mathbf{a}_H^\dagger \\ \mathbf{a}_V^\dagger \rightarrow \sqrt{\frac{1}{3}}\mathbf{a}_V^\dagger + i\sqrt{\frac{2}{3}}\mathbf{b}_V^\dagger \\ \mathbf{b}_H^\dagger \rightarrow \mathbf{b}_H^\dagger \\ \mathbf{b}_V^\dagger \rightarrow \sqrt{\frac{1}{3}}\mathbf{b}_V^\dagger + i\sqrt{\frac{2}{3}}\mathbf{a}_V^\dagger \end{cases} \quad (2.1a)$$

$$\text{PDBS}_a : \begin{cases} \mathbf{a}_H^\dagger \rightarrow \sqrt{\frac{1}{3}}\mathbf{a}_H^\dagger + i\sqrt{\frac{2}{3}}\mathbf{c}_H^\dagger \\ \mathbf{a}_V^\dagger \rightarrow \mathbf{a}_V^\dagger \end{cases} \quad (2.1b)$$

$$\text{PDBS}_b : \begin{cases} \mathbf{b}_H^\dagger \rightarrow \sqrt{\frac{1}{3}}\mathbf{b}_H^\dagger + i\sqrt{\frac{2}{3}}\mathbf{d}_H^\dagger \\ \mathbf{b}_V^\dagger \rightarrow \mathbf{b}_V^\dagger \end{cases}, \quad (2.1c)$$

where c and d are auxiliary loss modes which are not of any further importance.

For an initial input of two horizontally polarized photons, the output of the gate, after neglecting contributions with two photons in the same mode, is given by

$$\mathbf{a}_H^\dagger \mathbf{b}_H^\dagger \xrightarrow{\text{PDBS}_0} \mathbf{a}_H^\dagger \mathbf{b}_H^\dagger \xrightarrow{\text{PDBS}_{a,b}} \sqrt{\frac{1}{3}}\mathbf{a}_H^\dagger \sqrt{\frac{1}{3}}\mathbf{b}_H^\dagger = \sqrt{\frac{1}{9}}\mathbf{a}_H^\dagger \mathbf{b}_H^\dagger. \quad (2.2)$$

It equals the input besides an overall amplitude expressing that a coincidence event occurs with probability $\frac{1}{9}$. No interference takes place in this case. The perfect transmission for horizontal polarization ensures that the output mode of each photon provides unambiguous information about its input mode. The same is true for the input of one horizontally and one vertically polarized photon. As the horizontally polarized photon is transmitted at PDBS_0 , a coincidence event is detected only if the vertically polarized photon is transmitted as well

$$\mathbf{a}_H^\dagger \mathbf{b}_V^\dagger \xrightarrow{\text{PDBS}_0} \mathbf{a}_H^\dagger \sqrt{\frac{1}{3}}\mathbf{b}_V^\dagger \xrightarrow{\text{PDBS}_{a,b}} \sqrt{\frac{1}{3}}\mathbf{a}_H^\dagger \sqrt{\frac{1}{3}}\mathbf{b}_V^\dagger = \sqrt{\frac{1}{9}}\mathbf{a}_H^\dagger \mathbf{b}_V^\dagger, \quad (2.3a)$$

$$\mathbf{a}_V^\dagger \mathbf{b}_H^\dagger \xrightarrow{\text{PDBS}_0} \sqrt{\frac{1}{3}}\mathbf{a}_V^\dagger \mathbf{b}_H^\dagger \xrightarrow{\text{PDBS}_{a,b}} \sqrt{\frac{1}{3}}\mathbf{a}_V^\dagger \sqrt{\frac{1}{3}}\mathbf{b}_H^\dagger = \sqrt{\frac{1}{9}}\mathbf{a}_V^\dagger \mathbf{b}_H^\dagger, \quad (2.3b)$$

which happens again with probability $\frac{1}{9}$. The decisive difference appears for two vertically polarized photons entering the gate. Then, *two* possibilities, namely both photons being transmitted and both being reflected, can lead to a coincidence detection. If the photons are not distinguishable in any other degree of freedom, the output mode of each photon contains no information about the input mode where the photon was coming from and both possibilities interfere,

$$\mathbf{a}_V^\dagger \mathbf{b}_V^\dagger \xrightarrow{\text{PDBS}_0} \sqrt{\frac{1}{3}}\mathbf{a}_V^\dagger \sqrt{\frac{1}{3}}\mathbf{b}_V^\dagger + i\sqrt{\frac{2}{3}}\mathbf{a}_V^\dagger i\sqrt{\frac{2}{3}}\mathbf{b}_V^\dagger \xrightarrow{\text{PDBS}_{a,b}} \frac{1}{3}\mathbf{a}_V^\dagger \mathbf{b}_V^\dagger - \frac{2}{3}\mathbf{a}_V^\dagger \mathbf{b}_V^\dagger = -\sqrt{\frac{1}{9}}\mathbf{a}_V^\dagger \mathbf{b}_V^\dagger. \quad (2.4)$$

As can be seen, this interference causes the desired phase shift of π when both qubits are in the logical state $|1\rangle \hat{=} |V\rangle$. The overall success probability for this to happen is $\frac{1}{9}$. As explained in Sec. 1.3.1, the probabilistic nature of the setup is a consequence of the usage of purely linear optical elements.

2.1.2 A model for gate characterization

Working with real components naturally implies deviations from the ideal theoretical gate operation. The main source of error in the scheme is deficient interference of the photons at the PDBS₀. As can be seen from Eqn. (2.4), if the photons do not interfere, the probability to obtain a coincidence event is enhanced for the input $\mathbf{a}_V^\dagger \mathbf{b}_V^\dagger$. In this case not the amplitudes but the probabilities for both possibilities add up, resulting in a coincidence probability \wp_{vv} of

$$\wp_{vv} = \left(\frac{1}{3}\right)^2 + \left(-\frac{2}{3}\right)^2 = \frac{5}{9}, \quad (2.5)$$

which is by a factor of five higher than for the other input states.

Thus, non-perfect interference leads to input state dependent noise, a fact that will be relevant and visible in the experimental data.

A quantitative description thereof can be modeled in the following way: According to Eqn. (2.2) – Eqn. (2.4), the experimental phase gate operation $\text{CPHASE}_{\text{exp}}$ relying on the conditional detection of one photon in each mode can be decomposed as a sum of two matrices, \mathbf{M}_{tt} and \mathbf{M}_{rr} , which describe the process of transmitting or reflecting both photons,

$$\text{CPHASE}_{\text{exp}} = \mathbf{M}_{tt} + \mathbf{M}_{rr}, \quad (2.6)$$

with

$$\mathbf{M}_{tt} = \begin{pmatrix} \frac{1}{3} & 0 & 0 & 0 \\ 0 & \frac{1}{3} & 0 & 0 \\ 0 & 0 & \frac{1}{3} & 0 \\ 0 & 0 & 0 & \frac{1}{3} \end{pmatrix} \quad \text{and} \quad \mathbf{M}_{rr} = \begin{pmatrix} 0 & 0 & 0 & 0 \\ 0 & 0 & 0 & 0 \\ 0 & 0 & 0 & 0 \\ 0 & 0 & 0 & -\frac{2}{3} \end{pmatrix}. \quad (2.7)$$

If interference occurs only with a certain probability described by the parameter \mathcal{Q}' , these matrices act partly incoherent on an input state \wp , and it holds that

$$\begin{aligned} \text{CPHASE}_{\text{exp}} \wp \text{CPHASE}_{\text{exp}}^\dagger &= \mathcal{Q}'(\mathbf{M}_{tt} + \mathbf{M}_{rr}) \wp (\mathbf{M}_{tt} + \mathbf{M}_{rr})^\dagger \\ &+ (1 - \mathcal{Q}')(\mathbf{M}_{tt} \wp \mathbf{M}_{tt}^\dagger + \mathbf{M}_{rr} \wp \mathbf{M}_{rr}^\dagger). \end{aligned} \quad (2.8)$$

As can be see from Eqn. (2.8) for a non-vanishing incoherent contribution the experimental process is not trace preserving anymore as the output probability $\text{tr}(\text{CPHASE}_{\text{exp}} \wp \text{CPHASE}_{\text{exp}}^\dagger)$ becomes input state dependent. Furthermore, mixing can occur, i.e., pure states are not mapped onto pure states anymore.

Another fact that causes deviations from a perfect mode of operation is that the real transmission and reflection coefficients of PDBS₀ and PDBS_{a,b} do not match the ideal values. A detailed calculation assuming them to be variable shows that they have to fulfill a couple of conditions in order to correctly achieve the **CPHASE** action. (A detailed derivation of these conditions can be found in [121]).

First, the reflectivity of PDBS₀ should be zero for both modes,

$$\sqrt{R_H^{0,a}} = 0 = \sqrt{R_H^{0,b}}. \quad (2.9)$$

Second, for vertically polarization the reflectivity should be twice the transmissivity,

$$\sqrt{R_V^{0,a}} \sqrt{R_V^{0,b}} = 2\sqrt{T_V^{0,a}} \sqrt{T_V^{0,b}}. \quad (2.10)$$

Third, in both modes the overall transmission caused by PDBS_0 and $\text{PDBS}_{a,b}$ together should be the same for horizontal and vertical polarization,

$$\sqrt{T_H^{0,a}} \sqrt{T_H^a} = \sqrt{T_V^{0,a}} \sqrt{T_V^a} \quad \text{and} \quad \sqrt{T_H^{0,b}} \sqrt{T_H^b} = \sqrt{T_V^{0,b}} \sqrt{T_V^b}. \quad (2.11)$$

Under the assumption of a loss-free and symmetric PDBS_0 these conditions lead to the transmission and reflection coefficients described in the previous section.

2.1.3 Experimental results

In the following, the experimentally realized gate shall be characterized by so-called quantum process tomography (QPT) [123–125]. In general, any linear process can be characterized by performing QPT. Thereby, the process is represented by a superoperator $\hat{\mathbf{E}}$, which is decomposed in a linear combination of a basis of unitary transformations \mathbf{E}_i , with

$$\hat{\mathbf{E}}(\rho_{\text{in}}) = \rho_{\text{out}} = \sum_{ij} \chi_{ij} \mathbf{E}_i \rho_{\text{in}} \mathbf{E}_j^\dagger, \quad (2.12)$$

where the matrix χ completely describes the process. In order to obtain all components χ_{ij} , the normalized output density matrices ρ_{out}^k for a tomographic set of, usually separable, input states $\{\rho_{\text{in}}^k\}$ are measured.

Here, the tomographic set is chosen to be the set of the 16 states $\{|lm\rangle\langle lm|\}$ with $l, m \in \{H, V, +, L\}$. These states are prepared by feeding the first order emission of type II non-collinear SPDC into the phase gate and adjusting the photon's polarization through additional polarizers in the input modes a and b . The resulting output density matrices are reconstructed by quantum state tomography (QST) [22, 121, 126]. In QST a density matrix is decomposed in a sum of local (Pauli) operators which can be measured in the PA. The explicit way the QST is performed in the experiments presented here can be found in [121]. Due to the non-trace preserving character of the experimental gate, Eqn. (2.12) has to be adjusted such that

$$\rho_{\text{out}}^k = \frac{\hat{\mathbf{E}}(\rho_{\text{in}}^k)}{\text{tr}(\hat{\mathbf{E}}(\rho_{\text{in}}^k))} \Rightarrow \hat{\mathbf{E}}(\rho_{\text{in}}^k) = \text{tr}(\hat{\mathbf{E}}(\rho_{\text{in}}^k)) \rho_{\text{out}}^k, \quad (2.13)$$

to account for the fact that every output state ρ_{out}^k occurs with probability $\text{tr}(\hat{\mathbf{E}}(\rho_{\text{in}}^k))$. These probabilities are estimated from the diagonal entries of all measured output density matrices and χ_{ij} can be evaluated via Eqn. (2.12) and Eqn. (2.13). The result, χ_{exp} , is shown in Fig. 2.2(b)². For better comparison, the QPT matrix of the ideal CPHASE gate, χ_{th} , is shown in Fig. 2.2(a). In the representation the \mathbf{E}_i are taken as the Pauli operators with

$$\mathbf{E}_1 = \mathbb{1} \otimes \mathbb{1}, \mathbf{E}_2 = \mathbb{1} \otimes \sigma_x, \mathbf{E}_3 = -i \mathbb{1} \otimes \sigma_y, \mathbf{E}_4 = \mathbb{1} \otimes \sigma_z, \mathbf{E}_5 = \sigma_x \otimes \mathbb{1}, \dots, \mathbf{E}_{16} = \sigma_z \otimes \sigma_z, \quad (2.14)$$

and ideally

$$\begin{aligned} \text{CPHASE}_{\text{exp}} &= \frac{1}{6} (\mathbb{1} \otimes \mathbb{1} + \mathbb{1} \otimes \sigma_z + \sigma_z \otimes \mathbb{1} - \sigma_z \otimes \sigma_z) \\ &= \frac{1}{6} (\mathbf{E}_1 + \mathbf{E}_4 + \mathbf{E}_{13} - \mathbf{E}_{16}). \end{aligned} \quad (2.15)$$

²Only the real parts are shown since the imaginary parts are with an average of 0.000 ± 0.002 close to zero.

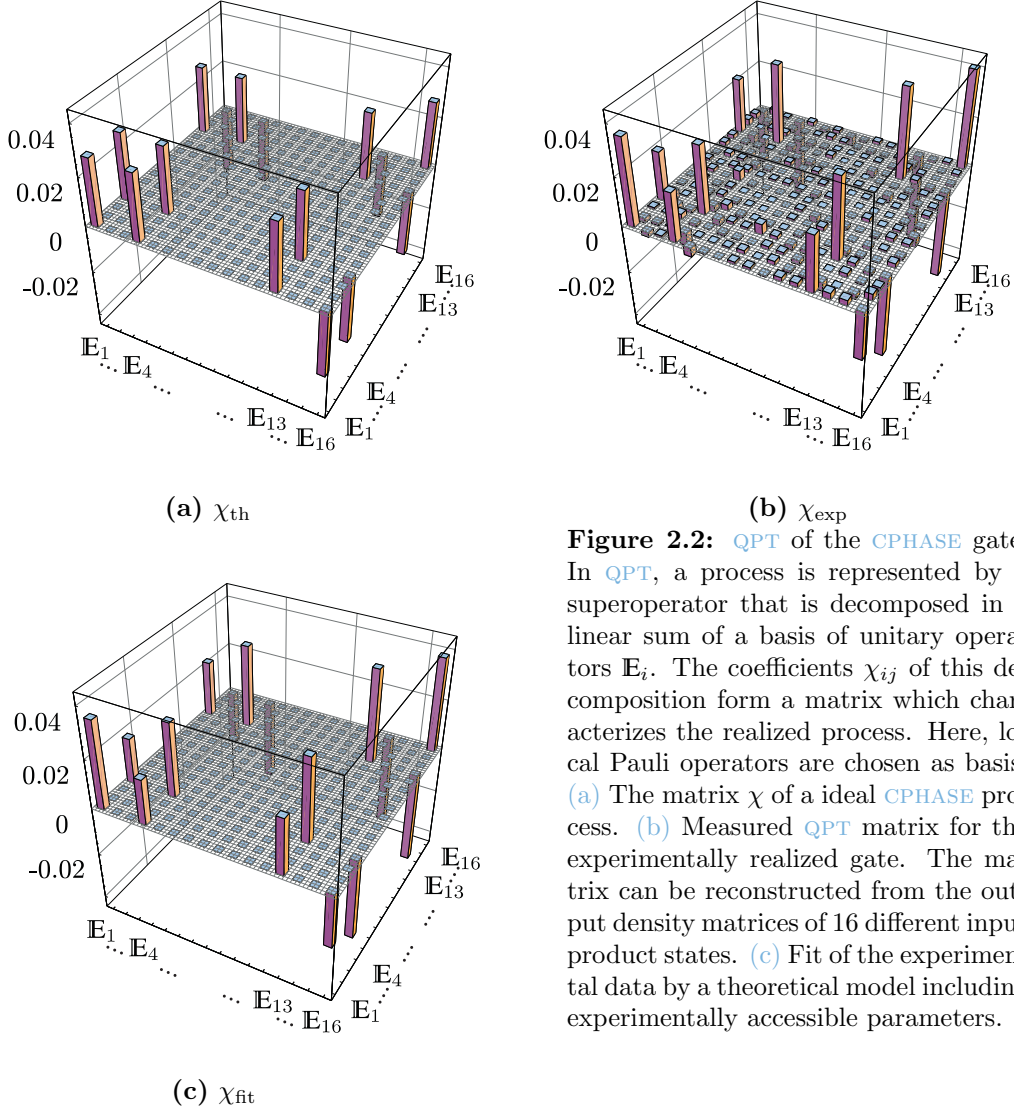


Figure 2.2: QPT of the CPHASE gate. In QPT, a process is represented by a superoperator that is decomposed in a linear sum of a basis of unitary operators \mathbb{E}_i . The coefficients χ_{ij} of this decomposition form a matrix which characterizes the realized process. Here, local Pauli operators are chosen as basis. (a) The matrix χ of an ideal CPHASE process. (b) Measured QPT matrix for the experimentally realized gate. The matrix can be reconstructed from the output density matrices of 16 different input product states. (c) Fit of the experimental data by a theoretical model including experimentally accessible parameters.

Comparing Fig. 2.2(a) and Fig. 2.2(b) reveals that the characteristic peaks of the theoretical matrix are reproduced in the experimental data. However, in the latter the off-diagonal elements are lowered indicating a lack of coherence in the process. A quantitative measure for the match of the two matrices is the process fidelity,

$$F_p = \frac{\text{tr}(\chi_{th}\chi_{exp})}{\text{tr}(\chi_{th})\text{tr}(\chi_{exp})}, \quad (2.16)$$

which yields $F_p = 0.816$. A problem of χ_{exp} , which is known to happen occasionally in QPT, is that it has non-physical negative eigenvalues due to Poissonian counting statistics. Usually, to circumvent this flaw, a maximum likelihood approach is used, in which a physical matrix is fitted to the experimental data. Yet, as the process is not unknown, it shall be described by a theoretical model including the experimentally accessible parameters introduced in the previous section. For simplicity, all transmissivities as well as reflectivities are assumed to be

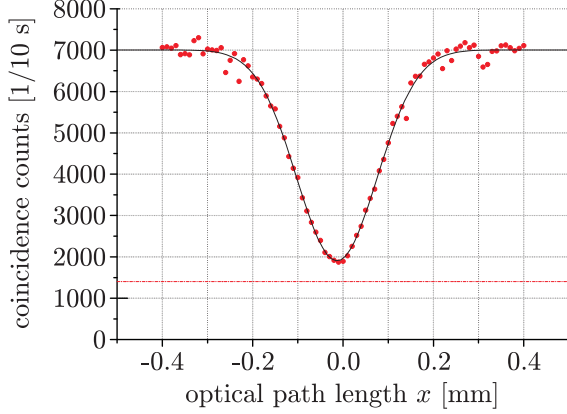


Figure 2.3: HOM interference measurement. For an input of two vertically polarized photons the optical path length is varied in mode a . For a difference in the path length that is significantly bigger than the coherence length of the photons no interference occurs as the photons are distinguishable by the time of arrival at the detectors. If the optical path lengths in both modes are equal the photons interfere and the coincidence count rate should ideally drop by a factor of 5.

equal for both modes and $\sqrt{R_H^0} \stackrel{!}{=} 0$. Consequently, a superoperator containing \mathcal{Q}' and the remaining reflection and transmission coefficients as free parameters is fitted to χ_{exp} resulting in χ_{fit} displayed in Fig. 2.2(c). The process fidelity for the fit is $F_p = 0.846$, a value that is comparable with the one for χ_{exp} . The noise occurring in χ_{exp} for the unexpected entries is not reproduced by χ_{fit} as it was not modeled. In order to judge how well the fit actually agrees with the experimental data, the values of the *fitted* parameters can be compared with their independently *measured* ones. This is the big advantage of using physically accessible parameters in the model compared to the standard maximum likelihood technique.

For experimentally quantifying the indistinguishability of the photons arriving at PDBS₀ and for the determination of \mathcal{Q}' , a Hong, Ou, Mandel (HOM) interference experiment is performed [127]. Prior to the detection the photons are spectrally selected by interference filters with a Gaussian transmission profile of width $\Delta\lambda = 2$ nm. Thus, in good approximation the photons' complex degree of temporal coherence can be assumed to be Gaussian as well, and the number of detected coincidences N_c is given as

$$N_c = C((T_{H/V}^0)^2 + (R_{H/V}^0)^2) \left(1 - \mathcal{Q}' \frac{2T_{H/V}^0 R_{H/V}^0}{(T_{H/V}^0)^2 + (R_{H/V}^0)^2} \exp\left(-\frac{x - x_0}{2\Delta^2}\right) \right). \quad (2.17)$$

Here, $x - x_0$ is the difference in the optical path length, x_0 the point for which the paths are equal, and $C((T_{H/V}^0)^2 + (R_{H/V}^0)^2)$ is the number of coincidences for a path length difference that significantly exceeds the coherence length Δ of the photons. Ideally ($\mathcal{Q}' = 1$), for $x - x_0 = 0$ the countrate for VV coincidences should drop by a factor of 5 (cp. also Eqn. (2.4) and Eqn. (2.5)).

Fig. 2.3 shows a measurement of this typical dip in the coincidence countrate versus the change in the optical path length of mode a . A fit of the data using Eqn. (2.17) with $C((T_{H/V}^0)^2 + (R_{H/V}^0)^2)$, x_0 , Δ , \mathcal{Q}' as parameters and assuming the ideal values for $T_{H,V}^0$ and $R_{H,V}^0$ allows the estimation of the interference quality to be $\mathcal{Q}' = 0.910 \pm 0.009$. In comparison, the fit of χ_{exp} yields a value of $\mathcal{Q}' = 0.904$ which is in good agreement.

The fitting procedure of χ_{exp} provides also estimations for the real values of the transmission and reflection coefficients. A ratio of $R_V^0/T_V^0 = 2.035$ is found which agrees well with the value of 2.019 ± 0.003 directly measured during the alignment of PDBS₀ (see [128]). The required equality for the overall transmission of PDBS₀ and PDBS _{a,b} for horizontal and vertical polarization is well reproduced in mode a , $\sqrt{T_H^{0,a}} \sqrt{T_H^a} = 1.00 \sqrt{T_V^{0,a}} \sqrt{T_V^a}$, whereas for mode b

a deviation, $\sqrt{T_H^{0,b}} \sqrt{T_H^b} = 1.16 \sqrt{T_V^{0,b}} \sqrt{T_V^b}$, occurs whose origin cannot be clearly identified. However, the value is consistent with the probability $\wp_{HV} = \text{tr} \left(\hat{\mathbb{E}}(|HV\rangle\langle HV|) \right) = 0.136$ derived from the diagonal entries of the measured output density matrices. Although the characteristics of PDBS_0 and $\text{PDBS}_{a,b}$ are not ideal, a more detailed study further varying the parameters of χ_{fit} proves that the main source of errors in the experimental gate is indeed the partial distinguishability of the photons leading to a lack of coherence in the interference [121].

Recapitulatory can be stated, that the fitted superoperator reproduces well the experimentally realized gate. This property makes it a useful tool for the estimation of the gate's performance in diverse applications. Some of them are presented in Chap. 3.

2.2 One setup for the observation of a whole family of states

The previous section introduced a linear optics setup which implements a two-qubit logic gate. Usually in linear optics quantum information processing the used linear optics network is especially tailored for the state to be observed. Here, a new scheme is presented which enables the observation of a whole family of states in a single setup by the tuning of one experimental parameter. The setup relies on the interference of the second order emission of type II non-collinear SPDC at a polarizing beam splitter. Prior to the interference the polarization of the photons in one mode is rotated by a HWP. Depending on its angular setting any weighted superposition of a GHZ state and a product of two Bell states can be observed. Thus, the output of the network parameterized by the weighting describes a family of states which is a particularly interesting subgroup of the generic family of states introduced in Eqn. (1.43). As already mentioned in Sec. 1.2.2, the members of this generic class exhibit many useful properties and play an important role in several applications of quantum information. Consequently, the possibility to generate a multitude of such states within a *single* experimental arrangement is of great advantage as it makes the supply of many different state sources needless.

In the following the linear optics setup is described and the explicit form of the family of output states is derived. After a discussion of general properties, common to the whole family, particular interesting members are discussed in detail. The experimental results of their observation are presented followed by a short discussion of the properties of each individual state with regard to applications. The explicit demonstration of their employment for a special task is postponed to Chap. 5 where the states are shown to be useful for the solution of a multi-agent quantum game.

2.2.1 The theoretical concept and the class of states

As stated above, the starting point for the observation of the states is the second order emission of non-collinear type II SPDC yielding four photons in two spatial modes a and c (cp. Eqn. (1.60)). These photons are overlapped on a PBS and afterwards symmetrically split up into four spatial modes, a, b, c, d , by two polarization independent beam splitters (BSS). Prior to the second order interference at the PBS the polarization of two of the photons is rotated by a HWP in mode c (see Fig. 2.4). Under the condition of detecting one photon in the PA of

each spatial mode the following state is observed,

$$|\Psi(\alpha)\rangle = \alpha |\text{GHZ}\rangle_{abcd} + \sqrt{1-\alpha^2} (|\psi^+\rangle_{ab} \otimes |\psi^+\rangle_{cd}), \quad (2.18)$$

with

$$|\text{GHZ}\rangle \equiv \frac{1}{\sqrt{2}} (|HHHH\rangle + |VVVV\rangle), \quad (2.19)$$

and $\alpha \in [-1, -\sqrt{\frac{2}{3}}] \cup [0, 1]$. This shall be derived in detail in the following by considering the action of each optical element. To this end, again the transformation of the bosonic creation and annihilation operators is used.

The initial state fed into the network reads

$$|\text{in}\rangle = \frac{1}{2\sqrt{3}} \left(\mathbf{a}_H^{\dagger 2} \mathbf{c}_V^{\dagger 2} + 2 \mathbf{a}_H^{\dagger} \mathbf{a}_V^{\dagger} \mathbf{c}_H^{\dagger} \mathbf{c}_V^{\dagger} + \mathbf{a}_V^{\dagger 2} \mathbf{c}_H^{\dagger 2} \right) |0\rangle. \quad (2.20)$$

It is transformed by the HWP(γ) in mode c into the intermediate state

$$\begin{aligned} |\text{mid}\rangle_1 = \frac{1}{2\sqrt{3}} & \left(\mathbf{a}_H^{\dagger 2} \left(\sin(2\gamma) \mathbf{c}_H^{\dagger} - \cos(2\gamma) \mathbf{c}_V^{\dagger} \right)^2 \right. \\ & + 2 \mathbf{a}_H^{\dagger} \mathbf{a}_V^{\dagger} \left(\cos(2\gamma) \mathbf{c}_H^{\dagger} + \sin(2\gamma) \mathbf{c}_V^{\dagger} \right) \left(\sin(2\gamma) \mathbf{c}_H^{\dagger} - \cos(2\gamma) \mathbf{c}_V^{\dagger} \right) \\ & \left. + \mathbf{a}_V^{\dagger 2} \left(\cos(2\gamma) \mathbf{c}_H^{\dagger} + \sin(2\gamma) \mathbf{c}_V^{\dagger} \right)^2 \right) |0\rangle, \quad (2.21) \end{aligned}$$

and the modes subsequently interfere at the PBS,

$$\text{PBS} : \begin{cases} \mathbf{a}_H^{\dagger} \rightarrow \mathbf{a}_H^{\dagger} \\ \mathbf{a}_V^{\dagger} \rightarrow i\mathbf{c}_V^{\dagger} \\ \mathbf{c}_H^{\dagger} \rightarrow \mathbf{c}_H^{\dagger} \\ \mathbf{c}_V^{\dagger} \rightarrow i\mathbf{a}_V^{\dagger} \end{cases}. \quad (2.22)$$

The resulting state behind the PBS will contain terms with more or less than two photons in one mode. However, as the registration of these contributions is ruled out by the conditional detection, they are not considered any further. Instead, the terms with exactly two photons in each of the two output modes of the PBS are given as

$$|\text{mid}\rangle_2 = \frac{1}{2\sqrt{3}} \left(\sin^2(2\gamma) (\mathbf{a}_H^{\dagger 2} \mathbf{c}_H^{\dagger 2} + \mathbf{a}_V^{\dagger 2} \mathbf{c}_V^{\dagger 2}) + 2 \cos(4\gamma) \mathbf{a}_H^{\dagger} \mathbf{a}_V^{\dagger} \mathbf{c}_H^{\dagger} \mathbf{c}_V^{\dagger} \right) |0\rangle. \quad (2.23)$$

This state is further processed by symmetrically splitting the photons with two beam splitters, BS_a, BS_c, into four modes according to

$$\text{BS}_a : \begin{cases} \mathbf{a}_H^{\dagger} \rightarrow \frac{1}{\sqrt{2}} \left(\mathbf{a}_H^{\dagger} + i\mathbf{b}_H^{\dagger} \right) \\ \mathbf{a}_V^{\dagger} \rightarrow \frac{1}{\sqrt{2}} \left(\mathbf{a}_V^{\dagger} + i\mathbf{b}_V^{\dagger} \right) \end{cases} \quad (2.24a)$$

$$\text{BS}_c : \begin{cases} \mathbf{c}_H^{\dagger} \rightarrow \frac{1}{\sqrt{2}} \left(\mathbf{c}_H^{\dagger} + i\mathbf{d}_H^{\dagger} \right) \\ \mathbf{c}_V^{\dagger} \rightarrow \frac{1}{\sqrt{2}} \left(\mathbf{c}_V^{\dagger} + i\mathbf{d}_V^{\dagger} \right). \end{cases} \quad (2.24b)$$

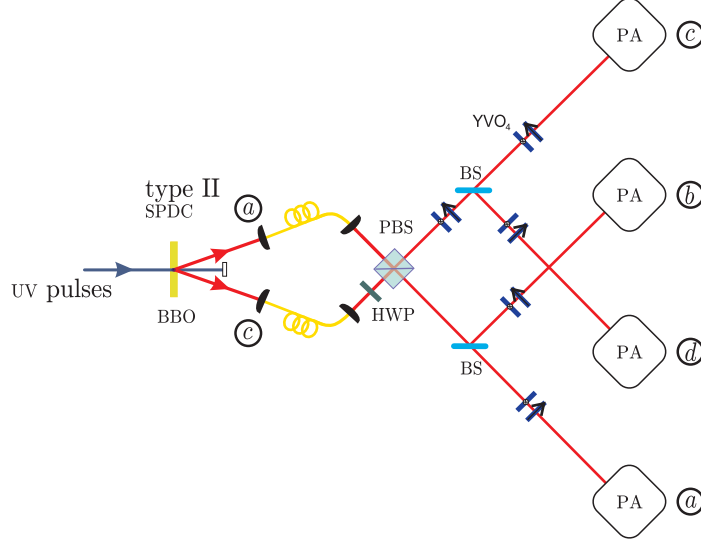


Figure 2.4: Setup for the observation of a whole family of states. The second order emission of non-collinear type II SPDC, yielding two horizontally and two vertically polarized photons in spatial modes a and c is overlapped at a PBS. Prior to the overlap the polarization of the photons in mode c is rotated by a HWP. After the interference at the PBS, the photons are symmetrically split in four spatial modes a, b, c, d . Under the condition of detecting one photon in the PA in each output mode the desired states are observed. The family of states is parameterized by the angular setting of the HWP. Relative phases between horizontal and vertical polarization of the photons can be adjusted by pairs of birefringent YVO_4 crystals.

Under the condition that the photons distribute at the BSs such that one is found in each spatial mode the final desired output state is

$$|\text{out}\rangle = -\frac{1}{4\sqrt{3}} \left(2 \sin^2(2\gamma) (a_H^\dagger b_H^\dagger c_H^\dagger d_H^\dagger + a_V^\dagger b_V^\dagger c_V^\dagger d_V^\dagger) \right. \\ \left. + \cos(4\gamma) (a_H^\dagger b_V^\dagger c_H^\dagger d_V^\dagger + a_H^\dagger b_V^\dagger c_V^\dagger d_H^\dagger + a_V^\dagger b_H^\dagger c_H^\dagger d_V^\dagger + a_V^\dagger b_H^\dagger c_V^\dagger d_H^\dagger) \right) |0\rangle. \quad (2.25)$$

This state is not normalized expressing the fact that the linear optics network works only with a certain probability. Taking this into account, it can be concluded that the setup leads to the observation of the (normalized) state³

$$|\Psi(\gamma)\rangle = \frac{2 \sin^2(2\gamma)}{\sqrt{5 - 4 \cos(4\gamma) + 3 \cos(8\gamma)}} (|HHHH\rangle + |VVVV\rangle) \\ + \frac{\cos(4\gamma)}{\sqrt{5 - 4 \cos(4\gamma) + 3 \cos(8\gamma)}} (|HVHV\rangle + |HVVH\rangle + |VHHV\rangle + |VHVH\rangle) \quad (2.26)$$

with probability

$$p_\Psi(\gamma) = \langle \text{out} | \text{out} \rangle = \frac{1}{48} (5 - 4 \cos(4\gamma) + 3 \cos(8\gamma)). \quad (2.27)$$

³The global phase of -1 can be omitted.

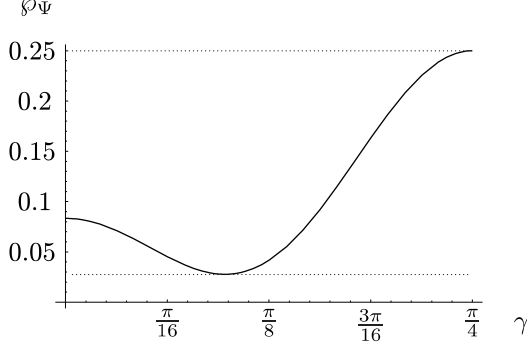


Figure 2.5: Probability that the photons leave the network one in each output mode, which is the condition to observe the state $|\Psi(\alpha)\rangle$. The probability $\wp_{\Psi}(\gamma)$ for this to happen depends on the angular setting γ of the **HWP** in front of the **PBS**. It reaches a maximum of 0.25 for $\gamma = 45^\circ$ and a minimum of ≈ 0.03 for $\gamma \approx 17.63^\circ$.

A plot of $\wp_{\Psi}(\gamma)$ is shown in Fig. 2.5. The probability that one photon is found in each output mode of the network depends obviously on γ , i.e., some states are produced more efficiently than others. It reaches a maximum of 0.25 for $\gamma = 45^\circ$ and a minimum of ≈ 0.03 for $\gamma \approx 17.63^\circ$.

Comparing Eqn. (2.26) and Eqn. (2.18) reveals the relation between the angle γ and the amplitude α ,

$$|\alpha| = \frac{2\sqrt{2}\sin^2(2\gamma)}{\sqrt{5 - 4\cos(4\gamma) + 3\cos(8\gamma)}} \quad \text{and} \quad \text{sgn}(\alpha) = \begin{cases} +1, & \text{for } 0 \leq \gamma \leq \frac{\pi}{8} \\ -1, & \text{for } \frac{\pi}{8} < \gamma \leq \frac{\pi}{4} \end{cases} \quad (2.28)$$

for $\gamma \in [0, \frac{\pi}{4}]$. Thus, by rotating the **HWP** prior to the interference at the **PBS** indeed the subgroup of G_{abcd} (see Eqn. (1.43)) denoted by Eqn. (2.18) can be observed. Precisely, this subgroup is defined by

$$\mathbf{a} = \mathbf{d} = \frac{2\sin^2(2\gamma)}{\sqrt{5 - 4\cos(4\gamma) + 3\cos(8\gamma)}} \quad (2.29a)$$

$$\mathbf{b} = \left| \frac{2\cos(4\gamma)}{\sqrt{5 - 4\cos(4\gamma) + 3\cos(8\gamma)}} \right| \quad (2.29b)$$

$$\mathbf{c} = 0. \quad (2.29c)$$

As \mathbf{a} , \mathbf{b} , \mathbf{c} , \mathbf{d} are by definition complex numbers with *non-negative* real part, the minus sign occurring in the function of Eqn. (2.29b) for $\gamma > \frac{\pi}{8}$ has to be absorbed in local unitaries.

For some reasons which will become clear later on, it is desirable to modify the setup in a way that it yields the state

$$|\Psi'(\alpha)\rangle = \alpha|\text{GHZ}'\rangle_{abcd} + \sqrt{1 - \alpha^2}(|\psi^+\rangle_{ab} \otimes |\psi^+\rangle_{cd}), \quad (2.30)$$

with

$$|\text{GHZ}'\rangle \equiv \frac{1}{\sqrt{2}}(|\text{HHVV}\rangle + |\text{VVHH}\rangle). \quad (2.31)$$

$|\Psi'(\alpha)\rangle$ and $|\Psi(\alpha)\rangle$ are, however, equal up to a local unitary operation. They differ in a bit flip, i.e., σ_x , on qubits a and b (or c and d) which can be implemented by inserting an additional **HWP** at an angle of $\frac{\pi}{4}$ in mode a (or c) right behind the **PBS**. As this additional element is not essential for the principal functioning of the linear optical network it was omitted in the above considerations. Accounted for, it would alter Eqn. (2.23) and Eqn. (2.25) just by exchanging

B_{-4}	$(1 - \alpha^2)$:	IIXX, IYY, XXII, YYII
B_{-3}	$(2\alpha^2 - 1)$:	IIZZ, ZZII
B_{-2}	$(\alpha\sqrt{2 - 2\alpha^2})$:	IXIX, IXXI, IYIY, IYYI, XIIX, XIXI, YIIY, YIYI
B_{-1}	$(-\alpha^2)$:	IZIZ, IZZI, ZIIZ, ZIZI
B_0	(1) :	IIII, XXXX, YYYY, ZZZZ
B_{+1}	(α^2) :	XYXY, XYYX, YXXY, YXYX
B_{+2}	$(-\alpha\sqrt{2 - 2\alpha^2})$:	XZXZ, XZZX, YZYZ, YZZY, ZXXZ, ZXZX, ZYYZ, ZYZY
B_{+3}	$(1 - 2\alpha^2)$:	XXYY, YYXX
B_{+4}	$(\alpha^2 - 1)$:	XXZZ, YYZZ, ZZXX, ZZYY

Table 2.1: Correlations of $|\Psi'(\alpha)\rangle$. The family of states $|\Psi'(\alpha)\rangle$ has at most 40 non-zero values of T_{ijkl} out of which 21 describe real four-qubit correlations. The correlations are all polynomials of α , and according to the explicit dependence, they form blocks, B_i .

\mathbf{a}_H^\dagger for \mathbf{a}_V^\dagger and vice versa. Naturally, $|\Psi'(\alpha)\rangle$ must form the same subgroup of G_{abcd} with identical conditions for \mathbf{a} , \mathbf{b} , \mathbf{c} , \mathbf{d} in Eqn. (2.29a) – Eqn. (2.29c). States of the structure of $|\Psi'(\alpha)\rangle$ are experimentally observed in the following, while $|\Psi(\alpha)\rangle$ is used in the experiment described in Chap. 5.

Before proceeding with the presentation of the experimental results, some general properties of this subgroup with respect to measurement correlations shall be discussed in the next section. The properties are not influenced in a relevant way by the local bit flips, but will be indicated if necessary.

2.2.2 Interesting states in terms of correlations

The states represented by the form of Eqn. (2.30) (and Eqn. (2.18)) can be conveniently characterized by their correlation tensor T_{ijkl} , with

$$|\Psi'(\alpha)\rangle\langle\Psi'(\alpha)| = \frac{1}{16} \sum_{ijkl} T_{ijkl} (\sigma_i \otimes \sigma_j \otimes \sigma_k \otimes \sigma_l), \quad (2.32)$$

where $i, j, k, l \in \{0, x, y, z\}$, $\sigma_0 \equiv \mathbb{1}$ and

$$T_{ijkl} \equiv \text{tr} \left(|\Psi'(\alpha)\rangle\langle\Psi'(\alpha)| \cdot (\sigma_i \otimes \sigma_j \otimes \sigma_k \otimes \sigma_l) \right). \quad (2.33)$$

Straight forward calculation shows that T_{ijkl} has at maximum 40 non-zero entries out of which 21 do not contain σ_0 and thus describe real four-qubit correlations. The entries are all polynomial in α and summarized in Tab. 2.1. Here and in the following, T_{ijkl} or the corresponding measurement settings will be often shortly denoted as "IJKL", such that, e.g., $IXYZ \hat{=} T_{0xyz}$. As can be seen the correlations are grouped in blocks, B_i , each of which exhibits the same dependence on α . These blocks become slightly reshuffled when considering $|\Psi(\alpha)\rangle$ instead of $|\Psi'(\alpha)\rangle$. The unitary transformation $(\mathbb{1} \otimes \mathbb{1} \otimes \sigma_x \otimes \sigma_x)$ relating these two states

leads to a minus sign (see Eqn. (1.21)) for particular terms when applied to the correlation operators, $(\mathbb{1} \otimes \mathbb{1} \otimes \sigma_x \otimes \sigma_x)^\dagger \cdot (\sigma_i \otimes \sigma_j \otimes \sigma_k \otimes \sigma_l) \cdot (\mathbb{1} \otimes \mathbb{1} \otimes \sigma_x \otimes \sigma_x)$,

$$\begin{aligned}
(\alpha\sqrt{2-2\alpha^2}): & \text{ IYIY, IYYI, YIHY, YIYI} & \longrightarrow & -(\alpha\sqrt{2-2\alpha^2}) \\
(-\alpha^2): & \text{ IZIZ, IZZI, ZIHZ, ZIZI} & \longrightarrow & +(\alpha^2) \\
(\alpha^2): & \text{ XYXY, XYYX, YXXY, YXYX} & \longrightarrow & -(\alpha^2) \\
(-\alpha\sqrt{2-2\alpha^2}): & \text{ XZXZ, XZZX, ZXXZ, ZXZX} & \longrightarrow & +(\alpha\sqrt{2-2\alpha^2}).
\end{aligned} \tag{2.34}$$

However, for many applications the absolute value of the correlations is important rather than their sign. The former is displayed in Fig. 2.6.

For particular values of α the polynomials intersect. The crossing points indicate distinguished states which have the property that two or more blocks of correlations take the same value. From this point of view these states can be considered as being interesting and possibly promising candidates for different applications. Indeed, well known four-qubit entangled states, such as the GHZ state ($\alpha = 1$) [62] and the state directly obtained from non-collinear SPDC ($\alpha = \sqrt{\frac{2}{3}}$) (see page 36 and [100]), correspond to the crossing points ($|\mathbf{B}_{+2}| = |\mathbf{B}_{+4}|, |\mathbf{B}_0| = |\mathbf{B}_{+1}| = |\mathbf{B}_{+3}|$) and ($|\mathbf{B}_{+3}| = |\mathbf{B}_{+4}|, |\mathbf{B}_{+1}| = |\mathbf{B}_{+2}|$). The state known as the symmetric four-qubit Dicke state with two excitations ($\alpha = \frac{1}{\sqrt{3}}$) belongs to the intersection points ($|\mathbf{B}_{+1}| = |\mathbf{B}_{+3}|, |\mathbf{B}_{+2}| = |\mathbf{B}_{+4}|$). It was recently experimentally observed and turned out to have as well interesting applications in quantum information [99, 121, 129]. The states associated with points ($|\mathbf{B}_{+2}| = |\mathbf{B}_{+3}|$) for $\alpha = \sqrt{\frac{1}{6}(3-\sqrt{3})}$, ($|\mathbf{B}_{+1}| = |\mathbf{B}_{+4}|$) for $\alpha = \frac{1}{\sqrt{2}}$ and ($|\mathbf{B}_{+2}| = |\mathbf{B}_{+3}|$) for $\alpha = \sqrt{\frac{1}{6}(3+\sqrt{3})}$ did not make any particular appearance in quantum information so far, but seem worth to be investigated in more detail. Especially, the state $|\Psi(\sqrt{\frac{1}{6}(3-\sqrt{3})})\rangle$ will be of relevance in Chap. 5.

Last, but not least, the points ($|\mathbf{B}_{+1}| = |\mathbf{B}_{+2}|, |\mathbf{B}_0| = |\mathbf{B}_{+3}| = |\mathbf{B}_{+4}|$) for $\alpha = 0$ denote a product state of two Bell pairs. This state, though being not four-qubit entangled, plays an important role (mainly) for quantum communication (see Sec. 3.1.4). Together with the GHZ state it is the only state within the family that is either perfectly ($|T_{ijkl}| = 1$) or not at all ($|T_{ijkl}| = 0$) correlated. In contrast, the states $|\Psi'(\frac{1}{\sqrt{2}})\rangle$ as well as $|\Psi'(\frac{1}{\sqrt{3}})\rangle$ and $|\Psi'(\sqrt{\frac{2}{3}})\rangle$ have two correlation values between zero and one ($|T_{ijkl}| = \frac{1}{2}, |T_{ijkl}| = \frac{1}{\sqrt{2}}$ and $|T_{ijkl}| = \frac{1}{3}, |T_{ijkl}| = \frac{2}{3}$, respectively), followed by the states $|\Psi'(\sqrt{\frac{1}{6}(3\pm\sqrt{3})})\rangle$ which have three ($|T_{ijkl}| = \frac{1}{6}(3\pm\sqrt{3}), |T_{ijkl}| = \frac{1}{\sqrt{3}}$).

A more detailed discussion on the general properties of $|\Psi'(\alpha)\rangle$ (and $|\Psi(\alpha)\rangle$) with respect to qubit permutation symmetry and the residual states after the measurement or the loss of qubits is outside the scope of this thesis, but will be carried out elsewhere. The work at hand aims at the demonstration of the functionality of the previously described linear optics network and the proof of its capability to serve as one source for the observation of many different states. To this end, the next section presents the experimental results obtained for the distinguished values of α .

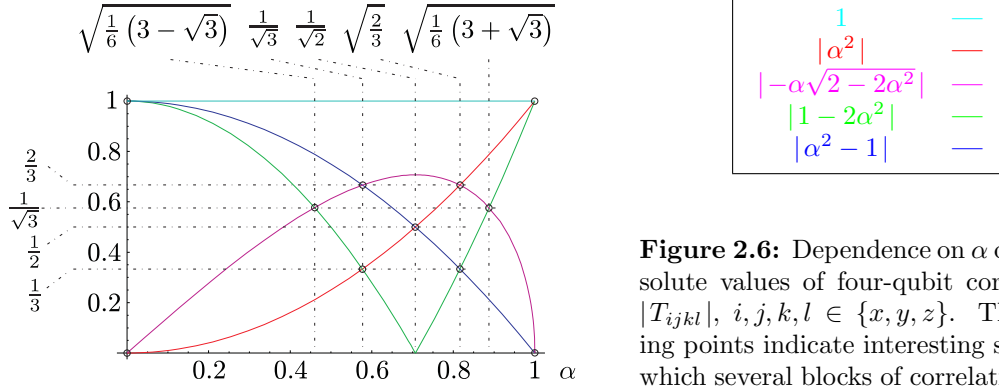


Figure 2.6: Dependence on α of the absolute values of four-qubit correlations $|T_{ijkl}|$, $i, j, k, l \in \{x, y, z\}$. The crossing points indicate interesting states for which several blocks of correlations take the same absolute value.

2.2.3 Experiment

Characterizing observed states

For the purpose of estimating how well each state can be obtained by the network, its fidelity is determined. The fidelity F is a distance measure between two states ρ_1 and ρ_2 [130],

$$F \equiv \left(\text{tr} \left(\sqrt{\sqrt{\rho_1} \cdot \rho_2 \cdot \sqrt{\rho_1}} \right) \right)^2. \quad (2.35)$$

In this thesis, the state ρ_1 is usually considered as the theoretical state that should ideally be obtained, whereas the state ρ_2 is the one that is actually observed in the experiment. As the former is in general pure, in contrast to the latter which is usually mixed, Eqn. (2.35) simplifies to

$$F = \text{tr}(\rho_1 \cdot \rho_2) = \langle \rho | \rho_2 | \rho \rangle, \quad (2.36)$$

with $\rho_1 = |\rho\rangle\langle\rho|$. That means, the fidelity expresses the probability that the observed state is projected onto the ideal one.

In order to see how the fidelity can be determined in practice, it is useful to express an experimentally observed state ρ_{exp}^α in terms of the correlation operators, analogous to Eqn. (2.32),

$$\rho_{\text{exp}}^\alpha = \frac{1}{16} \sum_{ijkl} c_{ijkl} (\sigma_i \otimes \sigma_j \otimes \sigma_k \otimes \sigma_l), \quad (2.37)$$

where $c_{ijkl} \equiv \text{tr}(\rho_{\text{exp}}^\alpha \cdot (\sigma_i \otimes \sigma_j \otimes \sigma_k \otimes \sigma_l))$. Consequently, the fidelity is given as

$$F = \langle \Psi'(\alpha) | \rho_{\text{exp}}^\alpha | \Psi'(\alpha) \rangle = \frac{1}{16} \sum_{ijkl} c_{ijkl} \underbrace{\langle \Psi'(\alpha) | (\sigma_i \otimes \sigma_j \otimes \sigma_k \otimes \sigma_l) | \Psi'(\alpha) \rangle}_{= T_{ijkl} \text{ (cp. Eqn. (2.32))}}. \quad (2.38)$$

While T_{ijkl} can be calculated, c_{ijkl} need to be derived from measurements. Although the latter constitutes in general a set of up to 256 values, it follows from Eqn. (2.38) that (in the case of $|\Psi'(\alpha)\rangle$ and $|\Psi(\alpha)\rangle$) at most 40 of them (for which $T_{ijkl} \neq 0$) are needed for the

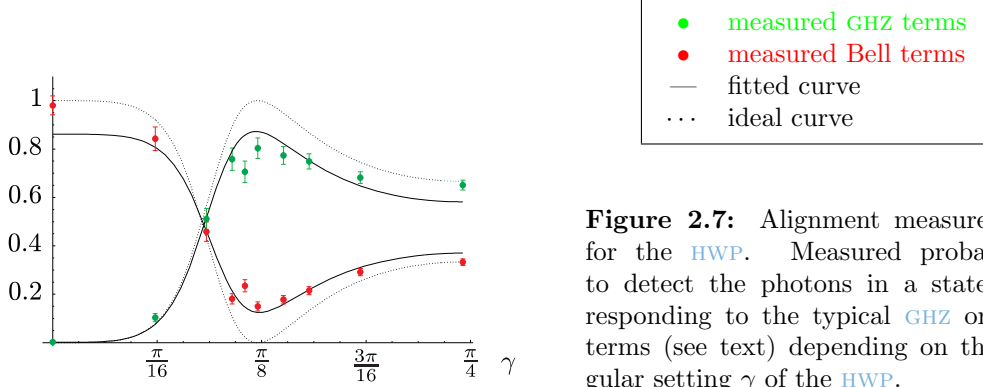


Figure 2.7: Alignment measurement for the **HWP**. Measured probability to detect the photons in a state corresponding to the typical **GHZ** or Bell terms (see text) depending on the angular setting γ of the **HWP**.

evaluation of the fidelity. Due to the special correlation structure of $|\Psi'(\alpha)\rangle^4$ it turns out that even a measurement of up to 21 four-qubit correlations is already sufficient (see App. A).

Alignment

The measurement of the correlations requires some basic alignment of the experimental setup. This concerns primarily proper adjustment of the **SPDC** source, angular calibration of the **HWP** in front of the **PBS** as well as the temporal and spatial mode overlap of the photons arriving at the **PBS**. Furthermore, the polarizing and non-polarizing beam splitters introduce unwanted relative phases between horizontal and vertical polarization which need to be compensated. The latter is achieved by pairs of **YVO₄** crystals (see Fig. 2.4) whose orientation is usually set once prior to the whole series of measurements. In contrast, the mode overlap needs to be adjusted (or at least checked) for each setting of α anew, as it is subject to misalignment within a period of typically a few days.

The angular calibration of the **HWP** is done in a separate setup but tested again within the network. For this purpose the typical **GHZ** and Bell terms are measured for varying γ . A measurement of

$$\left(\text{tr}(|HHVV\rangle\langle HHVV| \cdot \rho_{\text{exp}}^\alpha) + \text{tr}(|VVHH\rangle\langle VVHH| \cdot \rho_{\text{exp}}^\alpha)\right) \quad \text{and}$$

$$\begin{aligned} &\left(\text{tr}(|HVHV\rangle\langle HVHV| \cdot \rho_{\text{exp}}^\alpha) + \text{tr}(|HV VH\rangle\langle HV VH| \cdot \rho_{\text{exp}}^\alpha)\right) \\ &\quad + \text{tr}(|VHHV\rangle\langle VHHV| \cdot \rho_{\text{exp}}^\alpha) + \text{tr}(|VHVH\rangle\langle VHVH| \cdot \rho_{\text{exp}}^\alpha) \end{aligned}$$

is shown in Fig. 2.7. A fit of the data with the theoretically expected dependence allows the estimation of a possible angular offset and its subsequent correction. The resulting uncertainty in the angular setting is approximately $\pm 0.5^\circ$.

The **SPDC** source is aligned to produce in first order emission photon pairs in the state $|\psi^+\rangle$. Correlation measurements of these pairs yield typical values around 0.93 in the basis $\sigma_x \otimes \sigma_x$ and 0.98 in the basis $\sigma_z \otimes \sigma_z$.

The spatial and temporal indistinguishability of the photons is quantified by a **HOM** interference experiment similar to the one described in Sec. 2.1. While varying the optical path

⁴The correlation tensor of $|\Psi'(\alpha)\rangle$ and $|\Psi(\alpha)\rangle$ has the peculiar structure that all two-qubit correlations can be obtained from the corresponding four-qubit correlations with the detection system described in Sec. 1.3.3 on page 39.

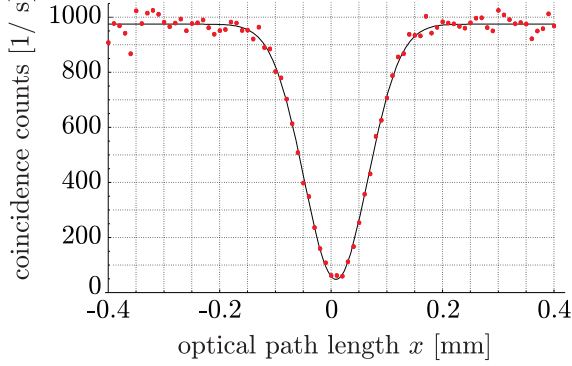


Figure 2.8: HOM interference measurement. Two-photon coincidences between mode a and c are recorded while the optical path length is varied in mode a . Which coincidence event shows the characteristic dip in the count rate depends on the angular setting γ of the HWP. For $\gamma = 45^\circ$ the photons are observed in the state $|\phi^-\rangle$ or $\frac{1}{2}|HH\rangle\langle HH| + \frac{1}{2}|VV\rangle\langle VV|$ if they are indistinguishable or perfectly distinguishable, respectively. Thus, for a measurement of $\sigma_x \otimes \sigma_x$ the event $++$ shows the characteristic drop in the rate.

length in mode a all possible coincidence events between modes a , b and c , d are recorded. Which event shows the characteristic drop in the count rate depends on the angular setting of the HWP in front of the PBS. For example for $\gamma = \frac{\pi}{4}$ the state after the PBS is given as,

$$|\text{mid}\rangle = \frac{1}{\sqrt{2}} \left(a_{H,t_1}^\dagger c_{H,t_2}^\dagger - a_{V,t_2}^\dagger c_{V,t_1}^\dagger \right) |0\rangle, \quad (2.39)$$

where $t_{1,2}$ denote an additional mode like, e.g., the photon's time of arrival. The state is a pure Bell state ($|\text{mid}\rangle = |\phi^-\rangle$) for $t_1 = t_2$ and turns more and more into an incoherent mixture of two horizontally and two vertically polarized photons for continuously increasing difference between t_1 and t_2 . This manifests in an increasing coincidence rate for the events $++$ and $--$ once the state is analyzed in the basis $\sigma_x \otimes \sigma_x$,

$$|\text{mid}\rangle = \frac{1}{2\sqrt{2}} \left(a_{+,t_1}^\dagger c_{+,t_2}^\dagger + a_{+,t_1}^\dagger c_{-,t_2}^\dagger + a_{-,t_1}^\dagger c_{+,t_2}^\dagger + a_{-,t_1}^\dagger c_{-,t_2}^\dagger - a_{+,t_2}^\dagger c_{+,t_1}^\dagger + a_{+,t_2}^\dagger c_{-,t_1}^\dagger + a_{-,t_2}^\dagger c_{+,t_1}^\dagger - a_{-,t_2}^\dagger c_{-,t_1}^\dagger \right) |0\rangle. \quad (2.40)$$

The result of such a measurement is shown in Fig. 2.8 for a $++$ coincidence detection between mode a and c . The quality of the mode overlap can be evaluated to be $\mathcal{Q} = 0.95 \pm 0.01$ (cp. page 49). Here and in all the measurements described in the following, spectral selection of the photons is achieved by interference filters (not shown in Fig. 2.4) with a bandwidth of 3 nm in modes a and c in front of the PBS.

Results

A product of two Bell pairs: $\alpha = 0$. The first crossing point in the absolute values of the correlations, $\alpha = 0$, corresponds to a product of two Bell pairs,

$$|\Psi'(0)\rangle = |\psi^+\rangle \otimes |\psi^+\rangle = \frac{1}{2} (|HVHV\rangle + |HV VH\rangle + |VHHV\rangle + |VHVH\rangle). \quad (2.41)$$

In this instance, the HWP in mode c has to be set to 0° as can be seen from Eqn. (2.28). Thereby, no second order interference takes place, but the photons are "sorted" at the PBS such that two photons with orthogonal polarization leave each of its output ports. The

entanglement in each pair is obtained after the symmetric splitting of the photons in the four final output modes at the **BS** prior to the **PA**.

The state $|\Psi'(0)\rangle$ is not four-qubit entangled and has 16 non-zero correlations out of which nine represent four-qubit correlations (see App. B.1.1). A measurement of these nine correlations yields a fidelity of the output state $\rho_{(\alpha=0)}$ of $F_{(\alpha=0)} = 0.874 \pm 0.013$. The same data set allows further the evaluation of the fidelity of each pair to be $F_{ab} = \text{tr}((\mathbf{F} \otimes \mathbb{1} \otimes \mathbb{1}) \rho_{(\alpha=0)}) = 0.931 \pm 0.012$ and $F_{cd} = \text{tr}((\mathbb{1} \otimes \mathbb{1} \otimes \mathbf{F}) \rho_{(\alpha=0)}) = 0.934 \pm 0.012$ with

$$\mathbf{F} = |\psi^+\rangle\langle\psi^+| = \frac{1}{4}(\mathbb{1} \otimes \mathbb{1} + \sigma_x \otimes \sigma_x + \sigma_y \otimes \sigma_y - \sigma_z \otimes \sigma_z). \quad (2.42)$$

The fidelity of the whole state is approximately the product of the pair fidelities. This needs not to be fulfilled in general, but is true for pure states. The entanglement of each pair can be successfully verified using a two-qubit witness [75, 76],

$$\mathbf{W} = \frac{1}{4}(\mathbb{1} \otimes \mathbb{1} - \sigma_x \otimes \sigma_x - \sigma_y \otimes \sigma_y + \sigma_z \otimes \sigma_z), \quad (2.43)$$

with $W_{ab} = \text{tr}((\mathbf{W} \otimes \mathbb{1} \otimes \mathbb{1}) \rho_{(\alpha=0)}) = -0.431 \pm 0.009$ and $W_{cd} = \text{tr}((\mathbb{1} \otimes \mathbb{1} \otimes \mathbf{W}) \rho_{(\alpha=0)}) = -0.434 \pm 0.009$; ideally $\langle\psi^+|\mathbf{W}|\psi^+\rangle = -0.5$.

As the state $|\Psi'(0)\rangle$ is a product state of two two-qubit states, it can be as well observed using two independent **SPDC** sources, each emitting the state $|\psi^+\rangle$ (see, e.g. [131] and Chap. 3). For some reasons this approach might be preferable in particular applications. The quality of the states obtained from both setups is, however, comparable.

Still unknown: $\alpha = \sqrt{\frac{1}{6}(3 - \sqrt{3})}$. The state corresponding to the next crossing point for $\alpha = \sqrt{\frac{1}{6}(3 - \sqrt{3})}$ was (to the author's knowledge) not mentioned so far in the quantum information literature,

$$\begin{aligned} |\Psi'(\sqrt{\frac{1}{6}(3 - \sqrt{3})})\rangle &\equiv |S^a\rangle = \sqrt{\frac{1}{6}(3 - \sqrt{3})}|\text{GHZ}\rangle + \sqrt{\frac{1}{6}(3 + \sqrt{3})}(|\psi^+\rangle \otimes |\psi^+\rangle) \\ &= \frac{1}{2} \left(\sqrt{1 - \frac{1}{\sqrt{3}}}(|\text{HHVV}\rangle + |\text{VVHH}\rangle) \right. \\ &\quad \left. + \sqrt{\frac{1}{6}(3 + \sqrt{3})}(|\text{HVHV}\rangle + |\text{HVVH}\rangle + |\text{VHHV}\rangle + |\text{VHVH}\rangle) \right). \end{aligned} \quad (2.44)$$

It will, however, appear in Chap. 5 in the context of multi-agent quantum games. As can be seen from Tab. 2.1 and Fig. 2.6 it has 40 non-zero correlations out of which 21 refer to four-qubit correlations. In contrast to the product of two Bell pairs these correlations are not perfect (see App. B.1.2), besides in the four standard bases **IIII**, **XXXX**, **YYYY**, **ZZZZ**.

In the setup the state is obtained for an angle setting of the **HWP** of $\gamma \approx 13.68^\circ$. The fidelity of the experimentally observed state $\rho_{(\alpha=\sqrt{\frac{1}{6}(3-\sqrt{3})})}$ is determined from a measurement of the state's 21 correlations to be $F_{(\alpha=\sqrt{\frac{1}{6}(3-\sqrt{3})})} = 0.755 \pm 0.014$. The results are summarized in Tab. B.4.

The symmetric four-qubit Dicke state: $\alpha = \frac{1}{\sqrt{3}}$. The next crossing point for $\alpha = \frac{1}{\sqrt{3}}$ corresponds to a state that is well known, the symmetric four-qubit Dicke state with two excitations,

$$\begin{aligned}
|\Psi'(\frac{1}{\sqrt{3}})\rangle \equiv |D_4^{(2)}\rangle &= \sqrt{\frac{1}{3}}|\text{GHZ}\rangle + \sqrt{\frac{2}{3}}(|\psi^+\rangle \otimes |\psi^+\rangle) \\
&= \frac{1}{\sqrt{6}}(|\text{HHVV}\rangle + |\text{VVHH}\rangle \\
&+ |\text{HVHV}\rangle + |\text{HVVH}\rangle + |\text{VHHV}\rangle + |\text{VHVH}\rangle).
\end{aligned} \tag{2.45}$$

Generally, a symmetric N -qubit Dicke state [132, 133] with M excitations is the equally weighted superposition of all permutations of N -qubit product states with M logical 1s and $(N - M)$ logical 0s, here denoted by $|D_N^{(M)}\rangle$. The Dicke states naturally appear as the common eigenstates of the total spin-squared and the spin z-component operators (where z is assumed to be the quantization direction) in spin one-half particle systems. Besides the state studied here, another well known example for a Dicke state is the N -qubit W state $|W_N\rangle$ (in the present notation $|D_N^{(1)}\rangle$) [134]. While other symmetric Dicke states have maximum overall spin, $D_4^{(2)}$ is the eigenstate which has minimum spin component along the quantization axis; a fact that leads to a set of interesting properties [99, 121, 129]. For instance, choosing a proper basis, the Dicke state allows to obtain either a three-qubit w state or a GHZ class state by a simple projective measurement on any of its qubits [135, 136]. This is remarkable as these resulting states cannot be transformed into each other by means of SLOCC (see Sec. 1.2.2). Furthermore, $D_4^{(2)}$ can be used as a resource for quantum information applications such as Telecloning [113], Open destination teleportation [137], and certain quantum versions of classical games [138].

The angular setting to obtain the Dicke state in the setup is $\gamma = 15^\circ$. A measurement of its 21 four-qubit correlations yields a fidelity of $F_{(\alpha=\frac{1}{\sqrt{3}})} = 0.709 \pm 0.013$. Using the generic witness of the Dicke state $\mathbb{W}_{D_4^{(2)}}$ with $\text{tr}(\mathbb{W}_{D_4^{(2)}} \rho_{(\alpha=\frac{1}{\sqrt{3}})}) = \frac{2}{3} - F_{(\alpha=\frac{1}{\sqrt{3}})}$, this fidelity is high enough to conclude that the experimentally observed state $\rho_{(\alpha=\frac{1}{\sqrt{3}})}$ is four-qubit entangled [139].

Due to the special structure of the state, there exists an alternative setup for the observation of $D_4^{(2)}$: As all terms in Eqn. (2.45) are equally weighted, the Dicke state can be seen as the superposition of the six possibilities to distribute two horizontally and two vertically polarized photons into four modes. Accordingly, the second order emission of collinear SPDC can be used to create four indistinguishable photons with appropriate polarizations in one spatial mode and distribute them with polarization independent BSs symmetrically onto four modes. As this type of setup does not involve interference it leads to a better state quality. Therefore, in applications which use the Dicke state only, this experimental configuration is preferable. It will also be used in Chap. 4.

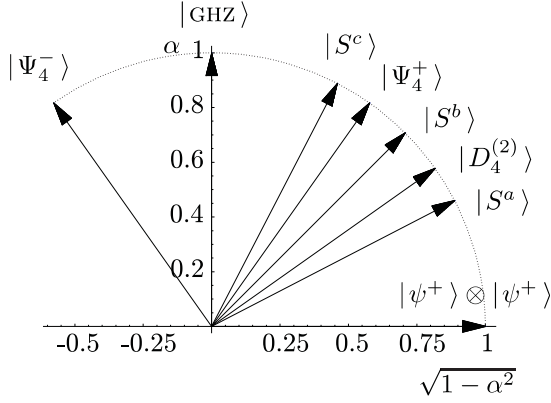


Figure 2.9: Pictorial representation of the plane in state space which is spanned by $|\text{GHZ}\rangle$ and $|\psi^+\rangle \otimes |\psi^+\rangle$. All states which can be obtained with the setup described in this section lie within this plane. Explicitly shown are the state vectors of the states for the distinguished values of α . All state vectors with $\alpha > 0$ are symmetric around $|S^b\rangle$ which lies central between $|\text{GHZ}\rangle$ and $|\psi^+\rangle \otimes |\psi^+\rangle$.

Still unknown: $\alpha = \frac{1}{\sqrt{2}}$. The corresponding state of the crossing point for $\alpha = \frac{1}{\sqrt{2}}$ is the intermediate state of the **GHZ** and the product of two Bell pairs,

$$\begin{aligned} |\Psi'(\frac{1}{\sqrt{2}})\rangle &\equiv |S^b\rangle = \frac{1}{\sqrt{2}}|\text{GHZ}\rangle + \frac{1}{\sqrt{2}}(|\psi^+\rangle \otimes |\psi^+\rangle) \\ &= \frac{1}{2} \left(|HHVV\rangle + |VVHH\rangle \right. \\ &\quad \left. + \frac{1}{\sqrt{2}}(|HVVH\rangle + |HVHV\rangle + |VHHV\rangle + |VHVV\rangle) \right). \end{aligned} \quad (2.46)$$

In the plane of state space spanned by $|\text{GHZ}\rangle$ and the product $|\psi^+\rangle \otimes |\psi^+\rangle$ it lies halfway between these states. This plane and the state vectors for different values of α are depicted in Fig. 2.9.

The correlation tensor of $|S^b\rangle$ has 36 non-zero terms, out of which 19 concern four-qubit correlations. A measurement of these correlations with $\gamma \approx 16.38^\circ$ yields a fidelity for the experimentally observed state $\rho_{(\alpha=\frac{1}{\sqrt{2}})}$ of $F_{(\alpha=\frac{1}{\sqrt{2}})} = 0.677 \pm 0.013$. In this instance, a statement about the four-qubit entanglement of the state is not possible.

Psi-four: $\alpha = \sqrt{\frac{2}{3}}$. The crossing point for $\alpha = \sqrt{\frac{2}{3}}$ corresponds to a state which has the reversed weighting compared to the Dicke state,

$$\begin{aligned} |\Psi'(\sqrt{\frac{2}{3}})\rangle &\equiv |\Psi_4^\pm\rangle = \sqrt{\frac{2}{3}}|\text{GHZ}\rangle \pm \sqrt{\frac{1}{3}}(|\psi^+\rangle \otimes |\psi^+\rangle) \\ &= \frac{1}{\sqrt{3}} \left(|HHVV\rangle + |VVHH\rangle \right. \\ &\quad \left. \pm \frac{1}{2}(|HVVH\rangle + |HVHV\rangle + |VHHV\rangle + |VHVV\rangle) \right). \end{aligned} \quad (2.47)$$

It is also well known and was first discussed as a four-photon entangled state that can be directly obtained from non-collinear **SPDC** [100]. To this end the overlap at the **PBS** is in principle not necessary and splitting the photons of the second order emission symmetrically in four output modes by two **BSS** is sufficient [111, 112]. Two **LU** equivalent versions of this state⁵, $|\Psi_4^+\rangle$ and $|\Psi_4^-\rangle$, can be found in literature and both can be observed in the present

⁵It holds, e.g., that $|\Psi_4^+\rangle = (\sigma_z \otimes \sigma_z \otimes \mathbb{1} \otimes \mathbb{1}) \cdot |\Psi_4^-\rangle$.

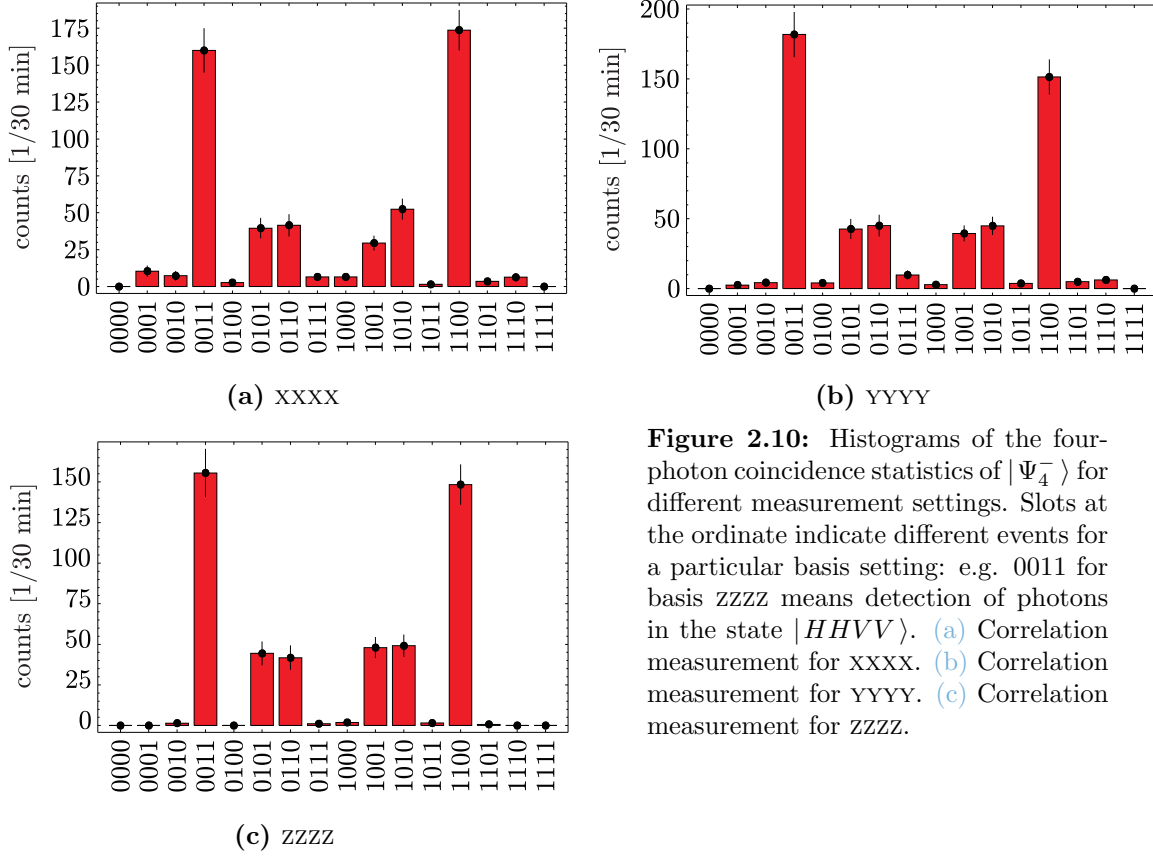


Figure 2.10: Histograms of the four-photon coincidence statistics of $|\Psi_4^-\rangle$ for different measurement settings. Slots at the ordinate indicate different events for a particular basis setting: e.g. 0011 for basis ZZZZ means detection of photons in the state $|HHVV\rangle$. (a) Correlation measurement for XXXX. (b) Correlation measurement for YYY. (c) Correlation measurement for ZZZ.

setup for $\gamma \approx 17.63^\circ$ and $\gamma = 45^\circ$, respectively. These states have special properties which make them useful for a couple of quantum information applications. For instance, the state $|\Psi_4^-\rangle$ is a four-qubit entangled state which is invariant under any local unitary operation acting in the same way on each qubit. Therefore, it plays an important role in decoherence free communication [114]. Other applications, for the states $|\Psi_4^\pm\rangle$ are, e.g., Telecloning [113] or four-party secret sharing [115, 140].

Like $D_4^{(2)}$, the state $|\Psi_4^\pm\rangle$ has also 40 non-zero terms of T_{ijkl} out of which 21 describe four-qubit correlations. Even the absolute values $|T_{ijkl}|$ are the same, but for different sets of $\{ijkl\}$. The results of a typical correlation measurement are shown for the state $|\Psi_4^-\rangle$ in Fig. 2.10 as they demonstrate the invariance property of the state with respect to some local unitary transformations. As just mentioned, if the applied operation is the same for each qubit, like a basis transformation between XXXX, YYY and ZZZ, the state remains unchanged. This can be seen in Fig. 2.10(a) – Fig. 2.10(c) which exhibit the same term structure for each basis.

The evaluation of all 21 correlations yields a fidelity of the experimental state $\rho_{(\alpha=\sqrt{\frac{2}{3}})}^-$ to the theoretical $|\Psi_4^-\rangle$ of $F_{(\alpha=\frac{2}{3})}^- = 0.904 \pm 0.014$ and of $\rho_{(\alpha=\sqrt{\frac{2}{3}})}^+$ to $|\Psi_4^+\rangle$ of $F_{(\alpha=\frac{2}{3})}^+ = 0.651 \pm 0.019$. These values differ significantly for both states. The reason is that the states are observed for different values of γ and that the state quality, in turn, depends on this angular setting. This is a particular feature of the used setup which will be discussed afterwards (see

Sec. 2.2.4).

With the generic witness operator presented in [70], $\mathbb{W}_{D_4^{(2)}}$ with $\text{tr}(\mathbb{W}_{D_4^{(2)}} \rho_{(\alpha=\sqrt{\frac{2}{3}})}) = \frac{3}{4} - F_{(\alpha=\sqrt{\frac{2}{3}})}$, at least one of the states, $\rho_{(\alpha=\sqrt{\frac{2}{3}})}^-$, can be proven to be four-qubit entangled.

For real applications, considering the difference in the state quality, it is sensible to use the setting $\gamma = 45^\circ$ and an additional HWP at an angle of 0° behind the PBS in order to obtain the state $|\Psi_4^+\rangle$.

Still unknown: $\alpha = \sqrt{\frac{1}{6}(3 + \sqrt{3})}$. Similar to the state $|\Psi_4^\pm\rangle$ which has reversed weighting than the Dicke state, the state which corresponds to the next crossing point for $\alpha = \sqrt{\frac{1}{6}(3 + \sqrt{3})}$,

$$\begin{aligned} |\Psi'(\sqrt{\frac{1}{6}(3 + \sqrt{3})})\rangle &\equiv |S^c\rangle = \sqrt{\frac{1}{6}(3 + \sqrt{3})}|\text{GHZ}\rangle + \sqrt{\frac{1}{6}(3 - \sqrt{3})}(|\psi^+\rangle \otimes |\psi^+\rangle) \\ &= \frac{1}{2} \left(\sqrt{1 + \frac{1}{\sqrt{3}}} (|\text{HHVV}\rangle + |\text{VVHH}\rangle) \right. \\ &\quad \left. + \sqrt{\frac{1}{6}(3 - \sqrt{3})} (|\text{HVHV}\rangle + |\text{HVVH}\rangle + |\text{VHHV}\rangle + |\text{VHVH}\rangle) \right), \end{aligned} \quad (2.48)$$

has reversed weighting than the state $|S^a\rangle$ and both lie centered around $|S^b\rangle$ (see Fig. 2.9). Consequently, $|S^c\rangle$ has the same number of non-zero correlations as $|S^a\rangle$ with the same absolute values of T_{ijkl} but for a different set of $\{ijkl\}$.

A measurement of these correlations results in a fidelity of the experimentally observed state $\rho_{(\alpha=\sqrt{\frac{1}{6}(3+\sqrt{3})})}$ to the theoretical state $|S^c\rangle$ of $F_{(\alpha=\sqrt{\frac{1}{6}(3+\sqrt{3})})} = 0.663 \pm 0.014$.

GHZ: $\alpha = 1$. Probably the most famous state of the family $|\Psi'(\alpha)\rangle$ is the GHZ state, lying at the crossing point for $\alpha = 1$,

$$\begin{aligned} |\Psi'(1)\rangle &= |\text{GHZ}\rangle \\ &= \frac{1}{\sqrt{2}} (|\text{HHVV}\rangle + |\text{VVHH}\rangle). \end{aligned} \quad (2.49)$$

It was already experimentally observed, not only with photonic qubits [141], and plays a central role in many quantum information applications [142–144].

Similar to the product of two Bell pairs, the GHZ state has also 16 non-zero terms of T_{ijkl} out of which nine correspond to four-qubit correlations, and all are perfect, i.e., $|T_{ijkl}| = 1$. However, in contrast to $|\psi^+\rangle \otimes |\psi^+\rangle$, the GHZ state is four-qubit entangled.

In the setup the state is observed for the setting $\gamma = 22.5^\circ$. As can be seen from Eqn. (2.21) and Eqn. (2.23), for this angular setting of the HWP the terms which are typical for the Bell pairs interfere destructively at the overlap. The remaining terms describe a superposition of the instances in which two photons of identical polarization leave the same output mode of the PBS.

A measurement of the nine correlations yields a fidelity of the experimentally observed state $\rho_{(\alpha=1)}$ of $F_{(\alpha=1)} = 0.750 \pm 0.013$. This value is well above the threshold of $F = 0.5$ to detect the experimental state to be four-qubit entangled with the generic GHZ witness [145].

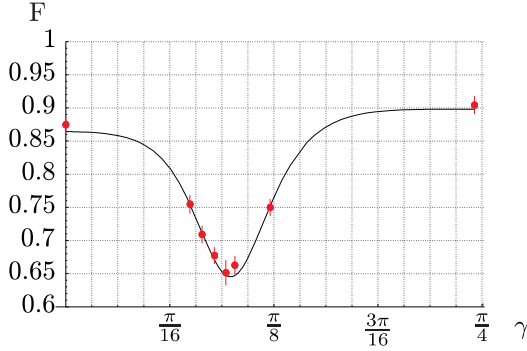
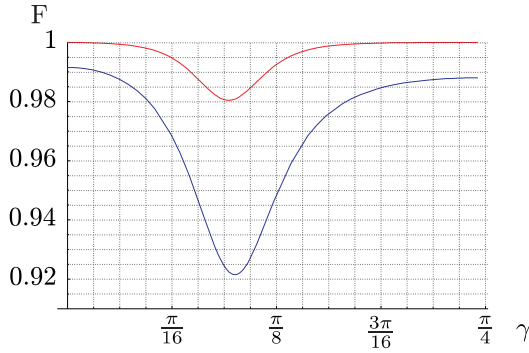
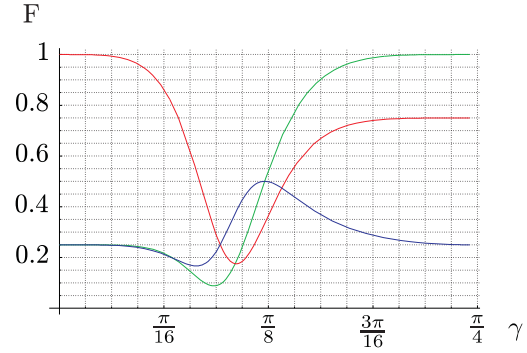


Figure 2.11: Experimentally measured fidelities F versus angular setting γ of the **HWP**. The fidelity of each state depends strongly on γ . This is not caused by misalignment of the setup but can be qualitatively attributed to different effects. A lack of perfect interference at the **PBS** caused by a remaining degree of distinguishability of the photons affects the state quality to a different degree for different γ .



(a)



(b)

Figure 2.12: Calculation of the resulting fidelities for different experimental imperfections. (a) Resulting fidelity including noise from third order **SPDC** emission (—) and for an angular offset in the alignment of the **HWP** in front of the **PBS** of 1° (—). (b) Resulting fidelity for incoherent second order **SPDC** emission (—), for distinguishable signal and idler photons (—) and for insufficient spatial mode overlap at the **PBS** (—).

2.2.4 Discussion of the results

The previously presented measurements of the states' fidelities show clearly that the linear optics network allows the observation of the family $|\Psi'(\alpha)\rangle$. The results are summarized in Fig. 2.11, where the fidelities F are plotted versus the angle γ of the **HWP**. It is noticeable that the obtained fidelities for the different states depend obviously on the setting of γ . In the case of $|\Psi_4^\pm\rangle$ the difference in the fidelities is significant (as the respective values for γ are different), although the two states are equivalent with respect to **LU**. As the alignment of the mode overlap at the **PBS**, quantified and checked by repeated **HOM** interference measurements (see page 57), as well as the alignment of the **SPDC** source was comparable for the whole series of measurements, this feature cannot be explained by misalignment of the setup and must therefore be intrinsic to the network.

There are a couple of reasons which lead to this fact. First of all the effective noise originating from higher order emissions of the photon source (see page 40) is dependent on γ . A calculation of the resulting fidelity including third order emissions is shown in Fig. 2.12(a) (blue curve). It reaches a minimum of around 0.92 for $\gamma \approx 18.36^\circ$. Second, an offset error in the alignment of the **HWP** in front of the **PBS** (as discussed on page 57) causes

an angular dependent impairment of the fidelities. The result is displayed in Fig. 2.12(a) (red curve) for an offset of 1° . As can be seen the effect is moderate and degrades the fidelity maximally by about 0.02 for $\gamma \approx 17.69^\circ$. Third, the various reasons for a given degree of distinguishability of the photons, and thus imperfect interference, have differently strong impact on different states. For example, assuming that there is, for what ever reason, some timing information left concerning the generation of the photons, the second order SPDC emission is, to a certain extent, described by two distinguishable pairs, rather than by a coherent four-photon emission (see page 36). Fed into the network, this would not affect the observation of the state $|\psi^+\rangle \otimes |\psi^+\rangle$ (see page 58 et seqq.), while being fatal for the one of other states containing four-photon entanglement. The fidelity for a completely incoherent emission is depicted in Fig. 2.12(b) (red curve). Here a minimum of around 0.18 is reached for $\gamma \approx 19.39^\circ$. An almost opposite behavior is expected for the following scenario: The second order emission be coherent, but the signal and idler photons be distinguishable by, e.g., their spectral width what is typical for SPDC with ultra short pump pulses (see page 38). This strongly affects the state $|\psi^+\rangle \otimes |\psi^+\rangle$, whereas it has no significance for the observation of $|\Psi_4^-\rangle$. The latter is a peculiar incident occurring in the network for $\gamma = 45^\circ$. For this particular angle setting the photons are "sorted" at the PBS such that the spectral information factors from the polarization information. As a result, the spectrum has no influence on the entanglement of the state. This was first discovered and also experimentally studied by Kurtsiefer *et al.* [146]. A calculation of the resulting fidelity for perfectly distinguishable photons is also displayed in Fig. 2.12(b) (green curve). The minimum of approximately 0.09 is reached for $\gamma \approx 16.94^\circ$. Another impairment of the fidelity which concerns $|\Psi_4^-\rangle$ as well as $|\psi^+\rangle \otimes |\psi^+\rangle$ and exhibits a modulation for median values of γ occurs for insufficient spatial mode overlap. A calculation thereof is shown in Fig. 2.12(b) (blue curve) for perfectly distinguishable photons. The strength of this effect can be approximately estimated from the HOM interference measurement (see page 57). Assuming that the difference in the optical path length can be adjusted to be zero, the reduction of the quality factor \mathcal{Q} by about 0.05 can be attributed to spatial mode mismatch.⁶

As can be seen, all effects seem to have their major significance for median values of γ . This observation is in agreement with the course of the measured fidelities plotted in Fig. 2.11. A parameterized superposition of the fidelity curves for the different effects is used to fit the data shown in Fig. 2.11. As it is difficult to separate the above described effects experimentally from each other and to estimate how strongly each of them actually contributes to the distribution of the measured fidelities, this fit has to be treated with care. It has to be seen as a qualitative rather than a quantitative explanation for the angular dependence of the fidelities. Furthermore, the different reasons for a partial distinguishability of the photons do not need to be independent and might partially account for each other.

However, very recent measurements with an increased spectral indistinguishability of the photons by the use of different interference filters⁷ yield an improvement of the fidelities of up to 0.1. With a fidelity range of 0.75 to 0.93 (instead of 0.66 to 0.90) the improvement concerns predominantly the median values of γ and thus damps the angular dependence.

⁶ For an angular setting of $\gamma = 45^\circ$ a possible spectral distinguishability of the photons has no effect on the dip visibility for the same reasons as discussed previously for $|\Psi_4^-\rangle$.

⁷The new filters have a transmission profile close to a rectangular distribution instead of a Gaussian one.

2.3 Conclusion

This chapter has presented two new linear optics networks. The first was a **CPHASE** gate which belongs to the set of universal quantum logic gates necessary for quantum computation. The design of the gate is particularly interesting for applications in multi-photon experiments as it constitutes an improvement of former realizations with respect to stability and reliability. This is achieved by replacing (phase-dependent) single-photon interferometers for different polarizations by a polarization-dependent (but phase-independent) two-photon interference. The performance of the experimental gate was characterized by quantum process tomography in combination with a theoretical model based on experimental parameters of the setup. Close examination of the results shows that the main deviation from optimal gate operation is due to a remaining degree of distinguishability of the photons causing imperfect interference. Still, as shall be demonstrated in the next Chapter, the gate is a useful tool in various applications.

The second network, fed with the second order emission of non-collinear type II **SPDC**, represents a tunable source of a whole family of states. This is a significant achievement as up to now the observation of a particular state required an individually tailored setup. With the previously described network many different states can be obtained within the same arrangement by the tuning of an easily accessible experimental parameter. Furthermore these states form a subgroup of an important generic family of four-qubit entangled states. The performance of the setup was characterized by selected fidelity measurements for distinguished states of the subgroup. These states can be obtained with fidelities which are comparable with the ones achieved in alternative, state tailored setups. The dependence of the state quality on the tuning parameter in case of imperfect interference is still suboptimal. However, this effect can be reduced by further technical improvements and first steps in this direction are promising. The applicability of the setup will be demonstrated in Chap. 5 where the obtained states are used for the implementation of a multi-agent quantum game.

Chapter 3

Applications of a controlled phase gate

In Chap. 2 a scheme for a simple linear optics phase gate was introduced. This chapter deals with the applications of this gate for different quantum information tasks. The setup is the same for all the applications described herein. However, the evaluation of the obtained data is done from different perspectives corresponding to the various applications. As explained in Sec. 1.2.3, a CPHASE gate can be used to transform between an entangled state and a product state basis. From this point of view it can be applied to entangle or disentangle states. The following two sections deal with the latter: there the gate is used to perform a complete Bell state analysis. The last section of this chapter is devoted to the entangling capabilities of the gate. In this respect it will be shown that a four-photon cluster state can be observed by entangling photons from two Bell pairs.

3.1 Teleportation and entanglement swapping with complete Bell state analysis

The processing of quantum information is inevitably connected with its transportation. As long as *quantum* channels are available, i.e., channels capable of carrying qubits, the latter task seems not to be a major problem. The situation changes, however, if exclusively *classical* channels, i.e., channels able to convey only classical bits, can be used. They are obviously not sufficient, as the information needed to describe the qubit's state is infinite (see Sec. 1.2.1). Thus, a classical approach of a local state measurement followed by an remote state preparation cannot be used to "transfer" an unknown quantum state from one location to another via the exchange of classical information.

However, quantum teleportation provides a method to faithfully transmit ("teleport") quantum information via a classical channel by exploiting entanglement as a resource [10]. The term "teleportation" was coined by Bennett *et al.* as in the protocol, which was proposed by them, a potential sender does neither need to know the state to be transmitted nor the location of an intended, arbitrarily remote receiver. The case in which the state to be teleported is not simply unknown, but not determined at all as it is itself part of an entangled state is called entanglement swapping [11]. As a result of the protocol, two qubits which have never interacted in the past become entangled. From this point of view it can thus be seen as the teleportation of entanglement. Both protocols, though being interesting on their own, are

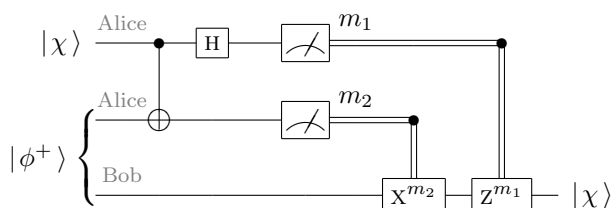


Figure 3.1: Circuit diagram for quantum teleportation. The circuit "teleports" an arbitrary unknown quantum state $|\chi\rangle$ from Alice's side to Bob's. Besides a shared maximally entangled state as resource it requires the exchange of classical information.

fundamental building blocks in many other quantum information and communication applications (see, e.g., [147–151]). Thus, their experimental implementation is of vital importance. In the following the two protocols shall be shortly recapitulated.

3.1.1 The protocols

Teleportation

Alice and Bob be two parties who are connected by a classical communication channel. Alice possess a qubit whose state $|\chi\rangle$ she wants to transmit to Bob. There be no quantum channel available between them at this moment. Yet, it is assumed that they share a maximally entangled two-qubit state, i.e., Alice and Bob possess each one of the qubits. For convenience this state be $|\phi^+\rangle$. The sharing of the state might have happened in earlier times when the parties met or howsoever. Alice and Bob can use the entanglement contained in the state as a resource to transmit quantum information by just sending classical bits. To this end, in the first step of the protocol, Alice needs to couple the state she intends to transmit to her part of the entangled pair. Precisely, she has to perform a projective von Neumann measurement on these two qubits in the Bell basis. This can be accomplished by the application of a CNOT gate followed by a HAD operation on $|\chi\rangle$ and subsequent measurement of both qubits in the computational basis, see Circ. 1.45. In the second step of the protocol she communicates the result m_1 for the first qubit and the result m_2 for the second qubit to Bob via the classical channel. Depending on these two bits of classical information, Bob applies one of four unitary operations, $(\sigma_x^{m_1} \cdot \sigma_z^{m_2})$, on his part of the shared state. As a result of this third and last step he obtains the quantum state to be transmitted. The corresponding quantum circuit is shown in Fig. 3.1. The proof for this circuit to work is easily given by straight forward calculation (see, e.g., [35]).

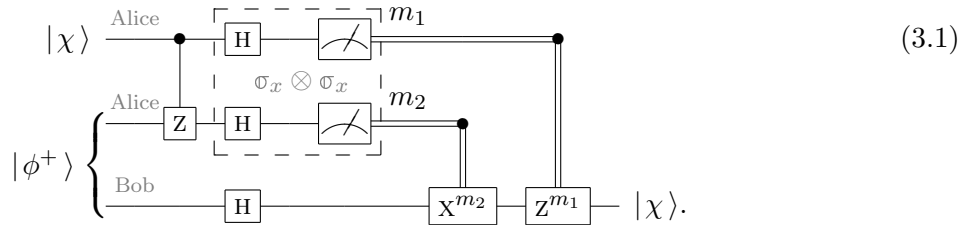
At this stage there are two things which are important to note:

The protocol does neither violate *causality* nor the so-called *no-cloning theorem*. The name "teleportation" might suggest an instantaneous state transfer, but this is easily seen to be wrong. In order to recover Alice's original state Bob must know the measurement result to properly apply one of the four transformations. Without this information, which can reach him maximally at the speed of light, the qubit he possesses is in a completely mixed state and thus contains zero information. Consequently, the quantum state is not instantaneously transferred.

What is generally known today as the "no-cloning theorem" is the observation that the linearity of quantum mechanics forbids the cloning or copying of an unknown quantum state [152, 153]. The fact that the teleportation protocol does not break with this law is ensured by the Bell projection measurement. Alice, by projecting the state to be teleported and her half

of the shared Bell pair into a common maximally entangled state, destroys all the information about the qubit on her side (see Sec. 1.2.2). Otherwise, if this measurement is not perfect, in the sense that Alice does not project onto a *maximally* entangled state and thus retains partial information on the initial state, Bob will not be able to recover the full information on his side.

Naturally, the Bell projection measurement can be equally well accomplished by the usage of a CPHASE instead of a CNOT gate. This leads to minor differences which shall be shortly discussed as the experiments presented later use the CPHASE. The equivalent quantum circuit in this case is given as,



The two HAD gates on Alice’s side followed by a measurement in the computational basis can be interpreted as a measurement in the basis $\sigma_x \otimes \sigma_x$. Together with the preceding CPHASE gate this corresponds also to a Bell projection measurement, however in a different Bell basis. The CPHASE transforms between the following product and entangled basis states,

$$|++\rangle \xleftrightarrow{\text{CPHASE}} \frac{1}{\sqrt{2}} (|0+\rangle + |1-\rangle) \equiv |\widetilde{\phi}^+\rangle \tag{3.2a}$$

$$|+-\rangle \xleftrightarrow{\text{CPHASE}} \frac{1}{\sqrt{2}} (|0-\rangle + |1+\rangle) \equiv |\widetilde{\psi}^+\rangle \tag{3.2b}$$

$$|-+\rangle \xleftrightarrow{\text{CPHASE}} \frac{1}{\sqrt{2}} (|0+\rangle - |1-\rangle) \equiv |\widetilde{\phi}^-\rangle \tag{3.2c}$$

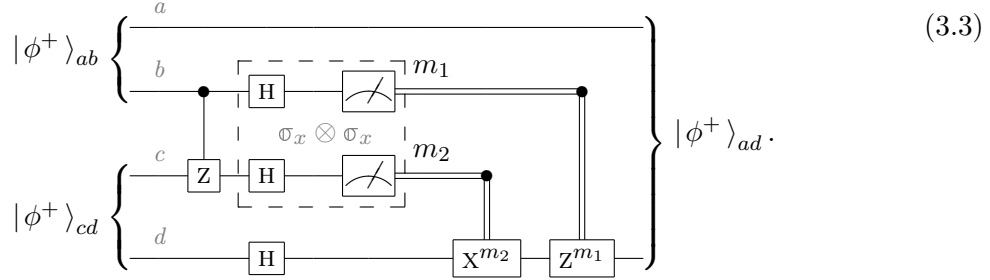
$$|--\rangle \xleftrightarrow{\text{CPHASE}} \frac{1}{\sqrt{2}} (|0-\rangle - |1+\rangle) \equiv |\widetilde{\psi}^-\rangle \tag{3.2d}$$

As this Bell basis differs from the standard one in a HAD rotation on the second qubit, Bob has to compensate for this difference in order to retrieve the original input state $|\chi\rangle$. This means, additionally to one of the four unitary operations ($\mathbb{1}, \sigma_x, \sigma_z, \sigma_x \cdot \sigma_z = i\sigma_y$), he applies a HAD gate on his qubit (cp. Circ. 3.1). The rest of the teleportation protocol runs exactly in the same way as described before.

Entanglement swapping

In the teleportation protocol the state to be teleported, though it might be arbitrary and unknown to Alice, is well defined. This is not the case if the input qubit itself is part of an entangled state. If the above described protocol is run analogously under such circumstances it is usually referred to as *entanglement swapping* [11]. The name was coined by Żukowski *et al.* as in this instance two particles can be entangled which do not share any common past. The entanglement is, so to say, "swapped" from one pair of qubits to another. The

corresponding quantum circuit is very similar to Circ. 3.1 and given as,



The starting point is given in form of two Bell states (for convenience they be both $|\phi^+\rangle$) with the qubits labeled by a, b, c, d . Rewriting this input state immediately reveals the concept of the protocol,

$$|\phi^+\rangle_{ab}|\phi^+\rangle_{cd} = \frac{1}{2} \left(|\widetilde{\phi}^+\rangle_{ad}|\widetilde{\phi}^+\rangle_{bc} + |\widetilde{\psi}^+\rangle_{ad}|\widetilde{\psi}^+\rangle_{bc} + |\widetilde{\phi}^-\rangle_{ad}|\widetilde{\phi}^-\rangle_{bc} + |\widetilde{\psi}^-\rangle_{ad}|\widetilde{\psi}^-\rangle_{bc} \right). \quad (3.4)$$

As can be seen, a projective measurement of qubits b and c in the Bell basis, projects qubits a and d likewise in a Bell state. In which Bell state the latter are projected depends on the outcome of the measurement on the former. To account for this, the corresponding local operations on qubit d are applied conditioned on the results m_1 and m_2 . Hence, the output state of qubits a and d equals the input state of qubits a, b or c, d , respectively. If it is, however, just important to entangle qubits a and d , the conditioned operations are not necessary and can be skipped. As a result qubits a, d will be in anyone of the four Bell states.

3.1.2 The implementation

As can be learned from the above discussion, the essential step involved in both protocols is the Bell projection measurement, which requires two-qubit logic gates. Hence, teleportation could be demonstrated already with a number of different systems, where the gate operations are possible [154–157]. However, while photons doubtlessly are the most proper quantum system for communication tasks, the implementation of two photon quantum gates is not straight forward as there is no photon-photon interaction with reasonable coupling strength (see Sec. 1.3). There are deterministic schemes realizing the gate operation which rely on entanglement in additional degrees of freedom, but they are not suited for teleportation [158]. Therefore, beginning with initial experiments [131, 159], two photon interference [160, 161] was employed to identify up to two of the four Bell states and, recently, a probabilistic identification of three Bell states using positive operator-valued measure (POVM)¹ operators was demonstrated [162, 163]. Quantum teleportation of a photon polarization state with complete Bell state analysis was also demonstrated using non-linear effects [164], though with vanishingly small probability. To perform similar experiments with linear optics gates was up to now not possible as the existing solutions [14–17] were not stable enough to be applied within multi-photon setups. This has changed, however, with the development of the simplified CPHASE gate described in Sec. 2.1. In the following, it will be shown that and how this gate can be used in a teleportation and entanglement swapping protocol.

¹A POVM is a set of Hermitian positive-semidefinite operators $\{\mathbf{O}_i\}$ which is complete, i.e., $\sum_i \mathbf{O}_i = \mathbb{1}$. It constitutes the most general formulation of a measurement.

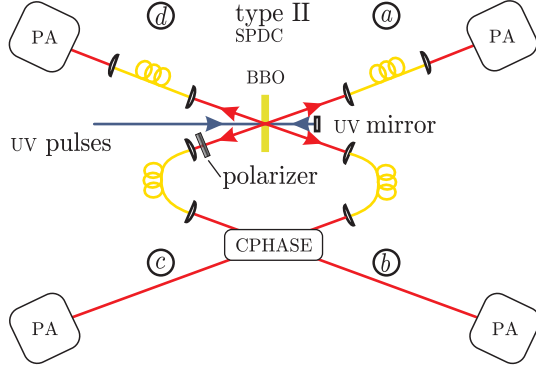


Figure 3.2: Setup for quantum teleportation and entanglement swapping. The required photon states are provided by a non-collinear SPDC of type II, which is operated in a double pass configuration. This enables photon pair emission into four modes a , b and c , d along the forward and backward direction of the pump beam. For the teleportation protocol the backward emission is used as heralded single photon source with mode d as trigger. The polarization state of the photon in mode c is set by a polarizer in front of the coupling and teleported to mode a .

In the experiment the input states are generated by non-collinear SPDC of type II (see Sec. 1.3.2) in which the BBO crystal is pumped in a double pass configuration. That means after passing the crystal the beam is reflected back by a UV-mirror in a distance of about 3 cm to enable SPDC also into a second pair of beams. Thus, pairs of photons are emitted along the forward *and* the backward direction of the pump beam, respectively. The photons propagating along the characteristic intersection lines of the emission cones are coupled into single mode fibers defining the four spatial modes a , b , c , d , (see Fig. 3.2). The modes b and c are coupled as input to the CPHASE gate. Spectral selection is achieved with narrow bandwidth interference filters (spectral width $\Delta\lambda = 2$ nm in the CPHASE gate and $\Delta\lambda = 3$ nm in modes a and d) before detection. The setup stays stable over several days with typical detection rates of about 180 fourfold coincidence counts per hour.

3.1.3 Experimental results for teleportation

The goal of quantum teleportation in this setup is to transfer the most general polarization state $|\chi\rangle_c = \alpha|H\rangle_c + \beta|V\rangle_c$ with arbitrary amplitudes α , β of the photon in mode c onto the photon in mode a . This requires a maximally entangled Bell state in modes a and b , as well as the complete Bell state projection measurement between the photons in mode b and c . The Bell state is obtained by proper alignment of the photon pair originating from the forward down conversion which is adjusted to yield state $|\phi^+\rangle$. The photon which will carry the state $|\chi\rangle_c$ is provided by the backward emission of the down conversion which is operated as a heralded single photon source [165–167] with the photon in mode d initializing the trigger. The polarization state $|\chi\rangle_c$ is prepared by a polarizer in front of the fiber coupler in mode c and proper alignment of the fibre’s polarization controller.

Teleported states

Four different input states $|H\rangle$, $|V\rangle$, $|+\rangle$, $|R\rangle$ are chosen to be teleported. For each of them a single qubit tomography of the corresponding output state is carried out in mode a . This yields the density matrices ρ_k , ($k \in \{H, V, +, R\}$), of the experimentally teleported states and allows the calculation of the fidelities, $F_k = \langle k | \mathbf{U}_{m_1, m_2} \rho_k \mathbf{U}_{m_1, m_2}^\dagger | k \rangle$ to the input states. The unitary operations, $\mathbf{U}_{m_1, m_2} = \sigma_z^{m_1} \cdot \sigma_x^{m_2} \cdot \text{HAD}$, are not physically implemented but applied

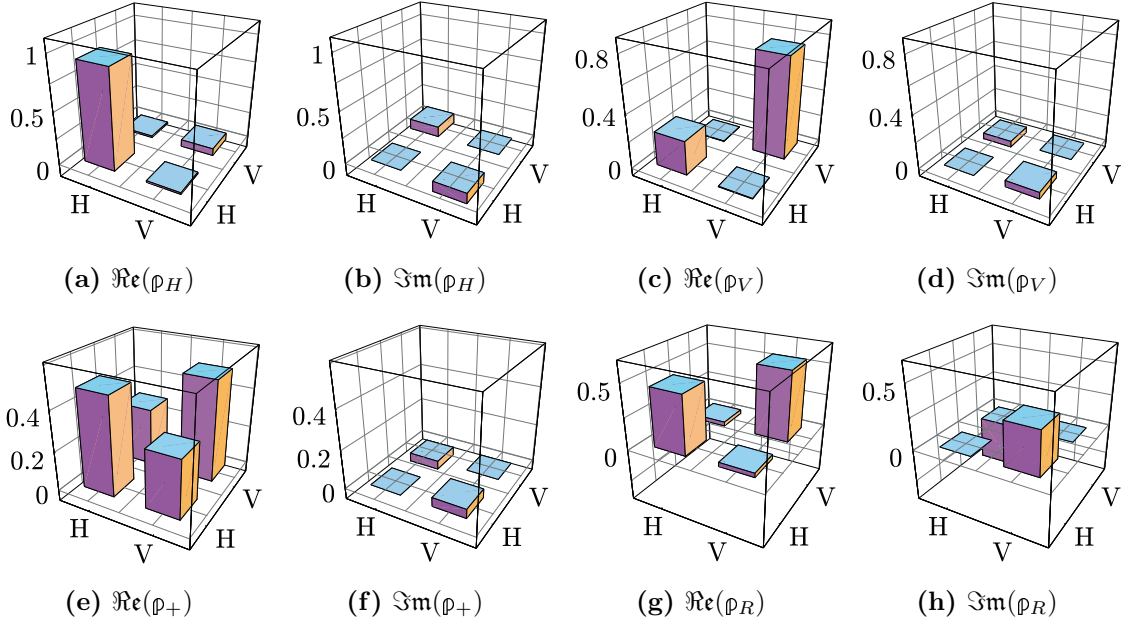


Figure 3.3: Experimentally determined density matrices of various teleported states. For each input state the data at the output was averaged over the four possible detections in the **CPHASE** gate. Prior to the averaging, the proper unitary transformation was applied to the data. (a) Real part and (b) imaginary part of the output density matrix for teleportation of $|H\rangle$. In this instance, lack of quality in the output state is primarily caused by imperfect input states. (c) Real part and (d) imaginary part of the output density matrix for teleportation of $|V\rangle$. This state is expected to be teleported worst as its quality is impaired at most for incoherent **CPHASE** operation. This is observable in the comparably high $|H\rangle\langle H|$ noise. (e) Real part and (f) imaginary part of the output density matrix for teleportation of $|+\rangle$ and (g) real part and (h) imaginary part of the output density matrix for teleportation of $|R\rangle$. These two states are supposed to be teleported approximately with the same quality. This is not exactly the case in the experiment due to additional imperfections besides lack of coherence in the gate and lack of quality of the input states.

to the data during the evaluation process. After averaging for each state over the different projection outcomes, m_1, m_2 , this results in $F_H = 0.93 \pm 0.02$, $F_V = 0.75 \pm 0.05$, $F_+ = 0.79 \pm 0.02$, $F_R = 0.84 \pm 0.03$. The real- and imaginary parts of ρ_k are graphically displayed in Fig. 3.3(a) – Fig. 3.3(h). As can be seen, the quality of the output states differs for the various input states. This can be understood by considering the influence of imperfect gate operation. In Sec. 2.1 it was concluded that for the experimental gate the main source of errors is a lack of coherence. Taking that into account, it is obvious that the teleportation works best for the state $|H\rangle$, as in this instance no interference is required. In contrast, from this point of view the output state for the input $|V\rangle$ is expected to be the worst. The states $|+\rangle$ and $|R\rangle$ should be teleported approximately at the same quality on average. However, for the state $|+\rangle$ the fidelity of the output state depends on the result of the projection in the **CPHASE** gate. It is worse for $m_1 = 0$ and better for $m_1 = 1$. A calculation using Eqn. (2.8) with $\mathcal{Q}' = 0.90$ is shown in Tab. 3.1(a). For comparison the measured results are summarized in Tab. 3.1(b). As can be seen, the measured fidelities exhibit roughly the expected behavior. Still, they are significantly worse than calculated. This is due to the fact that, naturally in

the experiment other effects occur in addition to the lack of coherence. Tab. 3.1(a) shows in square brackets the results of the output state fidelities for a calculation which uses the QPT matrix χ_{fit} and allows for imperfect input states $\rho_{a,b} \otimes \rho_c$ of the form

$$\rho_{a,b} = f_1 |\phi^+\rangle\langle\phi^+| + \frac{1-f_1}{4} \mathbb{1}^{\otimes 2} \quad (3.5a)$$

$$\rho_c = f_2 |k\rangle\langle k| + \frac{1-f_2}{2} \mathbb{1}, \quad (3.5b)$$

with $f_1 = 0.93$ and $f_2 = 0.95$. Comparing these values again with the experimental ones points up that the loss in quality for $|H\rangle$ is indeed not impaired by lack of coherence but mainly determined by impurity of the input states. For $|R\rangle$ obviously both effects are relevant. The model is not capable of explaining why the measured fidelities for every state, not only for $|+\rangle$, fluctuate for the different projections in the CPHASE gate. This must be due to noise effects which are not accounted for in χ_{fit} . These effects seem to be also responsible for the worse than expected fidelity of $|V\rangle$ and $|+\rangle$.

Despite all imperfections, it is important to note that the average fidelities are all well above the optimal classical limit² of $\frac{2}{3}$.

Quantum process tomography

The four input states, $|H\rangle$, $|V\rangle$, $|+\rangle$, $|R\rangle$, represent a tomographic set out of which a teleportation process tomography can be evaluated. Similarly as described for the CPHASE gate (see Sec. 2.1.3), such a tomography yields a matrix \mathcal{M}_{ij} which characterizes the performance of the teleportation process according to

$$\widehat{\mathbb{E}}(|k\rangle\langle k|) = \rho_k = \sum_{ij} \mathcal{M}_{ij} \mathbb{E}_i |k\rangle\langle k| \mathbb{E}_j^\dagger. \quad (3.6)$$

For the linear decomposition of the superoperator, $\widehat{\mathbb{E}}$, the basis of unitary transformations \mathbb{E}_i is here chosen to be

$$\mathbb{E}_1 = \mathbb{1}, \quad \mathbb{E}_2 = \sigma_x, \quad \mathbb{E}_3 = -i\sigma_y, \quad \mathbb{E}_4 = \sigma_z. \quad (3.7)$$

The experimentally measured matrix \mathcal{M}_{exp} is shown in Fig. 3.4. In this representation an ideal teleportation (\mathcal{M}_{th}) corresponds to the identity operation. Thus the height of the $(\mathbb{E}_1, \mathbb{E}_1)$ -entry of \mathcal{M}_{exp} directly gives the process fidelity,

$$F_p = \text{tr}(\mathcal{M}_{\text{th}}\mathcal{M}_{\text{exp}}), \quad (3.8)$$

which is the overlap between the experimentally obtained and the theoretically expected matrix. It measures the quality of the implemented teleportation process and reaches in the experiment a value of $F_p = 0.75$. The limiting factor of the process fidelity is the fidelity of the state which is teleported worst. Following the discussions of the previous section this is the state $|V\rangle$ for which the output state fidelity reaches an average value comparable to F_p .

The inherent quantum features of the teleportation process are best seen by performing entanglement swapping. In the experiment described before, the teleportation of a polarized

²The best fidelity which can be achieved by a local measurement of the state and a remote preparation after the exchange of classical information is $\frac{2}{3}$ for a single qubit averaged over all possible input states. For a comprehensive explanation see, e.g., [168].

(a) Calculated fidelities of the teleported output states

state	Fidelity for different projection results: m_1, m_2								Average fidelity	
	0, 0		0, 1		1, 0		1, 1			
$ H\rangle$	1.00	[0.93]	1.00	[0.93]	1.00	[0.93]	1.00	[0.93]	1.00	[0.93]
$ V\rangle$	0.83	[0.81]	0.83	[0.81]	0.83	[0.81]	0.83	[0.81]	0.83	[0.81]
$ +\rangle$	0.83	[0.77]	1.00	[0.94]	0.83	[0.77]	1.00	[0.94]	0.915	[0.855]
$ R\rangle$	0.91	[0.85]	0.91	[0.85]	0.91	[0.85]	0.91	[0.85]	0.91	[0.85]

(b) Measured fidelities of the teleported output states

state	Fidelity for different projection results: m_1, m_2				Average fidelity
	0, 0	0, 1	1, 0	1, 1	
$ H\rangle$	0.92 ± 0.05	0.94 ± 0.04	0.95 ± 0.04	0.93 ± 0.05	0.93 ± 0.02
$ V\rangle$	0.77 ± 0.06	0.80 ± 0.06	0.71 ± 0.07	0.71 ± 0.06	0.75 ± 0.05
$ +\rangle$	0.74 ± 0.04	0.96 ± 0.02	0.66 ± 0.05	0.86 ± 0.04	0.79 ± 0.02
$ R\rangle$	0.81 ± 0.05	0.85 ± 0.05	0.88 ± 0.04	0.81 ± 0.05	0.84 ± 0.03

Table 3.1: Table of the teleportation output states' fidelity for the different input states depending on the result of the Bell state projection measurement in the **CPHASE** gate. (a) Calculated fidelities of the output states using the **CPHASE** model of Eqn. (2.8) and assuming a quality parameter $\mathcal{Q}' = 0.90$. Values in square brackets are for a similar calculation using the **CPHASE QPT** matrix χ_{fit} and allowing additionally for imperfect input states. The state $|H\rangle$ is expected to be teleported best as it is not influenced by \mathcal{Q}' . In contrast the state $|V\rangle$ is maximally affected by \mathcal{Q}' and therefore teleported worst. Except for the state $|+\rangle$, the output fidelities are not dependent on the results of the Bell state projection. (b) Measured fidelities of the teleported output states. In the experiment the fidelities depend on the results of the Bell projection measurement. This effect cannot be explained by lack of coherence in the **CPHASE** gate or admixture of white noise in the input states.

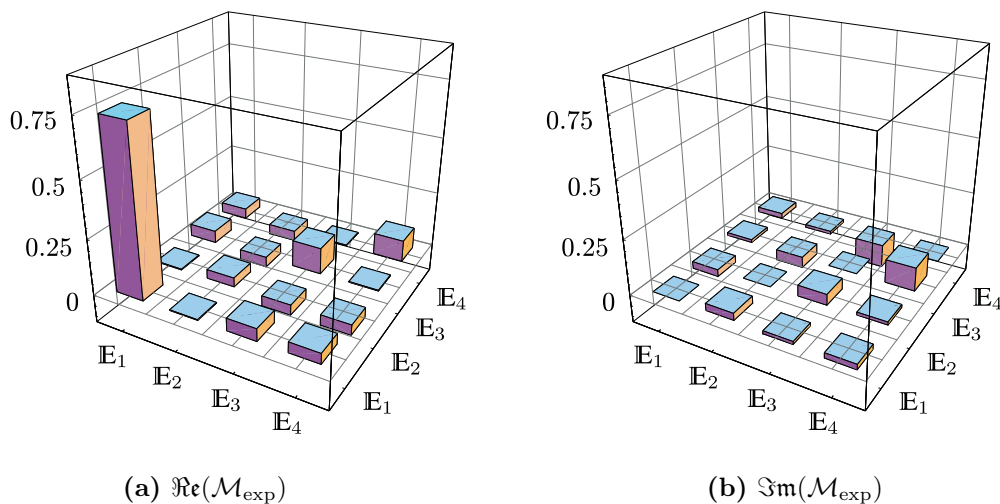


Figure 3.4: (a) Real part and (b) imaginary part of the experimentally reconstructed quantum process tomography matrix for the teleportation process. An ideal teleportation corresponds to the identity. Thus, the height of the $(\mathbb{E}_1, \mathbb{E}_1)$ entry directly gives the process fidelity F_p which is a measure for the performance of the protocol. It is bounded by the fidelity of the state which is teleported worst and reaches here $F_p = 0.75$.

photon does not succeed always, e.g., due to experimental restrictions like limited detection efficiencies etc. Hence it could be argued that the observed teleportation fidelities are a result of statistical averaging over many measurements. Such arguments can be directly refuted for entanglement swapping. Here, the teleported photon is part of an entangled pair, in that sense it is not polarized. Therefore, the outcome of a measurement on this photon considered apart is completely random. Thus, if the observed teleportation results for individual one-photon output states were attributed to statistical averaging, the analogue experimental procedure would unavoidably lead to a random result for the correlation measurements on two-photon output states. In the following, however, it will be proven that indeed quantum correlations can be observed. This confirms the entanglement contained in the swapped photon pair and proves that teleportation succeeds for every single instance.

3.1.4 Experimental results for entanglement swapping

In order to perform entanglement swapping, the **SPDC** is operated to emit photon pairs in the forward and in the backward direction, respectively; each in the state $|\phi^+\rangle$. After complete alignment procedure the pairs emitted in the forward (backward) direction exhibit polarization correlation visibilities of approximately 0.98 (0.98) in the computational basis, $\sigma_z \otimes \sigma_z$, and 0.94 (0.95) in the conjugate diagonal basis, $\sigma_x \otimes \sigma_x$. As before, the Bell projection measurement between the photons in modes b and c is accomplished by the use of the **CPHASE** gate. Like previously described, by projecting photons from these two modes onto a Bell state, the photons from mode a and d will be left likewise in a maximally entangled state. Which Bell state they form depends in turn on the result of the Bell state measurement in modes b and c (see Eqn. (3.4)).

Results for the output states

In order to determine how close the experimentally obtained states are to the expected ones and whether they are indeed entangled, a two-qubit state tomography is performed for the photons detected in modes a and d . This allows the reconstruction of the experimental states' density matrices ρ_l , ($l \in \{\phi^+, \psi^+, \widetilde{\phi}^-, \widetilde{\psi}^-\}$), which are displayed in Fig. 3.5. The measure-

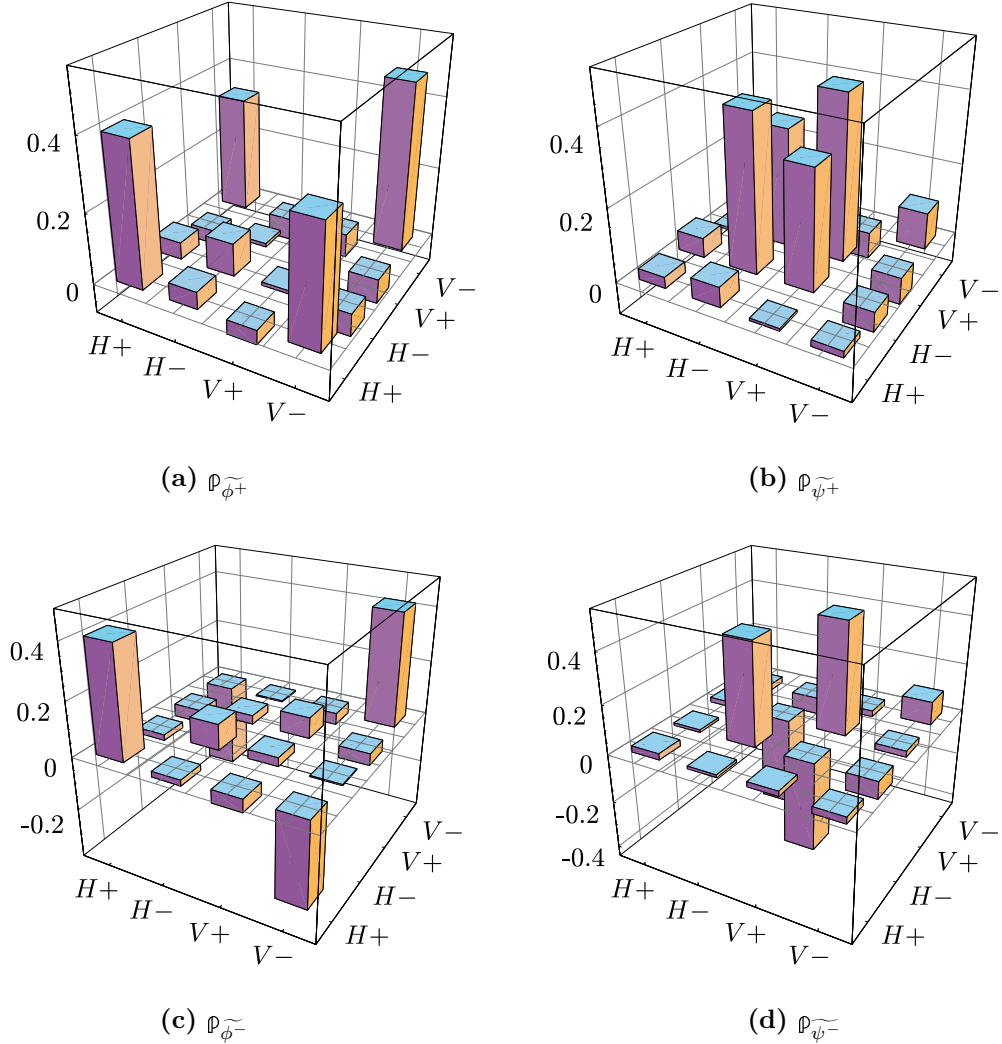


Figure 3.5: Real parts of the measured density matrices of the output states for the entanglement swapping protocol. (a) For projection of the photons in mode b and c onto $|++\rangle$, the photons in mode a and d are expected to be in the state $|\widetilde{\phi}^+\rangle$. (b) Analogously for a projection onto $|+-\rangle$, the photons in modes a and c are found in the state $|\psi^+\rangle$. (c) The state $|\widetilde{\phi}^-\rangle$ corresponds to projection onto the state $|--\rangle$. (d) For a projection onto $|+-\rangle$, the state $|\widetilde{\psi}^-\rangle$ should be obtained.

ment time for each of the nine basis settings of the tomography amounts to approximately 420 min. From the acquired data the states' fidelity F_l , as well as their logarithmic negativity \mathcal{N} (see Def. 1.2.8) can be calculated. The results are summarized in Tab. 3.2. As can be seen

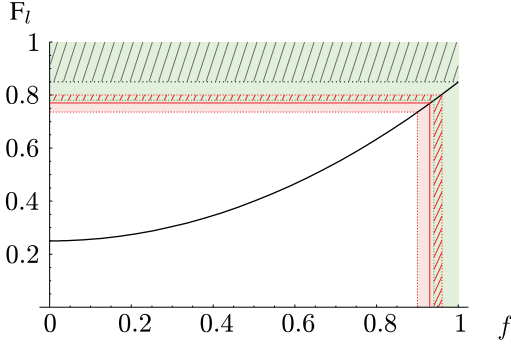


Figure 3.6: Fidelity F_l of the swapped output states depending on the ratio of white noise, $(1 - f)$, contained in the input states. Even for perfect ($f = 1$) input states, F_l cannot exceed 0.85 (shaded area). States with $F_l \geq 0.78$ violate a Bell inequality (green area). With a range of $0.73 \leq F_l \leq 0.80$ (red area) and an average of $F_l = 0.77$ (red line), the fidelity of the experimental states lies just at this limit.

an entangled state is obtained for each of the four Bell state projections in the **CPHASE** gate with fidelities of up to 0.80 relative to the corresponding expected Bell state. On average the fidelity is 0.77 for all simultaneously detected Bell states. The maximally possible fidelity to achieve is bounded by the imperfect gate operation. A simulation based on χ_{fit} reveals that even for a perfect input state, the output state fidelity cannot exceed 0.85. A calculation of F_l allowing for mixed input states ρ_{in} of the form

$$\rho_{\text{in}} = \rho_{a,b} \otimes \rho_{c,d} \quad (3.9)$$

with

$$\rho_{a,b} = \rho_{c,d} = f |\phi^+\rangle\langle\phi^+| + \frac{1-f}{4} \mathbb{1}^{\otimes 2} \quad (3.10)$$

is shown in Fig. 3.6. For the assumption Eqn. (3.10) the result is quadratic in f . The measured average value of $F_l = 0.77$ corresponds thereby approximately to $f = 0.93$. In any case, also for $\rho_{a,b} \neq \rho_{c,d}$, F_l does not depend on the result of the Bell projection measurement in the **CPHASE** gate. The reason for the quality difference between ρ_{ϕ^-} and ρ_{ψ^-} cannot be explained within this model and must be due to effects which are not accounted for by χ_{fit} .

Entangled states with a fidelity larger than $(2 + 3\sqrt{2})/8 \approx 0.78$ violate Bell-type inequalities [169]. According to the previous discussions this requires f to be greater than 0.94. Consequently, with an average fidelity of 0.77, the quality of the measured states is just at this limit and does not doubtlessly provide evidence for a violation of local realism. Therefore, in the following, it will be explicitly shown that the violation of a **CHSH** type Bell inequality (see page 11) is indeed possible.

Bell state observed	Fidelity F_l	Negativity \mathcal{N}
$ \widetilde{\phi}^+\rangle_{ad}$	0.777 ± 0.031	0.660 ± 0.051
$ \widetilde{\psi}^+\rangle_{ad}$	0.776 ± 0.029	0.666 ± 0.048
$ \widetilde{\phi}^-\rangle_{ad}$	0.736 ± 0.031	0.582 ± 0.055
$ \widetilde{\psi}^-\rangle_{ad}$	0.803 ± 0.027	0.720 ± 0.042

Table 3.2: Measured fidelities of the swapped states and the corresponding logarithmic negativity. For each projection in the **CPHASE** gate the photons in modes a and d are found in an entangled state.

Bell state	Correlation coefficient
$ \widetilde{\phi}^+\rangle_{ad}$	$\mathcal{S}_+ = -2.20 \pm 0.17$
$ \widetilde{\psi}^+\rangle_{ad}$	$\mathcal{S}_+ = 2.13 \pm 0.15$
$ \widetilde{\phi}^-\rangle_{ad}$	$\mathcal{S}_- = 2.12 \pm 0.16$
$ \widetilde{\psi}^-\rangle_{ad}$	$\mathcal{S}_- = -2.12 \pm 0.18$

Table 3.3: Measured value of the CHSH correlation coefficient. The swapped states violate the bound for local realistic theories by about one standard deviation.

Violation of local realism

Quantum teleportation enables efficient communication of quantum information between remote partners and thus is a core element of future long distance quantum networks. From that point of view entanglement swapping is particularly useful, provided it yields a swapped state which is entangled strongly enough such as to exhibit non-local correlations. To check the non-classical properties of the experimentally observed states, a CHSH type Bell inequality is measured, (see page 11). Using the CPHASE gate this can be done at the same time for all four Bell states by measuring the correlation coefficient,

$$|\mathcal{S}_{\pm}| := |\pm\langle\mathbf{A}, \mathbf{D}\rangle \mp \langle\mathbf{A}, \mathbf{D}'\rangle + \langle\mathbf{A}', \mathbf{D}\rangle + \langle\mathbf{A}', \mathbf{D}'\rangle|. \quad (3.11)$$

Herein, $\langle\mathbf{A}, \mathbf{D}\rangle$, $\langle\mathbf{A}, \mathbf{D}'\rangle$, $\langle\mathbf{A}', \mathbf{D}\rangle$ and $\langle\mathbf{A}', \mathbf{D}'\rangle$ are the expectation values of four local operators

$$\mathbf{A} = \sigma_x \quad (3.12a)$$

$$\mathbf{A}' = \sigma_z \quad (3.12b)$$

$$\mathbf{D} = \frac{1}{\sqrt{2}} \sigma_z + \frac{1}{\sqrt{2}} \sigma_x \quad (3.12c)$$

$$\mathbf{D}' = \frac{1}{\sqrt{2}} \sigma_x - \frac{1}{\sqrt{2}} \sigma_z, \quad (3.12d)$$

where \mathbf{A}, \mathbf{A}' are acting on qubits in mode a and \mathbf{D}, \mathbf{D}' on qubits in mode d . This corresponds to a polarization measurement under four sets of angles; 0° for \mathbf{A}' , -22.5° for \mathbf{D} , -45° for \mathbf{A} and -67.5° for \mathbf{D}' , respectively.

For local hidden variable models $|\mathcal{S}_{\pm}|$ is bounded from above by 2. In the experiment this limit can be violated for each of the four Bell states by about one standard deviation. The results are summarized in Tab. 3.3. As expected from the previous discussions the violation is tight and, due to the limited measurement time for each of the four cases, the error is relatively high. However, the average value of 2.14 ± 0.08 shows a significant violation of the Bell inequality.

3.1.5 Discussion

The distinction of all four Bell states is not a necessary ingredient in the teleportation and entanglement swapping protocol. The first realizations indeed used the projection onto a single Bell-state only, neglecting the other cases. This results in a success probability of $\frac{1}{4}$ [131, 159]. The best success probability achieved is $\frac{1}{2}$ and is known to be the theoretical limit when using linear optics without ancillary qubits [91, 160, 161, 170]. Even though in the scheme presented here no Bell state is neglected, the success probability is limited by the

efficiency of the gate operation, which is $\frac{1}{9}$, and therefore lower than in the other schemes. Still, the beauty in the application of the **CPHASE** gate is the possibility to detect all four Bell states in a setup just as simple as the (single-state) Bell state projection of the initial demonstration of quantum teleportation [159].

Moreover, for quantum teleportation and entanglement swapping, the detection of all four Bell states could be mimicked with a setup that distinguishes only a restricted number by randomly switching between the detected set of states. However, it has to be emphasized that this approach effectively causes only a statistical mixture of all four Bell states. In contrast, in the **CPHASE** gate scheme, a coherent Bell state projection is obtained once a single photon travels in each of the four modes prior to the detection. This is a fundamental difference and might be crucial for other tasks that rely on the analysis of Bell states or, more general, the successful application of linear optics gates. In the following, such other tasks will be presented.

3.2 Experimental direct measure of concurrence for mixed states

In Chap. 1 several tools for the characterization of entangled states have been introduced. Depending on the given experimental circumstances each of them has specific advantages and drawbacks. For instance, while Bell inequalities and entanglement witnesses usually require a comparably low number of observables to be measured, they are flawed by the fact that one specific parameter setting is applicable to a rather small set of entangled states. On the other hand, entanglement measures can be used for any state, but their functional relation to the state to be characterized is typically non-linear, or even worse, they involve un-physical operations that cannot be directly experimentally implemented. This means their evaluation requires the reconstruction of the state's density matrix by **QST** which entails a number of measurements exponentially increasing in the system size. In particular this holds for the negativity (see Def. 1.2.8) and the concurrence (see Def. 1.2.7), which are the most common computable entanglement measures.

For the determination of the latter, an alternative path was recently introduced, which utilizes measurements on multiple identically prepared quantum systems. It was shown that the concurrence of a bipartite qubit system can be measured directly without prior state reconstruction by collective measurements on a small number of copies [171, 172]. However, these measurements are based on the known algebraic solution for the concurrence and require a rather complex experimental setup. An experimental simplification is achieved for a generalization of the concurrence to systems of arbitrary finite dimensions [173], which, if restricted to qubits, is equivalent to the original definition [54]. As any m th degree polynomial function of a density matrix can be measured on an m -fold copy of the state [174], this approach accounts for the nonlinear dependence of the concurrence on the system state by considering a twofold copy of the density matrix. This method was first experimentally demonstrated by Walborn *et al.* [175]. In this work the authors assume the two copies to be pure states, which is not only a strong but also unrealistic assumption for any real experiment. In case that the copies are not pure, the measurement procedure for the direct evaluation of the concurrence needs to be refined [176]. In the following it will be shown how the **CPHASE** gate can be used to derive a lower bound on the concurrence of the observed states without any further restrictive assumptions. In order to obtain a correct estimation of the entanglement, not only

the mixedness of the states but also the imperfections of real gate operation have to be taken into account.

3.2.1 Theory

The everyday technique to infer information about the state of a quantum system is to measure observables, represented by Hermitian operators, \mathbf{O} , in the Hilbert space \mathbb{H} of the quantum system to be examined. The expectation value $\langle \psi | \mathbf{O} | \psi \rangle$ then allows to infer information about the underlying state $|\psi\rangle$. As mentioned above, the presently discussed measurement scheme is based on analyzing two identically prepared bipartite quantum systems. Formally, this implies that expectation values, $\langle \psi | \otimes \langle \psi | \mathbf{O}' | \psi \rangle \otimes |\psi\rangle$, are considered with respect to a twofold direct product of $|\psi\rangle$ with itself. The observable \mathbf{O}' is an operator on the extended Hilbert space $\mathbb{H} \otimes \mathbb{H}$.

In such extended Hilbert spaces, there are two different types of states with distinguished symmetry properties upon permutation. Symmetric states are invariant, whereas antisymmetric states acquire a minus sign under permutation. For the case of a qubit, the triplet states $|00\rangle$, $\frac{1}{\sqrt{2}}(|01\rangle + |10\rangle)$, and $|11\rangle$ form a basis of symmetric states, and the singlet $\frac{1}{\sqrt{2}}(|01\rangle - |10\rangle)$ is the sole antisymmetric state. These are exactly the eigenstates of the SWAP operation (see Eqn. (1.48)) for positive and negative eigenvalue, respectively. For reasons that shall be clear later on, it can be convenient to alternatively choose all the triplet states in form of the Bell states, $|\phi^\pm\rangle, |\psi^\pm\rangle$.

Given the ability to prepare a bipartite quantum system twice in the same fashion, and to distinguish symmetric from antisymmetric states, the concurrence of an arbitrary pure state can be measured [51, 54, 173, 177]. It is determined in terms of the probability to find the components of one subsystem of the duplicate quantum state in an antisymmetric state,

$$\mathcal{C}(\psi) = 2\sqrt{\wp_{--}} \equiv 2\sqrt{\langle \psi | \otimes \langle \psi | \mathbf{P}_{--} | \psi \rangle \otimes |\psi\rangle}, \quad (3.13)$$

with $\mathbf{P}_{--} \equiv (\mathbf{1} \otimes \text{SWAP} \otimes \mathbf{1}) \cdot (\mathbf{P}_- \otimes \mathbf{P}_-) \cdot (\mathbf{1} \otimes \text{SWAP} \otimes \mathbf{1})^\dagger$ and $\mathbf{P}_- \equiv |\psi^-\rangle \langle \psi^-|$. This is what was experimentally demonstrated in [175].

The intricacy concerning entangled states comes with mixing. For mixed states \wp the concurrence is defined via the optimization $\mathcal{C}(\wp) = \inf \sum_i \wp_i \mathcal{C}(\psi_i)$ over all sets of pure states $|\psi_i\rangle$, and probabilities \wp_i that are described by the density matrix \wp , i.e., that satisfy $\sum_i \wp_i |\psi_i\rangle \langle \psi_i| = \wp$. Such optimizations are rather extensive mathematical problems, and there is no prospect of finding exact general solutions beyond the case of two qubits. In particular, that means that it is practically impossible to redefine concurrence of mixed states in terms of a simple measurement prescription.

Still, lower bounds on the concurrence of arbitrary mixed states can be measured within the presently discussed framework of two identically prepared quantum states. The underlying idea is based on the fact that two identically prepared *pure* states form a globally symmetric object: that is, if the first-subsystem components are observed in a symmetric state, then also the second-subsystem components will be found in a symmetric state; and, similarly the observation of an antisymmetric state in the components of one subsystem projects the components of the other subsystem likewise in an antisymmetric state.

Consequently, the probability to find the components of the two different subsystems in states with different symmetry provides information on the mixing of the underlying state. Assuming a pure state, the concurrence is given in terms of the probability \wp_{--} to find the

twofold state $|\psi\rangle \otimes |\psi\rangle$ in locally antisymmetric states, but the larger the mixing is, the larger the deviation between this quantity and the actual value of the concurrence will be. For very weakly mixed states, \wp_{--} alone provides an approximation of the concurrence at the expense of overestimating its actual value.

For a more reliable estimation, such as a lower bound, the contribution which is due to mixing has to be subtracted from \wp_{--} . Indeed, it turns out that the concurrence of an arbitrary mixed state is bounded from below by $2\sqrt{\wp_{--} - \wp_{-+}}$, and by $2\sqrt{\wp_{--} - \wp_{+-}}$ [176], where \wp_{-+} is the probability to observe the first-subsystem part of $\rho \otimes \rho$ in an antisymmetric state, and simultaneously the second-subsystem part in a symmetric state, and vice versa for \wp_{+-} :

$$\wp_{-+} \equiv \text{tr}(\mathbf{P}_{-+} \rho \otimes \rho), \quad (3.14a)$$

$$\wp_{+-} \equiv \text{tr}(\mathbf{P}_{+-} \rho \otimes \rho), \quad (3.14b)$$

with $\mathbf{P}_{-+} \equiv (\mathbb{1} \otimes \text{SWAP} \otimes \mathbb{1}) \cdot (\mathbf{P}_- \otimes \mathbf{P}_+) \cdot (\mathbb{1} \otimes \text{SWAP} \otimes \mathbb{1})^\dagger$, $\mathbf{P}_{+-} \equiv (\mathbb{1} \otimes \text{SWAP} \otimes \mathbb{1}) \cdot (\mathbf{P}_+ \otimes \mathbf{P}_-) \cdot (\mathbb{1} \otimes \text{SWAP} \otimes \mathbb{1})^\dagger$ and $\mathbf{P}_+ \equiv \mathbb{1}^{\otimes 2} - |\psi^-\rangle\langle\psi^-|$. Here, it was implicitly assumed that \wp_{--} is larger than \wp_{-+} or \wp_{+-} . If this is not the case, then this implies that either the state is separable, i.e., its concurrence vanishes, or the state is too highly mixed, and the present bound fails to detect its entanglement.

In the following, the implementation of this measurement procedure using the **CPHASE** gate is discussed. The experiment gives evidence that the lower bound provides an accurate estimate of the actual value of concurrence for states that are getting mixed due to imperfections of state of the art experiments.

3.2.2 Experimental implementation

The setup for the direct measurement of concurrence is the same as depicted in Fig. 3.2. The concurrence of the states emitted by the **SPDC** is to be determined. The two **SPDC** sources are built in exactly the same manner and therefore the emission in the forward and backward direction can each be considered as providing one copy of the state in question. The **UV** mirror reflecting the pump beam in the backward direction is positioned 3 cm behind the down conversion crystal. The small distance (compared to 40 cm Rayleigh length of the pump beam) together with a proper tilt of the mirror leads to identical phase-matching conditions for both **SPDC** emissions. The single mode fiber couplers are aligned to select the same spectral range of down converted photons for all four modes. As before, the spectra are basically determined by narrow bandwidth interference filters ($\Delta\lambda = 3$ nm in modes a, d and $\Delta\lambda = 2$ nm in modes b, c).

The projection measurement onto the symmetric and antisymmetric subspace is accomplished by subjecting the components of the subsystems in modes b and c to a complete Bell state projection measurement. As mentioned before, the symmetric subspace is thereby spanned by $\{|\phi^\pm\rangle, |\psi^+\rangle\}$; and $|\psi^-\rangle$ is the only antisymmetric state. The distinction of all four Bell states at the same time can be achieved by a two qubit logic gate like a **CNOT** or **CPHASE** gate. The usage of the **CPHASE** instead of the **CNOT** gate in the present configuration implies that a Hadamard rotation is additionally applied to one copy of the input state. This is important to note, as for the direct measurement procedure of concurrence it is essential to project onto the standard Bell basis and not onto $\{|\widetilde{\phi}^\pm\rangle, |\widetilde{\psi}^\pm\rangle\}$. Only the former equals a distinction according to symmetric and antisymmetric. The circuit for the measurement

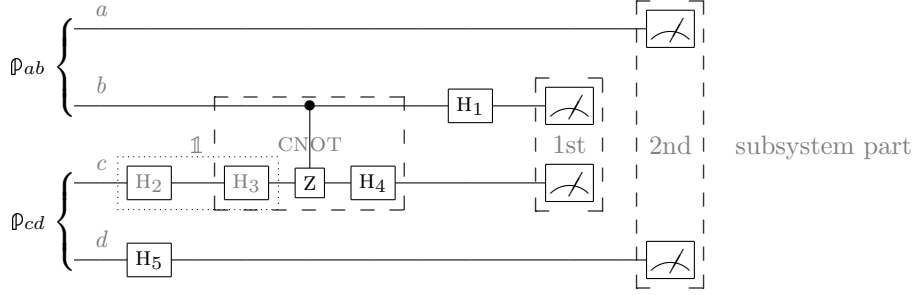


Figure 3.7: Circuit diagram for the direct measurement of concurrence. The usage of the **CPHASE** gate for the measurement procedure yields an estimation for $\mathcal{C}(\rho_{ab})\mathcal{C}((\text{HAD} \otimes \text{HAD}) \cdot \rho_{cd} \cdot (\text{HAD} \otimes \text{HAD})^\dagger)$. As the gates H_2 and H_3 form together the identity, they are not physically implemented.

procedure is drawn in Fig. 3.7. Comparing Fig. 3.7 with Fig. 1.6(h) shows that the **CPHASE** gate together with the Hadamard gates H_1 , H_3 and H_4 implements exactly Circ. 1.45 which is required for the projection in the standard Bell basis. As the sequence of gates H_2 and H_3 equals the identity, both gates are not physically realized in the setup. In this configuration, a measurement of the probabilities \wp_{--} , \wp_{+-} , \wp_{-+} yields a lower bound on the product of the concurrences of both input states according to

$$\mathcal{C}(\rho_{ab})\mathcal{C}(\rho'_{cd}) \geq \text{tr}(\rho_{ab} \otimes \rho'_{cd} \mathbf{V}_i), \quad (3.15)$$

with $\rho'_{cd} = (\text{HAD} \otimes \text{HAD}) \cdot \rho_{cd} \cdot (\text{HAD} \otimes \text{HAD})^\dagger$, $\mathbf{V}_1 = 4(\mathbf{P}_- - \mathbf{P}_+) \otimes \mathbf{P}_- = 4(\mathbf{P}_{--} - \mathbf{P}_{+-})$ and $\mathbf{V}_2 = 4\mathbf{P}_- \otimes (\mathbf{P}_- - \mathbf{P}_+) = 4(\mathbf{P}_{--} - \mathbf{P}_{-+})$.

3.2.3 Results

The determination of the probabilities \wp_{--} , \wp_{-+} , \wp_{+-} requires only three correlation measurements, XZZX , YZZY and ZZZZ , or if the Hadamard gates are already taken into account, ZXXX , YXXY and XXXX .

For the latter, the detection of photons in modes b and c in the state $|--\rangle$ corresponds to a projection onto the antisymmetric subspace. Thus, the share of these events in all detected coincidences directly gives the probability \wp_- to find the one subsystem part in the antisymmetric subspace. The remaining events where the photons in modes b and c are measured in the states $|++\rangle$, $|+-\rangle$ and $| -+\rangle$ lead accordingly to the probability to observe this subsystem part in the symmetric subspace. Correlation measurements of the form Z..X , Y..Y and X..Z allow the reconstruction of the fidelity of the qubits a and d on any of the four Bell states in analogy to Eqn. (2.38), (see also Eqn. (2.42)). The fidelity F_{ψ^-} to the state $|\psi^-\rangle$ equals thereby the probability to find the other subsystem part in the antisymmetric subspace, whereas $1 - F_{\psi^-}$ gives the probability to observe it in the symmetric subspace.

Finally, the evaluation of the quantities F_{ψ^-} and $1 - F_{\psi^-}$ for the modes a and d with respect to the different detection events in modes b and c yields all the conditional probabilities needed for the calculation of the concurrence according to Eqn. (3.15). For a measurement time of

approximately 420 min for each setting this results in

$$\begin{aligned}\wp_{--} &= 0.208 \pm 0.007, \\ \wp_{-+} &= 0.050 \pm 0.006, \\ \wp_{+-} &= 0.061 \pm 0.012,\end{aligned}\tag{3.16}$$

what corresponds to

$$\begin{aligned}\mathcal{C}(\wp_{ab})\mathcal{C}(\wp'_{cd}) &\geq 4(0.208 \pm 0.007 - 0.050 \pm 0.006) = 0.632 \pm 0.037 \\ &\geq 4(0.208 \pm 0.007 - 0.061 \pm 0.012) = 0.588 \pm 0.055.\end{aligned}\tag{3.17}$$

Assuming $\wp_{ab} = \wp'_{cd} = \wp$, this implies a concurrence value $\mathcal{C}(\wp) \geq 0.795$. For comparison, with the additional assumption made in [175] of having pure input states it holds that the probability \wp_- of finding the subsystem part b, c in the antisymmetric subspace is identical to the conditional probability \wp_{--} . With the obtained data, $\wp_- = 0.258 \pm 0.005$, what in turn would correspond to a concurrence value of $\mathcal{C}(\wp) = 2\sqrt{\wp_-} = 1.015 \pm 0.005$. As this value is bigger than one, it is un-physical and clearly an overestimation. This proves that the above scheme allowing for impurities of the input states leads indeed to a more reliable and realistic estimation of the actual entanglement contained in the initial states.

3.2.4 Influence of imperfect gate operation

Another important issue, besides the mixedness of the initial states, which was not taken into account so far, is the influence of imperfect gate operation. This shall be finally studied in the following. To this end, numerical simulations are performed using the QPT matrix, χ_{fit} , which was derived in Sec. 2.1.3.

At first, perfectly pure initial states, $|\phi^+\rangle \otimes |\phi^+\rangle$, are considered. A simulation of the measurement based on χ_{fit} yields

$$\begin{aligned}\wp_{--} &= 0.212, \\ \wp_{-+} &= \wp_{+-} = 0.038,\end{aligned}\tag{3.18}$$

which results in $\mathcal{C}(\wp_{ab})\mathcal{C}(\wp'_{cd}) \geq 0.696$ and consequently $\mathcal{C}(\wp) \geq 0.834$. As the initial states are pure, the non-vanishing values for \wp_{-+} and \wp_{+-} can only be caused by deficient gate operation. A comparison of Eqn. (3.16) and Eqn. (3.18) even suggests at first glance that the experimentally determined bound on the concurrence is more influenced by the gate than by the impurity of the initial states. To better judge how strong the gate influence actually is, the following calculation is carried out, (see Fig. 3.8(a)). For pairs of given, assumably measured probabilities $\{\wp_{--}, \wp_{+-}\}$ and $\{\wp_{--}, \wp_{-+}\}$, the minimal bound on the concurrence for a general input state is calculated which is still consistent with their assumed values. This means it is searched for an arbitrary state of the form,

$$\wp = \wp_{ab}^1 \otimes \wp_{cd}^2,\tag{3.19}$$

which has as low concurrence as possible in either subsystem, but still yields the values $\{\wp_{--}, \wp_{+-}\}$ or $\{\wp_{--}, \wp_{-+}\}$ when subjected to the measurement procedure described before. Fig. 3.8(b) shows the lower concurrence bound, $\inf(\mathcal{C}(\wp_{ab})\mathcal{C}(\wp'_{cd}))$, derived from $\{\wp_{--}, \wp_{+-}\}$ and $\{\wp_{--}, \wp_{-+}\}$ versus the calculated minimal bound, $\inf(\mathcal{C}(\wp_{ab})\mathcal{C}(\wp'_{cd}))_{\text{min}}$, of an arbitrary input state under the constraint to reproduce \wp_{--} and \wp_{+-} (green stars) or \wp_{--}

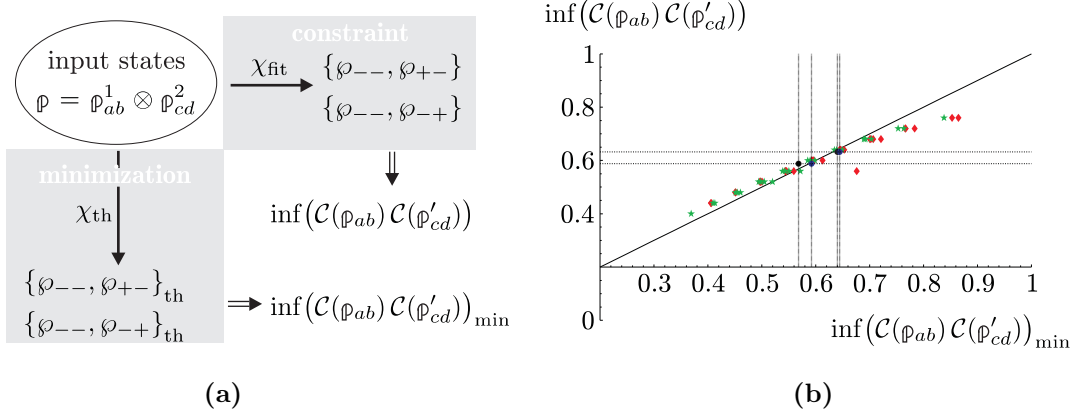


Figure 3.8: (a) Simulation scheme to obtain the minimal concurrence value. It is searched for the least entangled state of the form $\rho = \rho_{ab}^1 \otimes \rho_{cd}^2$ that still reproduces given pairs of $\{\varphi_{--}, \varphi_{+-}\}$ or $\{\varphi_{--}, \varphi_{-+}\}$ measured via χ_{fit} . (b) Simulated bound of the concurrence. $\inf(\mathcal{C}(\rho_{ab})\mathcal{C}(\rho'_{cd}))$ is derived using the measurement procedure with χ_{fit} , $\inf(\mathcal{C}(\rho_{ab})\mathcal{C}(\rho'_{cd}))_{\text{min}}$ is the constrained minimum to still reproduce the measured probabilities. (\star) Arbitrary $\{\varphi_{--}, \varphi_{+-}\}$, (\blacklozenge) arbitrary $\{\varphi_{--}, \varphi_{-+}\}$, (\bullet) $\{\varphi_{--} = 0.208, \varphi_{-+} = 0.05\}$ and $\{\varphi_{--} = 0.208, \varphi_{+-} = 0.061\}$ of $\inf(\mathcal{C}(\rho_{ab})\mathcal{C}(\rho'_{cd}))_{\text{min}} = 0.568$ is a little lower than $\inf(\mathcal{C}(\rho_{ab})\mathcal{C}(\rho'_{cd})) = 4(\varphi_{--} - \varphi_{+-}) = 0.588$ (black bullets). If the boundary conditions are tightened such that the input state should reproduce not only the measured values $\{\varphi_{--}, \varphi_{+-}\}$ or $\{\varphi_{--}, \varphi_{-+}\}$, but φ_{--} , φ_{+-} and φ_{-+} , the values $\inf(\mathcal{C}(\rho_{ab})\mathcal{C}(\rho'_{cd})) = 0.632$ and $\inf(\mathcal{C}(\rho_{ab})\mathcal{C}(\rho'_{cd}))_{\text{min}} = 0.644$ for $\{\varphi_{--}, \varphi_{-+}\}$ as well as $\inf(\mathcal{C}(\rho_{ab})\mathcal{C}(\rho'_{cd})) = 0.588$ and $\inf(\mathcal{C}(\rho_{ab})\mathcal{C}(\rho'_{cd}))_{\text{min}} = 0.592$ for $\{\varphi_{--}, \varphi_{+-}\}$ (blue bullets) are each in good agreement. In both cases a slight underestimation of the concurrence bound is obtained.

and φ_{-+} (red lozenges), respectively. As can be seen, for both cases the measurement procedure using the CPHASE gate tends to slightly underestimate the actual concurrence for high values whereas it provides a marginal overestimation for lower values. Explicitly, the least entangled state that still yields the experimentally measured values $\{\varphi_{--} = 0.208, \varphi_{-+} = 0.05\}$ has a concurrence of $\inf(\mathcal{C}(\rho_{ab})\mathcal{C}(\rho'_{cd}))_{\text{min}} = 0.640$, which is slightly higher than $\inf(\mathcal{C}(\rho_{ab})\mathcal{C}(\rho'_{cd})) = 4(\varphi_{--} - \varphi_{-+}) = 0.632$. In contrast, the value for $\{\varphi_{--} = 0.208, \varphi_{+-} = 0.061\}$ of $\inf(\mathcal{C}(\rho_{ab})\mathcal{C}(\rho'_{cd}))_{\text{min}} = 0.568$ is a little lower than $\inf(\mathcal{C}(\rho_{ab})\mathcal{C}(\rho'_{cd})) = 4(\varphi_{--} - \varphi_{+-}) = 0.588$ (black bullets). If the boundary conditions are tightened such that the input state should reproduce not only the measured values $\{\varphi_{--}, \varphi_{+-}\}$ or $\{\varphi_{--}, \varphi_{-+}\}$, but φ_{--} , φ_{+-} and φ_{-+} , the values $\inf(\mathcal{C}(\rho_{ab})\mathcal{C}(\rho'_{cd})) = 0.632$ and $\inf(\mathcal{C}(\rho_{ab})\mathcal{C}(\rho'_{cd}))_{\text{min}} = 0.644$ for $\{\varphi_{--}, \varphi_{-+}\}$ as well as $\inf(\mathcal{C}(\rho_{ab})\mathcal{C}(\rho'_{cd})) = 0.588$ and $\inf(\mathcal{C}(\rho_{ab})\mathcal{C}(\rho'_{cd}))_{\text{min}} = 0.592$ for $\{\varphi_{--}, \varphi_{+-}\}$ (blue bullets) are each in good agreement. In both cases a slight underestimation of the concurrence bound is obtained.

What can be learned from this simulation is that, without any further information about the input state, it is difficult to separate the influence of the gate operation from the one of the input state mixedness. If the input state is (nearly) pure, the imperfect gate operation can cause a significant underestimation of the concurrence. However, in the range of the measured values, Eqn. (3.16), the used measurement procedure does at least not overestimate the actual value of the concurrence.

3.2.5 Discussion

To summarize, in this section it was experimentally demonstrated that the CPHASE gate can be successfully applied to derive a lower bound on the concurrence of a given state by using the method described in [176]. In contrast to previous work [175], no additional assumptions about the purity of the state under investigation have been made. In order to prove that

the experimentally determined bound is indeed a reliable estimate, the influence of imperfect gate operation has been investigated. In particular, it was shown that the method does *not* overestimate the actual concurrence of the state, but can lead to an underestimation, which is, however, better than the other way round.

As the method requires only three measurement settings instead of nine for a full **QST** it might be advantageous in particular applications.

3.3 Observation of a four-photon Cluster state

In the previous sections the **CPHASE** gate was used to implement a complete Bell state projection measurement. In these applications the gate acts as a disentangling operation mapping four entangled Bell states onto four detectable product states. In the following last section the **CPHASE** gate is used for entangling qubits. In this context the observation of a four-photon Cluster state shall be discussed. Thereby the state is obtained by entangling photons of two Bell pairs. The resulting state and its properties are analyzed in detail in [121, 178]. Here, the results on the state observation are shortly recapitulated. The focus in the evaluation of the data is set in the following on the main application of cluster states: the measurement based quantum computing. Prior to the presentation of its experimental implementation and the discussion of the obtained results, a short introduction about cluster states and their role for measurement based computation is given.

3.3.1 The linear four-photon Cluster state

In Sec. 1.2.3 it was explained that in quantum computing the processing of information is associated with a unitary evolution of states.

Surprisingly, this (unitary) evolution of quantum information can very well go together with absolutely non-unitary, irreversible and destructive measurement processes – provided the information is embedded in entangled states [10, 147, 179]. This culminated in the discovery by Raussendorf and Briegel, suggesting universal computation by an algorithm-specific sequence of single-qubit measurements in combination with classical feed-forward transformations on the qubits of a, what they named, *cluster state* [12, 13]. In all of these so-called *measurement based quantum computation* schemes multi-qubit entanglement of the cluster state, or more generally, of graph states plays a central role [180–184].

A cluster state is an entangled state of many qubits that can be represented by a schematic presentation of its generation prescription, i.e., a cubic lattice in which the vertices are formed by two-level quantum systems and the grid lines correspond to next neighbor Ising type interactions between them, see Fig. 3.9(a). Cluster states $|C\rangle$ are fully described by a set of eigenvalue equations,

$$\mathbb{O}^i |C\rangle = (-1)^{k_i} |C\rangle \quad (3.20)$$

where the operator $\mathbb{O}^i = \sigma_x^i \otimes_{j \in nn(i)} \sigma_z^j$ corresponds to the application of σ_x on every qubit i of the lattice and σ_z on all its next neighbors (nn) j [185]. Therein, $\{k\} = \{k_i \in \{0, 1\}\}$ is an additional parameter that characterizes the particular cluster state.

A simple example of a linear four-qubit cluster state (see Fig. 3.9(b)) with $\{k\} = \{0, 0, 0, 0\}$

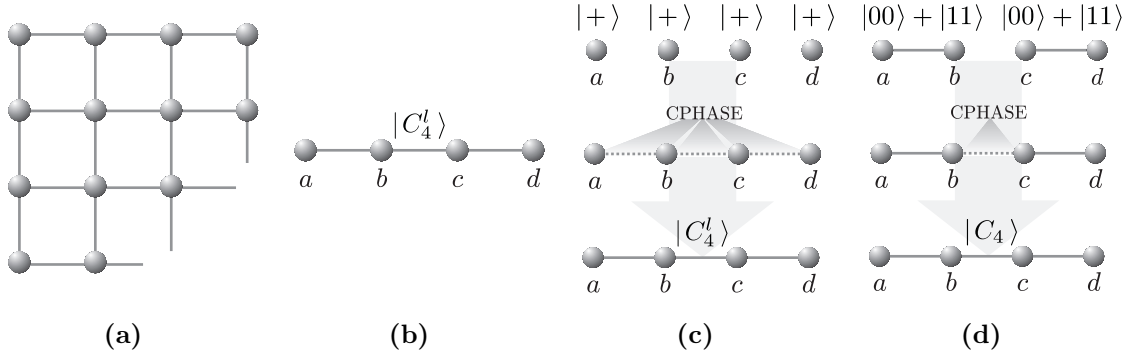


Figure 3.9: (a) Schematic figure of a cluster state. Vertices represent qubits and grid lines correspond to next neighbor Ising type interactions between them. (b) Schematic representation of the linear four-qubit cluster, $|C_4^l\rangle$. (c) Generation prescription of the four-qubit linear cluster. The qubits are initially prepared in the state $|+\rangle$ and entangled by the application of a CPHASE gate. (d) An alternative way for the experimental generation of a four-qubit cluster state starting from two entangled pairs of qubits. As qubits a, b and c, d are already entangled, the CPHASE has to be applied only once. The resulting state $|C_4\rangle$ is LU equivalent to $|C_4^l\rangle$.

leads to the following equations,

$$(\sigma_x \otimes \sigma_z \otimes \mathbb{1} \otimes \mathbb{1}) |C_4^l\rangle = |C_4^l\rangle \quad (3.21a)$$

$$(\sigma_z \otimes \sigma_x \otimes \sigma_z \otimes \mathbb{1}) |C_4^l\rangle = |C_4^l\rangle \quad (3.21b)$$

$$(\mathbb{1} \otimes \sigma_z \otimes \sigma_x \otimes \sigma_z) |C_4^l\rangle = |C_4^l\rangle \quad (3.21c)$$

$$(\mathbb{1} \otimes \mathbb{1} \otimes \sigma_z \otimes \sigma_x) |C_4^l\rangle = |C_4^l\rangle, \quad (3.21d)$$

which have the unique solution

$$|C_4^l\rangle = \frac{1}{2} \left(|+\rangle_a |0\rangle_b |+\rangle_c |0\rangle_d + |+\rangle_a |0\rangle_b |-\rangle_c |1\rangle_d + |-\rangle_a |1\rangle_b |-\rangle_c |0\rangle_d + |-\rangle_a |1\rangle_b |+\rangle_c |1\rangle_d \right). \quad (3.22)$$

The generic way of initializing such a cluster state is to prepare four qubits in the state $|+\rangle$ and sequentially apply the CPHASE in the computational basis between them, see Fig. 3.9(c). It can be seen from Eqn. (3.22) and Fig. 3.9(c) that for the generation of the linear four-qubit cluster the CPHASE gate has to be applied three times, what would be experimentally demanding using photonic qubits. To circumvent this problem, in the following the state $|C_4\rangle$ is considered, which is local-unitary equivalent to the linear four-qubit cluster,

$$|C_4\rangle = \frac{1}{2} \left(|0\rangle_a |0\rangle_b |0\rangle_c |0\rangle_d + |0\rangle_a |0\rangle_b |1\rangle_c |1\rangle_d + |1\rangle_a |1\rangle_b |0\rangle_c |0\rangle_d - |1\rangle_a |1\rangle_b |1\rangle_c |1\rangle_d \right). \quad (3.23)$$

$|C_4^l\rangle$ and $|C_4\rangle$ are transformed into each other by a HAD gate, acting on qubits a and d . The advantage of $|C_4\rangle$ is, that it can be generated from the product of two Bell pairs, $|\phi^+\rangle \otimes |\phi^+\rangle$, and a single application of CPHASE on qubits b and c , see Fig. 3.9(d). This is experimentally easier to implement and allows furthermore to exploit the entanglement inherent in the photon pairs produced by SPDC.

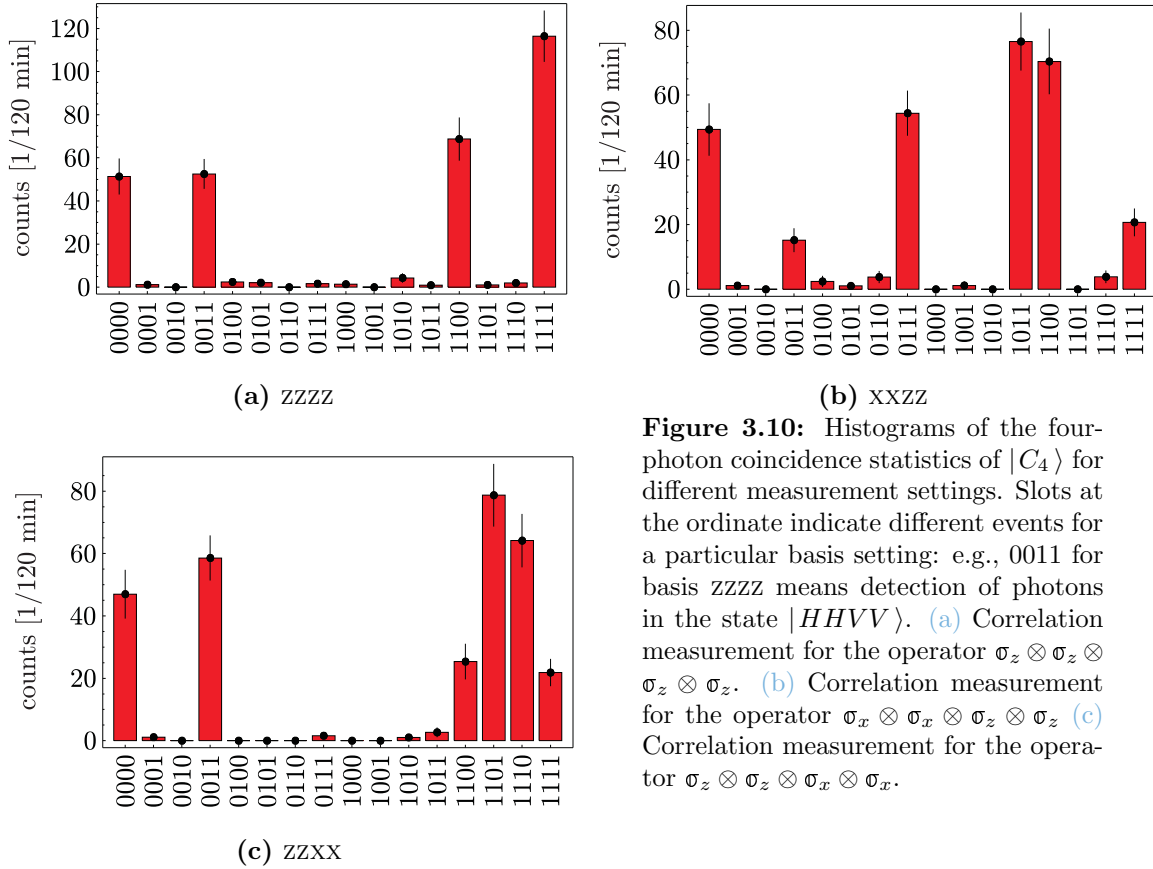


Figure 3.10: Histograms of the four-photon coincidence statistics of $|C_4\rangle$ for different measurement settings. Slots at the ordinate indicate different events for a particular basis setting: e.g., 0011 for basis ZZZZ means detection of photons in the state $|HHVV\rangle$. (a) Correlation measurement for the operator $\sigma_z \otimes \sigma_z \otimes \sigma_z \otimes \sigma_z$. (b) Correlation measurement for the operator $\sigma_x \otimes \sigma_x \otimes \sigma_z \otimes \sigma_z$. (c) Correlation measurement for the operator $\sigma_z \otimes \sigma_z \otimes \sigma_x \otimes \sigma_x$.

3.3.2 Experimental results

In order to observe the state $|C_4\rangle$, the setup described in the previous section in the context of entanglement swapping (Fig. 3.2) is used. This follows directly the generation prescription depicted in Fig. 3.9(d). Two photon pairs, each in the state $|\phi^+\rangle$, are emitted by the SPDC in the forward and backward direction of the pump beam. One photon of each pair (mode b and c) is fed as input into the CPHASE gate. Consequently, under the condition of detecting one photon in each mode the gate operation is applied and the cluster state is observed.

For its characterization, polarization analysis is performed in all four output modes. Fig. 3.10 displays the obtained four-fold coincidence counts for correlation measurements in three different bases, ZZZZ, XXZZ, ZZXX. In the computational basis, the typical four-term structure with peaks at $HHHH$, $HHVV$, $VVHH$, and $VVVV$ is clearly visible. The $VVVV$ -contribution is enhanced, mainly due to the vertically polarized noise originating from imperfect interference in the CPHASE gate (Fig. 3.10(a)). A slight asymmetry in the transmission amplitudes for vertical polarization in the two modes of the phase gate causes a raising of the $HHVV$ term. The measurement of the other bases proves the contributions to be in a coherent superposition. Exemplarily, the four-photon coincidence counts are shown when the photons in mode a, b (Fig. 3.10(b)), or the photons in mode c, d (Fig. 3.10(c)), respectively, are measured in the diagonal basis xx . The clear four term structure is present here as well, however, the imperfect interference results in additional terms of detections with $\pm\pm VV$ (b) or $VV\pm\pm$ (c), respectively. A detailed discussion of the influence on the state

quality resulting from imperfect gate operation can be found in [121, 184].

In order to evaluate the quality of the experimentally observed state ρ_{exp} the fidelity $F_{C_4} = \langle C_4 | \rho_{\text{exp}} | C_4 \rangle$ is determined. In analogy to Eqn. (2.38) this means a measurement of all non-zero correlations of the cluster state. In case of cluster states, or graph states in general, these correlations are given in terms of the so-called stabilizer operators [186]. These are all 16 elements of the group that is generated by the operators of the characteristic eigenvalue equations, Eqn. (3.21). The fidelity equals then the average absolute expectation value of the stabilizer operators which yields here for the obtained data $F_{C_4} = 0.741 \pm 0.013$. This value is greater than $\frac{1}{2}$ which is sufficient to prove the experimental state to be genuinely four-qubit entangled by using the generic witness operator [145].

3.3.3 Measurement based quantum computation

Once the cluster state is obtained it allows to demonstrate the principle of one of its main applications, namely measurement based quantum computation. To this end, a detailed explanation of the measurements and the correspondingly implemented computation will be given. Thereby the notation used in [180] is partly adopted. This allows an interpretation of the results obtained in Sec. 3.1.4 as four different computations.

In conventional quantum computation the information is encoded in qubits that are processed by the application of logical one- and two-qubit gates within a quantum circuit. In contrast, in a one-way quantum computer the logical qubits on which the computation is carried out do not need to coincide with the actual physical qubits forming the cluster state. The processing of the former is achieved by single qubit measurements of the latter according to an algorithm specific pattern. The cluster state serves thereby as a substrate for any kind of computation. Indeed, due to its entanglement, the individual physical qubits do not carry any information and the logical qubits are encoded non-locally in its correlations. Finally, the result of a computation is found in form of the specific state of particular read-out qubits. As the entanglement of the cluster state is destroyed by the single-qubit measurements during the process of computation, the state can be used only once. Therefore this scheme is often also referred to as one-way quantum computation in contrast to conventional quantum computation which is reversible.

With respect to such a computation two types of single qubit measurements need to be distinguished: Measurements in the computational basis remove or disconnect single qubits from the cluster resulting in a cluster state of a lower qubit number. Thus, these types of measurements can be used to shape or structure the cluster. Measurements in the basis $B(\alpha) = \{|\pm\alpha\rangle\}$ with $|\pm\alpha\rangle = \frac{1}{\sqrt{2}}(|0\rangle \pm \exp(i\alpha)|1\rangle)$ apply a rotation $\mathbf{R}_z(\alpha) \equiv \mathbf{U}(0, \alpha, 0, 0) = \exp(-i\alpha\frac{\sigma_z}{2})$ (cp. Eqn. (1.27)) on the logical qubit followed by a HAD gate. Together with the entanglement of the cluster, these measurements implement the logical operations required for a computation. In the following, the result for each type of measurement is presented.

As an example for the first type of measurement, qubit d is removed from the cluster resulting in the states

$$\begin{aligned} |C_3\rangle_{abc}^{\pm} &= \frac{1}{\sqrt{2}}(|00\pm\rangle_{abc} + |11\mp\rangle_{abc}) \\ &= \frac{1}{\sqrt{2}}(|\phi^+\rangle_{ab}|0\rangle_c \mp |\phi^-\rangle_{ab}|1\rangle_c) \end{aligned} \quad (3.24)$$

for the outcomes $+$ or $-$, respectively. The starting cluster state $|C_4\rangle$ differs from $|C_4^l\rangle$ by a

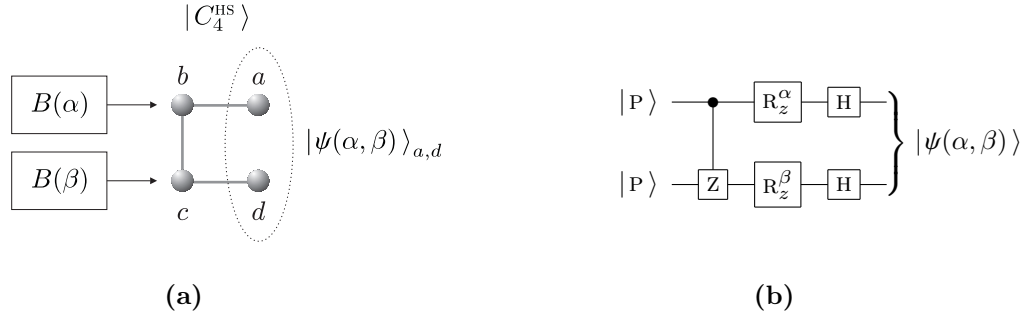


Figure 3.11: Scheme for measurement based quantum computation carried out on a four-qubit Horse-Shoe cluster, $|C_4^{\text{HS}}\rangle$. (a) The logical input qubits are encoded in the state of physical qubits b and c . The computation is performed by projective measurements in the bases $B(\alpha)$ and $B(\beta)$. Qubits a and d carry the logical output state, $|\psi(\alpha, \beta)\rangle_{a,d}$. (b) The corresponding quantum circuit for the logical qubits. A CPHASE gate is applied to the initial state $|P\rangle \otimes |P\rangle$, followed by the rotations $R_z(\alpha)$, $R_z(\beta)$ and a HAD gate.

HAD rotation on this qubit, therefore a measurement in the computational basis corresponds to σ_x instead of σ_z .

In the experiment the three-qubit cluster states are observed with fidelities $F_{C_3^+} = 0.756 \pm 0.028$ and $F_{C_3^-} = 0.753 \pm 0.026$. The fidelities are again determined from a measurement of the corresponding stabilizer operators and the values are significantly greater than $\frac{1}{2}$ what allows to proof genuine three-qubit entanglement of the experimental states [145]. Three qubit cluster states belong to the GHZ-class. Using Eqn. (1.38) the obtained fidelities are just at the limit to prove this unambiguously.

In order to demonstrate an example of a measurement of the second type, it is convenient to consider a cluster state which equals the four-qubit linear cluster in its mathematical form, but which has a slightly different graphical representation, see Fig. 3.11(a). Referring to its graph it was named "Horse-Shoe" cluster, $|C_4^{\text{HS}}\rangle$ in [180],

$$|C_4^{\text{HS}}\rangle = \frac{1}{2}(|H + H+\rangle + |H - V-\rangle + |V + V-\rangle + |V - H+\rangle). \quad (3.25)$$

The Horse-Shoe cluster equals also the state $|C\rangle$ up to a Hadamard transformation on the photons in modes a and d .

In the simple one-way quantum computation scheme presented here, the logical input qubits are encoded in the state of the two physical qubits on the left hand side (b and c in Fig. 3.11(a)) before the entangling operation (phase gate) acts on the qubits that are connected in the graph, i.e., between the pairs a, b and b, c and c, d . After this initialization, the computation is performed by application of projective measurements on all qubits apart from the pair on the right hand side (in Fig. 3.11(a), a and d). The qubits a and d carry the logical output state at the end of the computation. For a better illustration logical qubits are denoted for the rest of this section as

$$\begin{aligned} |0\rangle, \quad |P\rangle &= \frac{1}{\sqrt{2}}(|0\rangle + |1\rangle), \\ |1\rangle, \quad |M\rangle &= \frac{1}{\sqrt{2}}(|0\rangle - |1\rangle), \end{aligned} \quad (3.26)$$

to distinguish them from the physical qubits $|0\rangle$, $|1\rangle$, $|+\rangle$ and $|-\rangle$.

So the actual physical computation carried out on the Horse-Shoe cluster reads as follows,

$$\text{tr}_{b,c}\left((\mathbb{1} \otimes |\alpha\rangle\langle\alpha| \otimes |\beta\rangle\langle\beta| \otimes \mathbb{1}) \cdot |C_4^{\text{HS}}\rangle\right) = |\psi(\alpha, \beta)\rangle_{a,d}, \quad (3.27)$$

where the result is encoded in the state $|\psi(\alpha, \beta)\rangle_{a,d}$ (see Fig. 3.11(a)). On the level of the logical qubits this is equivalent to

$$(\text{HAD} \otimes \text{HAD}) \cdot (\mathbb{R}_z(\alpha) \otimes \mathbb{R}_z(\beta)) \cdot \text{CPHASE} \cdot (|P\rangle \otimes |P\rangle) = |\psi(\alpha, \beta)\rangle, \quad (3.28)$$

depicted in form of a quantum circuit in Fig. 3.11(b). As the qubits b and c are connected, a **CPHASE** operation acts on the logical input qubits prior to the single qubit rotations. This demonstrates how the entanglement in the cluster can be used to emulate non-local two-qubit operations required for universal computations.

In the experiment qubits b and c are measured in the XX basis what corresponds to rotations on the logical qubits according to four sets of angles $\{\alpha, \beta\} = \{0, 0\}, \{0, \pi\}, \{\pi, 0\}, \{\pi, \pi\}$. For the usage of $|C_4\rangle$ instead $|C_4^{\text{HS}}\rangle$, the output states are obtained up to another Hadamard transformation, which cancels with the **HAD** gate acting in the computation. Thus, the resulting transformation on the logical input state is $((\mathbb{R}_z(\alpha) \otimes \mathbb{R}_z(\beta)) \cdot \text{CPHASE})$ leading to

$$|\psi(0, 0)\rangle = \frac{1}{\sqrt{2}}(|0P\rangle + |1M\rangle), \quad (3.29a)$$

$$|\psi(0, \pi)\rangle = \frac{1}{\sqrt{2}}(|0M\rangle + |1P\rangle), \quad (3.29b)$$

$$|\psi(\pi, 0)\rangle = \frac{1}{\sqrt{2}}(|0P\rangle - |1M\rangle), \quad (3.29c)$$

$$|\psi(\pi, \pi)\rangle = \frac{1}{\sqrt{2}}(|0M\rangle - |1P\rangle). \quad (3.29d)$$

These are the states $|\widetilde{\phi}^+\rangle, |\widetilde{\psi}^+\rangle, |\widetilde{\phi}^-\rangle, |\widetilde{\psi}^-\rangle$, and as the logical output states in this instance are identical to the physical states of qubits a and d , the experimental result of this computation is the same as the one presented in Fig. 3.5 and Tab. 3.2.

3.3.4 Discussion

The realized computation scheme corresponds to the one presented in [180] achieving one output state with a slightly higher fidelity of 0.84 ± 0.03 despite of the lower fidelity of the cluster state itself. In contrast to [180], here four different single qubit rotations on the logical qubits have been implemented and the output states are all obtained at comparable quality. This proves the functionality of the small one-way computation for different computational settings. A possible next step is the implementation of the scheme in a way that different input states can be used. This can, however, also be solved by realizing a bigger cluster state that allows to first transform the logical qubits into the input state as part of the cluster scheme. Very important is further the feed-forward of measurement results which allows to make the computation deterministic. This route is followed in the group of Anton Zeilinger and was applied for the first time in [181].

The successful observation of the four-photon cluster state presented above is another proof for the applicability of the **CPHASE** gate. Together with the results discussed in Sec. 3.1 and Sec. 3.2 it shows that the gate can be used for entangling as well as disentangling qubits within tasks involving more than just two qubits. This makes the implemented **CPHASE** gate an indispensable tool in future multi-photon quantum information applications.

3.4 Conclusion

This chapter has presented three multi-photon applications of the **CPHASE** gate introduced in Chap. 2. The first two used the gate for a complete Bell state measurement. In this context for the first time, a teleportation and entanglement swapping protocol was performed where all four Bell states are distinguished by means of linear optics only. The teleported polarization states showed fidelities clearly above the classical bound. The quality of the implemented teleportation and the achievement of an efficient quantum channel was confirmed by reconstruction of the quantum process matrix. Running the entanglement swapping protocol yielded high fidelities and states which were entangled strong enough to violate a Bell inequality.

The complete Bell state measurement was further used for a direct measure of concurrence. The underlying method based on measurements on multiple identically prepared quantum systems was already demonstrated before, however under the very restrictive and unrealistic assumption of having pure states. Here, for the first time, a generalization of the method for mixed states was tested accounting for the imperfections of state-of-the-art technology which is used in current set-ups. Thereby it was particularly important to consider the influence of non-ideal gate operation. This allowed a realistic lower bound estimation on the concurrence of the prepared states.

In the last application the **CPHASE** gate was used to entangle the photons of two Bell pairs. This enabled the successful observation of a four photon cluster state with high fidelity. As the properties of the observed state were analyzed in detail elsewhere, the treatment of the results in this chapter was focused on a proof-of-principle demonstration of measurement based quantum computation. The two types of single-qubit measurements commonly applied in such computation schemes have been demonstrated. This comprised in particular the entangling operation of two encoded logical qubits.

To summarize, the analysis of data obtained within the same set-up from three different perspectives constitutes together an interesting proof that a universal two photon gate based on linear optics only can be successfully applied in tasks involving more than just two qubits. This is a further demonstration that meanwhile linear optics gates are no longer feasible just in principle but have reached a level of functionality and simplicity which allows their implementation in quantum information applications. If this is combined with recently developed active feed-forward techniques it might additionally open up new vistas for linear optics quantum computation.

Chapter 4

Discriminating multi-partite entangled states

In Chap. 1 it was mentioned that in the case of more than two qubits it is necessary to distinguish not only between separable and entangled but also between the different kinds of multi-partite entanglement. It was shown that witness operators provide a tool to distinguish the different degrees of separability from each other. Whereas for three qubits witness operators are still suited to distinguish GHZ- from W-type entanglement, there is no instructive method to do something similar for more than three qubits.

This chapter addresses the problem of experimentally discriminating different types of four qubit entanglement. For this purpose characteristic Bell operators are introduced which are shown to be suitable for this task [187]. Finally, it will be demonstrated that, provided additional information about the state space is available, these characteristic operators can be chosen without the constraint of excluding local realistic descriptions of the measurement results.

4.1 The problem of state discrimination

Entanglement is the crucial resource for quantum information processing and as such the "currency" to pay with in almost all applications. For two-partite quantum states measures have been developed that uniquely specify the value of this resource. In contrast, for n -partite states the picture changes significantly. First, it has to be distinguished not only between fully separable or entangled, but also between genuine n -partite, bi-, and tri- separable entangled states, etc. (see Sec. 1.2.2). Second, even states with the same level of separability are different in the sense that they have, for example, different Schmidt rank [188] or that they cannot be transformed into each other, e.g., by LU or, more generally, by SLOCC [18, 19]. From an experimental point of view, classifying states according to the latter property is very reasonable, as states from one SLOCC class are suited for the same multi-party quantum communication applications. Thus, for the usage of multi-partite states it is of importance to know not only the *amount* but also the *type* of entanglement contained in a particular state. In other words, the value *and* the type of the "currency" is what matters.

Tools to detect the entanglement of a state exist, most prominently entanglement witnesses [43]. An alternative method, relying on the correlations between results obtained by local measurements, are Bell inequalities. Being originally devised to test fundamental issues

of quantum physics they allow to distinguish entangled from separable two-qubit quantum systems [67, 189]. Bell inequalities, meanwhile extended to three- and more partite quantum states [190–195], can thus serve as witness for both entanglement and the violation of local realism. Recently it was observed that for each graph state all non-vanishing correlations (or even a restricted number thereof) form a Bell-inequality, which is maximally violated only by the respective quantum state [196–198]. In particular, the Bell inequality for the four-qubit cluster state is not violated at all by GHZ states [196]. Naturally, several questions arise: Is it in general possible to apply such Bell inequalities for the discrimination of particular states from other classes of multi-partite entangled states, if so, can they also be constructed and applied for non-graph states, and finally, are there other operators that allow to experimentally discriminate entanglement classes.

In this chapter these problems are addressed starting from Bell inequalities. A way is presented to construct Bell operators [38, 199] that are *characteristic* for a particular quantum state. Thereby the following definitions are used:

Definition 4.1.1 (Bell operator) *A Hermitian operator \mathbf{B} is called Bell operator if there exists a constant $\beta_{\text{LR}} \in \mathbb{R}$ and a state ρ such that $|\langle \mathbf{B} \rangle_{\text{avg}}| \leq \beta_{\text{LR}}$ for all local realistic theories and $\beta_{\text{LR}} < \text{tr}(\mathbf{B} \rho)$.*

Thereby $\langle \mathbf{B} \rangle_{\text{avg}} = E(\mathbf{B})$ is the weighted mean of measurement results in the local realistic theory for an observable \mathbf{B} which is represented by the operator \mathbf{B} in the quantum theory. This is analogous to Eqn. (1.14) and the considerations on page 12.

Definition 4.1.2 (Characteristic operator) *A Hermitian operator $\mathbf{D} : \mathbb{H} \rightarrow \mathbb{H}$ is called characteristic for a state $|X\rangle \in \mathbb{H}$, iff*

$$\mathbf{D}|X\rangle = \lambda_X|X\rangle, \quad \dim(\ker(\mathbf{D} - \lambda_X \mathbb{1}_{\mathbb{H}})) = 1 \quad \text{and} \quad |\lambda_X| = \sup(\{|\lambda| : \lambda \in \text{sp}(\mathbf{D})\}),$$

i.e., iff $|X\rangle$ is non-degenerate eigenvector of \mathbf{D} with maximal eigenvalue. Thereby, $\text{sp}(\mathbf{D})$ denotes the spectrum of \mathbf{D} .

With respect to experimental applications it is further desirable that the expectation value of each derived operator can be obtained by a minimal number of measurement settings. Under certain conditions, the initial requirement that the constructed operators have to be characteristic *and* in addition Bell operators can be relaxed, which allows further reduction of the number of settings. Comparison of the experimentally obtained expectation value with the maximal expectation values for states from other entanglement classes enables the distinction of an observed state from other multi-party entangled states.

4.2 Characteristic Bell inequalities – principle idea

In order to construct a Bell operator, the fact is exploited that certain correlations between measurement results on individual qubits are specific for multi-partite quantum states [194, 195]. As already denoted in Eqn. (2.32) and Eqn. (2.33), all correlations for a state $|X\rangle$ are summarized by the correlation tensor T . In the case of four qubits, $T_{ijkl} = \langle X | (\sigma_i \otimes \sigma_j \otimes \sigma_k \otimes \sigma_l) | X \rangle$, with $i, j, k, l \in \{0, x, y, z\}$, where $\sigma_0 = \mathbb{1}$. To obtain a Bell operator \mathbf{B}_X that is characteristic for a state $|X\rangle$, at first it is required that $|X\rangle$ is the eigenstate of \mathbf{B}_X with the highest eigenvalue λ_{max} . If, as imposed by Def. 4.1.2, the eigenstate is in addition

not degenerate, this immediately implies that \mathbb{B}_X acting on another state, cannot lead to an expectation value greater or equal λ_{\max} .

An operator, which is in general not a Bell operator, but trivially fulfills the condition to be characteristic for $|X\rangle$, is the projector or fidelity operator $\mathbb{F}_X = |X\rangle\langle X|$ (cp. Eqn. (2.32)) and

$$\mathbb{F}_X = \frac{1}{16} \sum_{i,j,k,l} T_{ijkl} (\sigma_i \otimes \sigma_j \otimes \sigma_k \otimes \sigma_l). \quad (4.1)$$

For most of the relevant quantum states the major part of the 256 coefficients T_{ijkl} is zero. Therefore, the number of measurement settings necessary for the evaluation of \mathbb{F}_X is much smaller than for a complete state tomography. Here, the non-vanishing terms are considered as relevant correlations for characterizing the state and taken as a starting point for the construction of \mathbb{B}_X . As shall be seen in the following two examples, there are quantum states for which a small subset of the relevant correlations is enough to construct \mathbb{B}_X . Once this is accomplished the upper bound, v_X^* , on the expectation values $v_Y = \langle Y | \mathbb{B}_X | Y \rangle = \langle \mathbb{B}_X \rangle_Y$ for states $|Y\rangle$ which belong to other classes than $|X\rangle$ can be calculated. Consequently, a state under investigation with $\langle \mathbb{B}_X \rangle_Z = v_Z$ cannot be an element of any class of states with $v_Y^* < v_Z$.

It has to be noted that $\langle \mathbb{B}_X \rangle$ induces a particular ordering of states which is neither absolute nor related to some entanglement of the states and, similarly to entanglement witnesses (see Def. 1.2.11), depends on the operator \mathbb{B}_X . Yet, \mathbb{B}_X does not only detect higher or lower degree of entanglement, but it distinguishes different types of entanglement. In this respect it can be said that a state with higher $\langle \mathbb{B}_X \rangle$ is more " $|X\rangle$ -type" entangled. The same is true for a mixed state ρ with expectation value $v_\rho = \text{tr}(\mathbb{B}_X \rho) = \langle \mathbb{B}_X \rangle_\rho$, in the sense that it cannot solely be expressed as a mixture of pure states $|Y_i\rangle$ with $v_{Y_i}^* < v_\rho$, but it has to contain contributions with a higher " X -type" entanglement.

Summarizing, the construction of a discrimination operator, which has $|X\rangle$ as non-degenerate eigenvector with the highest eigenvalue leads to a witness of " $|X\rangle$ -type" entanglement. After all, such an operator is neither unique, nor does it necessarily have to be a Bell operator. However, a Bell operator unconditionally detects the entanglement of the investigated state, even if the state space is not fully known. For example, witness operators might detect a state to be entangled though a description of measurement results based on local realistic models, or for that purpose, based on separable states in higher dimensional Hilbert spaces, is possible [200]. If the representation of the state is trusted, as will be shown below, even more efficient operators for state discrimination can be devised.

4.3 Examples with experimental results

The approach introduced above of discriminating entangled states by the usage of characteristic Bell operators shall be demonstrated in the following. At first the Bell inequality for the four-qubit cluster state derived in [196] is reviewed. Afterwards, two new Bell inequalities for two important four-qubit entangled states are set up and experimentally tested.

4.3.1 The four qubit cluster state

In [196], based on a GHZ argument for non-locality [62, 190], the authors derive a Bell inequality which is optimal for the linear four-qubit cluster state $|C_4^l\rangle$ (see Sec. 3.3). Adapted

State	under LU	under SLOCC
$ C_4\rangle$	1.000	1.000
$ \text{GHZ}\rangle$	0.500	1.000
$ D_4^{(2)}\rangle$	0.417	1.000
$ \Psi_4\rangle$	0.333	0.750
$ \text{w}\rangle$	0.625	0.750
$ \text{bi-sep}\rangle$	0.500	0.500
$ \text{sep}\rangle$	0.250	0.250

Table 4.1: Maximal expectation values of \mathbb{B}_{C_4} for several prominent examples of four-qubit states. The bounds are calculated numerically with respect to LU and SLOCC operations.

for the cluster state $|C_4\rangle$, the corresponding Bell operator reads,

$$\begin{aligned}
4\mathbb{B}_{C_4} &= \sigma_z \otimes \mathbb{1} \otimes \sigma_x \otimes \sigma_x + \sigma_x \otimes \sigma_y \otimes \sigma_x \otimes \sigma_y \\
&+ \sigma_x \otimes \sigma_y \otimes \sigma_y \otimes \sigma_x - \sigma_z \otimes \mathbb{1} \otimes \sigma_y \otimes \sigma_y,
\end{aligned} \tag{4.2}$$

with $\beta_{\text{LR}} = \frac{1}{2}$. It is constructed out of the state's stabilizers and optimized in the sense that it has $|C_4\rangle$ as eigenstate with the maximal eigenvalue $\lambda_{\text{max}} = 1$. However it is not characteristic according to Def. 4.1.2 as the maximal eigenvalues are degenerate, i.e., $\text{sp}(\mathbb{B}_{C_4}) = \{\pm 1\}$ and $\dim(\ker(\mathbb{B}_{C_4} \mp \mathbb{1})) = 2$. The corresponding orthogonal eigenvectors are $-|C_4\rangle$, $(\mathbb{1} \otimes \sigma_x \otimes \sigma_x \otimes \sigma_x) \cdot |C_4\rangle$ and $(\sigma_x \otimes \sigma_x \otimes \mathbb{1} \otimes \mathbb{1}) \cdot |C_4\rangle$, $(\sigma_x \otimes \mathbb{1} \otimes \sigma_x \otimes \sigma_x) \cdot |C_4\rangle$. Due to this degeneracy the authors' claim in [196] that \mathbb{B}_{C_4} "acts as a witness discriminating between $|C_4\rangle$, which violates it [the corresponding Bell inequality] up to the algebraic limit, and $|\text{GHZ}\rangle$, which does not violate it at all", is true only with respect to LU but not with respect to SLOCC. For both types of operations, Tab. 4.1 shows the bounds on the expectation value of \mathbb{B}_{C_4} acting on some classes of prominent four-qubit states (including a fully separable state, $|\text{sep}\rangle$, any bi-separable state, $|\text{bi-sep}\rangle$, as well as the four-partite entangled Dicke state $D_4^{(2)}$, the GHZ, w and Cluster (C_4) state itself). As can be seen, the GHZ as well as the Dicke state reach the same expectation value with respect to SLOCC and can thus not be discriminated against each other. The bounds were obtained by numerical optimization over either LU- or SLOCC-transformations, respectively. Thereby an LU operation is considered as an element of $SU(2)$ ¹, see Eqn. (1.27), an SLOCC operation as an element of $SL(2, \mathbb{C})$, see page 27 and the bi-separable states were taken as $|\text{GHZ}\rangle_{abc} \otimes |+\rangle_d$, $|\text{w}\rangle_{abc} \otimes |+\rangle_d$, $|\phi^+\rangle_{ab} \otimes |\phi^+\rangle_{cd}$ with all permutations between the qubits.

The expectation value $\langle \mathbb{B}_{C_4} \rangle$ can be evaluated for the data which was obtained in the experiment described in Sec. 3.3. The relevant correlation measurements are displayed in Fig. 4.1. The value $\langle \mathbb{B}_{C_4} \rangle_{\text{exp}}$ resulting from this data is 0.683 ± 0.03 which is sufficient, according to Tab. 4.1, to conclude that the experimentally observed state is not of Ψ_4 , $D_4^{(2)}$, GHZ or w type with respect to LU. Unfortunately, none of these states can be excluded with respect to SLOCC, what shows that the non-degeneracy requirement in Def. 4.1.2 is essential.

¹The determinant of the LU operation can be fixed to one ($SU(2)$). Otherwise ($U(2)$), the result would only differ by a constant complex factor which is not relevant.

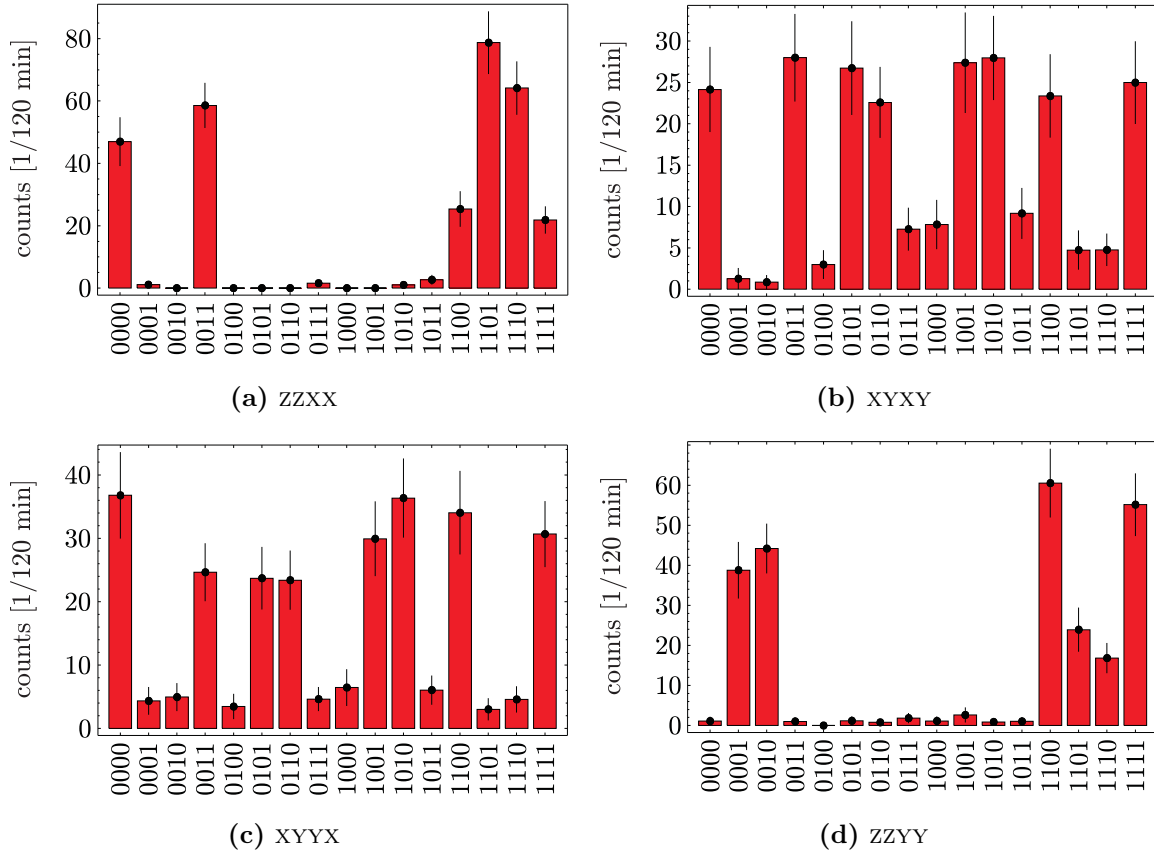


Figure 4.1: Histograms of the four-photon coincidence statistics of $|C_4\rangle$ for different measurement settings. Slots at the ordinate indicate different events for a particular basis setting: e.g. 0011 for basis ZZXX means detection of photons in the state $|HH--\rangle$. (a) Correlation measurement for the operator $\sigma_z \otimes \sigma_z \otimes \sigma_x \otimes \sigma_x$. (b) Correlation measurement for the operator $\sigma_x \otimes \sigma_y \otimes \sigma_x \otimes \sigma_y$. (c) Correlation measurement for the operator $\sigma_x \otimes \sigma_y \otimes \sigma_y \otimes \sigma_x$. (d) Correlation measurement for the operator $\sigma_z \otimes \sigma_z \otimes \sigma_y \otimes \sigma_y$.

In the following, two new Bell operators are introduced which are characteristic for two important states. As will be shown they allow indeed a discrimination of the experimentally observed state against states of other SLOCC classes.

4.3.2 The four-qubit singlet state

The first example is the entangled four-qubit singlet state which was already introduced in Sec. 2.2:

$$\begin{aligned}
 |\Psi_4^-\rangle &= \frac{1}{\sqrt{3}}(|0011\rangle + |1100\rangle - \frac{1}{2}(|0101\rangle \\
 &\quad + |0110\rangle + |1001\rangle + |1010\rangle)).
 \end{aligned}
 \tag{4.3}$$

This state is of particular interest as it has several applications in quantum information [113–115, 140, 201].

As discussed in Sec. 2.2, the fidelity operator for that state, \mathbb{F}_{Ψ_4} , contains 40 relevant correlation operators ($\sigma_i \otimes \sigma_j \otimes \sigma_k \otimes \sigma_l$), out of which 21 describe four-qubit correlations (i.e.

State	under LU	under SLOCC
$ \Psi_4\rangle$	1.000	1.000
$ D_4^{(2)}\rangle$	0.926	0.926
$ \text{GHZ}\rangle$	0.805	0.805
$ C_4\rangle$	0.515	0.764
$ w\rangle$	0.736	0.758
$ \text{bi-sep}\rangle$	0.722	0.749
$ \text{sep}\rangle$	0.217	0.217

Table 4.2: Maximal expectation values of \mathbf{B}_{Ψ_4} for several prominent examples of four-qubit states. The bounds are calculated numerically with respect to LU and SLOCC operations.

do not contain σ_0). These correlations can be used to determine the fidelity in an experiment. However, already 10 are enough to construct a characteristic Bell operator for $|\Psi_4\rangle$,

$$\begin{aligned}
6\mathbf{B}_{\Psi_4} = & \sigma_x \otimes \sigma_y \otimes \sigma_y \otimes \sigma_x + \sigma_y \otimes \sigma_x \otimes \sigma_y \otimes \sigma_x \\
& - \sigma_y \otimes \sigma_y \otimes \sigma_x \otimes \sigma_x + \sigma_x \otimes \sigma_z \otimes \sigma_x \otimes \sigma_z \\
& + \sigma_z \otimes \sigma_x \otimes \sigma_x \otimes \sigma_z - \sigma_z \otimes \sigma_z \otimes \sigma_x \otimes \sigma_x \\
& + \sigma_z \otimes \sigma_z \otimes \sigma_z \otimes \sigma_z - \sigma_y \otimes \sigma_y \otimes \sigma_z \otimes \sigma_z \\
& + \sigma_y \otimes \sigma_z \otimes \sigma_y \otimes \sigma_z + \sigma_z \otimes \sigma_y \otimes \sigma_y \otimes \sigma_z,
\end{aligned} \tag{4.4}$$

with maximal eigenvalue $\lambda_{\max} = 1$. With the chosen normalization the limit for any local realistic theory is obtained by replacing σ_i by some locally predetermined values $I_i = \pm 1$, leading to the inequality $|\langle \mathbf{B}_{\Psi_4} \rangle_{\text{avg}}| \leq \frac{2}{3}$. Table 4.2 shows the bounds on the expectation value of \mathbf{B}_{Ψ_4} acting on the same classes of prominent four-qubit states as before. Thus, this operator can be applied instead of the fidelity to discriminate an experimentally observed state with respect to other four-qubit states (even w.r.t. SLOCC). In particular, with the bound for an arbitrary bi-separable state, \mathbf{B}_{Ψ_4} provides also a sufficient condition to check for genuine four-partite entanglement.

These results can now be employed for the analysis of the data acquired with the setup described in Sec. 2.2. The fidelity of the experimental state $\rho_{\Psi_4^-}$, determined from 21 four-qubit correlations, is $F_{\Psi_4} = \text{tr}(\mathbf{F}_{\Psi_4} \rho_{\Psi_4^-}) = 0.904 \pm 0.014$. The analysis of the experimental state using the Bell operator \mathbf{B}_{Ψ_4} requires less than half of the measurement settings and leads to $\langle \mathbf{B}_{\Psi_4} \rangle_{\text{exp}} = 0.912 \pm 0.024$. This value is, according to Table 4.2, sufficient to prove that the experimental state is genuine four-qubit entangled and cannot be of w-, Cluster-, or GHZ-type in the sense described in Sec. 4.2.

4.3.3 The symmetric dicke state with two excitations

The class of states that can experimentally not be excluded as it has the second largest expectation value in Table 4.2 is represented by the so-called symmetric four qubit Dicke state with two excitations (see Sec. 2.2.3),

$$\begin{aligned}
|D_4^{(2)}\rangle = & \frac{1}{\sqrt{6}}(|0011\rangle + |0101\rangle + |0110\rangle \\
& + |1001\rangle + |1010\rangle + |1100\rangle).
\end{aligned} \tag{4.5}$$

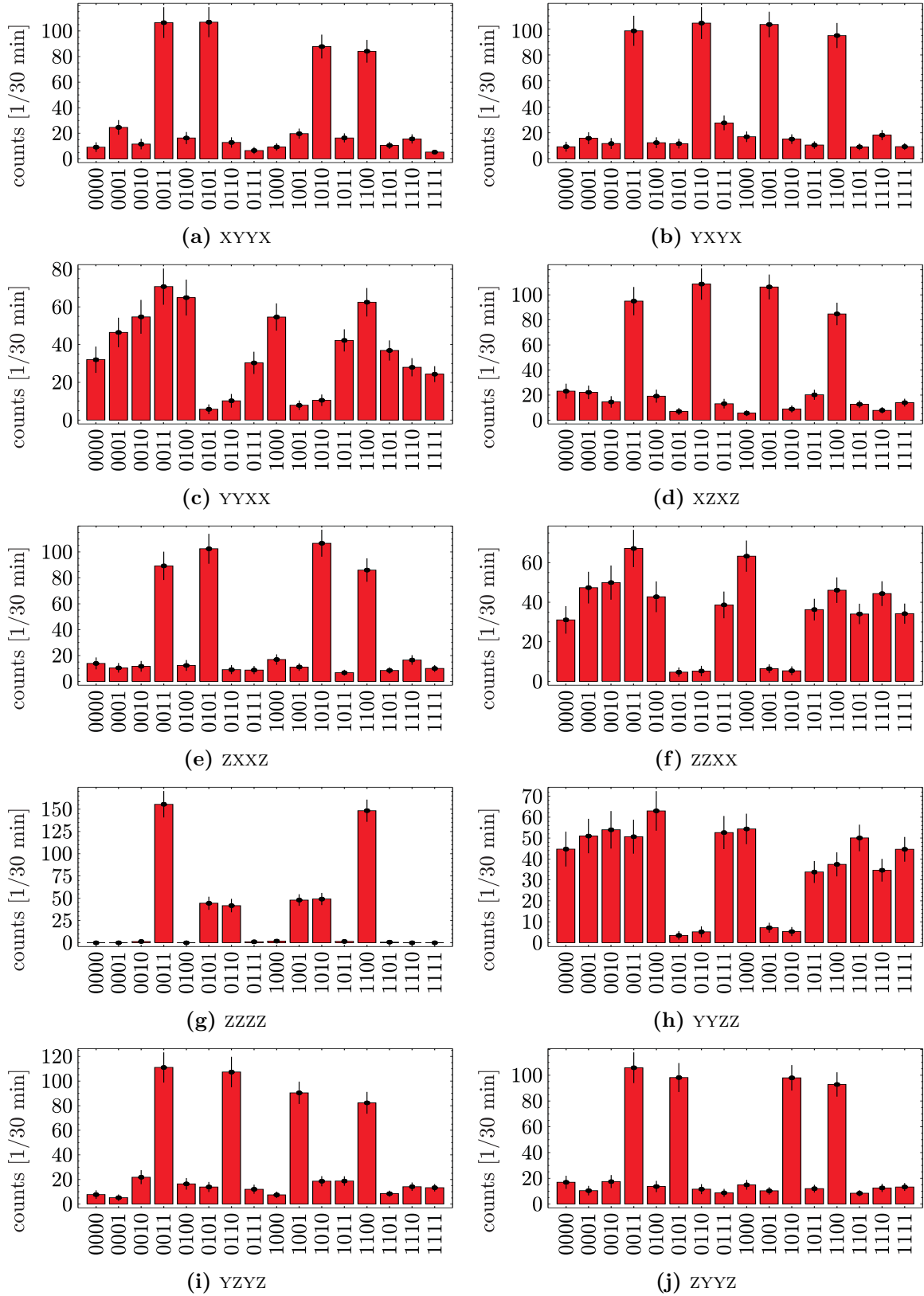


Figure 4.2: Statistics of the ten correlation measurements required for the evaluation of the operator \mathbb{B}_{Ψ_4} .

In turn, for the Dicke state a separate, characteristic Bell operator $\mathbb{B}_{D_4^{(2)}}$ can be constructed. Again, $|D_4^{(2)}\rangle$ has 40 correlation operators with non zero expectation value, out of which 21 describe original four-qubit correlations. Naturally, the exact values of the correlations T_{ijkl} differ compared to $|\Psi_4\rangle$ (cp. App. B.1.3 and App. B.1.5). In the case of $|D_4^{(2)}\rangle$ they are such that eight of the correlation operators are already sufficient for the construction of $\mathbb{B}_{D_4^{(2)}}$:

$$\begin{aligned} 6\mathbb{B}_{D_4^{(2)}} = & -\sigma_x \otimes \sigma_z \otimes \sigma_z \otimes \sigma_x - \sigma_x \otimes \sigma_z \otimes \sigma_x \otimes \sigma_z \\ & -\sigma_x \otimes \sigma_x \otimes \sigma_z \otimes \sigma_z + \sigma_x \otimes \sigma_x \otimes \sigma_x \otimes \sigma_x \\ & -\sigma_y \otimes \sigma_z \otimes \sigma_z \otimes \sigma_y - \sigma_y \otimes \sigma_z \otimes \sigma_y \otimes \sigma_z \\ & -\sigma_y \otimes \sigma_y \otimes \sigma_z \otimes \sigma_z + \sigma_y \otimes \sigma_y \otimes \sigma_y \otimes \sigma_y, \end{aligned} \quad (4.6)$$

with $\lambda_{\max} = 1$ for $|D_4^{(2)}\rangle$. This operator has a remarkable structure: It is of the form $\sigma_x \otimes \mathbb{M}_3 + \sigma_y \otimes \mathbb{M}'_3$, where \mathbb{M}_3 and \mathbb{M}'_3 are three-qubit Mermin inequality operators² [190], with

$$\mathbb{M}_3 = -\sigma_z \otimes \sigma_z \otimes \sigma_x - \sigma_z \otimes \sigma_x \otimes \sigma_z - \sigma_x \otimes \sigma_z \otimes \sigma_z + \sigma_x \otimes \sigma_x \otimes \sigma_x \quad (4.7)$$

and \mathbb{M}'_3 analog with σ_x replaced by σ_y . Thus, by applying a kind of GHZ-argument [62, 202], the bound for any local realistic theory can be easily determined. To illustrate this, the first block of $\mathbb{B}_{D_4^{(2)}}$ is written in the following form:

$$\begin{array}{cccc} \text{I} & \text{II} & \text{III} & \text{IV} \\ \sigma_x \otimes \sigma_z \otimes \sigma_z \otimes \sigma_x & & & \end{array} \quad (4.8a)$$

$$\begin{array}{cccc} \sigma_x \otimes \sigma_z \otimes \sigma_x \otimes \sigma_z & & & \end{array} \quad (4.8b)$$

$$\begin{array}{cccc} \sigma_x \otimes \sigma_x \otimes \sigma_z \otimes \sigma_z & & & \end{array} \quad (4.8c)$$

$$\begin{array}{cccc} \sigma_x \otimes \sigma_x \otimes \sigma_x \otimes \sigma_x & & & \end{array} \quad (4.8d)$$

As the observables σ_x and σ_z do not commute (see Eqn. (1.21)) it obviously holds that for column III, $\sigma_z \cdot \sigma_x \cdot \sigma_z = -\sigma_x$ and therefore (4.8a) · (4.8b) · (4.8c) = −(4.8d). In contrast, in any local realistic theory the product of outcomes for the subsequent measurements corresponding to operators (4.8a) to (4.8c) has to be equal to the outcome of the measurement corresponding to operator (4.8d). Applying such arguments for both blocks of Eqn. (4.6) leads to $\beta_{\text{LR}} = \frac{2}{3}$.

Table 4.3 shows the maximal expectation values of $\mathbb{B}_{D_4^{(2)}}$ with the same set of four-qubit states as before. Considering the structure of $\mathbb{B}_{D_4^{(2)}}$, further omitting correlation operators, for example one whole block $\sigma_x \otimes \mathbb{M}_3$ (or $\sigma_y \otimes \mathbb{M}'_3$), leaves a four-qubit Mermin-type Bell operator. The corresponding Bell inequality is still violated by $|D_4^{(2)}\rangle$. However, it is not characteristic anymore for $|D_4^{(2)}\rangle$ as it is maximally violated by the state $|\text{GHZ}\rangle_y = \frac{1}{\sqrt{2}}(|RRRR\rangle \pm |LLLL\rangle)$ and the bi-separable state $|\text{P} \cdot \text{GHZ}\rangle = \frac{1}{\sqrt{2}}(|+\rangle(|RRR\rangle \pm i|LLL\rangle))$. It is a particular property of the Dicke state to have correlations in two planes (x-z- and y-z-plane) of the Bloch sphere, whereas a GHZ state, for instance, is correlated only in one plane (here the x-z-plane). This quite characteristic feature is reflected in the construction of $\mathbb{B}_{D_4^{(2)}}$.

²Interestingly, the characteristic Bell operator for the symmetric six-qubit Dicke state with three excitations, $|D_6^{(3)}\rangle$, is of the same structure: $\sigma_x \otimes \mathbb{M}_5 + \sigma_y \otimes \mathbb{M}'_5$. The bound for local realistic theories in this case is 0.4 and the expectation value for the Dicke state is 1 compared to e.g. 0.85 for any six-qubit GHZ state.

State	under LU	under SLOCC
$ D_4^{(2)}\rangle$	1.000	1.000
$ \Psi_4\rangle$	0.889	0.889
$ \text{GHZ}\rangle$	0.833	0.833
$ C_4\rangle$	0.500	0.706
$ \text{bi-sep}\rangle$	0.667	0.667
$ w\rangle$	0.613	0.619
$ \text{sep}\rangle$	0.178	0.178

Table 4.3: Maximal expectation values of $\mathbb{B}_{D_4^{(2)}}$ for several prominent examples of four-qubit states. The bounds are calculated numerically with respect to LU and SLOCC operations.

The above considerations shall be again demonstrated by their application to real data. The observation of the state $|D_4^{(2)}\rangle$ was reported in Sec. 2.2.3. However, there is an alternative linear optics setup which can be used to obtain the Dicke state and which yields a slightly better state quality as it does not involve two-photon interference. This scheme exploits the fact that the Dicke state is an equally weighted superposition of all permutations to distribute two horizontally and two vertically polarized photons onto four spatial modes. Thus, the starting point is the second order emission of a collinear type-II SPDC process, leading to two horizontally and two vertically polarized photons in one spatial mode. These four photons are symmetrically split up into four output modes using three beam splitters with polarization independent splitting ratio. Under the condition that the photons are indistinguishable up to their polarization and that one of them is detected in coincidence in each of the four output modes, the desired state $D_4^{(2)}$ is observed (see Fig. 4.3). In the experiment, which is described in detail in [99, 121, 129], the state is obtained with a fidelity of $F = 0.844 \pm 0.008$ at a count rate of about 60 fourfold coincidence counts per minute.

In the following the data acquired with this arrangement is used. In order to still increase the state fidelity by a higher degree of the photons' indistinguishability, the filter bandwidth is reduced from 3 nm (as used in [99]) to 2 nm, resulting in $F = 0.919 \pm 0.019$. For the state's experimental analysis with the Bell operator (Eqn. (4.6)) the value $\langle \mathbb{B}_{D_4^{(2)}} \rangle_{\text{exp}} = 0.896 \pm 0.039$ is found. The data of the eight required correlation measurements is shown in Fig. 4.4. The reached value is high enough to conclude that the state is genuine four-qubit entangled and cannot be, e.g., of w-, Cluster- or GHZ-type. Yet, it is again just at the limit to separate against $|\Psi_4\rangle$.

4.4 Non-Bell operators

If there is no doubt about the structure of the state space, that means in this case that it is spanned by four qubits, other operators can be used equally well instead of the Bell operators. This can lead to a further reduction of the number of measurement settings. Starting with $\mathbb{B}_{D_4^{(2)}}$, some of the correlation operators can still be dropped, e.g., the terms $(\sigma_x \otimes \sigma_x \otimes \sigma_x \otimes \sigma_x)$ and $(\sigma_y \otimes \sigma_y \otimes \sigma_y \otimes \sigma_y)$. The resulting discrimination operator,

$$4\mathbb{D}_{D_4^{(2)}} = -\sigma_x \otimes \sigma_z \otimes \sigma_z \otimes \sigma_x - \sigma_x \otimes \sigma_z \otimes \sigma_x \otimes \sigma_z - \sigma_x \otimes \sigma_x \otimes \sigma_z \otimes \sigma_z \\ - \sigma_y \otimes \sigma_z \otimes \sigma_z \otimes \sigma_y - \sigma_y \otimes \sigma_z \otimes \sigma_y \otimes \sigma_z - \sigma_y \otimes \sigma_y \otimes \sigma_z \otimes \sigma_z, \quad (4.9)$$

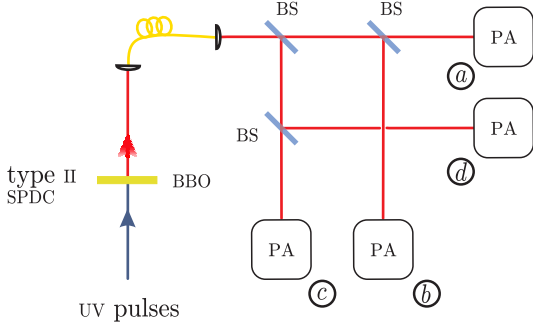


Figure 4.3: Schematic sketch of the alternative setup for the observation of the state $|D_4^{(2)}\rangle$. Two horizontally and two vertically polarized photons are emitted by the second order emission of collinear SPDC. The photons propagate initially in one spatial mode but are afterwards symmetrically split by three polarization independent BS. Under the condition of detecting one photon in the PA of each mode a, b, c, d , the state is observed.

is not a Bell operator anymore ($\beta_{LR} = \frac{3}{2}$), but is still characteristic, i.e., it has $|D_4^{(2)}\rangle$ as the only eigenstate with maximal eigenvalue $\lambda_{\max} = 1$. Interestingly, as seen in Tab. 4.4(a), it introduces a new ordering of states with a bigger separation between $|D_4^{(2)}\rangle$ and $|\Psi_4\rangle$. With $\langle \mathbf{D}'_{D_4^{(2)}} \rangle_{\text{exp}} = 0.904 \pm 0.050$ it is possible to discriminate against this state with a better significance. The reordering, which results in the GHZ state having now the second highest eigenvalue, indicates that this operator analyzes the various states from a different point of view. This is quite plausible as it uses different correlations for the analysis.

An even more radical change in the point of view is possible with the data dropped above, i.e., $(\sigma_x \otimes \sigma_x \otimes \sigma_x \otimes \sigma_x)$ and $(\sigma_y \otimes \sigma_y \otimes \sigma_y \otimes \sigma_y)$. Relying on the particular symmetries of the Dicke state, these measurements allow the evaluation of a discrimination operator, which was introduced as a spin witness in [203],

$$6 \mathbf{D}'_{D_4^{(2)}} = \left(\frac{1}{2} \sum_{i=1}^4 \sigma_x^i \right)^2 + \left(\frac{1}{2} \sum_{i=1}^4 \sigma_y^i \right)^2, \quad (4.10)$$

where, e.g., $\sigma_{x/y}^3 = \mathbb{1} \otimes \mathbb{1} \otimes \sigma_{x/y} \otimes \mathbb{1}$. Obviously this operator is the sum of the spin squared along x and y direction. As $|D_4^{(2)}\rangle$ is the only spin eigenstate which has maximal total spin and, at the same time, minimal spin along z direction (where z be the quantization axis) it maximizes the eigenvalue of this operator (which is also no Bell operator anymore, $\beta_{LR} = \frac{4}{3}$).

Comparing the observed value $\langle \mathbf{D}'_{D_4^{(2)}} \rangle_{\text{exp}} = 0.958 \pm 0.013$ with the bounds for other states (Tab. 4.4(b)), a discrimination of the experimental state against all states of the respective classes is possible with only two settings.

Analogous considerations can be applied for the construction of characteristic operators for other states, where the number of settings scales polynomially with the number of qubits compared to the exponentially increasing effort for quantum state tomography. Recently, such operators were introduced also for $|\Psi_4\rangle$ [204] and $|C_4\rangle$ [145].

The operator for $|\Psi_4\rangle$ requires for its evaluation only three measurement settings (XXXX, YYYY, ZZZZ) and is of the form

$$21 \mathbf{D}_{\Psi_4} = \mathbf{D}_x + \mathbf{D}_y + \mathbf{D}_z, \quad (4.11)$$

with

$$\mathbf{D}_k = \sigma_k^{\otimes 4} + 3 \left(\sigma_k^{1,2} + \sigma_k^{3,4} \right) - \frac{3}{2} \left(\sigma_k^{2,3} + \sigma_k^{2,4} + \sigma_k^{1,3} + \sigma_k^{1,4} \right), \quad (4.12)$$

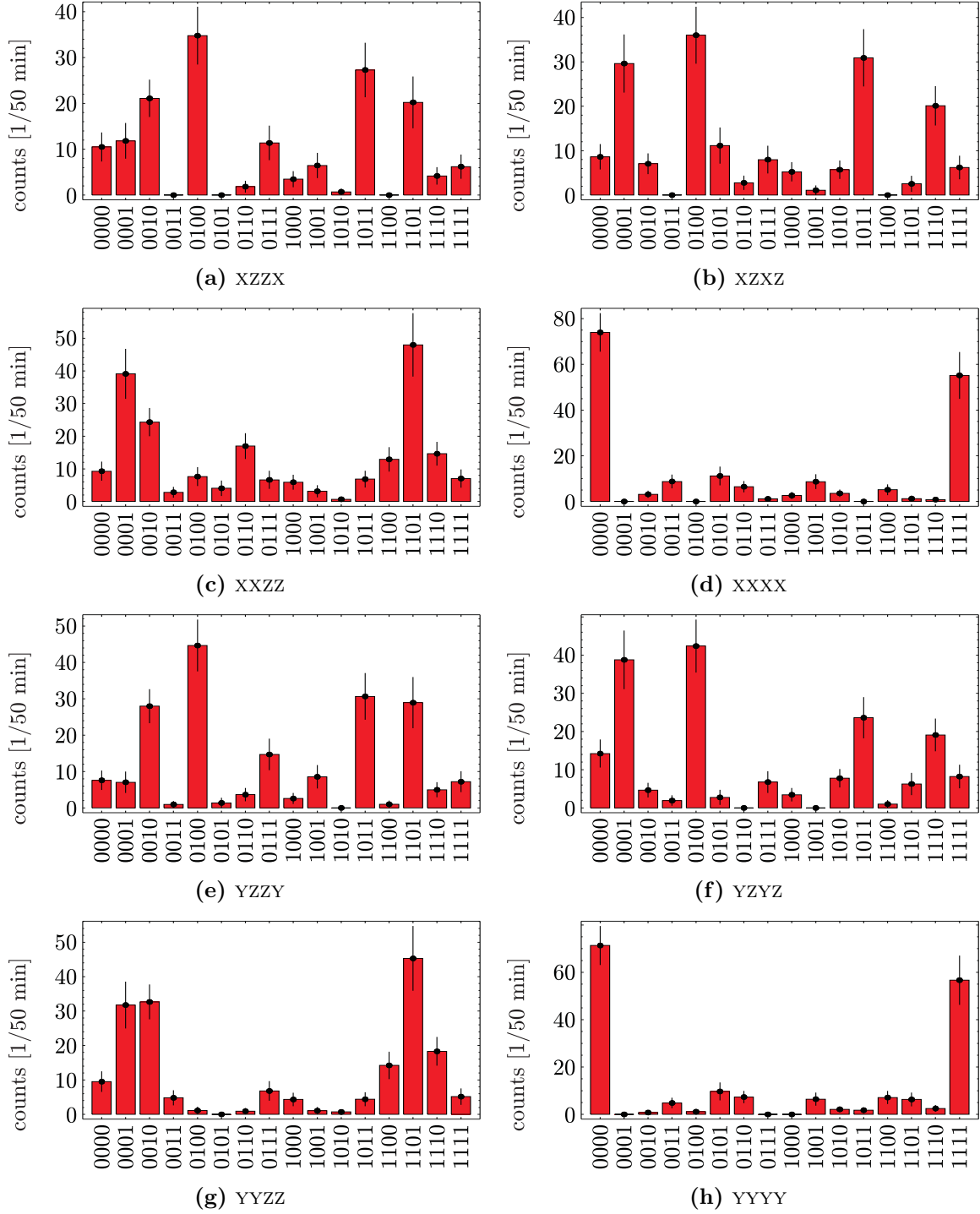


Figure 4.4: Statistics of the eight correlation measurements required for the evaluation of the operator $\mathbb{B}_{D_4^{(2)}}$.

(a)			
State	$ \langle \mathbf{D}_{D_4^{(2)}} \rangle $ (SLOCC)	$ \langle \mathbf{D}'_{D_4^{(2)}} \rangle $ (SLOCC)	
$ D_4^{(2)}\rangle$	1.000	1.000	
$ \text{GHZ}\rangle$	0.905	0.937	
$ C_4\rangle$	0.871	0.905	
$ \text{w}\rangle$	0.869	0.905	
$ \Psi_4\rangle$	0.869	0.901	
$ \text{bi-sep}\rangle$	0.750	0.872	
$ \text{sep}\rangle$	0.192	0.139	

(b)		(c)	
State	$ \langle \mathbf{D}_{\Psi_4} \rangle $ (SLOCC)	State	$ \langle \mathbf{D}_{C_4} \rangle $ (SLOCC)
$ \Psi_4\rangle$	1.000	$ C_4\rangle$	1.000
$ D_4^{(2)}\rangle$	0.905	$ D_4^{(2)}\rangle$	0.871
$ \text{GHZ}\rangle$	0.772	$ \Psi_4\rangle$	0.750
$ C_4\rangle$	0.741	$ \text{GHZ}\rangle$	0.750
$ \text{w}\rangle$	0.701	$ \text{w}\rangle$	0.750
$ \text{bi-sep}\rangle$	0.683	$ \text{bi-sep}\rangle$	0.750
$ \text{sep}\rangle$	0.619	$ \text{sep}\rangle$	0.625

Table 4.4: Maximal expectation values of alternative characteristic operators for (a) $|D_4^{(2)}\rangle$, (b) $|\Psi_4\rangle$ and (c) $|C_4\rangle$. The bounds for several prominent examples of four-qubit states are calculated numerically with respect to SLOCC operations.

where, e.g., $\sigma_k^{1,3} = \sigma_k \otimes \mathbb{1} \otimes \sigma_k \otimes \mathbb{1}$ and $k \in \{x, y, z\}$. It is characteristic for $|\Psi_4\rangle$, but not a Bell operator as, $\beta_{\text{LR}} = \frac{13}{7}$. Tab. 4.4(b) shows the bounds on the expectation value of \mathbf{D}_{Ψ_4} for the same set of four-qubit states as before. An experimental evaluation of \mathbf{D}_{Ψ_4} using the data obtained in Sec. 2.2.3 (see Fig. 2.10) yields $\langle \mathbf{D}_{\Psi_4} \rangle_{\text{exp}} = 0.903 \pm 0.018$. Comparing this value with Tab. 4.4(b) proves that the state is genuinely four-qubit entangled and cannot be of GHZ-, cluster-, or w-type. Unfortunately, the value is just at the limit to discriminate the experimentally observed state from the Dicke state. Still, the discrimination to all states is more significant in comparison to the usage of \mathbf{B}_{Ψ_4} .

The operator for $|C_4\rangle$ is, like \mathbf{B}_{C_4} , constructed from the cluster state stabilizer operators. It is of the form

$$8\mathbf{D}_{C_4} = (\sigma_z^{1,2} + \mathbb{1}^{\otimes 4}) \cdot (\mathbb{1} \otimes \sigma_z \otimes \sigma_x \otimes \sigma_x + \mathbb{1}^{\otimes 4}) + (\sigma_x \otimes \sigma_x \otimes \sigma_z \otimes \mathbb{1} + \mathbb{1}^{\otimes 4}) \cdot (\sigma_z^{3,4} + \mathbb{1}^{\otimes 4}) \quad (4.13)$$

and its evaluation requires two measurement settings (ZZXX, XXZZ). It is characteristic for $|C_4\rangle$ with $\lambda_{\text{max}} = 1$, but no Bell operator as the limit for any local realistic theory is $\beta_{\text{LR}} = 16$. The bounds on the expectation value of \mathbf{D}_{C_4} for other states are displayed in Tab. 4.4(c). Using the operator for the analysis of the cluster state which was observed in the experiment described in Sec. 3.3, yields $\langle \mathbf{D}_{C_4} \rangle_{\text{exp}} = 0.825 \pm 0.020$. According to Tab. 4.4(c), this value is not sufficient to discriminate the experimental state from the Dicke state. However, it allows to prove that the state is four qubit entangled and not of GHZ-, Ψ_4 -, or w-type. In contrast to the usage of \mathbf{B}_{C_4} , this discrimination can be accomplished indeed with respect to SLOCC operations.

4.5 Conclusion

In this chapter it was demonstrated that characteristic (Bell-)operators, i.e., operators for which a particular state only has maximal expectation value, allow to distinguish this state from the ones out of other classes of multi-partite entangled states. Thereby the properties of a *characteristic operator* were defined and shown to be reasonable in the sense that relaxing the imposed requirements does not lead to the desired result anymore. New operators for two important four-qubit entangled states were presented. They have been successfully applied to experimentally distinguish two important four-qubit entangled states from states of several other SLOCC classes. It was shown that other, already known witness operators for these states are also characteristic according to the introduced definition. Used in the experiment, they allowed the investigation of the observed states from a different perspective.

The simple, though not yet constructive, method to design these discrimination operators is based on the correlations between local measurement settings that are typical for the respective quantum state. As the number of measurement settings required for the evaluation of the operators is lower compared to standard analysis tools, like, e.g., QST or fidelity estimation, the experimental effort is significantly diminished. Demanding the discrimination operators to be Bell operators can be advantageous in case of limited knowledge about the state space. Otherwise, employing characteristic symmetries and properties of the state under investigation can even further reduce the effort to a number of settings which scales polynomially with the number of qubits. This renders the new method a truly efficient tool for the characterization of multi-partite entanglement.

Chapter 5

Experimental implementation of multi-agent quantum games

In Chap. 2 a linear optics network was introduced that enables the observation of a whole family of four-qubit entangled states. This chapter deals with the application of this setup for the first experimental realization of a multi-agent quantum game. The particular game which is implemented is the four-player quantum Minority game.

After a short introduction to the principles of (quantum) game theory, it is theoretically shown that for this game, with the family of initial states presented in Sec. 2.2, there is a symmetric Pareto optimal strategy profile that provides payoffs superior to that obtainable classically. The excess of the quantum payoff over the classical depends on the fidelity of the initial state. When the appropriate strategies are applied experimentally, the payoff values obtained lie well above the classical limit and thus prove the quantum version of the game to be superior to its classical counterpart.

5.1 Basics of (quantum) game theory

Game theory is a branch of applied mathematics which is used to mathematically describe the behavior of rational decision making in conflict situations. It has been used in economics, social sciences and biology to model situations in which decisions of particular individuals depend upon the choices of others. Meanwhile it found also applications in physics and computer science.

From a mathematical point of view a game is defined as a set of players, a set of rules according to which the players can choose their actions, and a set of payoff functions assigning rewards to the players for the different game outcomes. Thereby the payoff constitutes a measure for the desirability of a particular outcome of the game for a player. In the simplest version of a game the players can choose between two strategies and their choice can each be encoded in a single bit. Being involved with quantum information it seems natural to replace this classical bit by a qubit [205]. This translation of an originally classically formulated theory into the quantum realm can offer completely new prospects, just like it happened for quantum cryptography or quantum computing. As an elaborated introduction into (quantum) game theory would go beyond the scope of this thesis, the basic features and definitions necessary for the understanding of the following sections are demonstrated by means of a simple example involving two players. Probably the most famous is the so-called Prisoners' Dilemma.

The name stems from a short story about two prisoners on remand which have the chance to negotiate their respective time of imprisonment by either choosing to *defect* or *cooperate* during the interrogation. Any elaboration of the story is not of further importance as the underlying conflict applies anyway to various situation in everyday life. Important, however, is to note that each player has two strategies to play and is concerned exclusively with maximizing his own payoff irrespective of the reward of the other. A convenient way of representing this game is in its normal form, which consists of a matrix including the players, say A and B, their strategies, c and d, as well as the resulting payoffs (\cdot, \cdot) :

	A: c	A: d
B: c	(3,3)	(0,5)
B: d	(5,0)	(1,1)

Considering the distribution of the payoff it is obvious that with the aim of maximizing his own reward, rational choice of each player leads to both playing d, although each player's individual payoff would be greater if they both played c. This can be easily understood by running through the possibilities: Assuming A plays c, the obvious best choice for B is to play d as in this case he obtains 5 credits instead of only 3. Also in case A chooses d, for B to play d is the preferred strategy as he is rewarded at least 1 credit instead of 0. The same holds vice versa for A. The arising conflict can be formulated in an elegant way by defining the following two terms [206]:

Definition 5.1.1 (Nash equilibrium) *A game result from which no player can improve their payoff by a unilateral change in strategy is called Nash equilibrium (NE).*

Definition 5.1.2 (Pareto optimal) *A game result from which no player can improve their payoff without another player being worse off is called Pareto optimal (PO).*

Consequently, the *dilemma* in the Prisoners' Dilemma is the fact that the PO solution, which makes everybody "happy", is not a NE, i.e., it will not be reached within the game, as the game tends to end up in the equilibrium solution.

In a quantized version of the game [207] the players' actions are implemented by unitary operations on the qubits of a bi-partite (entangled) state. It can be shown that if entanglement is used, and under certain restrictions to the strategic space [208, 209], the players can escape the dilemma; a new NE appears in the game which is PO.

This was one of the first demonstrations that novel features can emerge if classical games are extended to the quantum domain. The quantum Prisoners' Dilemma was recently experimentally realized using quantum computers based on nuclear magnetic resonance [210] and linear optics [211]. In the following the first experimental implementation of a four-player quantum game is discussed.

5.2 The quantum Minority game

In this chapter a four-player quantum Minority game (QMG) with the continuous set of four-partite entangled states presented in Sec. 2.2 is studied theoretically¹, and its experimental proof-of-principal realization is demonstrated.

¹The theory was derived by Adrian P. Flitney within the framework of a collaboration with the author and his co-workers concerning the experimental implementation of multi-agent quantum games.

The Minority game [212] is a simple multi-player game for studying strategic decision making within a group of agents. It arose as a multi-agent iterative model of buying and selling in a market [213–215]. Similar to the Prisoners’ Dilemma, in each play the agents independently select between one of two options, labeled ”0” and ”1” (”buy” and ”sell”). Those that choose the minority win and are awarded a payoff of one unit, while the others loose and receive no payoff. Players utilize knowledge of past successful choices to optimize their strategy. Quantum versions of the one-shot Minority game have generated interest [216–220]. They provide a means of studying multi-partite entanglement in a competitive setting using game theoretic tools, and for small numbers of players are amenable to simulation using multi-photon entangled states.

The quantization of the Minority game is described as follows. Each of four players is given one qubit from a known four-partite entangled state. This state is an element of the subspace spanned by the four-qubit GHZ state and a product state of two Bell pairs. The players are permitted to act on their qubit with any local unitary operation. The choice of such an operator is the player’s strategy. During this stage coherence is maintained and no communication between the players is permitted. After the players’ actions, a referee measures the qubits in the computational basis and awards payoffs using the classical payoff scheme. In the dominant protocol of quantum games initialized by the quantization of the Prisoners’ Dilemma [207, 216], an entangling gate is used to produce a GHZ state from an initial state of $|00\dots 0\rangle$. After the players’ actions the inverse operator is applied to the multi-partite state. For the Minority game this last operator only has the effect of interchanging between states where the same player(s) win and so can be omitted without changing the expected payoffs. Although here no longer an initial GHZ state is considered, the construction of: *initial state* \rightarrow *player operations* \rightarrow *measurement in the computational basis* is maintained for simplicity, and to enable a comparison to be carried out with earlier results. This arrangement is consistent with the generalized quantum game formalisms of Lee and Johnson [221] and Gutoski and Watrous [222], and is particularly suited for an implementation using entangled photon states and linear optics quantum logic.

5.3 Theory

A four player QMG was first examined by Benjamin and Hayden [216], and later generalized to multiple players [217] and to the consideration of decoherence [218]. Formally the QMG is played by computing the state

$$\rho_{\text{fin}} = (\mathbf{A} \otimes \mathbf{B} \otimes \mathbf{C} \otimes \mathbf{D}) \cdot \rho_{\text{in}} \cdot (\mathbf{A} \otimes \mathbf{B} \otimes \mathbf{C} \otimes \mathbf{D})^\dagger, \quad (5.1)$$

where $\mathbf{A}, \mathbf{B}, \mathbf{C}, \mathbf{D}$ are the operators representing the strategies of the four players and ρ_{in} is some four-qubit input state. For convenience the players shall be named Alice (A), Bob (B), Charlie (C) and Debra (D). The qubits in ρ_{fin} are subsequently measured in the computational basis and payoffs are awarded using the classical payoff matrix. Work to date has concentrated on the consideration of an initial GHZ state. In contrast, here as initial state the family introduced in Sec. 2.2 is considered,

$$\begin{aligned} |\psi_{\text{in}}\rangle = |\Psi(\alpha)\rangle = & \frac{\alpha}{\sqrt{2}}(|0000\rangle + |1111\rangle) \\ & + \frac{\sqrt{1-\alpha^2}}{2}(|01\rangle + |10\rangle) \otimes (|01\rangle + |10\rangle), \end{aligned} \quad (5.2)$$

see Eqn. (2.18). To make allowances for some loss of fidelity in the experimental preparation of this state the initial state will be a mixed state represented by the density matrix

$$\rho_{\text{in}} = f|\psi_{\text{in}}\rangle\langle\psi_{\text{in}}| + \frac{1-f}{16} \sum_{ijkl=0,1} |ijkl\rangle\langle ijkl|, \quad (5.3)$$

where $f \in [0, 1]$ is a measure of the quality of production of the desired initial state. The second term in Eqn. (5.3) represents white noise [100]. The players' strategies are single-qubit unitary operators that can be parameterized in the form

$$\mathbf{S}(\theta, \beta_1, \beta_2) = \begin{pmatrix} \exp(i\beta_1) \cos\left(\frac{\theta}{2}\right) & i \exp(i\beta_2) \sin\left(\frac{\theta}{2}\right) \\ i \exp(-i\beta_2) \sin\left(\frac{\theta}{2}\right) & \exp(-i\beta_1) \cos\left(\frac{\theta}{2}\right) \end{pmatrix}, \quad (5.4)$$

where $\theta \in [0, \pi]$, $\beta_1, \beta_2 \in [-\pi, \pi]$. In the used construction of the QMG only the difference in the phases is relevant to the expected payoff, so it suffices to use a restricted set of operators where $\beta \equiv \beta_1 = -\beta_2$.

In the case where $\alpha = 1$ it is known that a symmetric NE occurs when all players choose the strategy [216]

$$\mathbf{S}\left(\frac{\pi}{2}, \frac{\pi}{8}, -\frac{\pi}{8}\right) = \frac{1}{\sqrt{2}} \begin{pmatrix} \exp(i\frac{\pi}{8}) & i \exp(-i\frac{\pi}{8}) \\ i \exp(i\frac{\pi}{8}) & \exp(-i\frac{\pi}{8}) \end{pmatrix}. \quad (5.5)$$

Although the value $\beta_1 = -\beta_2 = \frac{\pi}{8}$ is not the unique optimum, it is a focal point [223] that attracts the attention of the players since it is the simplest optimum value, and therefore there is no great difficulty in arriving at this NE. Given that at most one player of the four can be in the minority, $\frac{1}{4}$ is the greatest average payoff that can be expected. This is realized with the above strategy when the initial state has maximum fidelity. As $f \rightarrow 0$, the payoff reduces to $\frac{1}{8}$, the optimal payoff in a one-shot classical Minority game, where the players can do no better than choosing 0 or 1 with equal probability. This is as expected since in the absence of entanglement the QMG cannot give any advantage over its classical counter part.

A NE in the case of general α can be searched as follows. If there exists θ^*, β^* such that

$$\begin{aligned} \langle \$_{\text{D}} (\mathbf{S}(\theta^*, \beta^*, -\beta^*)^{\otimes 4}) \rangle &\geq \\ \langle \$_{\text{D}} (\mathbf{S}(\theta^*, \beta^*, -\beta^*)^{\otimes 3} \otimes \mathbf{S}(\theta, \beta, -\beta)) \rangle &\quad \forall \theta, \beta, \end{aligned} \quad (5.6)$$

then $\mathbf{S}(\theta^*, \beta^*, -\beta^*)$ is a symmetric NE strategy². Thereby $\$_{\text{D}} \equiv |0001\rangle\langle 0001| + |1110\rangle\langle 1110|$ denotes the payoff operator to Debra. There is no in principle objection to asymmetric NE strategy profiles, where the players choose different strategies. However, in practice these cannot be reliably achieved in the absence of communication between the participants since it is otherwise impossible for the players to know which of the different strategies to select. Necessary, but not sufficient, conditions for the existence of a symmetric NE are

$$\left. \frac{\partial \langle \$_{\text{D}} \rangle}{\partial \theta} \right|_{\theta=\theta^*, \beta=\beta^*} = 0, \quad \left. \frac{\partial \langle \$_{\text{D}} \rangle}{\partial \beta} \right|_{\theta=\theta^*, \beta=\beta^*} = 0, \quad (5.7a)$$

$$\left. \frac{\partial^2 \langle \$_{\text{D}} \rangle}{\partial \theta^2} \right|_{\theta=\theta^*, \beta=\beta^*} \leq 0, \quad \left. \frac{\partial^2 \langle \$_{\text{D}} \rangle}{\partial \beta^2} \right|_{\theta=\theta^*, \beta=\beta^*} \leq 0, \quad (5.7b)$$

where $\langle \$_{\text{D}} \rangle$ is the payoff on the right hand side of Eqn. (5.6). Inequalities in Eqn. (5.7b) indicate a local maximum in the payoff to Debra, however this may not be a global maximum.

²If Eqn. (5.6) holds for each player, this is nothing but a mathematical formulation of Def. 5.1.1.

An equality in Eqn. (5.7b) may mean a local maximum, minimum or an inflection point in the payoff. In the following all the symmetric NE strategies are enumerated by considering Eqn. (5.7a) – Eqn. (5.7b) over the range of $\alpha \in [0, 1]$.

If Alice, Bob and Charlie use the strategy $\mathbf{S}(\theta, \beta, -\beta)$ while Debra plays $\mathbf{S}(\theta', \beta', -\beta')$ then

$$\begin{aligned} \left. \frac{\partial \langle \$_{\text{D}} \rangle}{\partial \theta'} \right|_{\theta'=\theta, \beta'=\beta} &= \frac{\sin(2\theta)}{8} \left(2\alpha^2 + 2\alpha\sqrt{2-2\alpha^2} \cos(4\beta) \right. \\ &\quad \left. + (2\alpha^2 - 2 - 2\alpha\sqrt{2-2\alpha^2} \cos(4\beta) - \alpha^2 \cos^2(4\beta)) \sin^2(\theta) \right) \\ \left. \frac{\partial \langle \$_{\text{D}} \rangle}{\partial \beta'} \right|_{\theta'=\theta, \beta'=\beta} &= \frac{\alpha}{2} \sin(4\beta) \sin^2(\theta) \\ &\quad \times \left((\sqrt{2-2\alpha^2} + \alpha \cos(4\beta)) \sin^2(\theta) - 2\sqrt{2-2\alpha^2} \right). \end{aligned} \quad (5.8)$$

The variables θ, β need to be found for which these derivatives are simultaneously zero. Apart from the known NE for $\alpha = 1$ the only other symmetric NE occurs for $\alpha \leq \sqrt{\frac{2}{3}}$ when $\cos(4\beta) = 1$ and

$$\cos(\theta) = \sqrt{\frac{2-3\alpha^2}{2-\alpha^2+2\alpha\sqrt{2-2\alpha^2}}}. \quad (5.9)$$

The expected payoff to each player for this equilibrium is

$$\langle \$ \rangle = \frac{\alpha(2-3\alpha^2)(\alpha + \sqrt{2-2\alpha^2})}{4-2\alpha^2+4\alpha\sqrt{2-2\alpha^2}}, \quad (5.10)$$

which reaches a maximum value of $(3+2\sqrt{3})/(18+10\sqrt{3}) \approx 0.183$ at $\alpha = \sqrt{\frac{1}{6}(3-\sqrt{3})}$. Fig. 5.1(a) and Fig. 5.1(b) give the value of θ and the resulting payoff, respectively, for this solution.

Now the PO strategy profile is considered, i.e., the one from which no player can improve their result without another being worse off. This is in effect the best result for the players as a group. Again only symmetric strategy profiles are considered. That is, only values of θ^*, β^* are of interest for which

$$\langle \$ (\mathbf{S}(\theta^*, \beta^*, -\beta^*)^{\otimes 4}) \rangle \geq \langle \$ (\mathbf{S}(\theta, \beta, -\beta)^{\otimes 4}) \rangle \quad \forall \theta, \beta, \quad (5.11)$$

where $\$$ represents the payoff to any one of the four players for the indicated strategy profile. Suppose all players select the strategy $\mathbf{S}(\theta, \beta, -\beta)$ for some θ, β to be determined. The payoff to each player is

$$\begin{aligned} \langle \$ \rangle &= \frac{\sin^2(\theta)}{32} \left(8 - 2\alpha^2 + 8\alpha\sqrt{2-2\alpha^2} \cos(4\beta) - 2\alpha^2 \cos(8\beta) \right. \\ &\quad \left. + 2(4-3\alpha^2) \cos(2\theta) + 8\alpha\sqrt{2-2\alpha^2} \cos(4\beta) \cos(2\theta) \right. \\ &\quad \left. + 2\alpha^2 \cos(8\beta) \cos(2\theta) \right). \end{aligned} \quad (5.12)$$

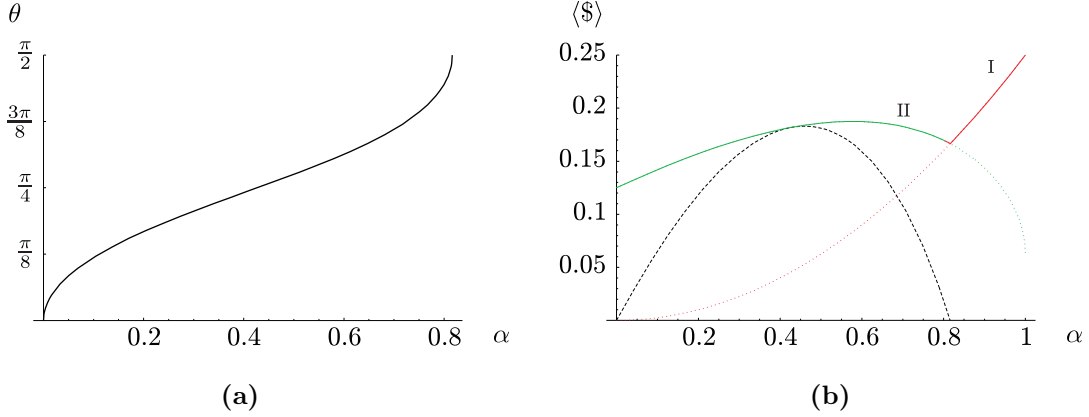


Figure 5.1: (a) The value of θ given by Eqn. (5.9) that, along with $\beta = 0$, gives a symmetric NE, as a function of the initial state parameter $\alpha \in [0, \sqrt{\frac{2}{3}}]$. The payoff for this equilibrium is given in Fig. 5.1(b) dashed curve. (b) Payoffs for the two maxima in Tab. 5.1, along with the symmetric NE payoff of Eqn. (5.10) (dashed line), as a function of the initial state parameter α . In I (—) the GHZ- and in II (—) the Bell-dominated regions are shown. The symmetric NE is maximal when $\alpha = \sqrt{\frac{2}{11}}$, while the peak of II occurs when $\alpha = \sqrt{\frac{1}{3}}$. The two PO payoff curves (I and II) meet at $\alpha = \sqrt{\frac{2}{3}}$.

A local maximum or minimum in the value of the payoff will have $\frac{\partial \langle \$ \rangle}{\partial \theta} = \frac{\partial \langle \$ \rangle}{\partial \beta} = 0$ where,

$$\begin{aligned} \frac{\partial \langle \$ \rangle}{\partial \theta} = & \frac{\sin(2\theta)}{4} \left(\alpha^2 \sin(2\theta) (1 - 2 \cos^2(4\beta) \sin^2(\theta)) \right. \\ & \left. + \cos(2\theta) (2 - 2\alpha^2 + 2\alpha \sqrt{2 - 2\alpha^2} \cos(4\beta)) \right); \end{aligned} \quad (5.13a)$$

$$\frac{\partial \langle \$ \rangle}{\partial \beta} = 2\alpha \sin^2(\theta) \sin(4\beta) (\alpha \cos(4\beta) \sin^2(\theta) - \sqrt{2 - 2\alpha^2} \cos^2(\theta)). \quad (5.13b)$$

The latter expression is zero if $\sin(\theta) = 0$, $\sin(4\beta) = 0$, or

$$\cos(4\beta) = \frac{\sqrt{2 - 2\alpha^2}}{\alpha} \cot^2(\theta). \quad (5.14)$$

Substituting the last expression into Eqn. (5.13a) and simplifying gives

$$\frac{\partial \langle \$ \rangle}{\partial \theta} = \frac{3\alpha^2 - 2}{4} \sin(2\theta), \quad (5.15)$$

which is equal to zero if $\sin(2\theta) = 0$ or $\alpha = \sqrt{\frac{2}{3}}$. From these results, Tab. 5.1 of extrema points and their corresponding payoffs can be calculated, where allowance has been made for non-unit fidelities f . The first two strategies are PO in the regions $\alpha \geq \sqrt{\frac{2}{3}}$ and $\alpha \leq \sqrt{\frac{2}{3}}$, respectively. Fig. 5.1(b) shows the payoffs for these cases for a fidelity of $f = 1$, along with the NE payoff of Eqn. (5.10). It has to be noted that the optimal strategy switches from $\mathbf{S}_I \equiv \mathbf{S}(\frac{\pi}{2}, \frac{\pi}{8}, -\frac{\pi}{8})$ for $\alpha > \sqrt{\frac{2}{3}}$ where the initial state is dominated by the GHZ part, to $\mathbf{S}_{II} \equiv \mathbf{S}(\frac{\pi}{4}, 0, 0)$ for $\alpha < \sqrt{\frac{2}{3}}$, where the initial state is dominated by the Bell pairs. At $\alpha = \sqrt{\frac{2}{3}}$

θ	β	$\langle \$ \rangle$	$\frac{\partial^2 \langle \$ \rangle}{\partial \theta^2}$	$\frac{\partial^2 \langle \$ \rangle}{\partial \beta^2}$
$\frac{\pi}{2}$	$\frac{\pi}{8}$	$\frac{1}{8} + \frac{f}{8}(2\alpha^2 - 1)$	$< 0 \forall \alpha > \sqrt{\frac{2}{3}}$	< 0
$\frac{\pi}{4}$	0	$\frac{1}{8} + \frac{f}{16}\alpha(2\sqrt{2-2\alpha^2} - \alpha)$	$< 0 \forall \alpha \neq \sqrt{\frac{2}{3}}$	$< 0 \forall \alpha < \sqrt{\frac{2}{3}}$
$\frac{\pi}{4}$	$\frac{\pi}{4}$	$\frac{1}{8} + \frac{f}{16}\alpha(-2\sqrt{2-2\alpha^2} - \alpha)$	$< 0 \forall \alpha \neq \sqrt{\frac{2}{3}}$	> 0
0	0	$\frac{1}{8} - \frac{f}{8}$	> 0	
	0	min		
0	$\frac{\pi}{4}$	$\frac{1}{8} - \frac{f}{8}$	> 0	0
$\frac{\pi}{2}$	0	$\frac{1}{8} - \frac{f}{8}$	> 0	> 0
$\frac{\pi}{2}$	$\frac{\pi}{4}$	$\frac{1}{8} - \frac{f}{8}$	> 0	> 0

Table 5.1: Table of θ and β that give rise to a local maximum or minimum expected payoff for a symmetric strategy profile $\mathbf{S}(\theta, \beta, -\beta)^{\otimes 4}$, along with the resulting payoff. The second derivatives of the payoff can be used to classify the extrema. Here, $f \in [0, 1]$ is the fidelity to which the initial state is prepared.

the components in the initial state are equally weighted and both strategies yield the same results.

There has been some recent interest in the correspondence between equilibria in quantum game theory and the violation of Bell inequalities [224, 225]. In the case considered here it is interesting that the curve for the symmetric PO payoff is the same as that for the maximal violation of the Mermin-Ardehali-Belinski-Klyshko (MABK) Bell inequality [226]. These findings are reported and discussed in detail in [227].

5.4 Experimental implementation and results

The implementation of the four-player quantum minority game consists of acting with the strategy operator on each qubit of the input state and afterwards measuring the resulting output state in different bases. The input states for different values of α are provided by the linear optics setup described in Sec. 2.2. The unitary transformation corresponding to the players' choice of a strategy is realized by a series of quarter-, half- and quarter-wave plates placed right before the PA in each of the four spatial modes. In order to play strategy I and to act with \mathbf{S}_I the angles of the wave plates are chosen as $\{-\frac{\pi}{8}, \frac{5\pi}{16}, 0\}$, for strategy II and \mathbf{S}_{II} as $\{\frac{\pi}{2}, \frac{\pi}{16}, \frac{\pi}{2}\}$.

First of all, the NE solution for $\alpha = 1$ shall be experimentally tested. The expected state after the application of strategy I, which is in this case the optimal one, is of the form

$$\begin{aligned}
(\mathbf{S}_I^{\otimes 4})|\text{GHZ}\rangle &= -\frac{1}{2\sqrt{2}}\left(|HHHV\rangle + |HHVH\rangle\right. \\
&\quad + |HVHH\rangle + |VHHH\rangle \\
&\quad - |VVVH\rangle - |VVHV\rangle \\
&\quad \left. - |VHVV\rangle - |HVVV\rangle\right) \\
&= \frac{i}{\sqrt{2}}(|RRRR\rangle - |LLLL\rangle).
\end{aligned} \tag{5.16}$$

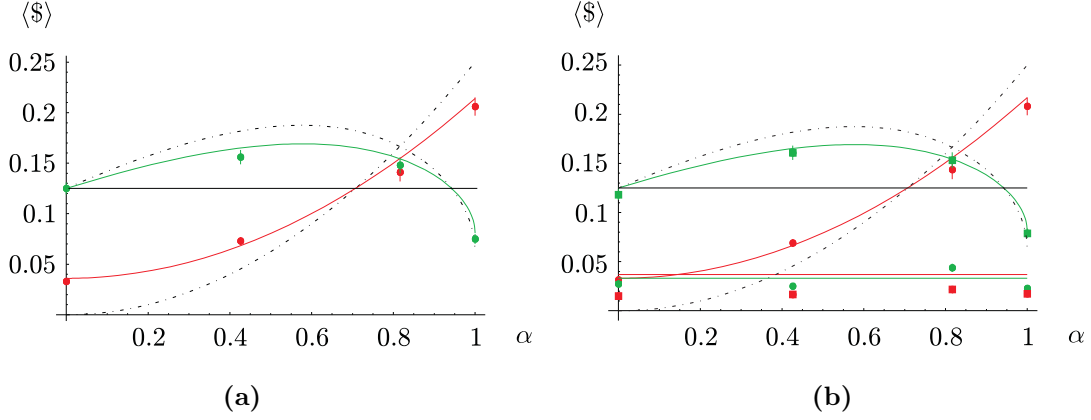


Figure 5.2: Experimentally measured payoffs. The data is fitted assuming a mixed input state of the form $f|\Psi(\alpha)\rangle\langle\Psi(\alpha)| + (1-f)/16\mathbb{1}^{\otimes 4}$. The maximum value achievable by classical means is $\frac{1}{8}$ (black line). The dashed line corresponds to the ideal case $f = 1$. (a) Payoff $\langle \$_{I,II} \rangle$ averaged over all four players dependent on α for strategy I (-●-) and strategy II (-●-), measured in the computational basis. (b) Payoff $\langle \$_{I,II} \rangle$ averaged over all four players dependent on α in the basis XXXX for strategy I (-●-) and strategy II (-●-) and in the basis YYYY for strategy I (-■-) and strategy II (-■-).

As can be seen, the transformed state is also of GHZ-type, and thus the fidelity

$$F = \langle \text{GHZ} | \mathbf{S}_I^{\dagger \otimes 4} \rho_{\alpha=1}^{\text{out}} \mathbf{S}_I^{\otimes 4} | \text{GHZ} \rangle \quad (5.17)$$

of the experimental state $\rho_{\alpha=1}^{\text{out}}$ equals the average expectation value of the GHZ stabilizer operators³ (cp. page 88). A measurement of the respective correlations is hence sufficient to evaluate the state fidelity. This requires nine measurement settings yielding a value of $F = 0.746 \pm 0.019$. For comparison, the fidelity of the untransformed initial GHZ state obtained with the setup is $F = 0.745 \pm 0.022$. Thus, application of the strategy operators leaves the quality of the observed state unchanged.

The payoff awarded to each player can be evaluated from the correlation measurement in the computational basis, zzzz. The obtained results are summarized in Tab. 5.2. The payoffs differ slightly for each player but are comparable within the measurement error. Averaged over all four players the payoff for $\alpha = 1$ and strategy I is $\langle \$_I \rangle_{\alpha=1} = 0.206 \pm 0.009$ which is well above the classical limit of $\frac{1}{8}$.

As shown theoretically in the previous section, the maximal achievable payoff depends on α and, moreover, an interesting change in the PO strategy occurs for $\alpha = \sqrt{\frac{2}{3}}$. This shall be verified experimentally in the following; in particular the dependence of the PO payoff on the value of α shall be reconstructed. To this end, measurements for other distinguished states, $|\Psi(0)\rangle$, $|\Psi(\sqrt{\frac{2}{11}})\rangle$, and $|\Psi(\sqrt{\frac{2}{3}})\rangle$ are performed. The results are summarized in Tab. 5.2 and the dependence of the average payoffs for strategy I and II is displayed in Fig. 5.2(a).

For other values of α , like in the GHZ case, the experimentally measured payoffs differ also slightly for each player but are in most instances comparable. The only exception occurs for player C and player A for $\alpha = \sqrt{\frac{2}{11}}$ and $\sqrt{\frac{2}{3}}$, respectively. The cause of this could

³A four-qubit GHZ state is also a graph state.

State	Strategy I		Strategy II	
	Player	payoff $\langle \$_I \rangle$	Player	payoff $\langle \$_{II} \rangle$
$ \Psi(0)\rangle$	A:	0.023 ± 0.004	A:	0.128 ± 0.012
	B:	0.028 ± 0.005	B:	0.117 ± 0.011
	C:	0.041 ± 0.006	C:	0.123 ± 0.011
	D:	0.042 ± 0.006	D:	0.131 ± 0.012
	Average:	0.033 ± 0.003	Average:	0.125 ± 0.006
$ \Psi(\sqrt{\frac{2}{11}})\rangle$	A:	0.058 ± 0.007	A:	0.148 ± 0.014
	B:	0.073 ± 0.008	B:	0.145 ± 0.014
	C:	0.104 ± 0.010	C:	0.161 ± 0.015
	D:	0.056 ± 0.007	D:	0.172 ± 0.015
	Average:	0.073 ± 0.004	Average:	0.156 ± 0.007
$ \Psi(\sqrt{\frac{2}{3}})\rangle$	A:	0.095 ± 0.015	A:	0.161 ± 0.016
	B:	0.155 ± 0.021	B:	0.133 ± 0.015
	C:	0.168 ± 0.021	C:	0.133 ± 0.014
	D:	0.145 ± 0.018	D:	0.165 ± 0.017
	Average:	0.141 ± 0.009	Average:	0.148 ± 0.008
$ \Psi(1)\rangle$	A:	0.202 ± 0.019	A:	0.061 ± 0.008
	B:	0.213 ± 0.020	B:	0.078 ± 0.009
	C:	0.185 ± 0.018	C:	0.068 ± 0.009
	D:	0.226 ± 0.019	D:	0.093 ± 0.010
	Average:	0.206 ± 0.009	Average:	0.075 ± 0.009

Table 5.2: Measured payoffs $\langle \$_{I,II} \rangle$ for strategy I and II played for four different initial states with distinguished values of α .

not yet doubtlessly be identified. The average payoffs follow the expected dependence for both strategies, once imperfect state quality is taken into account. To allow for loss in the states' fidelity the data in Fig. 5.2(a) is fitted assuming a mixed input state of the form of Eqn. (5.3). Although the assumptions to have an admixture of white noise and constant state quality for all values of α is only an approximation (see Sec. 2.2.4), the value of $f = 0.71 \pm 0.03$ obtained from the fit is in good agreement with the measured GHZ fidelity, where $F = (1 + 15f)/16 \approx 0.73$. A more detailed discussion of the results for each measured point is given in the following.

For $\alpha = 0$ a product of two Bell states is expected. As this state is not four-qubit entangled it should yield at maximum the classical payoff for strategy II. This is reproduced in the experiment with an average payoff of $\langle \$_{II} \rangle_{\alpha=0} = 0.125 \pm 0.006$. If the players chose to play strategy I zero payoff is expected for ideal, pure input states. However, for an increasing mixedness of the input states the payoff curves become more and more deformed into a

constant of the classical limit and finally equalize for $f \rightarrow 0$. This fact leads to a non-zero value for the experimentally measured average payoff for strategy I, $\langle \$I \rangle_{\alpha=0} = 0.033 \pm 0.003$.

Similar behavior is obtained for $\alpha = \sqrt{\frac{2}{11}}$, where the measured payoffs for strategy II, $\langle \$II \rangle_{\alpha=\sqrt{2/11}} = 0.156 \pm 0.007$, and strategy I, $\langle \$I \rangle_{\alpha=\sqrt{2/11}} = 0.073 \pm 0.004$, are lower and higher than expected, respectively. Still, the experimentally reached state quality is high enough to ensure for the proper strategy a payoff which exceeds the one maximally achievable in classical games.

As mentioned before, the next point, $\alpha = \sqrt{\frac{2}{3}}$ is special as both strategies lead to the same payoff. It is the point in which the players have to switch between the different strategies. The corresponding state, $|\Psi(\sqrt{\frac{2}{3}})\rangle \equiv |\Psi_4\rangle$, was already discussed several times within this work. The point's feature of being a quantum fulcrum is nicely reproduced in the experiment as well. As can be seen, both from Tab. 5.2 and Fig. 5.2(a), within the measurement errors the average payoff, $\langle \$I \rangle_{\alpha=\sqrt{2/3}} = 0.141 \pm 0.009$ and $\langle \$II \rangle_{\alpha=\sqrt{2/3}} = 0.148 \pm 0.008$, is the same for strategy I and II.

Finally, also the values obtained in the GHZ case fit well in the dependence prescribed by the previous points. Like for the other states, due to imperfect state quality the average payoff is slightly lower (higher) than the ideal value of $\frac{1}{4}$ ($\frac{1}{16}$) for strategy I (II).

Recapitulatory, it can be stated that for all values of α the players are awarded payoffs above the classical limit if they chose the proper strategy.

The realization of the Minority game presented here does not use an unentangling gate. Thus a measurement in the computational basis alone cannot prove that the higher than classical payoff values have their seeds in the four-qubit entanglement of $|\Psi(\alpha)\rangle$. In principle they could be caused by an admixture of the separable state

$$\rho_{\text{sep}} = \frac{1}{8} \left(|HHHV\rangle\langle HHHV| + \text{permutations} + |VVVH\rangle\langle VVVH| + \text{permutations} \right), \quad (5.18)$$

which yields a maximal "payoff" of $\frac{1}{4}$ when measured in the computational basis. However, measured in other bases, the state ρ_{sep} will not give a payoff above the classical limit.

In contrast the state $|\Psi(\alpha)\rangle$ has the extraordinary property that it exhibits the same term structure in the bases ZZZZ and XXXX when transformed by $\mathbf{S}_I^{\otimes 4}$ and in the bases ZZZZ and YYYY when transformed by $\mathbf{S}_{II}^{\otimes 4}$. Consequently, the strategies are still optimal, and if the payoff is evaluated analogously in these bases, the same dependence on α is expected. In order to prove this, the same measurements as before are performed in the bases XXXX and YYYY. The result is shown in Fig. 5.2(b).

For each basis and appropriate strategy indeed similar curves as for the computational basis are found. The applied fitting procedure is the same as before. The resulting values for f are slightly different for both bases ($f_x = 0.736 \pm 0.019$ and $f_y = 0.706 \pm 0.053$) but comparable with the one found for ZZZZ. The small asymmetry between the bases indicates that the experimental noise is indeed not purely white. The measured values of the averaged payoffs are summarized in Tab. 5.3. For the proper strategy they lie all above the classical limit also in these bases.

State	Strategy I	Strategy II
	in $(\sigma_x \otimes \sigma_x \otimes \sigma_x \otimes \sigma_x)$	in $(\sigma_y \otimes \sigma_y \otimes \sigma_y \otimes \sigma_y)$
	payoff $\langle \$_I \rangle$	payoff $\langle \$_{II} \rangle$
$ \Psi(0)\rangle$	0.031 ± 0.003	0.118 ± 0.006
$ \Psi(\sqrt{\frac{2}{11}})\rangle$	0.069 ± 0.004	0.161 ± 0.007
$ \Psi(\sqrt{\frac{2}{3}})\rangle$	0.144 ± 0.010	0.153 ± 0.008
$ \Psi(1)\rangle$	0.208 ± 0.009	0.079 ± 0.005

Table 5.3: Measured average payoffs $\langle \$_{I,II} \rangle$ for strategy I and II played for four different initial states with distinguished values of α . The payoff is not evaluated in the computational basis, but in the other two standard bases $(\sigma_x \otimes \sigma_x \otimes \sigma_x \otimes \sigma_x)$ and $(\sigma_y \otimes \sigma_y \otimes \sigma_y \otimes \sigma_y)$.

5.5 Conclusion

This chapter presented a theoretical study of the four-player quantum Minority game and its first experimental realization. In contrast to previous work a whole family of input states was considered.

It was shown that depending on the parameter which characterizes the family of states, different **PO** and **NE** solutions to the game exist. As long as the used input state is four-qubit entangled these solutions yield always a payoff which is higher than the one achievable in classical scenarios. In order to obtain the maximal possible reward the players have to adapt their strategy to the corresponding input state. Thereby exists a distinguished state at which the required change in strategy takes place. This fact appears to be rooted in the entanglement and correlation structure of the family of input states which changes between being dominated by its **GHZ** or Bell part, respectively.

These findings could be corroborated experimentally constituting a successful application of the linear optics network presented in Sec. 2.2. In particular, the experimentally achieved average payoffs lie all well above the classical limit, and their input state dependence could be well reproduced. An evaluation of the payoffs in different bases indicates the entanglement of the input states to be indeed the cause of the better than classical performance.

It can be stated that the study of quantum games is interesting in general as it provides another point of view to exploit preexisting classical frameworks as a base for finding new ways of understanding and using entanglement in quantum systems. While game theory is the mathematical language of competitive (classical) interactions, quantum game theory is the natural extension to consider competitive situations in quantum information settings. For example, eavesdropping in quantum communication (see, e.g., [228–230]) and optimal cloning [231] can be conceived as strategic games between two or more players. The particular game discussed here represents a different means of studying the entanglement structure of the used input states. As shown elsewhere [227], there exists even an interesting correspondence between the equilibria in the Minority game and the violation of Bell inequalities.

Conclusion and outlook

Prediction is very difficult, especially if it's about the future.

Niels Bohr

Setups of today's experiments on multi-photon entanglement can all be structured in the following way: They consist of a photon source, a linear optics network by which the photons are processed and the conditional detection of the photons at the output of the network.

This thesis has introduced two new linear optics networks and presented their application for several quantum information tasks. Thereby, the workhorse of multi-photon quantum information, spontaneous parametric down conversion (SPDC), was used in different configurations to provide the input states for the networks.

The first network was a controlled phase (CPHASE) gate which belongs to the set of universal quantum logic gates necessary for quantum computation. The new design of the gate is particularly interesting for applications in multi-photon experiments as it constitutes an improvement of former realizations with respect to stability and reliability. This was achieved by replacing (phase-dependent) single-photon interferometers for different polarizations by a polarization-dependent (but phase-independent) two-photon interference. The performance of the experimental gate was characterized by quantum process tomography in combination with a theoretical model based on experimental parameters of the setup.

One application of a CPHASE gate is its usage for the complete projection measurement of all four Bell states. In this context for the first time, a teleportation and entanglement swapping protocol was performed where all four Bell states are distinguished by means of linear optics only. Different polarization states have been teleported which showed fidelities clearly above the classical bound. The quality of the implemented teleportation and the achievement of an efficient quantum channel was confirmed by reconstruction of the quantum process matrix. Furthermore, also teleportation of entanglement was demonstrated. Thereby, the state to be teleported was completely indeterminate as it was itself part of an entangled state. Running this so-called entanglement swapping protocol yielded entangled output states with high fidelities between photons which have never interacted before. It could be even shown, that these states are entangled strong enough to violate a Bell inequality.

The distinction of all four Bell states enables also the projection of states onto the symmetric or antisymmetric subspace. As was shown recently for pure states, if such a projection is applied to the subsystem parts of two copies of the same quantum state, it allows the direct measurement of concurrence without quantum state tomography (QST). Within this work, for the first time, a generalization of the method for mixed states was tested experimentally, accounting for the imperfections of state-of-the-art technology. Detailed considerations about the influence of non-ideal gate operation allowed a realistic lower bound estimation about the

concurrence of the prepared states. These results prove the method for the direct measurement of concurrence to be an important tool for experiments with limitations on the number of measurements.

The **CPHASE** operation represents the central interaction in the generation principle of graph states, in particular cluster states. In this thesis, starting from two Bell states, the **CPHASE** gate could be successfully applied for the observation of a four-photon cluster state with high fidelity. The analysis of the results was focused on a proof-of-principle demonstration of the main usage of cluster states, namely measurement based quantum computation. The two fundamental types of single-qubit measurements commonly applied in such computation schemes have been demonstrated. This comprised the removal of physical qubits from the cluster, and the entangling operation of two encoded logical qubits. Although a four-qubit cluster provides only very restricted computational possibilities, the presented results are first promising steps towards future linear optics quantum computation at a larger scale.

The second network presented in this work, once fed with the second order emission of non-collinear type II **SPDC**, constitutes a tunable source of a whole family of states. This is a significant achievement as up to now the observation of a particular state required an individually tailored setup. With the network introduced here, many different states could be obtained within the same arrangement by the tuning of an easily accessible experimental parameter. These states form a subgroup of an important generic family of four-qubit entangled states, exhibit many useful properties and play a central role in several applications of quantum information. The performance of the setup was characterized by fidelity measurements for selected distinguished states of the subgroup. It was shown that these states can be obtained with high fidelities which are comparable with the ones achieved in alternative, state tailored setups. Consequently, the possibility to generate a multitude of such states within a *single* experimental setup is of great advantage as it represents an alternative to many different state sources.

The applicability of the setup was explicitly demonstrated by using the obtained states for the solution of a multi-party quantum information task. The task which was implemented is the four-player quantum Minority game which is a simple multi-player game for studying strategic decision making within a group of agents. In this game, each player acts locally with a unitary operator on a multi-qubit input state with the aim of maximizing a certain observable, the so-called payoff. In contrast to previous work, the optimal strategy for the players and the resulting payoffs were studied not only for a single input state, but for a whole family of states. The experimental verification of the theoretical findings was first made possible by the usage of the new linear optics network. It could be shown that for the whole family of states a greater than classically possible payoff is reached as long as four-photon entanglement is used as a resource. The study of quantum games can provide another point of view to exploit preexisting classical frameworks as a base for finding new ways of understanding and using entanglement in quantum systems. While game theory is the mathematical language of competitive (classical) interactions, quantum game theory is the natural extension to consider competitive situations in quantum information settings. For example, eavesdropping in quantum communication and optimal cloning can be conceived as strategic games between two or more players. The particular game discussed here represents thereby a different means of studying the entanglement structure of the used input states. Inspired by this, it could be shown elsewhere that there exists an interesting correspondence between the equilibria in the Minority game and the violation of Bell inequalities.

Another topic which was discussed within this thesis and which used the experimental data

obtained with both networks, is the experimental discrimination of different multi-partite entangled states. Whereas the characterization of entanglement is easy for two-partite quantum states, it turns out to be an increasingly difficult problem for more than two subsystems. For n -partite states it has to be distinguished not only between fully separable or entangled, but also between different kinds of separability. Classifications for states with the same level of separability exist for three and four qubits. However, from an experimental point of view, the introduced classifications seemed rather academic especially for four qubits, as there was no tool to easily assign an experimentally observed state to the one or the other class.

Here, a simple, though not yet constructive, method to discriminate a given experimental state from states of other entanglement classes was presented. It is based on *characteristic* operators which are formed by the correlations between local measurement settings that are typical for the respective quantum state. Such operators were introduced for important four-qubit entangled states and successfully applied to the experimental data gained during the presented experiments. As the number of measurement settings required for the evaluation of the operators is lower compared to standard, alternative analysis tools, like, e.g., QST or fidelity estimation, the experimental effort was significantly reduced. Demanding the discrimination operators to be additionally Bell operators can be advantageous in case of limited knowledge about the state space. Otherwise, employing characteristic symmetries and properties of the state under investigation can even further reduce the effort to a number of settings which scales polynomially with the number of qubits. Referring to this, already known operators could be identified to be characteristic for the investigated states and applied experimentally. In particular instances, they allowed an even more significant discrimination between the states. This proves the new method to be a practicable and efficient tool for the characterization of multi-partite entanglement which will also be important for future experiments.

Future experiments aiming at the observation of states with a higher qubit number will be, inevitably, even more concerned by the necessity of performing as few measurements as possible in an exponentially increasing state space. Despite such occurring challenges, the route to more photons is one that should be pursued, and experiments with up to six photons have been already successfully reported. In the long run, they might require better techniques, like other photon sources or different detectors, but reliable and versatile linear optics networks such as the one presented here will always play a central role. It would surely be interesting to operate the introduced networks with input states of an extended qubit number. This might lead to the observation of new entangled states or the solution of other quantum information problems. It is remarkable, that so far, already the biggest variety of entangled states was observed in photonic systems. Currently, they seem to provide an ideal testbed for the investigation of multi-partite entanglement on a smaller scale.

Admittedly, though linear optics quantum computing can be made near deterministic, photons do not seem to be the suitable quantum system for information processing and it is questionable whether quantum computers, – so they once will exist –, are based on photonic qubits. It is, however, for sure that photons are the best quantum system for a fast information transfer at low decoherence. They might provide the ideal "quantum-bus" between different quantum information processing and storage units. The role of linear optics quantum logic in such a scenario can be seen twofold: On the one hand, it might be useful to implement and support the interfaces between these units. On the other hand, it could take over some pre-processing of information already during a communication stage. The presented work can be seen as another small step to be on target for this vision.

Appendix A

Experimentally measured expectation values and their errors

This part of the appendix describes how expectation values of operators are determined experimentally. In particular, it is shown how the error on the expectation value of a given operator evolves depending on the number of measurement settings and the measurement time.

A.1 Evaluation of expectation values of operators

The state under investigation be $|\psi\rangle$. The results of any correlation measurement carried out on this state are summarized in form of the correlation tensor

$$T_{i_1, \dots, i_q} = \langle \psi | \sigma_{i_1} \otimes \dots \otimes \sigma_{i_q} | \psi \rangle, \quad (\text{A.1})$$

where q is the number of qubits and $i_1, \dots, i_q \in \{0, x, y, z\}$. So, for example for $q = 4$ and the measurement $i_1 i_2 i_3 i_4 = 0xyz$, the correlation is $T_{0xyz} = \langle \psi | \mathbb{1} \otimes \sigma_x \otimes \sigma_y \otimes \sigma_z | \psi \rangle \hat{=} \text{IXYZ}$, cp. Eqn. (2.33).

As any operator can be decomposed in terms of correlation operators,

$$\mathbf{O} = \sum_{\{(i_1, \dots, i_q)\}} \alpha_{i_1, \dots, i_q} (\sigma_{i_1} \otimes \dots \otimes \sigma_{i_q}), \quad (\text{A.2})$$

its expectation value can be accordingly expressed as a sum of correlations

$$\langle \mathbf{O} \rangle_\psi = \langle \psi | \mathbf{O} | \psi \rangle = \sum_{\{(i_1, \dots, i_q)\}} \alpha_{i_1, \dots, i_q} T_{i_1, \dots, i_q}, \quad (\text{A.3})$$

where $\alpha_{i_1, \dots, i_q} = \text{tr}(\mathbf{O} \cdot (\sigma_{i_1} \otimes \dots \otimes \sigma_{i_q}))$. While T_{i_1, \dots, i_q} depends on the state under investigation, the coefficients α_{i_1, \dots, i_q} are specific for the chosen operator. The latter can be calculated whereas the former need to be determined during the experiment, (cp. the considerations for the measurement of the fidelity on page 56).

In order to measure T_{i_1, \dots, i_q} , each correlation operator is further decomposed in local projectors of the form

$$\mathbf{P}_{i_1, \dots, i_q}^{b(q-1)b(q-2)\dots b0} = \mathbf{P}_{i_1}^{b0} \otimes \dots \otimes \mathbf{P}_{i_q}^{b(q-1)}, \quad (\text{A.4})$$

with

$$\mathbf{P}_{i_j}^{b(j-1)} = \begin{cases} \frac{\mathbb{1} + (-1)^{b(j-1)\sigma_{i_j}}}{2}, & \text{for } i_j \in \{x, y, z\} \\ \mathbb{1}, & \text{for } i_j \in \{0\}, \end{cases} \quad (\text{A.5})$$

$j = 1, \dots, q$ and $b(q-1)b(q-2)\dots b0$ the binary representation for an integer $k \in \{0, \dots, 2^q - 1\}$. For example, \mathbf{P}_{xxzz}^{0101} is the projector ($q = 4, k = 5$),

$$\mathbf{P}_x^1 \otimes \mathbf{P}_x^0 \otimes \mathbf{P}_z^1 \otimes \mathbf{P}_z^0 = \frac{\mathbb{1} + (-1)^1 \sigma_x}{2} \otimes \frac{\mathbb{1} + (-1)^0 \sigma_x}{2} \otimes \frac{\mathbb{1} + (-1)^1 \sigma_z}{2} \otimes \frac{\mathbb{1} + (-1)^0 \sigma_z}{2}. \quad (\text{A.6})$$

With this definition, it follows that

$$\sigma_{i_1} \otimes \dots \otimes \sigma_{i_q} = \sum_{k=0}^{2^q-1} \text{sign}(b(q-1)b(q-2)\dots b0) \mathbf{P}_{i_1, \dots, i_q}^{b(q-1)b(q-2)\dots b0}, \quad (\text{A.7})$$

with

$$\text{sign}(b(q-1)b(q-2)\dots b0) = (-1)^{\left(\sum_{j|i_j \neq 0} b(j-1)\right) \bmod 2}. \quad (\text{A.8})$$

Consequently, each correlation is determined by the probabilities,

$$\wp_{i_1, \dots, i_q}^{b(q-1)b(q-2)\dots b0} = \langle \psi | \mathbf{P}_{i_1, \dots, i_q}^{b(q-1)b(q-2)\dots b0} | \psi \rangle, \quad (\text{A.9})$$

for the different results of the local projectors (see page 39), and

$$T_{i_1, \dots, i_q} = \sum_{k=0}^{2^q-1} \text{sign}(b(q-1)b(q-2)\dots b0) \wp_{i_1, \dots, i_q}^{b(q-1)b(q-2)\dots b0}. \quad (\text{A.10})$$

In the experiment, the probabilities $\wp_{i_1, \dots, i_q}^{b(q-1)b(q-2)\dots b0}$ can be approximated by relative frequencies, $f_{i_1, \dots, i_q}^{b(q-1)b(q-2)\dots b0}$, which are obtained from the four-fold coincidence count rates of the corresponding detection event,

$$\wp_{i_1, \dots, i_q}^{b(q-1)b(q-2)\dots b0} \approx f_{i_1, \dots, i_q}^{b(q-1)b(q-2)\dots b0} = \frac{c_{i_1, \dots, i_q}^{b(q-1)b(q-2)\dots b0}}{\sum_{k=0}^{2^q-1} c_{i_1, \dots, i_q}^{b(q-1)b(q-2)\dots b0}}. \quad (\text{A.11})$$

Thereby, $c_{i_1, \dots, i_q}^{b(q-1)b(q-2)\dots b0}$ denotes the number of four-fold coincidence counts for the event $b(q-1)b(q-2)\dots b0$ in the basis i_1, \dots, i_q .

Finally, the expectation value of an operator is given as,

$$\begin{aligned} \langle \mathbf{O} \rangle_\psi &= \sum_{\{(i_1, \dots, i_q)\}} \alpha_{i_1, \dots, i_q} \sum_{k=0}^{2^q-1} \text{sign}(b(q-1)b(q-2)\dots b0) \wp_{i_1, \dots, i_q}^{b(q-1)b(q-2)\dots b0} \\ &\approx \sum_{\{(i_1, \dots, i_q)\}} \alpha_{i_1, \dots, i_q} \sum_{k=0}^{2^q-1} \text{sign}(b(q-1)b(q-2)\dots b0) f_{i_1, \dots, i_q}^{b(q-1)b(q-2)\dots b0}. \end{aligned} \quad (\text{A.12})$$

A.2 Errors of expectation values

In order to determine the error of the expectation value, $\Delta\langle\mathbf{O}\rangle_\psi$, as a function of the measured relative frequencies $f_{i_1,\dots,i_q}^{b(q-1)b(q-2)\dots b_0}$ Gaussian error propagation is applied,

$$\Delta\langle\mathbf{O}\rangle_\psi = \sqrt{\sum_{\{(i_1,\dots,i_q)\};k} \left(\frac{\partial\langle\mathbf{O}\rangle_\psi}{\partial f_{i_1,\dots,i_q}^{b(q-1)b(q-2)\dots b_0}} \Delta f_{i_1,\dots,i_q}^{b(q-1)b(q-2)\dots b_0} \right)^2}, \quad (\text{A.13})$$

where $\Delta f_{i_1,\dots,i_q}^{b(q-1)b(q-2)\dots b_0}$ is the error of $f_{i_1,\dots,i_q}^{b(q-1)b(q-2)\dots b_0}$.

Assuming that the coincidence counts $c_{i_1,\dots,i_q}^{b(q-1)b(q-2)\dots b_0}$ are statistically independent Poissonian random variables, and that the overall number of counts per measurement setting (i_1, \dots, i_q) for a given measurement time is $N_{i_1,\dots,i_q} \equiv \sum_{k=0}^{2^q-1} c_{i_1,\dots,i_q}^{b(q-1)b(q-2)\dots b_0} \gg 1$, it holds that¹ [22],

$$\Delta f_{i_1,\dots,i_q}^{b(q-1)b(q-2)\dots b_0} \approx \sqrt{\frac{c_{i_1,\dots,i_q}^{b(q-1)b(q-2)\dots b_0}}{N_{i_1,\dots,i_q}^2}} = \sqrt{\frac{f_{i_1,\dots,i_q}^{b(q-1)b(q-2)\dots b_0}}{N_{i_1,\dots,i_q}}}. \quad (\text{A.14})$$

Consequently, it follows for the error of the expectation value:

$$\Delta\langle\mathbf{O}\rangle_\psi = \sqrt{\sum_{\{(i_1,\dots,i_q)\}} \frac{1}{N_{i_1,\dots,i_q}} \alpha_{i_1,\dots,i_q}^2 \sum_{k=0}^{2^q-1} f_{i_1,\dots,i_q}^{b(q-1)b(q-2)\dots b_0}}. \quad (\text{A.15})$$

As $\sum_{k=0}^{2^q-1} f_{i_1,\dots,i_q}^{b(q-1)b(q-2)\dots b_0} = 1$ this yields finally,

$$\Delta\langle\mathbf{O}\rangle_\psi = \sqrt{\sum_{\{(i_1,\dots,i_q)\}} \frac{1}{N_{i_1,\dots,i_q}} \alpha_{i_1,\dots,i_q}^2}. \quad (\text{A.16})$$

In case that the number of total counts is the same for each measurement setting, $N_{i_1,\dots,i_q} = N$, this can be further simplified to,

$$\Delta\langle\mathbf{O}\rangle_\psi = \frac{1}{\sqrt{N}} \sqrt{\sum_{\{(i_1,\dots,i_q)\}} \alpha_{i_1,\dots,i_q}^2}. \quad (\text{A.17})$$

In experiments, the 1-operator is usually not measured, i.e., for a real measurement setting, (h_1, \dots, h_q) , it holds that $h_1, \dots, h_q \in \{x, y, z\}$. Every $(q-d)$ -qubit correlation T_{i_1,\dots,i_q}^d containing d -times $i_j = 0$, ($d \in \{1, \dots, q\}$) can be evaluated out of all s , ($s \in \{1, \dots, 3^d\}$), measured q -qubit correlations or measurement settings, (h_1, \dots, h_q) , which satisfy $h_l = i_l \forall i_l \neq 0$:

$$T_{i_1,\dots,i_q}^d = \frac{1}{s} \sum_{\{(h_1,\dots,h_q)|h_l=i_l\forall i_l\neq 0\}} \sum_{k=0}^{2^q-1} \text{sign}(b(q-1)b(q-2)\dots b_0) \wp_{h_1,\dots,h_q}^{b(q-1)b(q-2)\dots b_0}. \quad (\text{A.18})$$

In case that Eqn. (A.18) is applied for the evaluation of Eqn. (A.12) and Eqn. (A.13), the error $\Delta\langle\mathbf{O}\rangle_\psi$ cannot be written anymore in the compact form of Eqn. (A.16). The reason is

¹Terms of the order of $\frac{1}{N^3}$ are neglected.

that each frequency $f_{i_1, \dots, i_q}^{b(q-1)b(q-2)\dots b0}$ appears in Eqn. (A.12) not only once but several times with different coefficients α_{i_1, \dots, i_q} . That means, in general, after carrying out the partial derivatives in Eqn. (A.13), the frequencies within a correlation for fixed i_1, \dots, i_q do not sum up anymore to one. Still, the error is always of the form:

$$\Delta \langle \mathbf{O} \rangle_\psi = \frac{1}{\sqrt{N}} \mathcal{A}. \quad (\text{A.19})$$

However, the factor \mathcal{A} depends not only on the operator (and the state), but as well on the particular set of measurements which is used to evaluate $\Delta \langle \mathbf{O} \rangle_\psi$ and $\langle \mathbf{O} \rangle_\psi$.

A.3 Examples

Three examples of operators for the symmetric four-qubit Dicke state with two excitations, $|D_4^{(2)}\rangle$ are considered (see Sec. 2.2.3). The operators are, the characteristic Bell operator $\mathbf{O}_1 = \mathbf{B}_{D_4^{(2)}}$ (see Eqn. (4.6)), the fidelity operator $\mathbf{O}_2 = \mathbf{F}_{D_4^{(2)}}$, and the spin witness operator $\mathbf{O}_3 = \mathbf{D}'_{D_4^{(2)}}$ (see Sec. 4.4, Eqn. (4.10) and [203]) with

$$\begin{aligned} \mathbf{B}_{D_4^{(2)}} = & \frac{1}{6} \left(-\sigma_x \otimes \sigma_z \otimes \sigma_z \otimes \sigma_x - \sigma_x \otimes \sigma_z \otimes \sigma_x \otimes \sigma_z \right. \\ & - \sigma_x \otimes \sigma_x \otimes \sigma_z \otimes \sigma_z + \sigma_x \otimes \sigma_x \otimes \sigma_x \otimes \sigma_x \\ & - \sigma_y \otimes \sigma_z \otimes \sigma_z \otimes \sigma_y - \sigma_y \otimes \sigma_z \otimes \sigma_y \otimes \sigma_z \\ & \left. - \sigma_y \otimes \sigma_y \otimes \sigma_z \otimes \sigma_z + \sigma_y \otimes \sigma_y \otimes \sigma_y \otimes \sigma_y \right), \end{aligned} \quad (\text{A.20})$$

$$\mathbf{F}_{D_4^{(2)}} = \frac{1}{16} \sum_{\{(i_1, \dots, i_4)\}} \alpha_{i_1, \dots, i_4} (\sigma_{i_1} \otimes \dots \otimes \sigma_{i_4}), \quad (\text{A.21})$$

where $\alpha_{i_1, \dots, i_4} = \langle D_4^{(2)} | \sigma_{i_1} \otimes \dots \otimes \sigma_{i_4} | D_4^{(2)} \rangle$, and

$$\begin{aligned} \mathbf{D}'_{D_4^{(2)}} = & \frac{4}{3} \left(4 \mathbb{1}^{\otimes 4} + \mathbb{1} \otimes \mathbb{1} \otimes \sigma_x \otimes \sigma_x + \mathbb{1} \otimes \sigma_x \otimes \mathbb{1} \otimes \sigma_x + \mathbb{1} \otimes \sigma_x \otimes \sigma_x \otimes \mathbb{1} \right. \\ & + \sigma_x \otimes \mathbb{1} \otimes \mathbb{1} \otimes \sigma_x + \sigma_x \otimes \mathbb{1} \otimes \sigma_x \otimes \mathbb{1} + \sigma_x \otimes \sigma_x \otimes \mathbb{1} \otimes \mathbb{1} \\ & + \mathbb{1} \otimes \mathbb{1} \otimes \sigma_y \otimes \sigma_y + \mathbb{1} \otimes \sigma_y \otimes \mathbb{1} \otimes \sigma_y + \mathbb{1} \otimes \sigma_y \otimes \sigma_y \otimes \mathbb{1} \\ & \left. + \sigma_y \otimes \mathbb{1} \otimes \mathbb{1} \otimes \sigma_y + \sigma_y \otimes \mathbb{1} \otimes \sigma_y \otimes \mathbb{1} + \sigma_y \otimes \sigma_y \otimes \mathbb{1} \otimes \mathbb{1} \right). \end{aligned} \quad (\text{A.22})$$

A measurement of these operators can be used to acquire information about an experimentally prepared state. They can be even used to discriminate between different four-qubit entangled states, see Chap. 4.

The Bell operator consists of eight correlation terms whose measurement requires the eight settings

$$\begin{aligned} \mathbf{S}_{\mathbf{B}} = & \{(x, z, z, x), (x, z, x, z), (x, x, z, z), (x, x, x, x), \\ & (y, z, z, y), (y, z, y, z), (y, y, z, z), (y, y, y, y)\} \end{aligned} \quad (\text{A.23})$$

The fidelity operator decomposes into 40 correlation terms for which $\alpha_{i_1, \dots, i_4} \neq 0$. Out of these, 21 describe four-qubit correlations (see Sec. 2.2.3 and App. B.1.3). The measurement

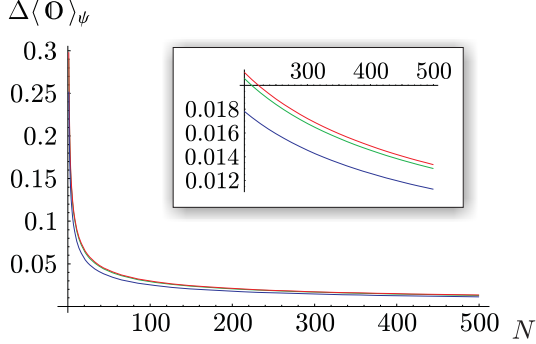


Figure A.1: Scaling of measurement errors. Error of the fidelity (—) $\Delta\langle\mathbb{F}_{D_4^{(2)}}\rangle_\psi$, the Bell (—) $\Delta\langle\mathbb{B}_{D_4^{(2)}}\rangle_\psi$, and witness (—) $\Delta\langle\mathbb{D}'_{D_4^{(2)}}\rangle_\psi$ operator for the Dicke state. The error on the expectation value of an operator, $\Delta\langle\mathbf{O}\rangle_\psi$, depends on the number of total counts, N , per measurement setting. For a fixed overall measurement time, N and thus the scaling behavior is related to the number of measurement settings required for the determination of $\langle\mathbf{O}\rangle_\psi$.

of these 21 four-qubit correlations suffices to evaluate the fidelity and needs accordingly 21 settings,

$$\mathcal{S}_F = \{(h_1, \dots, h_4) \mid \alpha_{h_1, \dots, h_4} \neq 0 \wedge h_1, \dots, h_4 \in \{x, y, z\}\}. \quad (\text{A.24})$$

In contrast, the spin witness operator comprises 13 correlation terms whose measurement take up only two settings,

$$\mathcal{S}_{D'} = \{(x, x, x, x), (y, y, y, y)\}. \quad (\text{A.25})$$

The error for the measured expectation value of the Bell-operator can be directly estimated using Eqn. (A.17):

$$\Delta\langle\mathbb{B}_{D_4^{(2)}}\rangle_\psi = \frac{1}{\sqrt{N}} \sqrt{8 \cdot \frac{1}{6^2}} = \frac{1}{\sqrt{N}} \cdot \frac{\sqrt{2}}{3}. \quad (\text{A.26})$$

For the calculation of the error on the expectation value of the fidelity and the spin witness operator, the factor \mathcal{A} in Eqn. (A.19) depends on the settings \mathcal{S}_F , $\mathcal{S}_{D'}$ and can be determined using Eqn. (A.18),

$$\Delta\langle\mathbb{F}_{D_4^{(2)}}\rangle_\psi = \frac{1}{\sqrt{N}} \underbrace{\sqrt{\frac{269}{21}}}_{\mathcal{A}_F}, \quad (\text{A.27})$$

$$\Delta\langle\mathbb{D}'_{D_4^{(2)}}\rangle_\psi = \frac{1}{\sqrt{N}} \underbrace{\sqrt{\frac{2}{3}}}_{\mathcal{A}_{D'}}. \quad (\text{A.28})$$

With these results, the scaling of the error for the three operators can be compared. To this end, the overall measurement time is assumed to be fixed. This implies that the total count rate per measurement setting is by a factor $\frac{21}{8}$ higher for $\mathbb{B}_{D_4^{(2)}}$ and by a factor $\frac{21}{2}$ for

State	Operator	\mathcal{A}	Number of settings	\mathcal{A}'
$ D_4^{(2)}\rangle$	$\mathbf{F}_{D_4^{(2)}}$	$\frac{\sqrt{\frac{269}{21}}}{12}$	21	0.298
	$\mathbf{B}_{D_4^{(2)}}$	$\frac{\sqrt{2}}{3}$	8	0.291
	$\mathbf{D}_{D_4^{(2)}}$	$\frac{\sqrt{\frac{3}{2}}}{2}$	6	0.327
	$\mathbf{D}'_{D_4^{(2)}}$	$\sqrt{\frac{2}{3}}$	2	0.252
$ \Psi_4^-\rangle$	\mathbf{F}_{Ψ_4}	$\frac{\sqrt{\frac{1111}{21}}}{24}$	21	0.303
	\mathbf{B}_{Ψ_4}	$\frac{\sqrt{\frac{5}{2}}}{3}$	10	0.364
	\mathbf{D}_{Ψ_4}	$\frac{11}{7\sqrt{3}}$	3	0.343
$ C_4\rangle$	\mathbf{F}_{C_4}	$\frac{1}{2\sqrt{2}}$	9	0.354
	\mathbf{B}_{C_4}	$\frac{1}{2}$	4	0.333
	\mathbf{D}_{C_4}	$\frac{1}{\sqrt{2}}$	2	0.333

Table A.1: Scaling of measurement errors. The error factor \mathcal{A} , the number of measurement settings and the relativ scaling factor \mathcal{A}' are given for some important operators of particular states.

$\mathbf{D}'_{D_4^{(2)}}$ compared to $\mathbf{F}_{D_4^{(2)}}$, such that

$$\Delta\langle\mathbf{F}_{D_4^{(2)}}\rangle_\psi = \frac{1}{\sqrt{N}} \frac{\sqrt{\frac{269}{21}}}{12} \approx \frac{1}{\sqrt{N}} \underbrace{0.298}_{\mathcal{A}'_{\mathbf{F}}} \quad (\text{A.29a})$$

$$\Delta\langle\mathbf{B}_{D_4^{(2)}}\rangle_\psi = \frac{1}{\sqrt{\frac{21}{8}N}} \frac{\sqrt{2}}{3} \approx \frac{1}{\sqrt{N}} \underbrace{0.291}_{\mathcal{A}'_{\mathbf{B}}} \quad (\text{A.29b})$$

$$\Delta\langle\mathbf{D}'_{D_4^{(2)}}\rangle_\psi = \frac{1}{\sqrt{\frac{21}{2}N}} \sqrt{\frac{2}{3}} \approx \frac{1}{\sqrt{N}} \underbrace{0.252}_{\mathcal{A}'_{\mathbf{D}'}} \quad (\text{A.29c})$$

The dependence on N is displayed in Fig. A.1. As can be seen, the error on the expectation value for the Bell operator scales negligibly better than the one for the fidelity operator. A considerably better scaling is achieved for the error on the expectation value for the spin witness operator. With respect to the experimental effort, the usage of $\mathbf{D}'_{D_4^{(2)}}$ is thus preferable to gain information about an experimental state.

Tab. A.1 shows in addition the error factor \mathcal{A} , as well as the number of required measurement settings and the accordingly corrected relative scaling factors \mathcal{A}' for other operators. These operators are used for the analysis of experimental states throughout this thesis (mainly in Chap. 4). By means of the values given in the table, the expected error on a measured quantity can be estimated prior to the actual measurement. This helps to rate the measurement time needed for a sufficient statistics.

Appendix B

Supplementary information and measured data

This part of the Appendix provides additional information and measured data for the different states investigated during the thesis. The data is only listed in form of tables without any further explanatory text. Explanations can be found in the respective sections where the states are studied.

B.1 For Chap. 2

This section lists explicitly the theoretical and experimentally measured correlations for the different states of the family $|\Psi'(\alpha)\rangle$ described in Sec. 2.2.

B.1.1 A product of two Bell pairs: $|\Psi'(0)\rangle$

Theoretical correlations

- (1): IIXX, IIYY, XXII, YYII
- (-1): IIZZ, ZZII
- (1): IIII, XXXX, YYYY, ZZZZ
- (1): XXYY, YYXX
- (-1): XXZZ, YYZZ, ZZXX, ZZYY

Table B.1: Theoretical values for the non-zero correlations of the state $|\Psi'(0)\rangle$.

Experimentally obtained results

III	1.000	\pm	0.009	XXXX	0.840	\pm	0.043
IIXX	0.891	\pm	0.025	XXYY	0.759	\pm	0.042
IYYI	0.866	\pm	0.024	XXZZ	-0.843	\pm	0.043
IIZZ	-0.980	\pm	0.025	YYXX	0.815	\pm	0.043
XXII	0.862	\pm	0.025	YYYY	0.733	\pm	0.042
YYII	0.883	\pm	0.024	YYZZ	-0.852	\pm	0.042
ZZII	-0.977	\pm	0.025	ZZXX	-0.870	\pm	0.044
Fidelity:	$F = 0.875 \pm 0.013$			ZZYY	-0.872	\pm	0.042
				ZZZZ	0.950	\pm	0.043

Table B.2: Measured non-zero two-qubit and four-qubit correlations for the state $|\Psi'(0)\rangle$, as well as resultant fidelity.

B.1.2 Still unknown: $|\Psi'(\sqrt{\frac{1}{6}(3 - \sqrt{3})})\rangle$

Theoretical correlations

$(\frac{1}{6}(3 + \sqrt{3}))$:	IIXX, IYYI, XXII, YYII
$(-\frac{1}{\sqrt{3}})$:	IIZZ, ZZII
$(\frac{1}{\sqrt{3}})$:	IXIX, IXXI, IYIY, IYYI, XIIX, XIXI, YIYY, YIYI
$(\frac{1}{6}(-3 + \sqrt{3}))$:	IZIZ, IZZI, ZIIZ, ZIZI
(1):	IIII, XXXX, YYYY, ZZZZ
$(\frac{1}{6}(3 - \sqrt{3}))$:	XYXY, XYYX, YXXY, YXYX
$(-\frac{1}{\sqrt{3}})$:	XZXZ, XZZX, YZYZ, YZZY, ZXXZ, ZXZX, ZYYZ, ZYZY
$(\frac{1}{\sqrt{3}})$:	XXYY, YYXX
$(\frac{1}{6}(-3 - \sqrt{3}))$:	XXZZ, YYZZ, ZZXX, ZZYY

Table B.3: Theoretical values for the non-zero correlations of the state $|\Psi'(\sqrt{\frac{1}{6}(3 - \sqrt{3})})\rangle$.

Experimentally obtained results

III	1.000	\pm 0.011	XXXX	0.710	\pm 0.051
IIXX	0.680	\pm 0.029	XXYY	0.471	\pm 0.050
IYY	0.656	\pm 0.028	XXZZ	-0.623	\pm 0.051
IIZZ	-0.606	\pm 0.029	XYXY	0.118	\pm 0.047
IXIX	0.316	\pm 0.029	XYYX	0.079	\pm 0.049
IXXI	0.323	\pm 0.029	XZXX	-0.399	\pm 0.049
IYIY	0.338	\pm 0.028	XZZX	-0.480	\pm 0.049
IYYI	0.362	\pm 0.028	YXXY	0.140	\pm 0.049
IZIZ	-0.175	\pm 0.028	YXYX	0.130	\pm 0.049
IZZI	-0.155	\pm 0.028	YYXX	0.460	\pm 0.051
XIIX	0.331	\pm 0.029	YYYY	0.663	\pm 0.050
XIXI	0.324	\pm 0.028	YYZZ	-0.643	\pm 0.049
XXII	0.675	\pm 0.029	YZYZ	-0.377	\pm 0.048
YIYY	0.333	\pm 0.028	YZZY	-0.370	\pm 0.047
YIYI	0.301	\pm 0.028	ZXXZ	-0.318	\pm 0.048
YYII	0.635	\pm 0.029	ZXZX	-0.346	\pm 0.048
ZIIZ	-0.164	\pm 0.028	ZYYZ	-0.338	\pm 0.049
ZIZI	-0.160	\pm 0.028	ZYZY	-0.386	\pm 0.050
ZZII	-0.621	\pm 0.028	ZZXX	-0.670	\pm 0.049
Fidelity: $F = 0.755 \pm 0.014$			ZZYY	-0.568	\pm 0.048
			ZZZZ	0.900	\pm 0.050

Table B.4: Measured non-zero two-qubit and four-qubit correlations for the state $|\Psi'(\sqrt{\frac{1}{6}(3-\sqrt{3})})\rangle$, as well as resultant fidelity.

B.1.3 The symmetric four-qubit Dicke state: $|\Psi'(\frac{1}{\sqrt{3}})\rangle$

Theoretical correlations

$(\frac{2}{3})$:	IIXX, IYY, XXII, YYII
$(-\frac{1}{3})$:	IIZZ, ZZII
$(\frac{2}{3})$:	IXIX, IXXI, IYIY, IYYI, XIIX, XIXI, YIYY, YIYI
$(-\frac{1}{3})$:	IZIZ, IZZI, ZIIZ, ZIZI
(1):	IIII, XXXX, YYYY, ZZZZ
$(\frac{1}{3})$:	XYXY, XYYX, YXXY, YXYX
$(-\frac{2}{3})$:	XZXX, XZZX, YYZ, YZZY, ZXXZ, ZXZX, ZYYZ, ZYZY
$(\frac{1}{3})$:	XXYY, YYXX
$(-\frac{2}{3})$:	XXZZ, YYZZ, ZZXX, ZZYY

Table B.5: Theoretical values for the non-zero correlations of the state $|\Psi'(\frac{1}{\sqrt{3}})\rangle$.

Experimentally obtained results

III	1.000	\pm 0.010	XXXX	0.701	\pm 0.049
IIXX	0.536	\pm 0.028	XXYY	0.318	\pm 0.047
IYY	0.578	\pm 0.028	XXZZ	-0.376	\pm 0.046
IIZZ	-0.400	\pm 0.027	XYXY	0.182	\pm 0.047
IXIX	0.370	\pm 0.027	XYYX	0.273	\pm 0.049
IXXI	0.425	\pm 0.028	XZXZ	-0.418	\pm 0.047
IYIY	0.358	\pm 0.028	XZZX	-0.397	\pm 0.045
IYYI	0.398	\pm 0.028	YXXY	0.221	\pm 0.047
IZIZ	-0.300	\pm 0.027	YXYX	0.226	\pm 0.048
IZZI	-0.252	\pm 0.026	YYXX	0.259	\pm 0.047
XIIX	0.422	\pm 0.028	YYYY	0.677	\pm 0.050
XIXI	0.370	\pm 0.027	YYZZ	-0.469	\pm 0.046
XXII	0.516	\pm 0.027	YZYZ	-0.497	\pm 0.047
YIIY	0.351	\pm 0.027	YZZY	-0.306	\pm 0.044
YIYI	0.360	\pm 0.028	ZXXZ	-0.405	\pm 0.048
YYII	0.541	\pm 0.028	ZXZX	-0.444	\pm 0.046
ZIIZ	-0.250	\pm 0.028	ZYYZ	-0.324	\pm 0.048
ZIZI	-0.245	\pm 0.027	ZYZY	-0.401	\pm 0.048
ZZII	-0.441	\pm 0.028	ZZXX	-0.606	\pm 0.047
Fidelity:	$F = 0.709 \pm 0.013$		ZZYY	-0.514	\pm 0.049
			ZZZZ	0.925	\pm 0.047

Table B.6: Measured non-zero two-qubit and four-qubit correlations for the state $|\Psi'(\frac{1}{\sqrt{3}})\rangle$, as well as resultant fidelity.

B.1.4 Still unknown: $|\Psi'(\frac{1}{\sqrt{2}})\rangle$

Theoretical correlations

$(\frac{1}{2})$:	IIXX, IYY, XXII, YYII
$(\frac{1}{\sqrt{2}})$:	IXIX, IXXI, IYIY, IYYI, XIIX, XIXI, YIIY, YIYI
$(-\frac{1}{2})$:	IZIZ, IZZI, ZIIZ, ZIZI
(1):	IIII, XXXX, YYYY, ZZZZ
$(\frac{1}{2})$:	XYXY, XYYX, YXXY, YXYX
$(-\frac{1}{\sqrt{2}})$:	XZXZ, XZZX, YYZZ, YZZY, ZXXZ, ZXZX, ZYYZ, ZYZY
$(-\frac{1}{2})$:	XXZZ, YYZZ, ZZXX, ZZYY

Table B.7: Theoretical values for the non-zero correlations of the state $|\Psi'(\frac{1}{\sqrt{2}})\rangle$.

Experimentally obtained results

III	1.000	\pm 0.010	XXXX	0.692	\pm 0.047
IIXX	0.445	\pm 0.026	XXZZ	-0.456	\pm 0.047
IYYI	0.491	\pm 0.027	XYXY	0.356	\pm 0.048
IXIX	0.354	\pm 0.027	XYYX	0.310	\pm 0.046
IXXI	0.394	\pm 0.027	XZXZ	-0.380	\pm 0.047
IYIY	0.362	\pm 0.027	XZZX	-0.414	\pm 0.047
IYYI	0.368	\pm 0.027	YXXY	0.355	\pm 0.046
IZIZ	-0.322	\pm 0.027	YXYX	0.334	\pm 0.048
IZZI	-0.410	\pm 0.028	YYYY	0.695	\pm 0.048
XIIX	0.393	\pm 0.027	YYZZ	-0.427	\pm 0.045
XIXI	0.411	\pm 0.027	YZYZ	-0.297	\pm 0.046
XXII	0.452	\pm 0.027	YZZY	-0.421	\pm 0.049
YIIY	0.366	\pm 0.027	ZXXZ	-0.380	\pm 0.045
YIYI	0.370	\pm 0.027	ZXZX	-0.443	\pm 0.047
YYII	0.425	\pm 0.026	ZYYZ	-0.419	\pm 0.045
ZIIZ	-0.370	\pm 0.026	ZYZY	-0.352	\pm 0.045
ZIZI	-0.351	\pm 0.027	ZZXX	-0.396	\pm 0.046
Fidelity:	$F = 0.677 \pm 0.013$		ZZYY	-0.536	\pm 0.047
			ZZZZ	0.901	\pm 0.047

Table B.8: Measured non-zero two-qubit and four-qubit correlations for the state $|\Psi'(\frac{1}{\sqrt{2}})\rangle$, as well as resultant fidelity.

B.1.5 Psi-four: $|\Psi_4\rangle$

Theoretical correlations

$(\frac{1}{3})$:	IIXX, IYYI, XXII, YYII
$(\frac{1}{3})$:	IIZZ, ZZII
$(\frac{2}{3})$:	IXIX, IXXI, IYIY, IYYI, XIIX, XIXI, YIIY, YIYI
$(-\frac{2}{3})$:	IZIZ, IZZI, ZIIZ, ZIZI
(1):	IIII, XXXX, YYYY, ZZZZ
$(\frac{2}{3})$:	XYXY, XYYX, YXXY, YXYX
$(-\frac{2}{3})$:	XZXZ, XZZX, YYZY, YZZY, ZXXZ, ZXZX, ZYYZ, ZYZY
$(-\frac{1}{3})$:	XXYY, YYXX
$(-\frac{1}{3})$:	XXZZ, YYZZ, ZZXX, ZZYY

Table B.9: Theoretical values for the non-zero correlations of the state $|\Psi_4^-\rangle$.

$$\begin{aligned}
(1 - \alpha^2): & \text{ IIXX, IYY, XXII, YYII} \\
(2\alpha^2 - 1): & \text{ IIZZ, ZZII} \\
(\alpha\sqrt{2} - 2\alpha^2): & \text{ XZXZ, XZZX, YZYZ, YZZY, ZXXZ, ZXZX, ZYYZ, ZYZY} \\
(-\alpha^2): & \text{ IZIZ, IZZI, ZIIZ, ZIZI} \\
(1): & \text{ IIII, XXXX, YYYYY, ZZZZ} \\
(\alpha^2): & \text{ XYXY, XYYX, YXXY, YXYX} \\
(-\alpha\sqrt{2} - 2\alpha^2): & \text{ IXIX, IXXI, IYIY, IYYI, XIIX, XIXI, YIIY, YIYI} \\
(1 - 2\alpha^2): & \text{ XXYY, YYXX} \\
(\alpha^2 - 1): & \text{ XXZZ, YYZZ, ZZXX, ZZYY}
\end{aligned}$$

Table B.10: Theoretical values for the non-zero correlations of the state $|\Psi_4^+\rangle$.

Experimentally obtained results

IIII	1.000	\pm 0.010	XXXX	0.858	\pm 0.047
IIXX	0.301	\pm 0.026	XXYY	-0.299	\pm 0.045
IYYI	0.299	\pm 0.026	XXZZ	-0.271	\pm 0.045
IIZZ	0.311	\pm 0.026	XYXY	0.582	\pm 0.044
IXIX	-0.590	\pm 0.027	XYYX	0.592	\pm 0.046
IXXI	-0.608	\pm 0.027	XZXZ	0.590	\pm 0.045
IYIY	-0.592	\pm 0.026	XZZX	0.588	\pm 0.045
IYYI	-0.629	\pm 0.027	YXXY	0.535	\pm 0.046
IZIZ	-0.624	\pm 0.027	YXYX	0.569	\pm 0.045
IZZI	-0.626	\pm 0.027	YYXX	-0.231	\pm 0.044
XIIX	-0.627	\pm 0.027	YYYY	0.834	\pm 0.047
XIXI	-0.611	\pm 0.026	YYZZ	-0.329	\pm 0.044
XXII	0.278	\pm 0.026	YZYZ	0.620	\pm 0.046
YIIY	-0.624	\pm 0.027	YZZY	0.568	\pm 0.046
YIYI	-0.609	\pm 0.027	ZXXZ	0.646	\pm 0.047
YYII	0.265	\pm 0.026	ZXZX	0.588	\pm 0.046
ZIIZ	-0.640	\pm 0.027	ZYYZ	0.640	\pm 0.046
ZIZI	-0.610	\pm 0.027	ZYZY	0.587	\pm 0.046
ZZII	0.286	\pm 0.027	ZZXX	-0.281	\pm 0.045
Fidelity:	$F = 0.904 \pm 0.014$		ZZYY	-0.263	\pm 0.045
			ZZZZ	0.973	\pm 0.049

Table B.11: Measured non-zero two-qubit and four-qubit correlations for the state $|\Psi_4^-\rangle$, as well as resultant fidelity.

III	1.000	± 0.015	XXXX	0.754	± 0.071
IHXX	0.337	± 0.039	XXYY	-0.163	± 0.072
IYYI	0.317	± 0.041	XXZZ	-0.365	± 0.076
IIZZ	0.051	± 0.043	XYXY	0.446	± 0.071
IXIX	0.342	± 0.041	XYYX	0.371	± 0.072
IXXI	0.331	± 0.040	XZXZ	-0.368	± 0.068
IYIY	0.374	± 0.041	XZZX	-0.382	± 0.070
IYYI	0.293	± 0.041	YXXY	0.433	± 0.069
IZIZ	-0.532	± 0.041	YXYX	0.468	± 0.072
IZZI	-0.491	± 0.041	YYXX	-0.098	± 0.065
XIIX	0.342	± 0.041	YYYY	0.704	± 0.072
XIXI	0.318	± 0.040	YYZZ	-0.298	± 0.073
XXII	0.405	± 0.042	YZYZ	-0.300	± 0.073
YIIY	0.417	± 0.041	YZZY	-0.321	± 0.071
YIYI	0.306	± 0.042	ZXXZ	-0.540	± 0.070
YYII	0.366	± 0.040	ZXZX	-0.312	± 0.068
ZIIZ	-0.452	± 0.041	ZYYZ	-0.273	± 0.071
ZIZI	-0.451	± 0.040	ZYZY	-0.394	± 0.069
ZZII	0.128	± 0.040	ZZXX	-0.187	± 0.066
Fidelity:	$F = 0.651 \pm 0.019$		ZZYY	-0.303	± 0.067
			ZZZZ	0.786	± 0.072

Table B.12: Measured non-zero two-qubit and four-qubit correlations for the state $|\Psi_4^+\rangle$, as well as resultant fidelity.

B.1.6 Still unknown: $|\Psi'(\sqrt{\frac{1}{6}(3 + \sqrt{3})})\rangle$

Theoretical correlations

$(\frac{1}{6}(3 - \sqrt{3}))$:	IHXX, IYYI, XXII, YYII
$(\frac{1}{\sqrt{3}})$:	IIZZ, ZZII
$(\frac{1}{\sqrt{3}})$:	IXIX, IXXI, IYIY, IYYI, XIIX, XIXI, YIIY, YIYI
$(\frac{1}{6}(-3 - \sqrt{3}))$:	IZIZ, IZZI, ZIIZ, ZIZI
(1):	IIII, XXXX, YYYY, ZZZZ
$(\frac{1}{6}(3 + \sqrt{3}))$:	XYXY, XYYX, YXXY, YXYX
$(-\frac{1}{\sqrt{3}})$:	XZXZ, XZZX, ZYZZ, YZZY, ZXXZ, ZXZX, ZYYZ, ZYZY
$(-\frac{1}{\sqrt{3}})$:	XXYY, YYXX
$(\frac{1}{6}(-3 + \sqrt{3}))$:	XXZZ, YYZZ, ZZXX, ZZYY

Table B.13: Theoretical values for the non-zero correlations of the state $|\Psi'(\sqrt{\frac{1}{6}(3 + \sqrt{3})})\rangle$.

Experimentally obtained results

III	1.000	\pm 0.011	XXXX	0.708	\pm 0.049
IIXX	0.320	\pm 0.028	XXYY	-0.223	\pm 0.049
IYYI	0.288	\pm 0.028	XXZZ	-0.258	\pm 0.047
IIZZ	0.200	\pm 0.029	XYXY	0.488	\pm 0.049
IXIX	0.292	\pm 0.028	XYYX	0.524	\pm 0.048
IXXI	0.343	\pm 0.028	XZXZ	-0.293	\pm 0.049
IYIY	0.268	\pm 0.028	XZZX	-0.336	\pm 0.050
IYYI	0.310	\pm 0.028	YXXY	0.455	\pm 0.049
IZIZ	-0.612	\pm 0.029	YXYX	0.467	\pm 0.049
IZZI	-0.543	\pm 0.029	YYXX	-0.281	\pm 0.049
XIIX	0.345	\pm 0.028	YYYY	0.763	\pm 0.048
XIXI	0.284	\pm 0.028	YYZZ	-0.222	\pm 0.049
XXII	0.312	\pm 0.028	YZYZ	-0.389	\pm 0.046
YIIY	0.328	\pm 0.028	YZZY	-0.289	\pm 0.047
YIYI	0.281	\pm 0.028	ZXXZ	-0.367	\pm 0.049
YYII	0.303	\pm 0.028	ZXZX	-0.336	\pm 0.049
ZIIZ	-0.552	\pm 0.029	ZYYZ	-0.309	\pm 0.048
ZIZI	-0.580	\pm 0.029	ZYZY	-0.357	\pm 0.049
ZZII	0.191	\pm 0.029	ZZXX	-0.179	\pm 0.047
Fidelity:	$F = 0.663 \pm 0.014$		ZZYY	-0.228	\pm 0.048
			ZZZZ	0.879	\pm 0.054

Table B.14: Measured non-zero two-qubit and four-qubit correlations for the state $|\Psi'(\sqrt{\frac{1}{6}(3 + \sqrt{3})})\rangle$, as well as resultant fidelity.

B.1.7 GHZ: $|\Psi'(1)\rangle$

Theoretical correlations

- (1): IIZZ, ZZII
(-1): IZIZ, IZZI, ZIIZ, ZIZI
(1): IIII, XXXX, YYYY, ZZZZ
(1): XYXY, XYYX, YXXY, YXYX
(-1): XXYY, YYXX

Table B.15: Theoretical values for the non-zero correlations of the state $|\Psi'(1)\rangle$.

Experimentally obtained results

III	1.000	\pm	0.010	XXXX	0.786	\pm	0.047
IIZZ	0.656	\pm	0.027	XXYY	-0.616	\pm	0.049
IZIZ	-0.800	\pm	0.027	XYXY	0.756	\pm	0.049
IZZI	-0.810	\pm	0.028	XYYX	0.675	\pm	0.048
ZIIZ	-0.790	\pm	0.028	YXXY	0.641	\pm	0.048
ZIZI	-0.819	\pm	0.028	YXYX	0.672	\pm	0.048
ZZII	0.666	\pm	0.028	YYXX	-0.609	\pm	0.048
Fidelity:	$F = 0.750 \pm 0.013$			YYYY	0.799	\pm	0.048
				ZZZZ	0.902	\pm	0.048

Table B.16: Measured non-zero two-qubit and four-qubit correlations for the state $|\Psi'(1)\rangle$, as well as resultant fidelity.

B.2 For Chap. 3

Measured stabilizer correlations for the observed cluster state described in Sec. 3.3. Ideally the values should be ± 1 .

III	1.000	\pm	0.017	XYXY	0.681	\pm	0.066
IIZZ	0.931	\pm	0.036	XYYX	0.729	\pm	0.062
IZXX	0.638	\pm	0.045	YXXY	0.681	\pm	0.064
IZYY	-0.626	\pm	0.067	YXYX	0.628	\pm	0.066
XXIZ	0.674	\pm	0.044	ZZZZ	0.931	\pm	0.064
XXZI	0.713	\pm	0.044	Fidelity:	$F = 0.741 \pm 0.013$		
YYIZ	-0.690	\pm	0.060				
YYZI	-0.679	\pm	0.043				
ZIXX	0.707	\pm	0.045				
ZIYY	-0.616	\pm	0.067				
ZZII	0.935	\pm	0.037				

Table B.17: Measured stabilizer correlations for the state $|C_4\rangle$, as well as resultant fidelity.

B.3 For Chap. 4

Measured non-zero two-qubit and four-qubit correlations for the symmetric four-qubit Dicke state with two excitations. The measurements were performed with 2 nm interference filters in the alternative setup described in [99].

III	1.000	\pm	0.009	XXXX	0.901	\pm	0.084
IIXX	0.613	\pm	0.027	XXYY	0.315	\pm	0.076
IYY	0.618	\pm	0.026	XXZZ	-0.458	\pm	0.078
IIZZ	-0.337	\pm	0.027	XYXY	0.363	\pm	0.089
IXIX	0.624	\pm	0.027	XYYX	0.345	\pm	0.076
IXXI	0.619	\pm	0.027	XZXZ	-0.594	\pm	0.083
IYIY	0.628	\pm	0.028	XZZX	-0.678	\pm	0.085
IYYI	0.632	\pm	0.027	YXXY	0.364	\pm	0.078
IZIZ	-0.320	\pm	0.026	YXYX	0.377	\pm	0.081
IZZI	-0.320	\pm	0.026	YYXX	0.470	\pm	0.078
XIIX	0.615	\pm	0.027	YYYY	0.860	\pm	0.086
XIXI	0.624	\pm	0.028	YYZZ	-0.598	\pm	0.084
XXII	0.632	\pm	0.027	YZYZ	-0.603	\pm	0.081
YIIY	0.628	\pm	0.026	YZZY	-0.683	\pm	0.079
YIYI	0.622	\pm	0.026	ZXXZ	-0.673	\pm	0.081
YYII	0.648	\pm	0.027	ZXZX	-0.543	\pm	0.083
ZIIZ	-0.337	\pm	0.027	ZYYZ	-0.555	\pm	0.078
ZIZI	-0.305	\pm	0.026	ZYZY	-0.517	\pm	0.079
ZZII	-0.292	\pm	0.026	ZZXX	-0.664	\pm	0.079
Fidelity:	$F = 0.919 \pm 0.019$			ZZYY	-0.468	\pm	0.077
				ZZZZ	0.864	\pm	0.083

Table B.18: Measured non-zero two-qubit and four-qubit correlations for the state $|D_4^{(2)}\rangle$, as well as resultant fidelity.

Acronyms and abbreviations

epr Einstein, Podolski, Rosen

chsh Clauser, Horne, Shimony, Holt

ppt positive partial transpose

locc local operations and classical communication

lu local unitary

slocc stochastic local operations and classical communication

ghz Greenberger, Horne, Zeilinger

cnot controlled not

xor exclusive or

cphase controlled phase

hwp half-wave plate

qwp quarter-wave plate

yvo₄ Yttrium Vanadate

klm Knill, Laflamme, Milburn

loqc linear optics quantum computation

loql linear optics quantum logic

spdc spontaneous parametric down conversion

cw continuous wave

uv ultraviolet

ir infrared

shg second harmonic generation

lbo Lithium Borate

ti:sa Titanium doped Sapphire

nd:yvo₄ Neodymium doped Yttrium Vanadate

bbo β -Barium Borate

apd avalanche photo diodes

pa polarization analysis

pbs polarizing beam splitter

pdbb polarization dependent beam splitter

qpt quantum process tomography

qst quantum state tomography

hom Hong, Ou, Mandel

bs beam splitter

povm positive operator-valued measure

qmg quantum Minority game

ne Nash equilibrium

po Pareto optimal

mabk Mermin-Ardehali-Belinski-Klyshko

lmu Ludwig-Maximilians-University

cern Conseil Européen pour la Recherche Nucléaire

opal Omni Purpose Apparatus for Lep

mpq Max-Planck-Institute of Quantum Optics

Bibliography

- [1] A. Einstein, B. Podolsky and N. Rosen. Can Quantum-Mechanical Description of Physical Reality Be Considered Complete?, *Phys. Rev.* **47**, 777 (1935).
- [2] E. Schrödinger. Die gegenwärtige Situation in der Quantenmechanik, *Naturwissenschaften* **23**, 807 (1935).
- [3] C.H. Bennett and D.P. DiVincenzo. Quantum information and computation, *Nature* **404**, 247 (2000).
- [4] B. Schumacher. Quantum coding, *Phys. Rev. A* **51**, 2738 (1995).
- [5] N. Gisin, G.G. Ribordy, W. Tittel and H. Zbinden. Quantum cryptography, *Rev. Mod. Phys.* **74**, 145 (2002).
- [6] E. Knill, R. Laflamme and G.J. Milburn. A scheme for efficient quantum computation with linear optics, *Nature* **409**, 46 (2001).
- [7] P. Kok, W.J. Munro, K. Nemoto, T.C. Ralph, J.P. Dowling and G.J. Milburn. Linear optical quantum computing with photonic qubits, *Rev. Mod. Phys.* **79**, 135 (2007).
- [8] J.L. O'Brien. Optical Quantum Computing, *Science* **318**, 1567 (2007).
- [9] J.W. Pan, Z.B. Chen, M. Żukowski, H. Weinfurter and A. Zeilinger. Multi-photon entanglement and interferometry, *arXiv:0805.2853 [quant-ph]* (2008).
- [10] C.H. Bennett, G. Brassard, C. Crépeau, R. Jozsa, A. Peres and W.K. Wootters. Teleporting an unknown quantum state via dual classical and Einstein-Podolsky-Rosen channels, *Phys. Rev. Lett.* **70**, 1895 (1993).
- [11] M. Żukowski, A. Zeilinger, M.A. Horne and A.K. Ekert. "Event-ready-detectors" Bell experiment via entanglement swapping, *Phys. Rev. Lett.* **71**, 4287 (1993).
- [12] R. Raussendorf and H.J. Briegel. A One-Way Quantum Computer, *Phys. Rev. Lett.* **86**, 5188 (2001).
- [13] R. Raussendorf, D.E. Browne and H.J. Briegel. Measurement-based quantum computation on cluster states, *Phys. Rev. A* **68**, 022312 (2003).
- [14] T.C. Ralph, N.K. Langford, T.B. Bell and A.G. White. Linear optical controlled-NOT gate in the coincidence basis, *Phys. Rev. A* **65**, 062324 (2002).

- [15] H.F. Hofmann and S. Takeuchi. Quantum phase gate for photonic qubits using only beam splitters and postselection, *Phys. Rev. A* **66**, 024308 (2002).
- [16] J.L. O'Brien, G.J. Pryde, A.G. White, T.C. Ralph and D. Branning. Demonstration of an all-optical quantum controlled-NOT gate, *Nature* **426**, 264 (2003).
- [17] J.L. O'Brien, G.J. Pryde, A. Gilchrist, D.F.V. James, N.K. Langford, T.C. Ralph and A.G. White. Quantum Process Tomography of a Controlled-NOT Gate, *Phys. Rev. Lett.* **93**, 080502 (2004).
- [18] W. Dür, G. Vidal and J.I. Cirac. Three qubits can be entangled in two inequivalent ways, *Phys. Rev. A* **62**, 062314 (2000).
- [19] F. Verstraete, J. Dehaene, B.D. Moor and H. Verschelde. Four qubits can be entangled in nine different ways, *Phys. Rev. A* **65**, 052112 (2002).
- [20] L. Lamata, J. Leon, D. Salgado and E. Solano. Inductive classification of multipartite entanglement under stochastic local operations and classical communication, *Phys. Rev. A* **74**, 052336 (2006).
- [21] L. Lamata, J. Leon, D. Salgado and E. Solano. Inductive entanglement classification of four qubits under stochastic local operations and classical communication, *Phys. Rev. A* **75**, 022318 (2007).
- [22] D.F.V. James, P.G. Kwiat, W.J. Munro and A.G. White. Measurement of qubits, *Phys. Rev. A* **64**, 052312 (2001).
- [23] R. Horodecki, P. Horodecki, M. Horodecki and K. Horodecki. Quantum entanglement, *arXiv:quant-ph/0702225* (2007).
- [24] A. Pais. Einstein and the quantum theory, *Rev. Mod. Phys.* **51**, 863 (1979).
- [25] D.N. Mermin. Is the moon there when nobody looks? Reality and the quantum theory, *Physics Today* **4**, 38 (1985).
- [26] J.S. Bell. On the Einstein-Podolsky-Rosen paradox, *Physics* **1**, 195 (1964).
- [27] J.F. Clauser, M.A. Horne, A. Shimony and R.A. Holt. Proposed Experiment to Test Local Hidden-Variable Theories, *Phys. Rev. Lett.* **23**, 880 (1969).
- [28] S.J. Freedman and J.F. Clauser. Experimental Test of Local Hidden-Variable Theories, *Phys. Rev. Lett.* **28**, 938 (1972).
- [29] A. Aspect, P. Grangier and G. Roger. Experimental Tests of Realistic Local Theories via Bell's Theorem, *Phys. Rev. Lett.* **47**, 460 (1981).
- [30] G. Weihs, T. Jennewein, C. Simon, H. Weinfurter and A. Zeilinger. Violation of Bell's Inequality under Strict Einstein Locality Conditions, *Phys. Rev. Lett.* **81**, 5039 (1998).
- [31] A. Aspect. Bell's inequality test: more ideal than ever, *Nature* **398**, 189 (1999).
- [32] M.A. Rowe, D. Kielpinski, V. Meyer, C.A. Sackett, W.M. Itano, C. Monroe and D.J. Wineland. Experimental violation of a Bell's inequality with efficient detection, *Nature* **409**, 791 (2001).

- [33] S. Gröblacher, T. Paterek, R. Kaltenbaek, Č. Brukner, M. Żukowski, M. Aspelmeyer and A. Zeilinger. An experimental test of non-local realism, *Nature* **446**, 871 (2007).
- [34] A. Holevo. Bounds for the quantity of information transmitted by a quantum communication channel., *Problemy Peredachi Informatsii* **9(3)**, 3 (1973).
- [35] M.A. Nielsen and I.L. Chuang: *Quantum Computation and Quantum Information*, Cambridge Univ. Press, 2000.
- [36] D. Deutsch. Quantum theory, the church-turing principle and the universal quantum computer, *Proceedings of the Royal Society of London Series A* **400**, 97 (1985).
- [37] D. Deutsch and R. Jozsa. Rapid Solution of Problems by Quantum Computation, *Proceedings of the Royal Society of London Series A* **439**, 553 (1992).
- [38] S.L. Braunstein, A. Mann and M. Revzen. Maximal violation of Bell inequalities for mixed states, *Phys. Rev. Lett.* **68**, 3259 (1992).
- [39] A. Zeilinger. Quantum teleportation and the non-locality of information, *Royal Society of London Philosophical Transactions Series A* **355(1733)**, 2401 (1997).
- [40] R. Horodecki, P. Horodecki and M. Horodecki. Violating Bell inequality by mixed states: necessary and sufficient condition, *Phys. Lett. A* **200**, 340 (1995).
- [41] Č. Brukner and A. Zeilinger. Information and fundamental elements of the structure of quantum theory, *arXiv:quant-ph/0212084* (2002).
- [42] A. Peres. Separability Criterion for Density Matrices, *Phys. Rev. Lett.* **77**, 1413 (1996).
- [43] M. Horodecki, P. Horodecki and R. Horodecki. Separability of mixed states: necessary and sufficient conditions, *Phys. Lett. A* **223**, 1 (1996).
- [44] A. Sanpera, R. Tarrach and G. Vidal. Quantum separability, time reversal and canonical decompositions, *arXiv:quant-ph/9707041* (1997).
- [45] V. Vedral and M.B. Plenio. Entanglement measures and purification procedures, *Phys. Rev. A* **57**, 1619 (1998).
- [46] M. Horodecki, P. Horodecki and R. Horodecki. Limits for Entanglement Measures, *Phys. Rev. Lett.* **84**, 2014 (2000).
- [47] G. Vidal. Entanglement monotones, *J. Mod. Optic.* **47**, 355 (2000).
- [48] M. Horodecki, P. Horodecki and R. Horodecki. Mixed-State Entanglement and Distillation: Is there a “Bound” Entanglement in Nature?, *Phys. Rev. Lett.* **80**, 5239 (1998).
- [49] P. Horodecki. Separability criterion and inseparable mixed states with positive partial transposition, *Phys. Lett. A* **232**, 333 (1997).
- [50] C.H. Bennett, H.J. Bernstein, S. Popescu and B. Schumacher. Concentrating partial entanglement by local operations, *Phys. Rev. A* **53**, 2046 (1996).
- [51] C.H. Bennett, D.P. DiVincenzo, J.A. Smolin and W.K. Wootters. Mixed-state entanglement and quantum error correction, *Phys. Rev. A* **54**, 3824 (1996).

- [52] M.J. Donald, M. Horodecki and O. Rudolph. The uniqueness theorem for entanglement measures, *J. Math. Phys.* **43**, 4252 (2002).
- [53] S. Hill and W.K. Wootters. Entanglement of a Pair of Quantum Bits, *Phys. Rev. Lett.* **78**, 5022 (1997).
- [54] W.K. Wootters. Entanglement of Formation of an Arbitrary State of Two Qubits, *Phys. Rev. Lett.* **80**, 2245 (1998).
- [55] C. Altafini and T.F. Havel. Reflection symmetries for multiqubit density operators, *J. Math. Phys.* **47**, 032104 (2006).
- [56] G. Vidal and R.F. Werner. Computable measure of entanglement, *Phys. Rev. A* **65**, 032314 (2002).
- [57] M.B. Plenio. Logarithmic Negativity: A Full Entanglement Monotone That is not Convex, *Phys. Rev. Lett.* **95**, 090503 (2005).
- [58] R.F. Werner. Quantum states with Einstein-Podolsky-Rosen correlations admitting a hidden-variable model, *Phys. Rev. A* **40**, 4277 (1989).
- [59] C. Carathéodory. Über den Variabilitätsbereich der Koeffizienten von Potenzreihen, die gegebene Werte nicht annehmen., *Math. Ann.* **64**, 95 (1907).
- [60] C.H. Bennett, S. Popescu, D. Rohrlich, J.A. Smolin and A.V. Thapliyal. Exact and asymptotic measures of multipartite pure-state entanglement, *Phys. Rev. A* **63**, 012307 (2001).
- [61] N. Linden and S. Popescu. On Multi-Particle Entanglement, *Fortschr. Phys.* **46**, 567 (1998).
- [62] D. Greenberger, M.A. Horne and A. Zeilinger: *Going beyond Bell's Theorem*, Kluwer Academic, Dordrecht, 1989.
- [63] A. Acin, D. Bruss, M. Lewenstein and A. Sanpera. Classification of Mixed Three-Qubit States, *Phys. Rev. Lett.* **87**, 040401 (2001).
- [64] V. Coffman, J. Kundu and W.K. Wootters. Distributed entanglement, *Phys. Rev. A* **61**, 052306 (2000).
- [65] R. Lohmayer, A. Osterloh, J. Siewert and A. Uhlmann. Entangled Three-Qubit States without Concurrence and Three-Tangle, *Phys. Rev. Lett.* **97**, 260502 (2006).
- [66] C. Eltschka, A. Osterloh, J. Siewert and A. Uhlmann. Three-tangle for mixtures of generalized GHZ and generalized W states, *arXiv:0711.4477 [quant-ph]* (2007).
- [67] B.M. Terhal. Bell inequalities and the separability criterion, *Phys. Lett. A* **271**, 319 (2000).
- [68] M. Lewenstein, B. Kraus, J.I. Cirac and P. Horodecki. Optimization of entanglement witnesses, *Phys. Rev. A* **62**, 052310 (2000).

- [69] M. Lewenstein, B. Kraus, P. Horodecki and J.I. Cirac. Characterization of separable states and entanglement witnesses, *Phys. Rev. A* **63**, 044304 (2001).
- [70] M. Bourennane, M. Eibl, C. Kurtsiefer, S. Gaertner, H. Weinfurter, O. Gühne, P. Hyllus, D. Bruss, M. Lewenstein and A. Sanpera. Experimental Detection of Multipartite Entanglement using Witness Operators, *Phys. Rev. Lett.* **92**, 087902 (2004).
- [71] E. Strømmer. Positive linear maps of operator algebras, *Acta Mathematica* **110**, 233 (1963).
- [72] S.L. Woronowicz. Positive maps of low dimensional matrix algebras, *Rep. Mat. Phys.* **10**, 165 (1976).
- [73] M. Choi. Positive linear maps, *Proc. Sympos. Pure Math.* **38**, 583 (1982).
- [74] A. Jamiołkowski. Linear transformations which preserve trace and positive semidefiniteness of operators., *Rep. Math. Phys.* **3**, 275 (1972).
- [75] O. Gühne, P. Hyllus, D. Bruß, A. Ekert, M. Lewenstein, C. Macchiavello and A. Sanpera. Detection of entanglement with few local measurements, *Phys. Rev. A* **66**, 062305 (2002).
- [76] O. Gühne, P. Hyllus, D. Bruß, A. Ekert, M. Lewenstein, C. Macchiavello and A. Sanpera. Experimental detection of entanglement via witness operators and local measurements, *J. Mod. Optic.* **50**, 1079 (2003).
- [77] O. Gühne and N. Lütkenhaus. Nonlinear entanglement witnesses, covariance matrices and the geometry of separable states, *Journal of Physics: Conference Series* **67**, 012004 (11pp) (2007).
- [78] J. Eisert, F.G.S.L. Brandão and K.M.R. Audenaert. Quantitative entanglement witnesses, *New J. Phys.* **9**, 46 (2007).
- [79] D. Deutsch. Quantum Computational Networks, *Proceedings of the Royal Society of London Series A* **425**, 73 (1989).
- [80] T. Sleator and H. Weinfurter. Realizable Universal Quantum Logic Gates, *Phys. Rev. Lett.* **74**, 4087 (1995).
- [81] A. Barenco, C.H. Bennett, R. Cleve, D.P. DiVincenzo, N. Margolus, P. Shor, T. Sleator, J.A. Smolin and H. Weinfurter. Elementary gates for quantum computation, *Phys. Rev. A* **52**, 3457 (1995).
- [82] M. Žnidarič, O. Giraud and B. Georgeot. Optimal number of controlled-NOT gates to generate a three-qubit state, *Phys. Rev. A* **77**, 032320 (2008).
- [83] G.C. Guo and Y.S. Zhang. Scheme for preparation of the W state via cavity quantum electrodynamics, *Phys. Rev. A* **65**, 054302 (2002).
- [84] D.P. DiVincenzo. The Physical Implementation of Quantum Computation, *Fortschr. Phys.* **48**, 771 (2000).

- [85] S. Braunstein and H.K. Lo. Experimental Proposals for Quantum Computation, *Fortschr. Phys. (Special Issue)* **48**, 769 (2000).
- [86] V.B. Berestetskii, E.M. Lifshitz and L.P. Pitaevskii: *Quantum Electrodynamics*, , volume 4 Course of Theoretical Physics 2. edition. Pergamon International Library, 1982.
- [87] B.E.A. Saleh and M.C. Teich: *Fundamentals of Photonics*, John Wiley & Sons, Inc., 1991.
- [88] D.S. Kliger, J.W. Lewis and C.E. Randall: *Polarized Light in Optics and Spectroscopy*, Academic Press Limited, 1990.
- [89] C. Schmid: *Kompakte Quelle verschränkter Photonen und Anwendungen in der Quantenkommunikation*, Ludwig-Maximilians-Universität München, Diplomarbeit, 2004.
- [90] M. Reck, A. Zeilinger, H.J. Bernstein and P. Bertani. Experimental realization of any discrete unitary operator, *Phys. Rev. Lett.* **73**, 58 (1994).
- [91] N. Lütkenhaus, J. Calsamiglia and K.A. Suominen. Bell measurements for teleportation, *Phys. Rev. A* **59**, 3295 (1999).
- [92] D. Bruß and G. Leuchs, editors *Lectures on Quantum Information*, Wiley-VCH, 2006.
- [93] L. Mandel and E. Wolf: *Optical Coherence and Quantum Optics*, Cambridge University Press, 1995.
- [94] D.N. Klyshko: *Photons and Nonlinear Optics*, Gordon & Breach Science Publishers Ltd, 1988.
- [95] P.G. Kwiat, K. Mattle, H. Weinfurter, A. Zeilinger, A.V. Sergienko and Y. Shih. New high-intensity source of polarization-entangled photon pairs, *Phys. Rev. Lett.* **75**, 4337 (1995).
- [96] P.G. Kwiat, P.H. Eberhard, A.M. Steinberg and R.Y. Chiao. Proposal for a loophole-free Bell inequality experiment, *Phys. Rev. A* **49**, 3209 (1994).
- [97] Y.H. Shih and A.V. Sergienko. Observation of quantum beating in a simple beam-splitting experiment: Two-particle entanglement in spin and space-time, *Phys. Rev. A* **50**, 2564 (1994).
- [98] T.B. Pittman, Y.H. Shih, A.V. Sergienko and M.H. Rubin. Experimental tests of Bell's inequalities based on space-time and spin variables, *Phys. Rev. A* **51**, 3495 (1995).
- [99] N. Kiesel, C. Schmid, G. Tóth, E. Solano and H. Weinfurter. Experimental Observation of Four-Photon Entangled Dicke State with High Fidelity, *Phys. Rev. Lett.* **98**, 063604 (2007).
- [100] H. Weinfurter and M. Żukowski. Four-photon entanglement from down-conversion, *Phys. Rev. A* **64**, 010102 (2001).
- [101] M. Żukowski, A. Zeilinger and H. Weinfurter. Entangling Photons Radiated by Independent Pulsed Sources, *Annals of the New York Academy of Sciences* **755**, 91 (1995).

- [102] M. Halder, A. Beveratos, N. Gisin, V. Scarani, C. Simon and H. Zbinden. Entangling independent photons by time measurement, *Nat. Phys.* **3**, 692 (2007).
- [103] R. Ursin, F. Tiefenbacher, T. Schmitt-Manderbach, H. Weier, T. Scheidl, M. Lindenthal, B. Blauensteiner, T. Jennewein, J. Perdigues, P. Trojek, B. Omer, M. Fürst, M. Meyenburg, J. Rarity, Z. Sodnik, C. Barbieri, H. Weinfurter and A. Zeilinger. Entanglement-based quantum communication over 144 km, *Nat. Phys.* **3**, 481 (2007).
- [104] G. Di Giuseppe, L. Haiberger, F. De Martini and A.V. Sergienko. Quantum interference and indistinguishability with femtosecond pulses, *Phys. Rev. A* **56**, R21 (1997).
- [105] C. Kurtsiefer, M. Oberparleiter and H. Weinfurter. High-efficiency entangled photon pair collection in type-II parametric fluorescence, *Phys. Rev. A* **64**, 023802 (2001).
- [106] M.H. Rubin. Transverse correlation in optical spontaneous parametric down-conversion, *Phys. Rev. A* **54**, 5349 (1996).
- [107] W.P. Grice and I.A. Walmsley. Spectral information and distinguishability in type-II down-conversion with a broadband pump, *Phys. Rev. A* **56**, 1627 (1997).
- [108] T.E. Keller and M.H. Rubin. Theory of two-photon entanglement for spontaneous parametric down-conversion driven by a narrow pump pulse, *Phys. Rev. A* **56**, 1534 (1997).
- [109] W.P. Grice, R. Erdmann, I.A. Walmsley and D. Branning. Spectral distinguishability in ultrafast parametric down-conversion, *Phys. Rev. A* **57**, R2289 (1998).
- [110] M. Atatüre, A.V. Sergienko, B.M. Jost, B.E.A. Saleh and M.C. Teich. Partial Distinguishability in Femtosecond Optical Spontaneous Parametric Down-Conversion, *Phys. Rev. Lett.* **83**, 1323 (1999).
- [111] M. Eibl, S. Gaertner, M. Bourennane, C. Kurtsiefer, M. Żukowski and H. Weinfurter. Experimental Observation of Four-Photon Entanglement from Parametric Down-Conversion, *Phys. Rev. Lett.* **90**, 200403 (2003).
- [112] S. Gaertner, M. Bourennane, M. Eibl, C. Kurtsiefer and H. Weinfurter. High-fidelity source of four-photon entanglement, *Appl. Phys. B: Lasers Opt.* **77**, 803 (2003).
- [113] M. Muraio, D. Jonathan, M.B. Plenio and V. Vedral. Quantum telecloning and multi-particle entanglement, *Phys. Rev. A* **59**, 156 (1999).
- [114] M. Bourennane, M. Eibl, S. Gaertner, C. Kurtsiefer, A. Cabello and H. Weinfurter. Decoherence-Free Quantum Information Processing with Four-Photon Entangled States, *Phys. Rev. Lett.* **92**, 107901 (2004).
- [115] S. Gaertner, C. Kurtsiefer, M. Bourennane and H. Weinfurter. Experimental Demonstration of Four-Party Quantum Secret Sharing, *Phys. Rev. Lett.* **98**, 020503 (2007).
- [116] S. Gaertner, H. Weinfurter and C. Kurtsiefer. Fast and compact multichannel photon coincidence unit for quantum information processing, *Review of Scientific Instruments* **76**, 123108 (2005).
- [117] N. Kiesel, C. Schmid, U. Weber, R. Ursin and H. Weinfurter. Linear Optics Controlled-Phase Gate Made Simple, *Phys. Rev. Lett.* **95**, 210505 (2005).

- [118] C. Schmid, N. Kiesel, U. Weber, R. Ursin and H. Weinfurter. Experimental analysis of a simple linear optics phase gate, *International Journal of Quantum Information (IJQI)* **5**, 235 (2007).
- [119] N.K. Langford, T.J. Weinhold, R. Prevedel, K.J. Resch, A. Gilchrist, J.L. O'Brien, G.J. Pryde and A.G. White. Demonstration of a Simple Entangling Optical Gate and Its Use in Bell-State Analysis, *Phys. Rev. Lett.* **95**, 210504 (2005).
- [120] R. Okamoto, H.F. Hofmann, S. Takeuchi and K. Sasaki. Demonstration of an Optical Quantum Controlled-NOT Gate without Path Interference, *Phys. Rev. Lett.* **95**, 210506 (2005).
- [121] N. Kiesel: *Experiments on Multiphoton Entanglement*, Ludwig-Maximilians-Universität München, Dissertation, 2007.
- [122] W. Wieczorek, C. Schmid, N. Kiesel, R. Pohlner, O. Gühne and H. Weinfurter. Experimental observation of an entire family of four-photon entangled states, *Phys. Rev. Lett.* **101**, 010503 (2008).
- [123] I.L. Chuang and M.A. Nielsen. Prescription for experimental determination of the dynamics of a quantum black box, *J. Mod. Optic.* **44**, 2455 (1997).
- [124] J.F. Poyatos, J.I. Cirac and P. Zoller. Complete Characterization of a Quantum Process: The Two-Bit Quantum Gate, *Phys. Rev. Lett.* **78**, 390 (1997).
- [125] M.W. Mitchell, C.W. Ellenor, S. Schneider and A.M. Steinberg. Diagnosis, Prescription, and Prognosis of a Bell-State Filter by Quantum Process Tomography, *Phys. Rev. Lett.* **91**, 120402 (2003).
- [126] J. Řeháček and M.G.A. Paris, editors *Lecture Notes in Physics: Quantum State Estimation*, Springer, 2004.
- [127] C.K. Hong, Z.Y. Ou and L. Mandel. Measurement of subpicosecond time intervals between two photons by interference, *Phys. Rev. Lett.* **59**, 2044 (1987).
- [128] U. Weber: *Das optische Phasengatter und Beobachtung eines vier-Photonen Cluster-Zustands*, Ludwig-Maximilians-Universität München, Diplomarbeit, 2005.
- [129] C. Schmid, N. Kiesel, W. Laskowski, E. Solano, G. Tóth, M. Zukowski and W. H.: *The Entanglement of the Symmetric Four-Photon Dicke State*, In *Quantum Communication and Security, Proceedings of the NATO Advanced Research Workshop on Quantum Communication and Security*, edited by M. Żukowski, S. Kilin and J. Kowalik. IOS Press (ISBN 978-1-58603-749-9) (Sep. 2007) page 113.
- [130] A. Uhlmann. The "transition probability" in the state space of a *-algebra, *Rep. Mat. Phys.* **9**, 273 (1976).
- [131] J.W. Pan, D. Bouwmeester, H. Weinfurter and A. Zeilinger. Experimental Entanglement Swapping: Entangling Photons That Never Interacted, *Phys. Rev. Lett.* **80**, 3891 (1998).
- [132] R.H. Dicke. Coherence in Spontaneous Radiation Processes, *Phys. Rev.* **93**, 99 (1954).

- [133] J.K. Stockton, J.M. Geremia, A.C. Doherty and H. Mabuchi. Characterizing the entanglement of symmetric many-particle spin-(1/2) systems, *Phys. Rev. A* **67**, 022112 (2003).
- [134] H. Häffner, W. Hänsel, C.F. Roos, J. Benhelm, D. Chek-al kar, M. Chwalla, T. Körber, U.D. Rapol, M. Riebe, P.O. Schmidt, C. Becher, O. Gühne, W. Dür and R. Blatt. Scalable multiparticle entanglement of trapped ions, *Nature* **438**, 643 (2005).
- [135] C. Schmid, N. Kiesel, W. Wieczorek, R. Pohlner and H. Weinfurter: *Multiphoton entanglement engineering via projective measurements*, volume 6780. SPIE (2007) page 67800E.
- [136] W. Wieczorek, C. Schmid, N. Kiesel and H. Weinfurter. Experimental multi-photon entanglement engineering via projective measurements, *To be published* .
- [137] Z. Zhao, Y.A. Chen, A.N. Zhang, T. Yang, H.J. Briegel and J.W. Pan. Experimental demonstration of five-photon entanglement and open-destination teleportation, *Nature* **430**, 54 (2004).
- [138] J. Shimamura, S.K. Ozdemir, F. Morikoshi and N. Imoto. Entangled states that cannot reproduce original classical games in their quantum version, *Phys. Lett. A* **328**, 20 (2004).
- [139] G. Tóth. Detection of multipartite entanglement in the vicinity of symmetric Dicke states, *J. Opt. Soc. Am. B* **24**, 275 (2007).
- [140] C. Schmid, P. Trojek, S. Gaertner, M. Bourennane, C. Kurtsiefer, M. Żukowski and H. Weinfurter. Experimental quantum secret sharing, *Fortschr. Phys.* **54**, 831 (2006).
- [141] C.A. Sackett, D. Kielpinski, B.E. King, C. Langer, V. Meyer, C.J. Myatt, M. Rowe, Q.A. Turchette, W.M. Itano, D.J. Wineland and C. Monroe. Experimental entanglement of four particles, *Nature* **404**, 256 (2000).
- [142] J.W. Pan, M. Daniell, S. Gasparoni, G. Weihs and A. Zeilinger. Experimental Demonstration of Four-Photon Entanglement and High-Fidelity Teleportation, *Phys. Rev. Lett.* **86**, 4435 (2001).
- [143] M. Hillery, V. Bužek and A. Berthiaume. Quantum secret sharing, *Phys. Rev. A* **59**, 1829 (1999).
- [144] J.K. Pachos, W. Wieczorek, C. Schmid, N. Kiesel, R. Pohlner and H. Weinfurter. Revealing anyonic statistics with multiphoton entanglement, *arXiv:0710.0895 [quant-ph]* (2007).
- [145] G. Tóth and O. Gühne. Detecting Genuine Multipartite Entanglement with Two Local Measurements, *Phys. Rev. Lett.* **94**, 060501 (2005).
- [146] C. Kurtsiefer: *Private communications*, . (2007).
- [147] D. Gottesman and I.L. Chuang. Demonstrating the viability of universal quantum computation using teleportation and single-qubit operations, *Nature* **402**, 390 (1999).

- [148] H.J. Briegel, W. Dür, J.I. Cirac and P. Zoller. Quantum Repeaters: The Role of Imperfect Local Operations in Quantum Communication, *Phys. Rev. Lett.* **81**, 5932 (1998).
- [149] W. Dür, H.J. Briegel, J.I. Cirac and P. Zoller. Quantum repeaters based on entanglement purification, *Phys. Rev. A* **59**, 169 (1999).
- [150] L.M. Duan, M.D. Lukin, J.I. Cirac and P. Zoller. Long-distance quantum communication with atomic ensembles and linear optics, *Nature* **414**, 413 (2001).
- [151] E. Waks, A. Zeevi and Y. Yamamoto. Security of quantum key distribution with entangled photons against individual attacks, *Phys. Rev. A* **65**, 052310 (2002).
- [152] W.K. Wootters and W.H. Zurek. A single quantum cannot be cloned, *Nature* **299**, 802 (1982).
- [153] D. Dieks. Communication by EPR devices, *Phys. Lett. A* **92**, 271 (1982).
- [154] M.A. Nielsen, E. Knill and R. Laflamme. Complete quantum teleportation using nuclear magnetic resonance, *Nature* **396**, 52 (1998).
- [155] A. Furusawa, J.L. Sørensen, S.L. Braunstein, C.A. Fuchs, H.J. Kimble and E.S. Polzik. Unconditional Quantum Teleportation, *Science* **282**, 706 (1998).
- [156] M. Riebe, H. Häffner, C.F. Roos, W. Hänsel, J. Benhelm, G.P.T. Lancaster, T.W. Körber, C. Becher, F. Schmidt-Kaler, D.F.V. James and R. Blatt. Deterministic quantum teleportation with atoms, *Nature* **429**, 734 (2004).
- [157] M.D. Barrett, J. Chiaverini, T. Schaetz, J. Britton, W.M. Itano, J.D. Jost, E. Knill, C. Langer, D. Leibfried, R. Ozeri and D.J. Wineland. Deterministic quantum teleportation of atomic qubits, *Nature* **429**, 737 (2004).
- [158] C. Schuck, G. Huber, C. Kurtsiefer and H. Weinfurter. Complete Deterministic Linear Optics Bell State Analysis, *Phys. Rev. Lett.* **96**, 190501 (2006).
- [159] D. Bouwmeester, J.W. Pan, K. Mattle, M. Eibl, H. Weinfurter and A. Zeilinger. Experimental Quantum Teleportation, *Nature* **390**, 575 (1997).
- [160] H. Weinfurter. Experimental Bell-state analysis, *Europhys. Lett.* **25**, 559 (1994).
- [161] S.L. Braunstein and A. Mann. Measurement of the Bell operator and quantum teleportation, *Phys. Rev. A* **51**, R1727 (1995).
- [162] J.A.W. van Houwelingen, A. Beveratos, N. Brunner, N. Gisin and H. Zbinden. Experimental quantum teleportation with a three-Bell-state analyzer, *Phys. Rev. A* **74**, 022303 (2006).
- [163] J.A.W. van Houwelingen, N. Brunner, A. Beveratos, H. Zbinden and N. Gisin. Quantum Teleportation with a Three-Bell-State Analyzer, *Phys. Rev. Lett.* **96**, 130502 (2006).
- [164] Y.H. Kim, S.P. Kulik and Y. Shih. Quantum Teleportation of a Polarization State with a Complete Bell State Measurement, *Phys. Rev. Lett.* **86**, 1370 (2001).

- [165] C.K. Hong and L. Mandel. Experimental realization of a localized one-photon state, *Phys. Rev. Lett.* **56**, 58 (1986).
- [166] A.I. Lvovsky, H. Hansen, T. Aichele, O. Benson, J. Mlynek and S. Schiller. Quantum State Reconstruction of the Single-Photon Fock State, *Phys. Rev. Lett.* **87**, 050402 (2001).
- [167] T. Pittman, B. Jacobs and J. Franson. Heralding single photons from pulsed parametric down-conversion, *Opt. Commun.* **246**, 545 (2005).
- [168] S.L. Braunstein, C.A. Fuchs and H.J. Kimble. Criteria for continuous-variable quantum teleportation, *J. Mod. Optic.* **47**, 267 (2000).
- [169] C.H. Bennett, G. Brassard, S. Popescu, B. Schumacher, J.A. Smolin and W.K. Wootters. Purification of Noisy Entanglement and Faithful Teleportation via Noisy Channels, *Phys. Rev. Lett.* **76**, 722 (1996).
- [170] L. Vaidman and N. Yoran. Methods for reliable teleportation, *Phys. Rev. A* **59**, 116 (1999).
- [171] P. Horodecki. Measuring Quantum Entanglement without Prior State Reconstruction, *Phys. Rev. Lett.* **90**, 167901 (2003).
- [172] H.A. Carteret. Noiseless Quantum Circuits for the Peres Separability Criterion, *Phys. Rev. Lett.* **94**, 040502 (2005).
- [173] F. Mintert, M. Kus and A. Buchleitner. Concurrence of mixed multipartite quantum states, *Phys. Rev. Lett.* **95**, 260502 (2005).
- [174] T.A. Brun. Measuring polynomial functions of states, *Quantum Information & Computation* **4**, 401 (2004).
- [175] S.P. Walborn, P.H. Souto Ribeiro, L. Davidovich, F. Mintert and A. Buchleitner. Experimental determination of entanglement with a single measurement, *Nature* **440**, 1022 (2006).
- [176] F. Mintert and A. Buchleitner. Observable Entanglement Measure for Mixed Quantum States, *Phys. Rev. Lett.* **98**, 140505 (2007).
- [177] P. Rungta, V. Bužek, C.M. Caves, M. Hillery and G.J. Milburn. Universal state inversion and concurrence in arbitrary dimensions, *Phys. Rev. A* **64**, 042315 (2001).
- [178] N. Kiesel, C. Schmid, U. Weber, G. Toth, O. Guhne, R. Ursin and H. Weinfurter. Experimental Analysis of a Four-Qubit Photon Cluster State, *Phys. Rev. Lett.* **95**, 210502 (2005).
- [179] M.A. Nielsen. Quantum computation by measurement and quantum memory, *Phys. Lett. A* **308**, 96 (2003).
- [180] P. Walther, K.J. Resch, T. Rudolph, E. Schenck, H. Weinfurter, V. Vedral, M. Aspelmeyer and A. Zeilinger. Experimental one-way quantum computing, *Nature* **434**, 169 (2005).

- [181] R. Prevedel, P. Walther, F. Tiefenbacher, P. Bohi, R. Kaltenbaek, T. Jennewein and A. Zeilinger. High-speed linear optics quantum computing using active feed-forward, *Nature* **445**, 65 (2007).
- [182] C.Y. Lu, X.Q. Zhou, O. Gühne, W.B. Gao, J. Zhang, Z.S. Yuan, A. Goebel, T. Yang and J.W. Pan. Experimental entanglement of six photons in graph states, *Nat. Phys.* **3**, 91 (2007).
- [183] M.S. Tame, R. Prevedel, M. Paternostro, P. Böhi, M.S. Kim and A. Zeilinger. Experimental Realization of Deutsch's Algorithm in a One-Way Quantum Computer, *Phys. Rev. Lett.* **98**, 140501 (2007).
- [184] C. Schmid, N. Kiesel, W. Wieczorek and H. Weinfurter. The entanglement of the four-photon cluster state, *New J. Phys.* **9**, 236 (2007).
- [185] R. Raussendorf: *Measurement-based quantum computation with cluster states*, LMU München: Fakultät für Physik, Dissertation, 2003.
- [186] D. Gottesman. Class of quantum error-correcting codes saturating the quantum Hamming bound, *Phys. Rev. A* **54**, 1862 (1996).
- [187] C. Schmid, N. Kiesel, W. Laskowski, W. Wieczorek, M. Żukowski and H. Weinfurter. Discriminating Multipartite Entangled States, *Phys. Rev. Lett.* **100**, 200407 (2008).
- [188] B.M. Terhal and P. Horodecki. Schmidt number for density matrices, *Phys. Rev. A* **61**, 040301 (2000).
- [189] N. Gisin. Bell's inequality holds for all non-product states, *Phys. Lett. A* **154**, 201 (1991).
- [190] D.N. Mermin. Quantum mysteries revisited, *Am. J. Phys.* **58**, 731 (1990).
- [191] A.V. Belinskii and D.N. Klyshko. Interference of light and Bell's theorem, *Phys.-Usp.* **36**, 653 (1993).
- [192] W. Laskowski, T. Paterek, M. Żukowski and Č. Brukner. Tight Multipartite Bell's Inequalities Involving Many Measurement Settings, *Phys. Rev. Lett.* **93**, 200401 (2004).
- [193] K. Nagata, W. Laskowski, M. Wieśniak and M. Żukowski. Rotational Invariance as an Additional Constraint on Local Realism, *Phys. Rev. Lett.* **93**, 230403 (2004).
- [194] R.F. Werner and M.M. Wolf. All-multipartite Bell-correlation inequalities for two dichotomic observables per site, *Phys. Rev. A* **64**, 032112 (2001).
- [195] M. Żukowski and Č. Brukner. Bell's Theorem for General N-Qubit States, *Phys. Rev. Lett.* **88**, 210401 (2002).
- [196] V. Scarani, A. Acin, E. Schenck and M. Aspelmeyer. Nonlocality of cluster states of qubits, *Phys. Rev. A* **71**, 042325 (2005).
- [197] O. Gühne, G. Tóth, P. Hyllus and H.J. Briegel. Bell Inequalities for Graph States, *Phys. Rev. Lett.* **95**, 120405 (2005).

- [198] G. Tóth, O. Gühne and H.J. Briegel. Two-setting Bell inequalities for graph states, *Phys. Rev. A* **73**, 022303 (2006).
- [199] R.F. Werner and M.M. Wolf. Bell's inequalities for states with positive partial transpose, *Phys. Rev. A* **61**, 062102 (2000).
- [200] A. Acin, N. Gisin and L. Masanes. From Bell's Theorem to Secure Quantum Key Distribution, *Phys. Rev. Lett.* **97**, 120405 (2006).
- [201] J. Lau, S. Gaertner, N. Kiesel, M. Bourennane and H. Weinfurter. Experimental Quantum Telecloning, *in preparation* (2007).
- [202] D.M. Greenberger, M.A. Horne, A. Shimony and A. Zeilinger. Bell's theorem without inequalities, *Am. J. Phys.* **58**, 1131 (1990).
- [203] G. Tóth and O. Gühne. Entanglement detection in the stabilizer formalism, *Phys. Rev. A* **72**, 022340 (2005).
- [204] O. Gühne, C.Y. Lu, W.B. Gao and J.W. Pan. Toolbox for entanglement detection and fidelity estimation, *Phys. Rev. A* **76**, 030305 (2007).
- [205] D.A. Meyer. Quantum Strategies, *Phys. Rev. Lett.* **82**, 1052 (1999).
- [206] J.F. Nash. Equilibrium Points in n-Person Games, *Proceedings of the National Academy of Sciences* **36**, 48 (1950).
- [207] J. Eisert, M. Wilkens and M. Lewenstein. Quantum Games and Quantum Strategies, *Phys. Rev. Lett.* **83**, 3077 (1999).
- [208] S.C. Benjamin and P.M. Hayden. Comment on "Quantum Games and Quantum Strategies", *Phys. Rev. Lett.* **87**, 069801 (2001).
- [209] J. Eisert, M. Wilkens and M. Lewenstein. Eisert, Wilkens, and Lewenstein Reply:, *Phys. Rev. Lett.* **87**, 069802 (2001).
- [210] J. Du, H. Li, X. Xu, M. Shi, J. Wu, X. Zhou and R. Han. Experimental Realization of Quantum Games on a Quantum Computer, *Phys. Rev. Lett.* **88**, 137902 (2002).
- [211] R. Prevedel, A. Stefanov, P. Walther and A. Zeilinger. Experimental realization of a quantum game on a one-way quantum computer, *New J. Phys.* **9**, 205 (2007).
- [212] D. Challet and Y.C. Zhang. Emergence of cooperation and organization in an evolutionary game, *Physica A: Statistical and Theoretical Physics* **246**, 407 (1997).
- [213] N.F. Johnson, S. Jarvis, R. Jonson, P. Cheung, Y.R. Kwong and P.M. Hui. Volatility and agent adaptability in a self-organizing market, *Physica A: Statistical Mechanics and its Applications* **258**, 230 (1998).
- [214] R. Savit, R. Manuca and R. Riolo. Adaptive Competition, Market Efficiency, and Phase Transitions, *Phys. Rev. Lett.* **82**, 2203 (1999).
- [215] D. Challet, M. Marsili and Y.C. Zhang. Modeling market mechanism with minority game, *Physica A: Statistical Mechanics and its Applications* **276**, 284 (2000).

- [216] S.C. Benjamin and P.M. Hayden. Multiplayer quantum games, *Phys. Rev. A* **64**, 030301 (2001).
- [217] Q. Chen, Y. Wang, J.T. Liu and K.L. Wang. N-player quantum minority game, *Phys. Lett. A* **327**, 98 (2004).
- [218] A.P. Flitney and L.C.L. Hollenberg: *Quantum minority game utilizing various forms of entanglement*, volume 6802. SPIE (2007) page 680209.
- [219] A.P. Flitney and A.D. Greentree. Coalitions in the quantum Minority game: Classical cheats and quantum bullies, *Phys. Lett. A* **362**, 132 (2007).
- [220] A.P. Flitney and L.C.L. Hollenberg. Multiplayer quantum minority game with decoherence, *Quant. Inf. Comp.* **7**, 111 (2007).
- [221] C.F. Lee and N.F. Johnson. Efficiency and formalism of quantum games, *Phys. Rev. A* **67**, 022311 (2003).
- [222] G. Gutoski and J. Watrous. Toward a general theory of quantum games, *arXiv:quant-ph/0611234* (2007).
- [223] T.C. Schelling: *The Strategy of Conflict*, Harvard University Press, Cambridge, MA, 1960.
- [224] J. Silman, S. Machnes and N. Aharon. On the relation between Bell inequalities and nonlocal games, *arXiv:0710.3322v3 [quant-ph]* (2008).
- [225] T. Cheon and A. Iqbal. Bayesian Nash Equilibria and Bell Inequalities, *J. Phys. Soc. Jpn.* **77**, 024801 (2008).
- [226] D.N. Mermin. What's wrong with these Elements of Reality, *Physics Today* **43**, 9 (1990).
- [227] A.P. Flitney, M. Schlosshauer, C. Schmid, W. Laskowski and L.C.L. Hollenberg. Equivalence between Bell inequalities and quantum game theory, *arXiv:0803.0579 [quant-ph]* (2008).
- [228] N. Gisin and B. Huttner. Quantum cloning, eavesdropping and Bell's inequality [Physics Letters A 228 (1997) 13], *Phys. Lett. A* **232**, 463 (1997).
- [229] A.K. Ekert. Quantum cryptography based on Bell's theorem, *Phys. Rev. Lett.* **67**, 661 (1991).
- [230] C.H. Bennett, F. Bessette, G. Brassard, L. Salvail and J. Smolin. Experimental quantum cryptography, *Journal of Cryptology* **5**, 3 (1992).
- [231] R.F. Werner. Optimal cloning of pure states, *Phys. Rev. A* **58**, 1827 (1998).

Danksagung / Acknowledgements

Approaching the end, I would like to thank all the people who contributed to the success of this work.

First of all, I would like to thank my supervisor Prof. Harald Weinfurter for giving me the opportunity to join his group and to work in this interesting field of research. I appreciated very much the pleasant working atmosphere, the freedom to realize own ideas and the chances to get in contact with colleagues in numerous national and international conferences.

My very special thanks goes to my colleague Nikolai Kiesel. The years working with him were really great from a professional as well as personal point of view. I like to thank also Witel Wieczorek who complemented our "Garching Team" with fresh impetus and new ideas. I think we three had a really nice and fruitful collaboration. In this context i acknowledge also the dedicated contributions of Ulrich Weber and Reinhold Pohlner to our experiments.

Further, i would like to thank Roland Krischek and Pavel Trojek for refreshing and stimulating discussions.

I am also very grateful that i got the chance to collaborate with many nice and brilliant people from other groups of whom i would like to especially mention, Andreas Buchleitner, Adrian Flitney, Otfried Gühne, Wiesław Laskowski, Florian Mintert, Enrique Solano, Géza Tóth, Rupert Ursin and Marek Żukowski.

I thank furthermore all former and present members of the "Garching fraction" for their contribution to the pleasant working atmosphere, in particular, Mohamed Bourenane, Manfred Eibl, Daniel Lampert-Richart and Yousef Nazirizadeh.

For a lot of small favors, for hosting us once a week and for organizing breakfast i like to express my gratitude to the present and former members of the "City fraction", Juliane Bahe, Stefan Berner, Andreas Deeg, Martin Fürst, Florian Henkel, Fredrik Hocke, Gerhard Huber, Christian Jakob, Michael Krug, Christian Kurtsiefer, Jan Lich, Davide Marangon, Markus Rau, Nadja Regner, Wenjamin Rosenfeld, Daniel Schlenk, Tobias Schmitt-Manderbach, Sebastian Schreiner, Carsten Schuck, Asli Ugur, Jürgen Volz, Johannes Vrana, Chunlang Wang, Markus Weber, Henning Weier.

Finally, i thank Heike Schwager for her personal support and proof-reading of my manuscript.

Last, but not least, to my parents, I am deeply indebted to them for their love and the absolute support they have given me all the way. Thank you very much!

Curriculum Vitae

Personal data

Name: Christian Immanuel Thaddäus Schmid
Date of birth: 1979-02-09
Place of birth: Landshut, Bavaria, Germany

Education

School

1985 – 1989 Primary school, Seligenthal in Landshut
1989 – 1998 Grammar school, Hans-Carossa-Gymnasium in Landshut
1998 Final secondary-school examinations, "Abitur"

University

1998 – 2004 Study of physics at the Ludwig-Maximilians-University (LMU) in Munich
2000 Intermediate diploma ("Vordiplom") in physics, awarded by the LMU
2001 Summer student at Conseil Européen pour la Recherche Nucléaire (CERN)
Studies within the Omni Purpose Apparatus for Lep (OPAL) experiment on:
"Invariant mass correlations in π^0 - π^0 and η - π^0 decays"
2004 Diploma in physics, awarded by the LMU
Thesis in the Experimental Quantum Physics group of Prof. Dr. Harald Weinfurter
at the Max-Planck-Institute of Quantum Optics (MPQ) in Garching on:
*"Compact source of polarization entangled photons
and applications in quantum communication"*

Post-graduate

2004 – 2008 Postgraduate studies
PhD thesis in the Experimental Quantum Physics group
of Prof. Dr. Harald Weinfurter at the MPQ in Garching on:
"Multi-photon entanglement and applications in quantum information"

The author's publication list

Publications related to this work

- N. Kiesel, C. Schmid, U. Weber, R. Ursin and H. Weinfurter. Linear Optics C-Phase gate made simple, *Phys. Rev. Lett.* **95**, 210505 (2005).
- N. Kiesel, C. Schmid, U. Weber, O. Guehne, G. Toth, R. Ursin and H. Weinfurter. Experimental Analysis of a Four-Qubit Photon Cluster State, *Phys. Rev. Lett.* **95**, 210502 (2005).
- N. Kiesel, C. Schmid, G. Toth, E. Solano and H. Weinfurter. Experimental Observation of Four-Photon Entangled Dicke State with High Fidelity. *Phys. Rev. Lett.* **98**, 063604 (2007).
- C. Schmid, N. Kiesel, U. Weber, R. Ursin and H. Weinfurter. Experimental Analysis of a simple linear optics phase gate, *Int. J. Quant. Inf.* **5**, 235 (2007).
- C. Schmid, N. Kiesel, W. Laskowski, E. Solano, G. Toth, M. Żukowski and H. Weinfurter. The Entanglement of the Symmetric Four-Photon Dicke state, QUANTUM COMMUNICATION AND SECURITY, Marek Żukowski, Sergei Kilin, Janusz Kowalik (Eds.) *Proceedings of the NATO Advanced Research Workshop on Quantum Communication and Security*, Gdansk, Poland, 10-13 September 2006, p. 113, IOS Press (ISBN 978-1-58603-749-9), Netherlands, (2007).
- C. Schmid, N. Kiesel, W. Wieczorek and H. Weinfurter. The entanglement of the four-photon cluster state, *New. J. Phys.* **9**, 236 (2007).
- W. Wieczorek, N. Kiesel, C. Schmid and H. Weinfurter. Efficient non-tomographic tools for the characterization of multipartite entanglement, QUANTUM COMMUNICATION, MEASUREMENT AND COMPUTING, Osamu Hirota, Jeffrey H. Shapiro, Masahide Sasaki (Eds.) *Proceedings of the 8th International Conference on Quantum Communication, Measurement and Computing*, Tsukuba, Japan, 28. Nov. - 03. Dec. 2006, p. 487, NICT Press (ISBN 978-4-904020-005), Japan, (2007).
- C. Schmid, N. Kiesel, W. Wieczorek, R. Pohlner and H. Weinfurter. Multiphoton entanglement engineering via projective measurements, *SPIE Proceedings* **6780**, 67800E (2007).
- A. P. Flitney, M. Schlosshauer, C. Schmid, W. Laskowski, L. C. L. Hollenberg. Equivalence between Bell inequalities and quantum game theory, *arXiv:0803.0579 [quant-ph]* (2008).

- C. Schmid, N. Kiesel, W. Laskowski, W. Wieczorek, M. Żukowski and H. Weinfurter. Discriminating multi-partite entangled states, *Phys. Rev. Lett.* **100**, 200407 (2008).
- W. Wieczorek, C. Schmid, N. Kiesel, R. Pohlner, O. Gühne and H. Weinfurter. Experimental observation of an entire family of four-photon entangled states, *Phys. Rev. Lett.* **101**, 010503 (2008).
- C. Schmid, N. Kiesel, U. K. Weber, R. Ursin, A. Zeilinger and H. Weinfurter. Quantum teleportation and entanglement swapping with linear optics logic gates, to be published.
- W. Wieczorek, C. Schmid, N. Kiesel and H. Weinfurter. Experimental multi-photon entanglement engineering via projective measurements, in preparation.
- C. Schmid, A. P. Flitney, W. Wieczorek, N. Kiesel, H. Weinfurter and L. C. L. Hollenberg. Experimental implementation of a four-player quantum Minority game, in preparation.
- C. Schmid, F. Mintert, N. Kiesel, W. Wieczorek, A. Buchleitner and H. Weinfurter. Experimental direct measure of concurrence for mixed states, in preparation.

Other publications

- P. Trojek, C. Schmid, M. Bourennane, C. Kurtsiefer, and H. Weinfurter. Compact source of polarization-entangled photon pairs, *Optics Express* **12**, 276-281 (2004).
- P. Trojek, C. Schmid, M. Bourennane, Časlav Brukner, M. Żukowski, and H. Weinfurter. Experimental quantum communication complexity, *Phys. Rev. A* **72**, R 050305 (2005).
- C. Schmid, P. Trojek, M. Bourennane, C. Kurtsiefer, M. Żukowski and H. Weinfurter. Experimental Single Qubit Quantum Secret Sharing, *Phys. Rev. Lett.* **95**, 230505 (2005).
- C. Schmid, P. Trojek, S. Gaertner, M. Bourennane, C. Kurtsiefer, M. Żukowski and H. Weinfurter. Experimental quantum secret sharing, *Fortschr. Phys.* **54**, 831 (2006).
- C. Schmid, P. Trojek, M. Bourennane, C. Kurtsiefer, M. Żukowski, and H. Weinfurter. Schmid et al. Reply, *Phys. Rev. Lett.* **98**, 028902 (2007).
- M. Bourennane, C. Schmid, P. Trojek, C. Kurtsiefer, Č. Brukner, M. Żukowski and H. Weinfurter. Experimental Single Qubit Quantum Multiparty Communication, QUANTUM COMMUNICATION AND SECURITY, Marek Żukowski, Sergei Kilin, Janusz Kowalik (Eds.) *Proceedings of the NATO Advanced Research Workshop on Quantum Communication and Security*, Gdansk, Poland, 10-13 September 2006, p. 22, IOS Press (ISBN 978-1-58603-749-9), Netherlands, (2007).
- J. K. Pachos, W. Wieczorek, C. Schmid, N. Kiesel, R. Pohlner, H. Weinfurter. Revealing anyonic statistics with multiphoton entanglement, *arXiv:0710.0895 [quant-ph]* (2007).

Book contributions

- C. Schmid, P. Trojek, S. Gaertner, M. Bourennane, C. Kurtsiefer, M. Żukowski and H. Weinfurter. Experimental quantum secret sharing, in *Elements of Quantum Information*, Wiley-Vch, W. P. Schleich and H. Walther (Eds.), p. 303, (2007), ISBN 978-3527407255.

Patents

Single-particle quantum-enhanced secret sharing

Publication number: *WO2006074153*

Publication date: *2006-07-13*

Inventors: *Bourennane Mohamed (SE); Kurtsiefer Christian (SG); Schmid Christian (DE); Trojek Pavel (DE); Weinfurter Harald (DE); Żukowski Marek (PL)*

Applicant: *Magiq Technologies Inc. (US); Bourennane Mohamed (SE); Kurtsiefer Christian (SG); Schmid Christian (DE); Trojek Pavel (DE); Weinfurter Harald (DE); Żukowski Marek (PL)*

Classification:

– international: *H04K1/00; H04K1/00;*

– European: *H04L9/08Q*

Application number: *WO2006US00072 20060103*

Priority number(s): *US20050640248P 20050103*